



Pugh, Lynsey A. (2011) *Understanding catalytic processes used in the fragrance industry*. PhD thesis.

<http://theses.gla.ac.uk/2704/>

Copyright and moral rights for this thesis are retained by the author

A copy can be downloaded for personal non-commercial research or study

This thesis cannot be reproduced or quoted extensively from without first obtaining permission in writing from the Author

The content must not be changed in any way or sold commercially in any format or medium without the formal permission of the Author

When referring to this work, full bibliographic details including the author, title, awarding institution and date of the thesis must be given

Understanding catalytic processes used in the fragrance industry



Lynsey.A. Pugh ©

A Thesis Presented to the University of Glasgow for the Degree of
Doctor of Philosophy

Abstract

The fragrance and flavour industry is a multi-billion dollar business, therefore the production of fragrance compounds in high yields with low production of waste is of great commercial interest. Currently Innospec produce lilestralis as one of their main fragrance compounds. Lilestralis has a fresh, floral note reminiscent of lily of the valley. Due to this pleasant odour it is used in soaps, detergents and cosmetic perfumes.

However there are various aspects of the production process that are not meeting their potential. Benzaldehyde is a key intermediate in the production of lilestralis and is currently produced from toluene via benzyl chloride. This process is not an environmentally friendly route and its replacement with a suitable alternative is highly desirable. In our investigations various alternative routes were studied including the oxidation of toluene, hydrogenation of benzoic acid and the hydroformylation reaction between isopropyl benzene and 1,3,5- trioxane. Various reactor set-ups (eg gas phase, liquid phase, trickle beds etc) and methods of analysis (GC, HPLC) were used to investigate these reactions. However both the toluene oxidation over $\text{VO}_x/\text{Al}_2\text{O}_3$ and hydroformylation reactions over sulphated zirconia proved unsuccessful. The hydrogenation of benzoic acid was found to produce the desired product, however the acid corroded the rig and prevented further work being carried out.

Another aspect of the commercial process which required optimisation was the dehydrogenation reaction of liliol alcohol. The current process involves the use of a copper chromite catalyst that has been found to deactivate over time. The replacement of this catalyst would provide clear environmental benefits and the possibility of greater yields. To obtain an understanding of the processes involved during the process, various studies were carried out on the starting materials and suggested that several reactions were proceeding concurrently. It was also reported that if lilestralis was not removed from the system as soon as possible it would further react and produce by-products. Studies into activation suggested that pre-activating the catalyst prior to use had a positive effect on the reaction, as an increase in conversion was apparent. Investigations into alternative catalysts were also studied. Copper chromite catalysts from different manufactures were studied and it was found that the copper chromite modified with 120 ppm Na showed less deactivation over the period studied. This may have been due to

additives that are present within the catalyst that reduce sintering. Non chromite containing catalysts such as Cu/ZnO/Al₂O₃ and 10% Cu/SiO₂ were also studied. Both these catalysts have been previously studied in dehydrogenation reactions and were thought to be suitable alternatives for copper chromite. However extensive leaching of copper within both catalysts occurred and hence were not suitable.

Acknowledgments

There are many people that I would like to thank for their help and support throughout my PhD. First and foremost I would like to thank my supervisor Prof David Jackson. He was never too busy to help answer my many questions and dilemmas that often occurred. If it wasn't for his guidance and confidence in me I may never have made it to the end through the many problems.

Secondly I would like to thank my industrial supervisors Dr Ian McRobbie and Dr Neil Fairfax from Innospec for all their help and support throughout my PhD.

I would also like to thank some other people from the chemistry department that helped me:

- ☆ My second supervisor Dr Justin Hargreaves for his help with any questions and problems that puzzled me
- ☆ Ron Spence- my PhD would never have been completed if it wasn't for Ron's help and expertise. The lab would collapse if he wasn't there or on holiday, EMERGENCY EMERGENCY!!
- ☆ Andy Monaghan - thanks for helping me with my BETs, TGAs, XRDs and any other problems I had. Also for the endless chats about football and all other pressing matters!!
- ☆ Kim Wilson- for CHN analysis
- ☆ Jim Gallagher – for help running SEM images

I would also like to thank the catalysis group past and present. They have all made the last 3 years enjoyable and fun. I will miss the random but funny chat in the office.

Thanks especially to Claire, Mark, Fee, Stuart, Anne-Marie and Liam for their help at the start and whom I shared many nights out with throughout the 3 years. Thanks also go to Javed, Bilal, Ailsa and Alex for also being about to lend a hand in the lab and for the many laughs we had.

I would also like to thank Natalie for all her help with XRD and helping to keep me sane throughout the 3 years. I couldn't have asked for a better friend. Also thanks to Stephanie and Claire for their friendship throughout my time at Uni.

Special thanks go to my mum, dad, gran and papa. If it wasn't for their continual support, love and guidance I would never have got to where I am today. Also for the continual hand outs of money, I will try and re-pay you one day!!

Finally I would like to say a big thank you to Stuart for all his help and continual support. He deserves a medal for putting up with all the tears, the moaning and the tantrums when things went wrong.

Declaration

This work contained in this thesis, submitted for the degree of Doctor of Philosophy, is my own work except where due reference is made to other authors. No material within this thesis has been previously submitted for a degree at this or any other university.

Lynsey A. Pugh

Table of Contents

Abstract.....	1
1 Introduction	19
1.1 Fragrance and flavour Industry.....	19
1.2 Naturals and synthetics.....	21
1.2.1 Naturals	21
1.2.2 Synthetics	22
1.3 Volatility	23
1.4 Project aims.....	24
2 Benzaldehyde production	25
2.1 Introduction	25
2.1.1 Benzaldehyde	25
2.1.2 Production methods	26
2.1.3 Possible methods	28
2.1.4 Toluene.....	29
2.1.5 Benzoic acid.....	32
2.1.6 Hydroformylation.....	36
2.1.7 Project aim	39
2.2 Experimental	40
2.2.1 Catalyst characterisation.....	40
2.2.2 Toluene Oxidation	42
2.2.3 Benzoic acid hydrogenation.....	47
2.2.4 Hydroformylation reactions.....	52
2.3 Results & Discussion.....	57
2.3.1 Toluene Oxidation	57
2.3.2 Benzoic acid hydrogenation.....	64
2.3.3 Hydroformylation reactions.....	74
2.4 Conclusions	85
3 Liquid phase dehydrogenation	86
3.1 Introduction	86
3.1.1 Lilestralis.....	86
3.1.2 Possible methods	87
3.1.3 Stability of lilestralis	88

3.1.4	Dehydrogenation Reactions.....	90
3.1.5	Copper catalysts.....	90
3.1.6	Copper chromite	90
3.1.7	Project outline.....	93
3.2	Experimental.....	94
3.2.1	LPD Reactor	94
3.2.2	GC method	95
3.2.3	Catalyst.....	96
3.2.4	Reduction of copper chromite catalysts	97
3.2.5	Extraction methods.....	100
3.2.6	Air sensitive XRD	101
3.2.7	Lewis acid site determination	102
3.2.8	Calibrations	102
3.2.9	Product analysis	105
3.2.10	Materials	108
3.2.11	Calculations	108
3.3	Results & discussion.....	109
3.3.1	Catalyst characterisation.....	109
3.3.2	Material investigation	142
3.3.3	Catalyst activation.....	167
3.3.4	Concentration variation	191
3.3.5	Alternative copper chromite.....	196
3.3.6	Alternative catalysts.....	206
3.4	Conclusions	220
4	References.....	222

List of Figures

Figure 1-1 Worldwide market shares of the flavour industry for the years 1999 and 2005	20
Figure 1-2 Market share of the individual sectors of the flavour and fragrance industry (2002,	20
Figure 1-3 Industrial usage of flavour and fragrance materials (2)	21
Figure 1-4 Structure of a perfume (3)	23
Figure 1-5 Lilestralis production.....	24
Figure 2-1 Perfumery materials from benzaldehyde (4)	26
Figure 2-2 Oxidation of toluene	29
Figure 2-3 The model of Mars and VanKrevelen on catalytic oxidation (29)	31
Figure 2-4 The catalytic mechanism of Ph-CHO production from Ph-COOH over metal oxide (47)	33
Figure 2-5 Product distribution in the deoxygenation of benzoic acid over ZrO_2 as a function of temperature (11).....	34
Figure 2-6 Product distribution in the deoxygenation of benzoic acid over ZnO as a function of temperature (11).....	35
Figure 2-7 Stoichiometry of the hydroformylation reaction (51)	36
Figure 2-8 Schematic diagram of hydroformylation reaction.....	38
Figure 2-9 Schematic diagram of trickle bed reactor.....	44
Figure 2-10 Soxhlet extraction apparatus.....	47
Figure 2-11 Benzoic acid saturator design	48
Figure 2-12 Benzoic acid ethanol feed set-up.....	48
Figure 2-13 Schematic diagram of gas phase reactor for benzoic acid hydrogenation	50
Figure 2-14 HPLC solvent profile.....	51
Figure 2-15 Gas phase reactor set-up for hydroformylation reaction	53
Figure 2-16 XRD 3.5% vanadium supported on alumina	59
Figure 2-17 XRD 8% vanadium supported on alumina	59
Figure 2-18 Complete combustion of toluene	60
Figure 2-19 XRD fresh $Zr(OH)_4$ uncalcined.....	64
Figure 2-20 Hot stage XRD $Zr(OH)_4$ in N_2 atmosphere at room temperature, 100°C, 200°C, 300°C, 400°C, 500°C and 600°C.....	65

Figure 2-21 Variation of the relative phase of the polymorph mixture as a function of temperature (88).....	66
Figure 2-22 TGA weight and derivative weight profile of $Zr(OH)_4$ in N_2 from 25°C to 600°C	67
Figure 2-23 HPLC trace from benzoic acid hydrogenation reaction 3, after 23 hours	68
Figure 2-24 HPLC trace from benzoic acid hydrogenation reaction 3, after 48 hours	70
Figure 2-25 HPLC trace from benzoic acid hydrogenation reaction 3, after 114 hours	71
Figure 2-26 Selective hydrogenation of acetic acid to acetaldehyde (91)	72
Figure 2-27 Schematic diagram of hydroformylation reaction.....	74
Figure 2-28 XRD uncalcined sulphated zirconia, laboratory prepared	75
Figure 2-29 XRD calcined sulphated zirconia laboratory prepared, 550°C for 8 hours.....	76
Figure 2-30 TPO weight and derivative weight profile: gas phase reaction between 3.5: 1 Isopropyl benzene: 1, 3, 5 trioxane, reaction conditions 300°C, 50ml.min ⁻¹ N_2 , feed rate 2.2ml.h ⁻¹	77
Figure 2-31 TPO weight and CO ₂ mass profile: gas phase reaction between 3.5: 1 Isopropyl benzene: 1, 3, 5 trioxane, reaction conditions 300°C, 50ml.min ⁻¹ N_2 , feed rate 2.2ml.h ⁻¹	78
Figure 2-32 TPO weight and formaldehyde mass profile : gas phase reaction between 3.5: 1 Isopropyl benzene: 1, 3, 5 trioxane, reaction conditions 300°C, 50ml.min ⁻¹ N_2 , feed rate 2.2ml.h ⁻¹	79
Figure 2-33 TPO weight and derivative weight profile: gas phase reaction between 10: 1 Isopropyl benzene: 1, 3, 5 trioxane, reaction conditions 300°C, 50ml.min ⁻¹ N_2 , feed rate 2.2ml.h ⁻¹	80
Figure 2-34 Chromatograms of CO ₂ and SO ₂ evolved from fresh and deactivated sulphates sol-gel process zirconia in TGA/FT-IR under air flow (94)	81
Figure 2-35 Carbon deposition on sulphated sol-gel zirconia in the isomerisation of <i>n</i> -butane at 200°C as a function of time (93).....	82
Figure 2-36 XRD commercial MEL chemicals 7% sulphated zirconium, uncalcined	83
Figure 2-37 XRD commercial MEL chemicals 7% sulphated zirconia -calcined 600°C for 3 hours in static air.....	83
Figure 3-1 Synthetic aldehydic muguet odourants (97)	86
Figure 3-2 Differences in odour profiles of muguet odourants (97)	87
Figure 3-3 Production of hydrocinnamaldehydes (4)	88
Figure 3-4 Autoxidation of lilestralis (4).....	89

Figure 3-5 Schematic diagram of LPD reactor.....	95
Figure 3-6 Glass line set-up for catalyst reduction	98
Figure 3-7 p-LOL weight calibration	103
Figure 3-8 p-LAL weight calibration	103
Figure 3-9 p-LOL concentration calibration	104
Figure 3-10 p-LAL concentration calibration.....	104
Figure 3-11 XRD pattern spent high activity catalyst from production plant.....	110
Figure 3-12 XRD pattern of spent low activity catalyst from production plant.....	110
Figure 3-13 XRD pattern of spent low and high activity catalyst from production plant..	111
Figure 3-14 TPO high activity spent catalyst (30-1000°C, 10 degC.min ⁻¹ , 2% O ₂ /Ar).....	112
Figure 3-15 TPO derivative weight and heat profile for high activity catalyst (30-1000°C, 10 degC.min ⁻¹ , 2% O ₂ /Ar).....	113
Figure 3-16 TPO Low activity spent catalyst profile (30-1000°C, 10 degC.min ⁻¹ , 2% O ₂ /Ar)	114
Figure 3-17 TPO derivative weight and heat profile for low activity catalyst (30-1000°C, 10 degC.min ⁻¹ , 2% O ₂ /Ar).....	114
Figure 3-18 TG of metallic copper (ramp rate 5degCmin ⁻¹) (110)	115
Figure 3-19 Hot stage XRD of fresh BASF copper chromite catalyst, carried out under 5%H ₂ /N ₂ atmosphere. Scans recorded at 25°C, 150°C, 200°C, 250°C and 300°C.....	117
Figure 3-20 TPR fresh copper chromite weight loss profile (30-500°C, 5%H ₂ /N ₂ , ramp rate of 10 degC.min ⁻¹).....	118
Figure 3-21 TPR derivative weight and heat profile fresh copper chromite (30-500°C, 5%H ₂ /N ₂ , ramp rate of 10 degC.min ⁻¹).....	119
Figure 3-22 The scheme of the reversible reduction of copper chromite. Triangles indicate (a) tetrahedral positions; squares indicate (d) octahedral positions; hatched areas indicate (c) octahedral positions (119)	120
Figure 3-23 TPR-TPO process of copper chromite a) Reduction: 30-500°C, 5%H ₂ /N ₂ , ramp rate of 10 degC.min ⁻¹ then allowed to stabilise in Argon for 20minutes b) Oxidation: 30-500°C, 2% O ₂ /Ar, ramp rate of 10 degC.min ⁻¹ then allowed to stabilise in Argon for 20minutes	121
Figure 3-24 TPR weight and derivative weight profile from 1 st reduction in reduction/oxidation process of fresh copper chromite (30-500°C, 5%H ₂ /N ₂ , ramp rate of 10 degC.min ⁻¹)	122
Figure 3-25 Thermal analysis of copper chromite comparison (114).....	123

Figure 3-26 XRD of post hot stage copper chromite (reduced: 25-300°C, 5% H ₂ /N ₂) after 1 week of air exposure.....	126
Figure 3-27 Comparison of a) fresh copper chromite and b) post hot stage XRD catalyst (reduced: 25-300°C, 5% H ₂ /N ₂) allowed to oxidise in air for 1 week.....	127
Figure 3-28 TPR weight profile of reduced copper chromite sample allowed to oxidise for 1 week then re-analysed (25-500°C, 5% H ₂ /N ₂).....	128
Figure 3-29 TPD profile of BASF copper chromite post pyridine adsorption (m/z= 52, 79). Conditions: 25-300°C, ramp rate of 10 degC.min ⁻¹ , 90 ml.min ⁻¹ Ar.....	129
Figure 3-30 XRD of fresh copper chromite 120 ppm Na.....	131
Figure 3-31 TPR of fresh copper chromite 120 ppm Na (30-500°C, ramp rate 10 degC.min ⁻¹ , 5% H ₂ /N ₂)	132
Figure 3-32 TPD profile of Sud chemie copper chromite 120 ppm Na post pyridine adsorption (m/z= 52, 79). Conditions: 25-300°C, ramp rate of 10 degC.min ⁻¹ , 90 ml.min ⁻¹ Ar.....	133
Figure 3-33 XRD of fresh Copper chromite 1600 ppm Na	134
Figure 3-34 TPR of fresh copper chromite 1600 ppm Na (30-500°C, ramp rate 10 degC.min ⁻¹ , 5% H ₂ /N ₂)	134
Figure 3-35 TPD profile of Sud chemie copper chromite 1600 ppm Na post pyridine adsorption (m/z= 52, 79). Conditions: 25-300°C, ramp rate of 10 degC.min ⁻¹ , 90 ml.min ⁻¹ Ar.....	135
Figure 3-36 TPR weight loss profile of fresh Cu/ZnO/Al ₂ O ₃ (30-500°C, ramp rate 10 degC.min ⁻¹ , 5% H ₂ /N ₂)	136
Figure 3-37 Hot Stage XRD CuO/ZnO/Al ₂ O ₃ carried out under 5%H ₂ /N ₂ atmosphere. Scans recorded at 25°C, 50°C, 100°C, 150°C, 200°C and 250°C.....	137
Figure 3-38 XRD of fresh silica support (Caricat Q10).....	138
Figure 3-39 XRD of calcined 10% copper silica catalyst.....	139
Figure 3-40 TGA uncalcined 10% Cu/SiO ₂ (30-500°C, ramp rate 10 degC.min ⁻¹ , Ar)	139
Figure 3-41 TPR of calcined 10% Cu/SiO ₂ (30-500°C, ramp rate 10 degC.min ⁻¹ , 5% H ₂ /N ₂)	140
Figure 3-42 GC trace: sample from reactor pot.....	143
Figure 3-43 GC trace: sample from collecting flask	143
Figure 3-44 Inert bed from production plant.....	144
Figure 3-45 Post reaction XRD comparison between a) fresh and b) used copper chromite from reaction between inert bed and catalyst (230°C, 57 mbar).....	145

Figure 3-46 GC trace inert bed & p-LOL 0-2 hours.....	146
Figure 3-47 Conversion of p-LOL and p-LAL yield in the reaction between p-LOL & copper chromite (0-2 hours: 203°C, 57 mbar, starting material rate addition 20g/h then 2-6.5 hours: 230°C, 270 mbar, rate of addition of p-LOL 50g/h)	148
Figure 3-48 Selectivity for all other by-products for reaction between p-LOL and copper chromite (0-2 hours: 203°C, 57 mbar, starting material rate addition 20g/h then 2-6.5 hours: 230°C, 270 mbar, rate of addition of p-LOL 50g/h)	149
Figure 3-49 Tishchenko reaction mechanism	150
Figure 3-50 Inert bed production.....	150
Figure 3-51 Reaction equations	152
Figure 3-52 Conversion of p-LOL and p-LAL yield for the reaction between p-LOL and copper chromite (230°C, 270 mbar, rate of addition of p-LOL: 13.5g/10 min then 5g/h)	153
Figure 3-53 Selectivity for all other by-products for the reaction between p-LOL and copper chromite (230°C, 270 mbar, rate of addition of p-LOL: 13.5g/10 min then 5g/h)	154
Figure 3-54 GC trace p-LAL and catalyst flask sample	155
Figure 3-55 GC trace p-LAL and catalyst reactor sample	156
Figure 3-56 Post reaction XRD from reaction between p-LAL, copper chromite & N ₂ (230°C, 400 mbar) (Key: star – Cu ⁰ , Circle – CuO).....	157
Figure 3-57 Conversion of p-LAL in reaction between p-LAL, copper chromite & H ₂ (230°C, 400 mbar, 20 ml.min ⁻¹ 5%H ₂ /Ar)	158
Figure 3-58 Selectivity of reaction between p-LAL, copper chromite & H ₂ (230°C, 400 mbar, 20 ml.min ⁻¹ 5%H ₂ /Ar)	158
Figure 3-59 Conversion of p-LAL in standard reaction between p-LAL and copper chromite (230°C, 57 mbar)	159
Figure 3-60 Selectivity of by-products in standard reaction between p-LAL and copper chromite (230°C, 57 mbar).....	160
Figure 3-61 Post reaction XRD standard reaction between p-LAL and unreduced copper chromite (230°C, 57 mbar).....	160
Figure 3-62 Conversion of p-LAL in a standard reaction between p-LAL & reduced copper chromite (230°C, 57 mbar).....	162
Figure 3-63 Selectivity of by-products in a standard reaction between p-LAL & reduced copper chromite (230°C, 57 mbar)	162

Figure 3-64 Conversion of p-LAL in the reaction between p-LAL and a) unreduced copper chromite & no inert bed b) unreduced copper chromite & inert bed and c) pre-reduced copper chromite & inert bed	163
Figure 3-65 By-product formation	165
Figure 3-66 Autoxidation of lilestralis (4).....	166
Figure 3-68 Data logger temperature profile from reaction where plant ratio studied (ratio used: 1 g catalyst: 10 g inert bed: 490 g p-LOL, conditions: 230°C, 57 mbar)	168
Figure 3-69 Conversion of p-LOL & p-LAL yield for reaction between p-LOL and non activated copper chromite: short reaction (230°C, 57 mbar).....	169
Figure 3-70 Data logger temperature profile from plant rate of addition of p-LOL (13.5g in 1 st 10 minutes then 5g/h, conditions: 230°C, 57 mbar).....	171
Figure 3-71 Post reaction XRD from standard reaction between p-LOL and copper chromite (230°C, 57 mbar).....	172
Figure 3-72 P-LAL yield comparison for standard reaction involving p-LOL and copper chromite (230°C, 57 mbar).....	173
Figure 3-73 p-LAL average yield for standard reaction involving p-LOL and copper chromite (230°C, 57 mbar).....	174
Figure 3-74 Post reaction XRD 2hour reaction between p-LOL and copper chromite (230°C, 57 mbar)	175
Figure 3-75 Post reaction XRD comparison of a) 2hr and b) 6.5hr reaction between p-LOL and copper chromite.....	175
Figure 3-76 Conversion of p-LOL & p-LAL yield for part 1 of sequential addition involving p-LOL and copper chromite (230°C, 57 mbar)	177
Figure 3-77 Conversion of p-LOL & p-LAL yield for part 2 of sequential addition involving p-LOL and copper chromite (230°C, 57 mbar)	177
Figure 3-78 Conversion of p-LOL & p-LAL yield for sequential addition reaction involving p-LOL and copper chromite (230°C, 57 mbar)	178
Figure 3-79 Conversion of p-LOL & p-LAL yield for reaction involving p-LOL and <i>in-situ</i> activation of copper chromite: short reaction (230°C, 57 mbar)	179
Figure 3-80 Conversion of p-LOL & p-LAL yield for reaction involving p-LOL and <i>ex-situ</i> activation of copper chromite: short reaction (230°C, 57 mbar)	180
Figure 3-81 p-LAL yield activation comparison between reaction involving a) no catalyst activation b) <i>in-situ</i> activation and c) <i>ex-situ</i> activation of copper chromite.....	181

Figure 3-82 Conversion of p-LOL & p-LAL yield for reaction involving p-LOL and non activated copper chromite: extended reaction (230°C, 57 mbar).....	182
Figure 3-83 Selectivity for all other by products for reaction involving p-LOL and non activated copper chromite: extended reaction (230°C, 57 mbar).....	183
Figure 3-84 Post reaction XRD from reaction involving p-LOL and no activated copper chromite: extended reaction (230°C, 57 mbar).....	183
Figure 3-85 Conversion of p-LOL & p-LAL yield for reaction involving p-LOL and <i>in-situ</i> activation of copper chromite: extended reaction (230°C, 57 mbar, N ₂)	184
Figure 3-86 Selectivity for all other by products for reaction involving p-LOL and <i>in-situ</i> activation of copper chromite: extended reaction (230°C, 57 mbar, N ₂)	185
Figure 3-87 Conversion & p-LAL yield for reaction involving p-LOL and <i>in-situ</i> activation of copper chromite: extended reaction (230°C, 57 mbar, 5% H ₂ /Ar)	186
Figure 3-88 for all other by products for reaction involving p-LOL and <i>in-situ</i> activation of copper chromite: extended reaction (230°C, 57 mbar, 5% H ₂ /Ar)	187
Figure 3-89 Deactivation comparison of 10 hour reaction between p-LOL and copper chromite with a) no activation b) <i>in-situ</i> activation then reaction carried out under N ₂ .	188
Figure 3-90 Methanol synthesis activities on Cu based catalysts with different metallic copper crystallite sizes (147).....	189
Figure 3-91 Deactivation comparison of 10 hour reaction between p-LOL and copper chromite with a) <i>in-situ</i> activation then reaction carried out under N ₂ b) <i>in-situ</i> activation then reaction carried out under 5% H ₂ /Ar	190
Figure 3-92 Conversion of p-LOL and p-LAL yield for 2.5 g catalyst: 50 g inert bed: 13 g p-LOL in 1 st 10min then 5 g/h (230°C, 57 mbar).....	191
Figure 3-93 Conversion of p-LOL and p-LAL yield for 1 g catalyst: 50 g inert bed: 13 g p-LOL in 1 st 10min then 5 g/h (230°C, 57 mbar)	192
Figure 3-94 p-LAL yield comparison for catalyst mass a) 5 g b) 2.5 g c) 1 g , reaction conditions: 230°C, 57mbar.....	193
Figure 3-95 Conversion of p-LOL and p-LAL yield for 2.5 g catalyst: 25 g inert bed: 13 g p-LOL in 1 st 10min then 5 g/h (230°C, 57 mbar).....	194
Figure 3-96 Conversion of p-LOL and p-LAL yield for 5 g catalyst: 50 g inert bed: 10 g in 1 st 10 min then 10 g/h p-LOL	194
Figure 3-97 Data logger temperature profile from reaction involving increased feed rate: 5 g catalyst: 50 g inert bed: 10 g in 1 st 10 min then 10 g/h p-LOL (230°C, 57 mbar).....	195

Figure 3-98 Conversion of p-LOL & p-LAL yield for reaction between p-LOL and non activated copper chromite 120 ppm Na (230°C, 57 mbar).....	197
Figure 3-99 Selectivity for all other by products for reaction involving p-LOL and non activated copper chromite 120 ppm Na (230°C, 57 mbar).....	198
Figure 3-100 Conversion of p-LOL & p-LAL yield for reaction between p-LOL and <i>in-situ</i> copper chromite 120 ppm Na (230°C, 57 mbar).....	200
Figure 3-101 Selectivity for all other by products for reaction involving p-LOL and <i>in-situ</i> activated copper chromite 120 ppm Na (230°C, 57 mbar).....	201
Figure 3-102 Conversion of p-LOL & p-LAL yield for reaction between p-LOL and non activated copper chromite 1600 ppm Na (230°C, 57 mbar).....	202
Figure 3-103 Relation of relative ratio of the dehydrogenation of benzyl alcohol vs concentration of aq. NaOH (163).....	203
Figure 3-104 Selectivity for all other by products for reaction involving p-LOL and non activated copper chromite 1600 ppm Na (230°C, 57 mbar).....	203
Figure 3-105 Comparison of p-LAL yield for unreduced catalysts for a) BASF copper chromite b) copper chromite 120 ppm Na and c) copper chromite 1600ppm Na.....	204
Figure 3-106 Comparison of by-product yield for unreduced catalysts a) BASF copper chromite b) copper chromite 120 ppm Na and c) copper chromite 1600ppm Na.....	205
Figure 3-107 Conversion of p-LOL & p-LAL yield for reaction between p-LOL and non activated CuO/ZnO/Al ₂ O ₃ (230°C, 57 mbar).....	207
Figure 3-108 Post reaction XRD from standard reaction between p-LOL and CuO/ZnO/Al ₂ O ₃ (230°C, 57 mbar).....	208
Figure 3-109 Leaching of Cu species. Naphthalene 10 mg; 1.0M H ₂ O ₂ aqueous solution, 10 ml; CuO/Al ₂ O ₃ , 20 mg; reaction temperature 100°C (170).....	209
Figure 3-110 Liquid UV analysis of a) p-LAL after exposure to Cu/ZnO/Al ₂ O ₃ b) copper (II) acetate in acetone.....	210
Figure 3-111 Conversion of p-LOL & p-LAL yield for reaction between p-LOL and <i>in-situ</i> activated CuO/ZnO/Al ₂ O ₃ (230°C, 57 mbar).....	211
Figure 3-112 SEM images of a) fresh and b) post reaction sample from reduced CuO/ZnO/Al ₂ O ₃ reaction	211
Figure 3-113 Conversion of p-LOL & p-LAL yield for reaction between p-LOL and non activated 10% Cu/SiO ₂ (230°C, 57 mbar).....	213
Figure 3-114 Post reaction XRD from standard reaction between p-LOL and non activated 10%Cu/SiO ₂ (230°C, 57 mbar).....	214

Figure 3-115 Conversion of p-LOL & p-LAL yield for reaction between p-LOL and <i>ex-situ</i> activated 10% Cu/SiO ₂ (230°C, 57 mbar).....	215
Figure 3-116 Post reaction XRD from standard reaction between p-LOL and <i>ex-situ</i> activated 10%Cu/SiO ₂ (230°C, 57 mbar).....	216
Figure 3-117 SEM images of a) fresh 10%Cu/SiO ₂ b) post reaction unreduced c) post reaction reduced	217
Figure 3-118 Catalyst & p-LOL experiment after a) 10 days, b) 20 days and c) 40 days ...	219

List of Tables

Table 1 Sales figures for flavour and fragrance industry (1).....	19
Table 2 Natural oils price and usage (4).....	22
Table 3 Catalytic oxidation of toluene with single components catalysts (25)	30
Table 4 Hydrogenation of benzoic acid with modification of the ZrO ₂ catalyst (18)	34
Table 5 Support properties of γ - alumina.....	45
Table 6 Catalytic reactions	46
Table 7 Hydroformylation vapour phase reactions	54
Table 8 7% Sulphated zirconia properties	54
Table 9 Hydroformylation liquid reactions	56
Table 10 Physiochemical characterisation of vanadium catalysts (75)	58
Table 11 Crystallite size of hot stage XRD Zr(OH) ₄	65
Table 12 Percentage of components BASF copper chromite	96
Table 13 Properties of BASF copper chromite.....	96
Table 14 Percentage of components Sud-Chemie copper chromite.....	97
Table 15 Typical weight % of each component in copper methanol synthesis catalysts (72)	99
Table 16 Silica Q10 support properties.....	100
Table 17 Possible products	106
Table 18 Material suppliers and purity	108
Table 19 CHN analysis results for spent Innospec catalysts	109
Table 20 BET analysis Copper chromite.....	118
Table 21 BET analysis 120 ppm Na Copper chromite	132
Table 22 BET analysis 1600 ppm Na Copper chromite	135
Table 23 BET analysis CuO/ZnO/Al ₂ O ₃	137
Table 24 BET analysis 10% Cu/SiO ₂	141
Table 25 p-LOL & catalyst material addition.....	147
Table 26 Compound names from GC trace (figures 3-54 & 3-55)	156
Table 27 Crystallite size comparison between hot stage XRD and 6.5 h reaction	172
Table 28 Crystallite size comparison between 2 h reaction and 6.5 h reaction.....	176
Table 29 Crystallite size comparison between hot stage, 2 h, 6.5 h and 10 h reaction ...	184
Table 30 Crystallite size comparison between 10 h no activation reaction and <i>in-situ</i> activation N ₂	188

Table 31 Crystallite size comparison between 10 h reaction carried out in N ₂ and 5% H ₂ N ₂	190
Table 32 Catalyst comparison for Lewis acid sites.....	196
Table 33 Catalyst comparison for Lewis acid sites 2.....	201
Table 34 Typical weight % of each component in copper methanol synthesis catalysts (72)	206
Table 35 BET CuO/ZnO/Al ₂ O ₃	212
Table 36 Crystallite size Cu/SiO ₂	216
Table 37 BET 10% Cu/SiO ₂	217

1 Introduction

1.1 Fragrance and flavour Industry

The fragrance and flavour industry is a multibillion dollar business. It covers a variety of different areas such as personal hygiene and care products, perfumes, laundry, detergents, foods and the tobacco industry. The top ten companies in the world in the industry dominate over 65% of the total market sales. As shown in table 1 the fragrance industry is a growing business, as the total market sales have nearly doubled over the last 10 years.

Table 1 Sales figures for flavour and fragrance industry (1)

Year	Total Market (\$, values in billions)	Top 10 companies (%)	All other companies (%)
1999	12.9	64.6	35.4
2005	16.0	66	34
2006	18.0	65.9	34.1
2007	19.8	68.7	31.3
2008	20.3	70.7	29.3
2009	20.0	72.4	27.6

It is shown in figure 1-1 that the market share percentages did not change dramatically over the period from 1999 to 2005. The percentage in Asia did increase slightly by 3% showing that there is a greater demand for flavour and fragrance products.

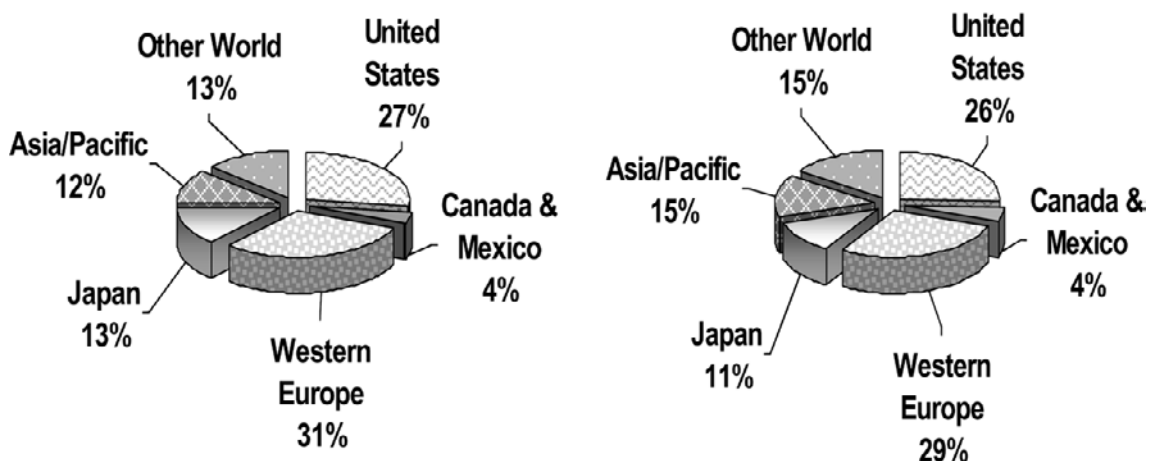


Figure 1-1 Worldwide market shares of the flavour industry for the years 1999 and 2005

(estimated by Freedonia; see: www.leffingwell.com/1372pr.pdf) (2)

The USA however is the major consumer of fragrance and flavour products (2). Although they only account for approximately 15% of the world population, their overall demand for fragrance and flavour was 71% in 1999 and 66% in 2004 of the total world demand (1, 2).

When the flavour and fragrance industry is divided into two sections the market share is approximately a 50:50 split. Figure 1-2 shows the market share for individual sectors for the combined industry.

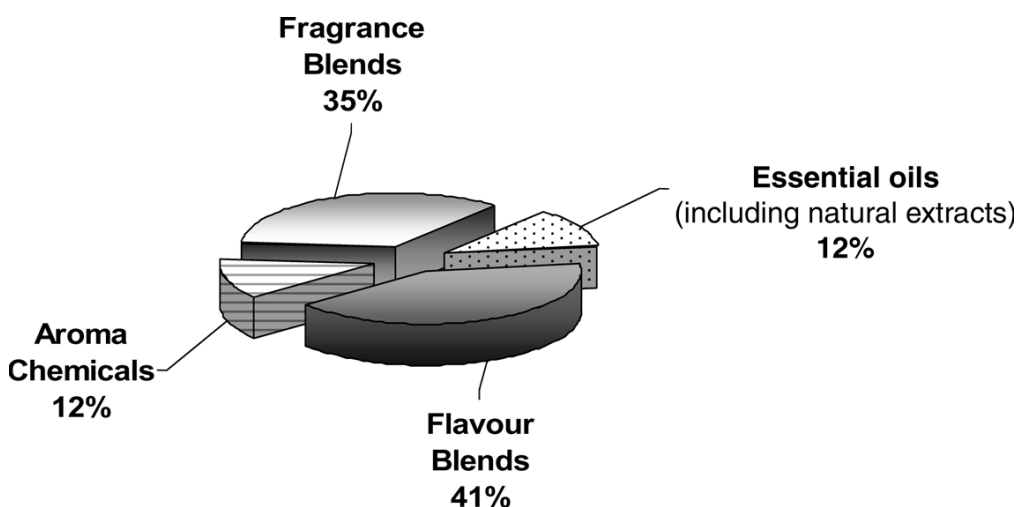


Figure 1-2 Market share of the individual sectors of the flavour and fragrance industry (2002, estimated by Freedonia Group, C&EN estimates) (2)

1.2 Naturals and synthetics

Fragrance and flavour compounds fall into two main categories: synthetics and naturals.

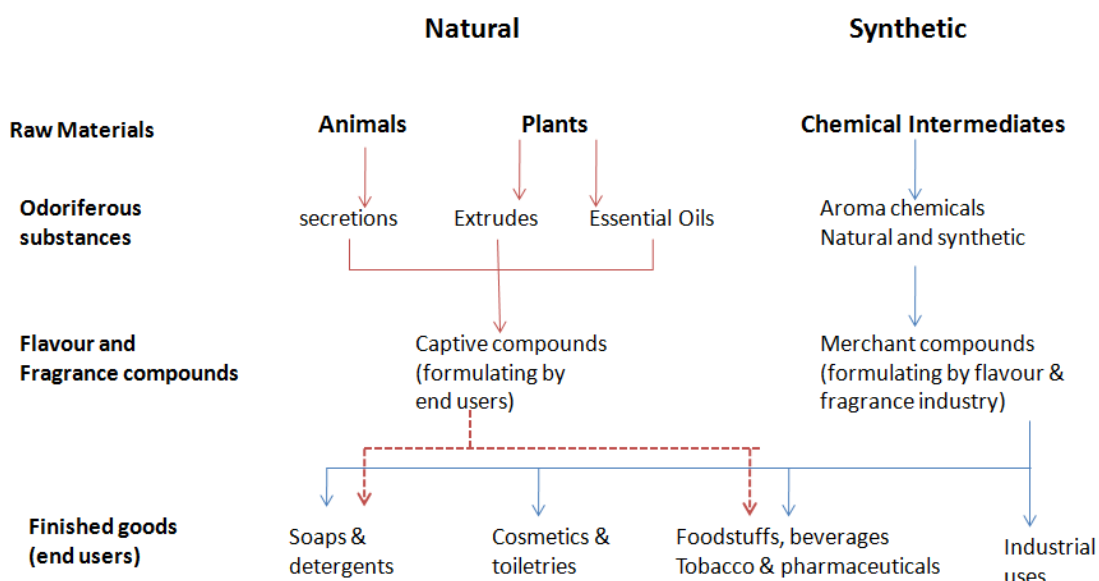


Figure 1-3 Industrial usage of flavour and fragrance materials (2)

1.2.1 Naturals

Natural materials are obtained from natural sources by the application of physical separation techniques such as extraction and distillation (3). In perfumery, natural compounds have been used as raw materials for many thousands of years. There are many sources for these materials, such as entire plants, flowers, fruits, seeds, leaves, woods, roots, resins and animal secretions. Some of the most commonly used natural compounds include the oil from oranges (~15,000 tonnes per annum produced), citronella, vanilla, peppermint, cornmint and lemon. The price of natural oils can vary considerably in price and volume used each year as shown in table 2.

Table 2 Natural oils price and usage (4)

Natural Oil	Annual Usage (tonnes)	Price per kg
Lavendar	250-300	£15-30
Rose	15-20	£1000-3000
Jasmine	12	£2000
Eucalyptus	2000	£5

Up until this century perfume was very expensive and only the wealthiest people could afford it. This was due to perfumers only having natural sources to rely on. Most of the ingredients that are required are expensive to obtain and in limited supply. An example of this is Jasmine. It takes 7,000,000 flowers to produce just 1kg of oil (4).

1.2.2 Synthetics

For the perfumer today there are thousands of synthetically produced aromas that are available. Many of these scents have been discovered in nature and have subsequently been synthesised, for example vanillin (3). The fragrance characteristic of the synthetic material nearly always mimics that of the natural source. Natural-identical materials are normally less expensive than the natural source. For example jasmine, the synthetic material is approximately one tenth the price of the natural material (4). The simpler analogues of this are even cheaper by at least an order of magnitude. In 1866 benzaldehyde was one of the first materials to be produced industrially from toluene. Hydrocarbons produced from the petroleum industry and monoterpenes from turpentine were the starting point in the synthesis of many new aromas. Aldehydes that were produced were the inspiration for a number of perfumes such as Chanel No.5 and Arpège (3).

1.3 Volatility

To be perceived a fragrance must be volatile. Some perfumery materials can last a few minutes where as others can last weeks. There are many important factors that come into play such as functional groups, molecular structure and molecular mass. Masses of around 200 occur frequently where as masses over 300 are exceptions (5). The odour of a perfume changes during evaporation due to the different volatilities of the materials present. This can be divided into 3 sections: top notes, middle notes and base notes (end note). The base notes consist of the least volatile compounds and hence last the longest, the middle notes are of medium volatility and the top notes are the most volatile. Often to prevent the more volatile compounds evaporating fixatives are added (3, 5).

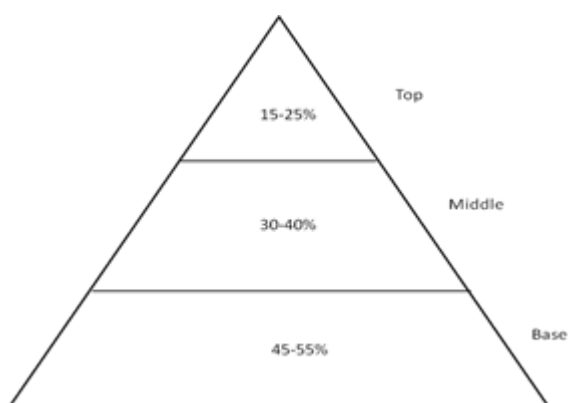


Figure 1-4 Structure of a perfume (3)

The balance between these three notes is of great important in a perfume, especially the extent to which the perfume diffuses during evaporation. Due to their variation of volatility, natural compounds are often hard to classify as notes. Top notes are often fresh notes such as linalool, lavender, citrus oils, rose oxide and *cis*-3- hexanol. Floral notes are often classed as middle notes such as terpineol, rose alcohols and many of the important compounds used in making muguet and jasmin. Eugenol and spicy oriental notes come at the bottom of the middle notes close to the base notes. Vanillin, oakmoss, musks and woody materials are all base notes (3).

1.4 Project aims

Currently Innospec produces lilestralis as one of their main fragrance compounds. Figure 1-5 shows how this is achieved. There are various aspects of this process that are not meeting their potential. Benzaldehyde is a key intermediate in the production of lilestralis and is currently produced from toluene via benzyl chloride. This process is not an environmentally friendly route. Another aspect is the liquid phase dehydrogenation (LPD) reaction of lilol alcohol. This involves a copper chromite catalyst that deactivates over time. The replacement of this catalyst would provide environmental benefits and the possibility of greater yields.

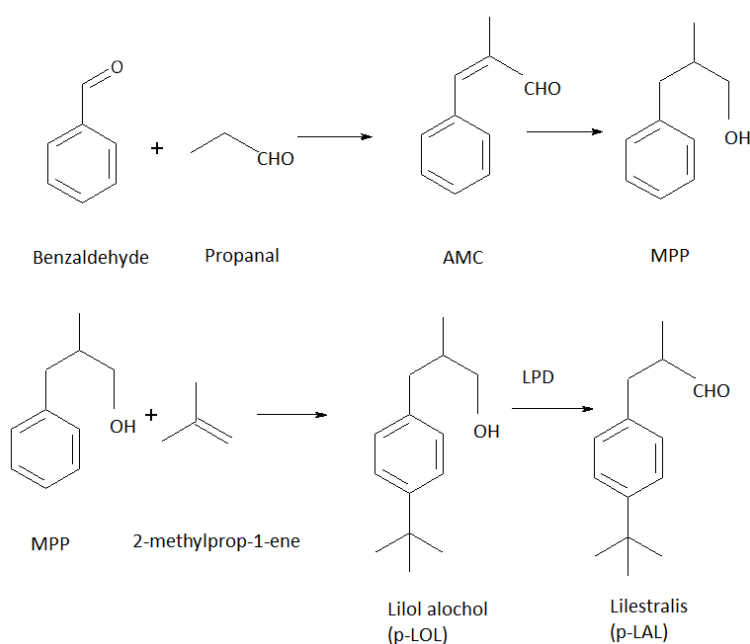


Figure 1-5 Lilestralis production

The work within this thesis has been separated into two sections: i) Benzaldehyde production and ii) optimisation of the dehydrogenation of p-LOL to p-LAL.

The aim of this project was to

1. Investigate a more environmentally friendly route to produce benzaldehyde for the start of the process
2. Investigate the dehydrogenation process of p-LOL to p-LAL

2 Benzaldehyde production

2.1 Introduction

2.1.1 Benzaldehyde

Benzaldehyde is the simplest aromatic aldehyde. It has a bitter almond-like odour and taste and can be found naturally in over fifty different oils. Natural bitter almond oil which consists of almost all benzaldehyde also contains small portions of hydrocyanic acid, which is poisonous for humans and has to be removed before being sold for flavourings and perfumery. Benzaldehyde is used in the manufacture of a variety of different products such as perfumes, dyes, medicinals and photographic films. Figure 2-1 shows some perfumery materials made from benzaldehyde. In the fragrance industry benzaldehyde itself is not used to any great extent but it is used commonly as a raw material in the production of many aromatic compounds (6).

Benzaldehyde comes in the form of a colourless liquid, however when this is exposed to air, oxidation occurs and the corresponding acid is formed. Benzoic acid is a solid white crystalline substance, so when produced can be easily recognised from the liquid aldehyde.

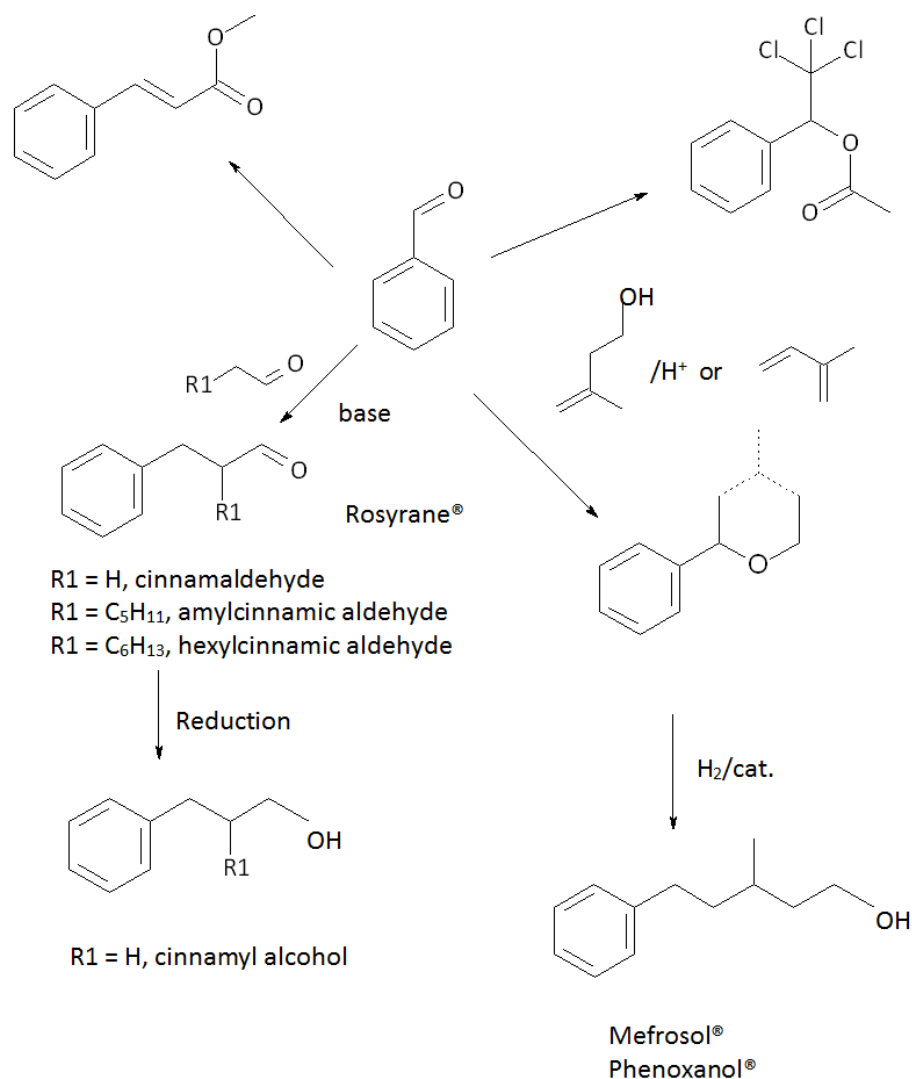


Figure 2-1 Perfumery materials from benzaldehyde (4)

2.1.2 Production methods

Over the years there have been various ways in which benzaldehyde has been produced. Two methods that are industrially important are the hydrolysis of benzal chloride and the air oxidation of toluene (7). Other methods which have also been studied include the oxidation of benzyl alcohol (8, 9) and the hydrogenation of benzoic acid (10, 11).

Today most of the world's synthetic benzaldehyde is produced from the air oxidation of toluene in both the liquid and gas phase (7). This process however requires high temperature and pressures and the yield produced from these reactions is low due to by-product formation. Several methods over the years have been studied for the production

of benzaldehyde from a toluene precursor. One of the most recent methods employed was the liquid phase air oxidation of toluene. Patent EP 1,088,810 (12) stated that the process involved providing a continuous flow of air in the presence of a catalyst (Fe, Co, Mn, Mo and Ni), a co-catalyst (manganese or copper salts), a promoter, a bromine source (cobalt bromide, zinc bromide or sodium bromide) and a carboxylic acid solvent. The carboxylic acid was selected from the group consisting of acetic acid, propionic acid, and benzoic acid ranging between 0.005 to 0.3 wt. times with respect to toluene. The reaction was carried out between 60-130°C using pressures in the range of 1-10 bar. However the reaction provided a fairly low conversion (< 25%) and selectivity to benzaldehyde (40-50%). The main by-products produced were benzyl alcohol and benzoic acid without any trace of benzyl bromide. One of the stated advantages for the process is that the air oxidation of toluene and its derivatives provide a green technology path for the production of benzaldehyde (12).

Toluene oxidation often has major drawbacks such as employing high temperatures and generating large quantities of carbon dioxide, which contribute to global warming. These drawbacks are primarily the reason as to why these processes do not appear attractive. Another problem is the low conversions and selectivity's that are often yielded. US patent 3,579,589 (13) describes the vapour phase oxidation of toluene at temperatures below 250°C in the presence of a catalyst composition containing phosphoric acid and palladium. The process however has two major drawbacks. Firstly to attain a high selectivity to benzaldehyde (>70%), conversion of toluene has to be kept very low (<4%), and secondly significant amounts of carbon dioxide are produced during the process. Similarly US Patent 4,137,259 (14) also describes a vapour phase oxidation process of toluene to benzaldehyde and benzoic acid. A silver-iron vanadate on silica catalyst was employed at temperatures ranging from 300-500°C. This process also reported fairly low conversions of toluene (21%) and selectivity to benzaldehyde (33%) (14).

An alternative method for the production of benzaldehyde is via the hydrolysis of benzal chloride. Patent 4,450,298 (15) describes a vapour phase process for the hydrolysis of benzal chloride using activated carbon, which has been treated with either an acid (e.g. sulphuric acid) or impregnated with a metal chloride such as ferric chloride and/or a metal sulphate such as cupric sulphate as a catalyst. Water and benzal chloride are continuously pumped into a vaporiser between 200 - 340°C and then passed over the

catalyst which is maintained at steady temperature (acid treated catalyst: 150 – 200°C, impregnated catalysts: 100 - 300°C). High yields of benzaldehyde (>96%) were reported when tested with both acid and impregnated catalysts.

Another process used in the production of benzaldehyde is the hydrogenation of benzoic acid. In 1988, Mitsubishi Chemical Corporation (MCC) established a commercial process by the direct hydrogenation of aromatic carboxylic acids to the corresponding aldehydes using a chromium-modified ZrO_2 (Cr/ZrO_2) (16). Patent US 4,613,700 (17) states that the process is carried out in the vapour phase using a flow system at temperatures around 350-400°C and at atmospheric pressure. The concentration of carboxylic acid in the reaction system is generally in the range of 0.1 to 10 vol% of hydrogen. The space velocity of hydrogen is generally in the range from 100 to 10,000 h^{-1} in terms of gas hourly space velocity (GHSV) and carboxylic acid fed is about 0.01 to 1 h^{-1} in terms of liquid hourly space velocity (LHSV) (17). Benzoic acid is fed into the vapouriser molten where it is quickly mixed with hydrogen and evaporated. The mixture is pre-heated before being introduced to the catalyst bed. The effluent is condensed to separate liquid products and excess hydrogen is recycled (18). The process is able to achieve a high benzaldehyde selectivity (95.6%) and conversion of benzoic acid (98.0%). When un-modified ZrO_2 was tested the conversion was significantly lower (51.2%) but selectivity was comparable (97.3%) (18).

2.1.3 Possible methods

There are various ways in which benzaldehyde can be prepared. There were three areas of interest that were studied in this thesis:

- toluene oxidation
- benzoic acid hydrogenation
- hydroformylation

2.1.4 Toluene

Toluene is the most important aromatic hydrocarbon (19) and is used as a starting material in the manufacture of a large number of industrial chemicals. The main chemical use is in the production of benzene and xylenes (20). It can be found naturally in crude oil or produced in the process of refining oil into petrol. In 2006 the world demand was approximately 23 million tonnes (20).

Toluene also contributes to the increasing amount of volatile organic compounds (VOCs) in the atmosphere. The presence of this material in civil and industrial emissions is why several strategies have been identified to reduce this (21). Benzyl alcohol, benzaldehyde, benzoic acid and chloro derivatives are all produced from toluene.

2.1.4.1 Toluene Oxidation

Several methods have been studied for the oxidation of toluene to benzaldehyde. The general equation is shown in figure 2-2. The oxidation of toluene to benzaldehyde shown in step 1 also produces water.

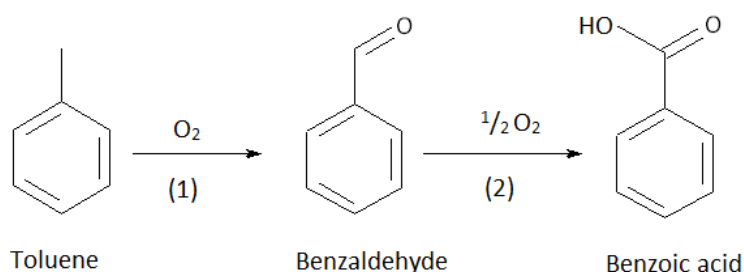


Figure 2-2 Oxidation of toluene

The oxidation of toluene can take place in both the gas and liquid phase. High yields are difficult to attain in the gas phase, hence why industry favours the liquid phase (22, 23). There are many drawbacks however in the liquid phase such as undesired product formation, corrosion problems, pollution and high cost on successive separation methods (24). Over oxidation to benzoic acid is also a major problem.

2.1.4.2 Toluene oxidation with molecular oxygen

Molecular oxygen is often used as a reactant in the gaseous phase toluene oxidation (24), however only few papers report using it in the liquid phase. J.Xu *et al* reported that using toluene, molecular oxygen and a copper based heterogeneous catalyst, benzaldehyde could be produced along with benzoic acid and benzyl alcohol in the liquid phase (25). They also studied using various metals supported on γ -alumina to see the difference in selectivity and conversion. Table 3 shows the results using the different metals.

Table 3 Catalytic oxidation of toluene with single components catalysts (25)

Entry	Catalyst	Conversion ^[b] (mol %)	Product selectivities (%)			
			CHO ^[c]	CH ₂ OH ^[c]	COOH ^[c]	Others
1	No catalyst	0	–	–	–	–
2	γ -Al ₂ O ₃	2.0	50.1	49.9	0	0
3	Fe/Al ₂ O ₃	1.1	95.7	4.3	0	0
4	Mn/Al ₂ O ₃	1.4	87.5	12.5	0	0
5	Zn/Al ₂ O ₃	1.8	88.5	11.5	0	0
6	Co/Al ₂ O ₃	2.0	77.8	20.6	0	1.6
7	Cu/Al ₂ O ₃	2.5	85.7	13.0	0	1.3

The major problem is getting the selectivity and conversion both high.

Metalloporphyrins have also been an area of interest due to their environmentally friendly conditions (19). Research has been carried out using these substances as catalysts in the presence of toluene and molecular oxygen.

2.1.4.3 Toluene oxidation using air

The oxidation of toluene can also take place using air as the oxidant. Cobalt bromide is a possible catalyst to oxidise toluene in air to benzaldehyde (19, 26). The drawback however is it has a low yield and poor selectivity to the desired product. The bromide also causes corrosion problems.

Metalloporphyrins are also of interest in this area due to having a conversion of 8.9% and selectivity of 60% to benzaldehyde (19).

2.1.4.4 Vanadium catalyst

Many oxidation reactions use a vanadium containing catalysts. Bulushev *et al* indicated that for the selective oxidation of hydrocarbons, vanadium oxides with a 2-D network were more active than bulk V_2O_5 crystallites which showed low activity (27). It was also found that the selectivity to benzaldehyde was higher when the strength of the $V=O$ was weaker (28). A Mars and VanKrevelen mechanism consisting of two steps is one of the proposed systems that may be occurring. Figure 2-3 Shows how this occurs. The hydrocarbon is adsorbed onto the catalyst surface and is converted into products using an oxygen atom from the lattice and at this point the catalyst is also reduced. The second stage involves the reduced catalyst reoxidising to its original form (29).

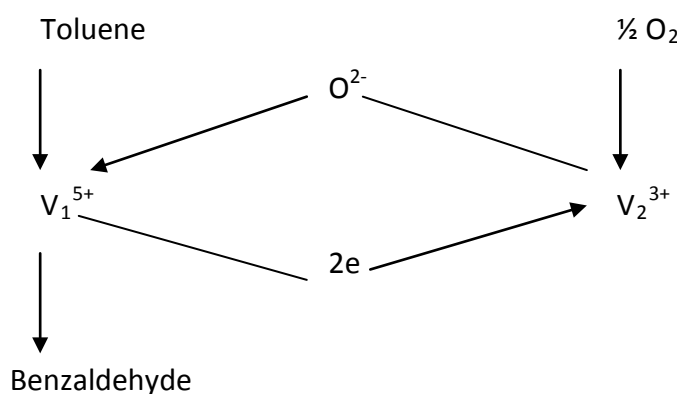


Figure 2-3 The model of Mars and VanKrevelen on catalytic oxidation (29)

The vanadium catalyst may show different catalytic activity and selectivity due to the nature of the support (eg SiO_2 , Al_2O_3 , TiO_2 , ZrO_2 , MgO) and the vanadium content (30-35). An efficient system in the partial oxidation of hydrocarbons is V_2O_5/TiO_2 .

Different promoters such as silver and nickel are often used to see the effect this has on the selectivity and conversion. More than often the conversion and selectivity is both enhanced. The greatest effect however is when they are in a V-Ag-Ni-O complex (36). The conversion and selectivity is increased significantly with V-Ag-Ni-O (conversion 8%, selectivity 95%) compared to V_2O_5 (conversion 2.5%, selectivity 60%). Ag and Ni were used as promoters as they were found to decrease the surface acidity and enhance the redox cycles of vanadium sites which help gain higher conversions and selectivity's.

2.1.5 Benzoic acid

Benzoic acid is a derivative of benzene and is the simplest aromatic acid. It is a white solid at room temperature with a strong characteristic odour and has a melting point of 122.4°C. Benzoic acid occurs naturally in gum benzoin which is found in the benzoin tree of Southeast Asia and also in many types of berries (37).

Industrially benzoic acid is produced by the liquid phase oxidation of toluene. The estimated global production capacity of benzoic acid is 638 000 tonnes per year, although over half of this is converted directly to phenol (38). Benzoic acid produced in Europe is further used to produce many other chemicals such as caprolactam and benzoyl chloride (38). One of the common uses for benzoic acid is as a food preservative. Both the acid and its sodium salt, sodium benzoate are used to preserve many different kinds of foods, including fruit juices, soft drinks, pickles, and salad dressings preferably in a pH range below 4.5. In some countries the limit amount allowed in food can often be as high as 1.25% (37).

2.1.5.1 Hydrogenation of benzoic acid

The catalytic hydrogenation of benzoic acid to benzaldehyde is a “green” technology (39). It is also an alternative to current selective oxygenation of benzene (40) or toluene (19) that are characterized by low yields or not being environmentally friendly (19, 40, 41). Over oxidation to benzoic acid is also a major problem in these reactions.

The hydrogenation of benzoic acid has been studied using various metal oxide catalysts such as ZrO₂ (18), ZnO (11, 16, 42, 43), CeO₂ (44, 45), and Mo Oxides (11, 16, 43-46). For these hydrogenation reactions a Mars and Van Krevelen mechanism has been proposed (47). Figure 2-4 demonstrates this mechanism

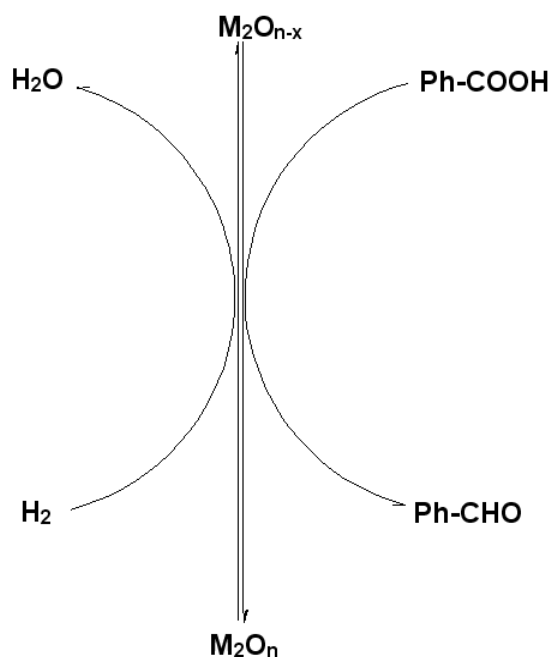


Figure 2-4 The catalytic mechanism of Ph-CHO production from Ph-COOH over metal oxide (47)

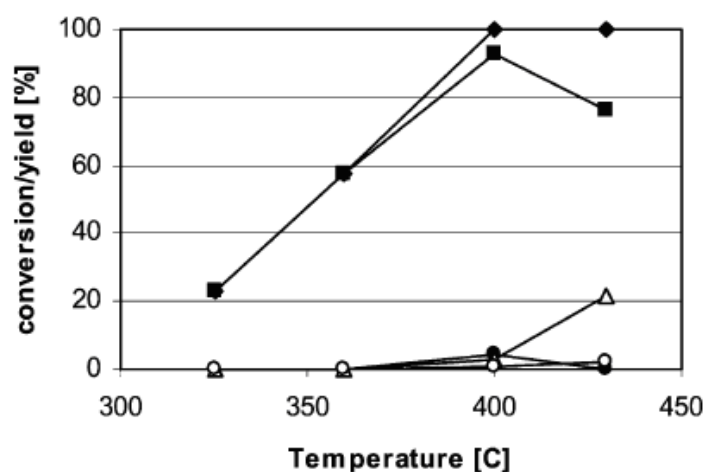
As shown in figure 2-4 the metal oxide is activated by reduction and oxygen vacancies are formed. The carboxyl oxygen atom of benzoic acid is then captured by the vacancies and this produces benzaldehyde. The catalytic behaviour is affected by the arrangement of these vacancies on the surface.

2.1.5.2 ZrO₂

ZrO₂ is found to be a good catalyst for the hydrogenation of carboxylic acids into the corresponding aldehydes due to its high selectivity to the aldehyde and its acid tolerant character (18). It has been shown that the activation of hydrogen on ZrO₂ is more difficult than for ZnO (11, 48) due to the energy barrier for the formation of oxygen vacancies being much higher for ZrO₂. This is due to difference in the oxygen-metal bond strength (11). Both of these catalysts are not easily reducible.

ZrO₂ is very selective to the formation of benzaldehyde. In the gaseous phase, by-product formation is only significant at elevated temperature when the conversion of benzoic acid to benzaldehyde is almost complete. Toluene is the main by-product produced (11).

Figure 2-5 shows the product distribution and conversion of benzoic acid in the gaseous phase.



Symbols: (◆) benzoic acid conversion; (■) benzaldehyde yield; (●) benzylalcohol yield; (Δ) toluene yield; (○) benzene yield.

H₂ flow rate 40 ml/min; benzoic acid partial pressure 13 mbar; benzoic acid $W/F = 0.39$ kg/mol h.

Figure 2-5 Product distribution in the deoxygenation of benzoic acid over ZrO₂ as a function of temperature (11).

Modification of ZrO₂ with additives (eg Pb²⁺, Ir³⁺, Cr³⁺ and Mn²⁺) were studied to see if the conversions could be enhanced (18). With all these types of modification the conversion was enhanced greatly while maintaining the high selectivity to benzaldehyde. Table 4 shows the results from this.

Table 4 Hydrogenation of benzoic acid with modification of the ZrO₂ catalyst (18)

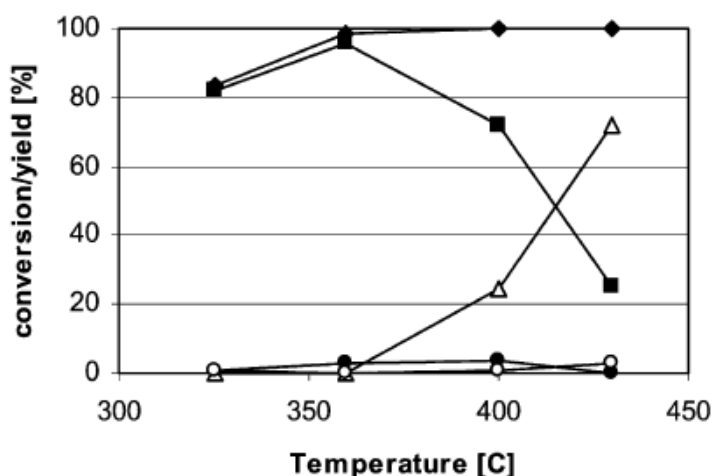
Reaction conditions: H₂ GHSV = 625 h⁻¹, benzoic acid/H₂ = 2/98 vol.-%, under atmospheric pressure

Additives	Temperature (°C)	Conversion of benzoic acid (%)	Selectivity to benzaldehyde (%)
None	350	51	97
Pb	310	89	96
In	330	100	91
Cr	350	98	96
Mn	350	70	97
Ca	350	50	98

Using the modified catalysts also resulted in less coke formation due to the coke formation site being poisoned by the metal ions (18).

2.1.5.3 ZnO

ZnO is also a catalyst used for the hydrogenation of benzoic acid to benzaldehyde as it shows high selectivity (>95%) to the aldehyde and high conversions. It is similar to ZrO_2 as it has strong metal-oxygen bonds and is not easily reducible. However reactions take place faster on ZnO due to hydrogen being more easily activated (11). Hölderich *et al* reported that ZnO had very weak acid sites and relatively strong basic sites. The formation of toluene as a by-product is enhanced by strong acidic sites (16, 42). Selectivity to toluene is higher with ZnO rather than ZrO_2 due to oxygen vacancies being more easily created. Due to basic nature of ZnO the carboxylic acid has a higher coverage on the catalyst as it favours more basic environments. Figure 2-6 shows the product distribution for ZnO.



Symbols: (◆) benzoic acid conversion; (■) benzaldehyde yield; (●) benzylalcohol yield; (Δ) toluene yield; (○) benzene yield.

H_2 flow rate 40 ml/min; benzoic acid partial pressure 13 mbar; benzoic acid $W/F = 0.39$ kg/molh.

Figure 2-6 Product distribution in the deoxygenation of benzoic acid over ZnO as a function of temperature (11)

2.1.5.4 CeO_2

CeO_2 is another suitable catalyst for the hydrogenation of benzoic acid as it displays high activity and selectivity towards the aldehyde. It is a good oxide to use because of its redox couple (Ce^{4+}/Ce^{3+}) which can transform easily. This means that oxygen vacancies can be formed and eliminated rapidly (39, 49). One of the main problems is coking of the catalyst

which leads to deactivation, however the catalyst can be regenerated by eliminating the coke and then exhibits almost the same reactivity (50).

2.1.6 Hydroformylation

Hydroformylation reactions, also known as “oxo synthesis,” were first discovered in 1938 by Otten Roelen (ref). The reaction involves adding one equivalent of both CO and H₂ (synthesis gas) to an alkene to produce linear and branched aldehydes (51).

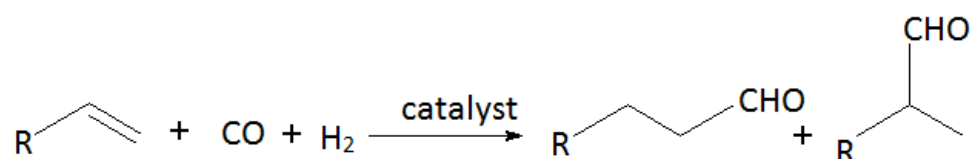


Figure 2-7 Stoichiometry of the hydroformylation reaction (51)

The synthesised aldehydes can subsequently be used to produce a variety of other species such as alcohols, carboxylic acids, diols, acetals, ethers and esters (52). More than 7 million tonnes, in particular *n*-aldehydes, are produced annually in the bulk and specialty chemicals industries (53). Typically cobalt and rhodium based catalysts are the two main types used to carry out these reactions. Mainly cobalt catalysts were originally employed in the production, however rhodium is currently used in many commercial processes in a homogenous phase (54). This is due to the milder conditions required and the higher straight: branched chain ratio produced, as straight chain is generally the desired product.

2.1.6.1 Carbonylation of benzene

Benzene is known to be one of the least reactive compounds and conversion to useful chemical products would be of great value. Benzaldehyde is one of those useful products that can be produced from the direct catalytic carbonylation of benzene (55).

The carbonylation of benzene with carbon monoxide is known to require Lewis and Brønsted acid sites (56). Zeolites are believed to have both types of acid sites present. Clingenpeel and Biaglow (56) carried out work on the carbonylation of benzene using a

zeolite catalyst. They found that benzoic acid could be produced using a zeolite H-Y catalyst and benzaldehyde from an AlCl_3 doped H-Y from the direct reaction between benzene and CO. It was found that the formation of benzoic acid was favourable while in the presence of AlCl_3 -free zeolite while the presence of AlCl_3 promoted the formation of benzaldehyde.

Benzaldehyde can also be produced from the carbonylation of benzene using oxygen as the oxidant. Yields of 37.3 % and selectivity of 80% towards the aldehyde can be achieved under mild conditions (130°C) using O_2 as the oxidant in the catalyst system of $\text{Co}(\text{OAc})_2/\text{CCl}_3\text{COOH}/\text{pyridine}$. Different additives were studied such as 2,2-bipyridine, iminazole, PPh_3 and $\text{P}(n\text{-Bu})_3$. When PPh_3 was used as an additive the selectivity of the reaction changed as benzoic acid was now the major product (55).

2.1.6.2 Benzene and formaldehyde

The alkylation reaction between benzene and formaldehyde using a standard Friedel-Crafts' catalyst has been performed for many years. The main product produced is diphenylmethane with benzyl alcohol as an intermediate. The reaction between benzene and formaldehyde may be able to provide a 'green route' to the production of benzyl alcohol as currently this occurs by the hydrolysis of benzyl chloride. Work has been carried out on this alternative route using ZSM-5 as a catalyst (57).

2.1.6.3 Sulphated zirconium

Solid acid catalysts are an important class of materials used in industry today. They have many applications, for example in the petroleum industry they are used for alkylation, isomerisation and cracking reactions (58-62). Over the years they have attracted a lot of attention due to their strong acidity and high activity in light alkane conversions at low temperatures (63). They often catalyse reactions which are not catalysed by conventional solid acids (64) such as the alkylation of alkanes by alkenes (65), the activation of ethane (66) and the Friedel-Crafts type alkylation (67) and acylation (68) of hydrocarbons with an inert molecule such as carbon monoxide (69). Sulphated zirconia is often classed as a superacid which is defined as an acid stronger than 100% sulphuric and perchloric acid (64).

Sulfation affects the physical properties of the catalyst, such as increasing the surface area and lowering the crystallinity (70). When polymorphism occurs in oxides, sulfation often stabilises one favoured form. In the case of zirconia it can exist in monoclinic, tetragonal, cubic and orthorhombic crystal phases. However when the catalyst is doped with sulphate, the tetragonal form is favoured over the commonly encountered monoclinic phase (70, 71).

2.1.6.4 Possible route

It was decided to study the reaction between isopropyl benzene and 1, 3, 5 trioxane over a solid acid catalyst. Figure 2-8 shows the possible products. The aim was to produce p-methyl benzaldehyde.

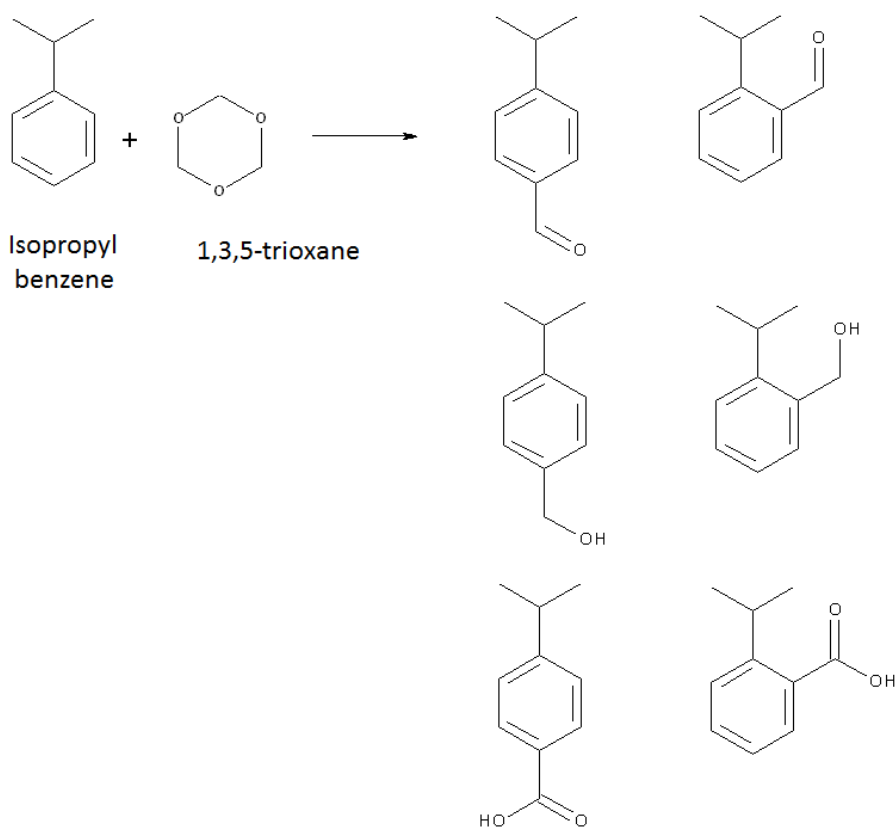


Figure 2-8 Schematic diagram of hydroformylation reaction

2.1.7 Project aim

The aim for this section of the project was to:

1. Investigate alternative routes for the production of benzaldehyde and minimise side products
2. To obtain good selectivity and conversion
3. For the process to be greener than current route

2.2 Experimental

2.2.1 Catalyst characterisation

2.2.1.1 Thermo-gravimetric analysis (TGA)

Thermo-gravimetric analysis was performed on post reaction catalysts using a combined TGA/DSC SDT Q600 thermal analyser coupled to an ESS mass spectrometer for evolved gas analysis. A ramp rate of 10 degC.min⁻¹ was used. TGA was carried out using Argon. Temperature programmed oxidations (TPO) were carried out using 100 ml.min⁻¹ 5% O₂/Ar. Temperature programmed reductions (TPR) were carried out using 100 ml.min⁻¹ 5% H₂/N₂. For mass spectrometry analysis, various relevant masses were followed depending on the sample being studied but typically 2, 14, 15, 16, 28, 29, 30, 32, 40, 44, 46 were followed.

2.2.1.2 X-Ray Diffraction (XRD)

2.2.1.3 Siemens D5000

Flat plate X-ray diffraction patterns were obtained using a Siemens D5000 x-ray diffractometer (40 kV, 40 mA, monochromatised) using a CuK alpha source (1.5418 Å). The scanning rate was 5-85° 2θ with a scanning rate of 1 second / step and a step size of 0.02°. Analysis was carried out at room temperature and pressure.

Hot stage XRD was also carried out on the D5000. Identical process conditions were used as that for the flat plate however the sample was heated in either N₂ or 5% H₂/N₂ depending on the sample and scans were taken at room temperature and then 100°C increments afterwards.

2.2.1.4 Siemens D8000

Air sensitive XRD was carried out on a Siemens D8000 x-ray diffractometer (40 kV, 40 mA, monochromatised) using a CuK alpha source (1.5418 Å). The scanning rate was 5-85° 2θ with a scanning rate of 1 second / step and a step size of 0.02°.

2.2.1.5 Scherrer equation

The Scherrer equation was used to calculate the crystallite size from XRD data. The following equation was used to:

Scherrer equation: $d = K\lambda / \beta \cos\theta$

d = diffracting domain size

$K = 0.9$

λ = wavelength of x-rays: 1.5406

θ = 2 theta angle of peak

β = full peak width at half maximum (FWHM)

2.2.1.6 Surface Area Analysis

Brunauer, Emmett, Teller (BET) analysis was used to determine the total surface area of the catalyst. This was carried out using a Micromeritics Gemini III 2375 surface area analyser. Before analysis was carried out approximately 0.04 g of catalyst was placed in a glass tube and purged with nitrogen overnight at 110°C.

$$\frac{P}{V(P_0 - P)} = \frac{1}{V_m C} + \frac{(C - 1)P}{V_m C P_0}$$

Where V = volume of gas adsorbed at pressure P

V_m = volume of gas adsorbed in monolayer, same units as V

P_0 = saturation pressure of adsorbate gas at the experimental temperature

C = a constant related exponentially to the heats of adsorption and liquefaction of the gas

$$C = e^{(q_1 - q_L)/RT}$$

Where q_1 = heat of adsorption on the first layer

q_L = heat of liquefaction of adsorbed gas on all other layers

R = gas constant

A graph of $P/V(P_0 - P)$ versus P/P_0 should produce a straight line, the slope and intercept of which can be used to evaluate V_m and C . From this $V_m = 1/(S + I)$ Where S is the slope, equal to $(C - 1)/V_m C$ and I is the intercept, equal to $1/V_m C$. The surface area of the catalyst can then be calculated from V_m if average are occupied by an adsorbate molecule is known (72). Nitrogen was used as the adsorbate.

2.2.1.7 Scanning Electron Microscopy (SEM)

SEM analysis was carried out on a Philips XL30 SEM-FEG operating at 20 KV in high vacuum mode with a working distance of 10 mm. Different levels of magnification were used to enhance images. An electrically conductive double sided adhesive carbon disc was pressed onto a 12.5 mm diameter aluminium pin stab. The catalyst was then loaded onto the exposed conductive carbon adhesive. The sample was loaded in to the equipment for analysis.

2.2.1.8 UV-Vis spectroscopy

UV-Vis analysis was carried out on a Varian Cary 500 scan UV-Vis NIR spectrophotometer. Scans were run from 200-800 nm. Samples were diluted using either acetone or water depending on the material.

2.2.2 Toluene Oxidation

2.2.2.1 Reactor

The oxidation of toluene was carried out using a trickle bed reactor. Liquid and gas entered at the top of the reactor, passed through the catalyst and exited via the bottom. The flow of the liquid was such that it kept the catalyst wet but the bed was never saturated.

2.2.2.2 Reaction Procedure

The trickle bed reactor was glass vessel, length 35 cm with an internal diameter of 2.5 cm. The catalyst once charged into the reactor, was held in place by a sinter 5 cm from the

bottom of the reactor vessel. The liquid flow rate was controlled using an HPLC pump (Gilson model 302) and the gas flow was controlled using mass flow controllers (Brooks, maximum pressure 100 bar, flow range 0-100 ml min⁻¹). Air and nitrogen were available as gas feeds when required. The liquid was pumped into the reactor where a 'shower head' distributor was employed at the exit of the fluid stream. This allowed a more dispersed fluid distribution over the catalyst. The reaction temperature was varied using a furnace with a temperature controller (Eurotherm 818P), accuracy $\pm 1\text{K}$. The temperature was measured outside of the reactor wall at half the catalyst bed height by a thermocouple. A needle valve at the exit stream was used to control the reactor pressure. Typically 3 g of catalyst was split into three equal portions. This first portion was loaded into the reactor, which was then gently tapped until the catalyst had settled. SiC (180 μm < 355) fines were then added until the majority of the catalyst was covered. The reactor was tapped again until the SiC filled the void space. This procedure was repeated three times (variation of Al-Dahhan and Duduković packing method (73)). The catalyst was then heated to reaction temperature in air at a flow rate of 421 ml.min⁻¹. A high flow rate was required to obtain a 1:1 ratio of oxygen to toluene. Once at temperature toluene (1.5 ml.min⁻¹) was introduced into the system. Samples were taken at intervals from the outlet stream and analysed using GC (74).

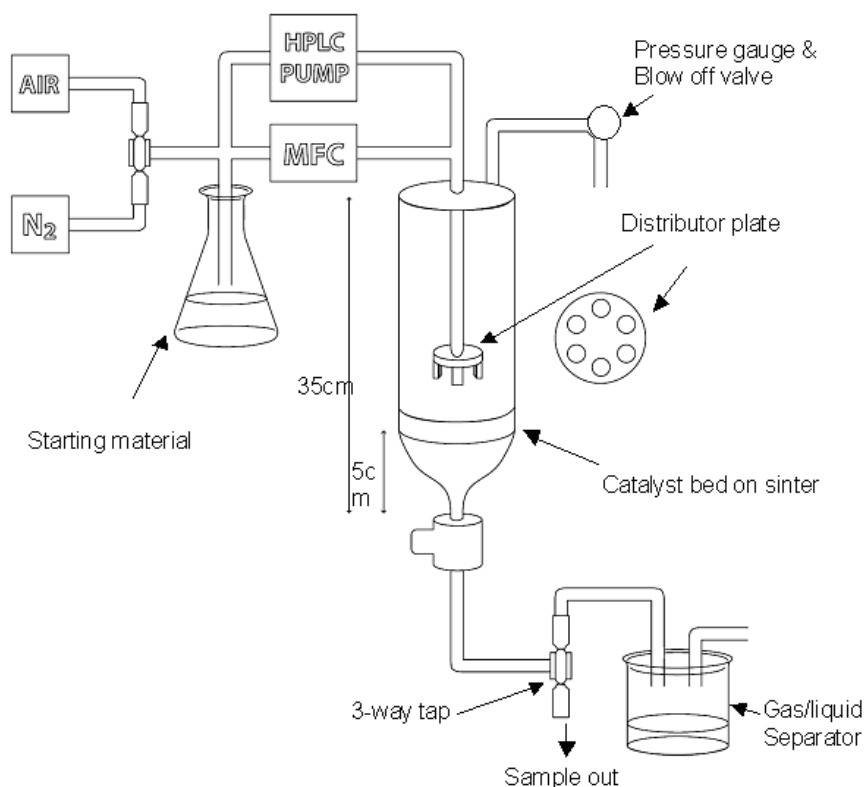


Figure 2-9 Schematic diagram of trickle bed reactor

2.2.2.3 Gas chromatography- Mass spectrometry method (GC-MS)

Liquid analysis was carried out on a Trace GC 2000 Series with an AS 3000 auto sampler. This is coupled to a Voyager MD800 mass spectrometer.

2.2.2.4 Column conditions

Column- Chrompack DB-5 25m

Sample Volume 1 μ L

Inlet temperature - 240°C

Carrier gas – helium at constant flow 1.5 ml.min⁻¹

Ramp Rate –hold at 60°C for 6 minutes then ramp at 20 degC.min⁻¹ to 180°C and hold for 1 min

2.2.2.5 Calibrations

Calibrations were not carried for the oxidation of toluene as the reaction proved unsuccessful. It was decided to carry out several reactions to see if products were produced and then only if successful would calibrations be carried out.

2.2.2.6 Catalyst Preparation

Catalysts used in these studies had been made by Dr S. Rugmini. Both 3.5% and 8% $\text{VO}_x/\text{Al}_2\text{O}_3$ were used. These had been made using an incipient wetness technique before being dried.

2.2.2.7 Support Properties

The support used for these catalysts was a ϑ - alumina supplied by Johnson Matthey, UK. The support properties are shown in table 5

Table 5 Support properties of ϑ - alumina

Surface Area (m^2g^{-1})	101
Pore Volume (ml g^{-1})	0.60

2.2.2.8 Preparation Procedure

The catalysts were prepared by incipient wetness impregnation using ϑ - alumina as the support. The alumina was predried at 80°C overnight before impregnation. To prepare the catalyst an aqueous NH_4VO_3 (>99%, Aldrich) solution was used. To this oxalic acid (99%, Aldrich) was added to achieve high VO_x loadings. After impregnation the samples were then mixed at 77°C for 2 hours using a rotavap. They were dried by purging with air at 120°C overnight and then calcined for 6 hours at 550°C (75)

2.2.2.9 Toluene reactions

The experiments were carried out using both vanadium supported on alumina catalysts. The catalysts were ground using a mortar and pestle before being sieved to between 250 and 450 microns which was used during the catalytic tests. Listed below in table 6 are the catalysts and the conditions:

Table 6 Catalytic reactions

Metal	Support	Reaction Temperature
3.5% Vanadium	Alumina	100°C
3.5% Vanadium	Alumina	150°C
8% Vanadium	Alumina	70°C
8% Vanadium	Alumina	100°C

2.2.2.10 Soxhlet extraction

Soxhlet extractions were carried out to remove any soluble species from post-reaction catalysts. Typically 0.3 g of catalyst was placed into the thimble and then placed into the soxhlet chamber (figure 2-10). Ethanol was the solvent used to carry out this extraction. Ethanol was placed in the boiling flask and heated to reflux in an oil bath. The system operates by vapour from the solvent rising up until it reaches the condenser where it turns into liquid and drips back down into the thimble. This process continues until the extraction chamber is full of solvent. When this occurs the chamber empties into the flask via the siphon arm. The process was left to repeat itself overnight to ensure all soluble material is extracted from the catalyst sample. Post extraction sample was analysed on the GC.

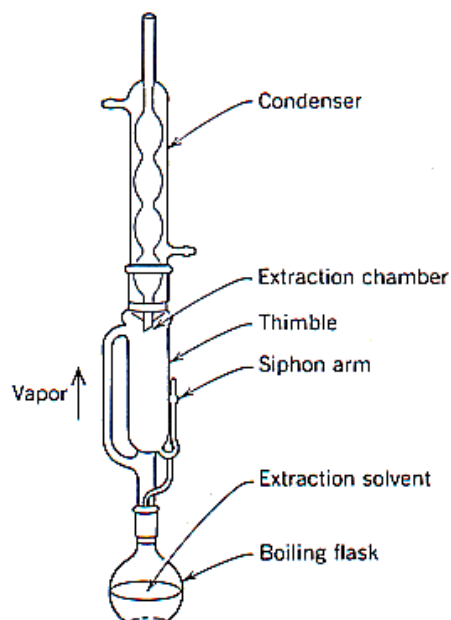


Figure 2-10 Soxhlet extraction apparatus

2.2.3 Benzoic acid hydrogenation

2.2.3.1 Reactor Design

For the hydrogenation of benzoic acid a reactor had to be designed and built. Benzoic acid is solid at room temperature and the unit had to be constructed to introduce it into the system in the gas phase.

Specifications of the reactor:

- Be able to introduce benzoic acid in the gas phase
- Reactor to be kept at sufficient temperature to avoid solid acid forming in system (200-250°C)
- Ethanol was to be pumped into system after reactor tube to dissolve starting material and products

To allow the introduction of benzoic acid into system in the vapour phase a stainless steel saturator was used. The solid benzoic acid was placed into the saturator and then connected to the unit. The top of the saturator was connected to a thin pipe through which carrier gas ($40 \text{ ml} \cdot \text{min}^{-1} \text{ H}_2$) was bubbled through the molten solid. Thermocouples

were used to maintain the temperature (220°C) of the trace heating. Figure 2-11 shows a diagram of this.

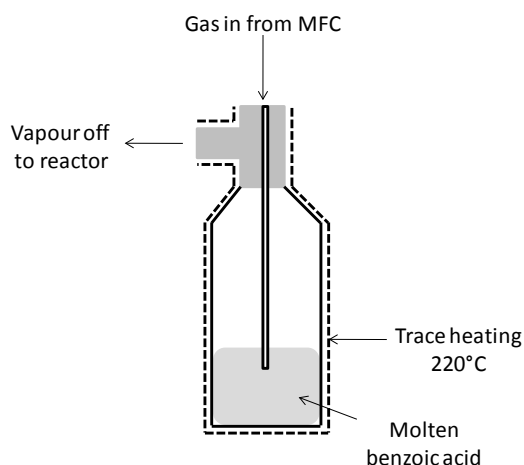


Figure 2-11 Benzoic acid saturator design

A major issue was benzoic acid plating out inside the reactor. To avoid this issue all connections between the saturator and reactor were trace heated and maintained a temperature of 220°C.

After the reactor an ethanol feed was pumped into the system to dissolve any starting material and products that were then collected as liquid samples. To ensure that the ethanol trickled down the whole circumference of the pipe the ethanol was pumped in through a capillary to increase the pressure and simulate a spray effect (figure 2-12).

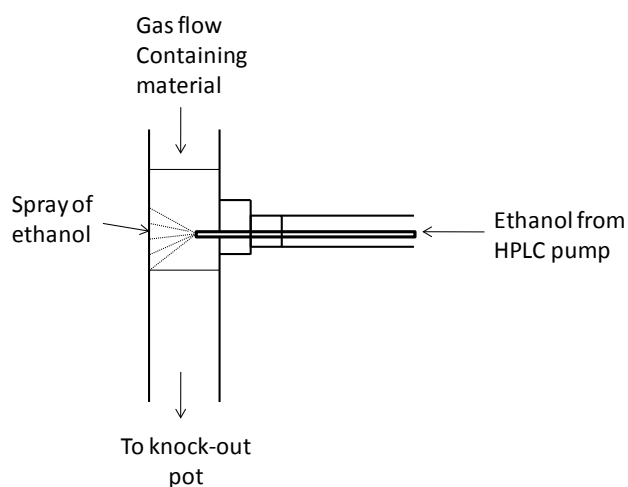


Figure 2-12 Benzoic acid ethanol feed set-up

Liquid samples could then be collected out of the knock out pot and analysed using HPLC.

2.2.3.2 Gas phase reactor

A glass-lined tube (60 cm, 0.5 inch diameter) containing a 30 cm thermocouple at the top. Boiling stones were used to pack the reactor, the catalyst was situated touching the tip of the thermocouple. Once loaded a metal sinter was then placed at the bottom of the reactor to hold everything in place.

The catalyst (0.5 g) was loaded into a reactor vessel and then placed in a furnace (LPC elements, 240 V, 1500 W), Figure 2-13. Gas flow rates were controlled using mass flow controllers (Brooks, maximum pressure 100bar, flow range 0-700 ml.min⁻¹) and a flow controller (West controller Ltd). 40ml.min⁻¹ hydrogen gas was passed through the molten benzoic acid in the saturator (220°C) producing a vapour pressure (0.0228 moles.day⁻¹), which is continually passed over the reactor at 400°C. All connections and pipe work from the saturator to reactor were kept above 220°C to avoid condensation of reactants. The system was run at 10 barg pressure maintained using a back pressure regulator (Swagelock). Ethanol (100 ml.day⁻¹) was pumped into the system after the reactor tube to dissolve any products and unreacted starting material. Liquid samples are collected in the chilled knock out pot (approx 5°C) and analysed using HPLC.

2.2.3.3 Catalyst preparation

Zirconium oxide was prepared from zirconium hydroxide powder (MEL Chemicals, 99% purity), however the powder was too fine and had to be pressed using stainless steel dies. The pellet produced was ground using a mortar and pestle before being sieved between 250 and 450 microns which was used during the catalytic tests.

2.2.3.4 Catalyst Calcination

The Zr(OH)₄ was calcined in the reactor before the reaction took place. A TGA mimicking the activation conditions showed that 0.691 g of Zr(OH)₄ was required to produce 0.5 g ZrO₂. The active phase of the catalyst was produced by flowing 40ml.min⁻¹ N₂ over the catalyst at 600°C. A ramp rate of 10 degC.min⁻¹ was used.

2.2.3.5 Reactor procedure

Figure 2-13 shows a schematic diagram of the layout of the apparatus. Before the reaction was started, *in-situ* catalyst activation was carried out. This was achieved by heating the catalyst to 600°C at a ramp of 10 degC.min⁻¹ in flowing N₂ (40 ml.min⁻¹).

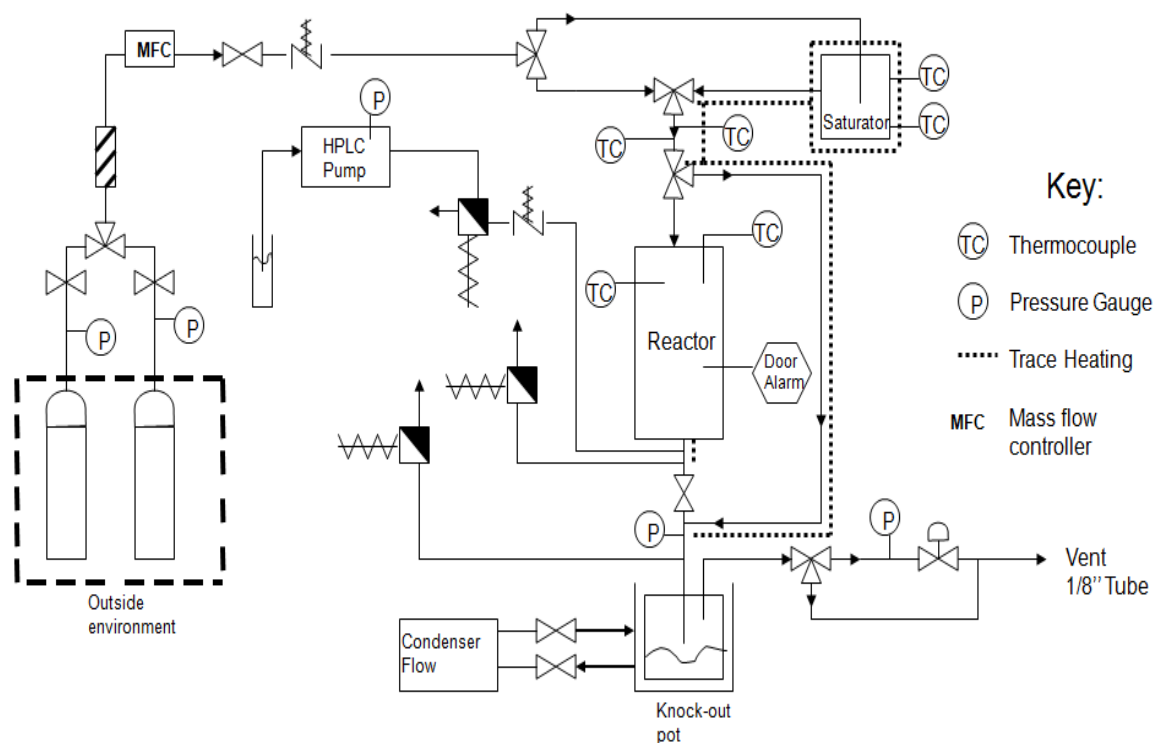


Figure 2-13 Schematic diagram of gas phase reactor for benzoic acid hydrogenation

The reactor was cooled to reaction temperature and flushed in 40 ml.min⁻¹ H₂. The system was then pressurised to 2 barg pressure with hydrogen, bypassing the saturator. The trace heating and saturator were then brought to temperature. Ethanol was pumped into the system. Valves are then opened to allow gas to flow through saturator and over reactor. The reaction started at this point. System was then pressurised up to 10 barg. First sample was taken approximately 24 hours into reaction and then every 24 hours afterwards. Samples were analysed using HPLC.

2.2.3.6 High Performance Liquid Chromatography (HPLC)

HPLC is an analytical technique used to identify compounds in a solution. It is not limited by the volatility or stability of the sample. It can be used to separate, identify, purify and quantify various compounds in a solution. Chromatographic separation in HPLC relies upon both the interactions between sample molecules and both the mobile and the stationary phases.

2.2.3.7 HPLC method

Analysis was carried out on a Hewlett Packard (HP) 1050 series HPLC with a HP 3396 series III integrator. A thermo Scientific BDS Hypersil C18 column was used (dimension: 250 x 4.6 mm, particle size: 5 micrometres). The mobile phase consisted of a 2 solvents- solvent A: Water with 5% phosphoric acid, solvent B: Acetonitrile. Figure 2-14 shows the solvent profile.

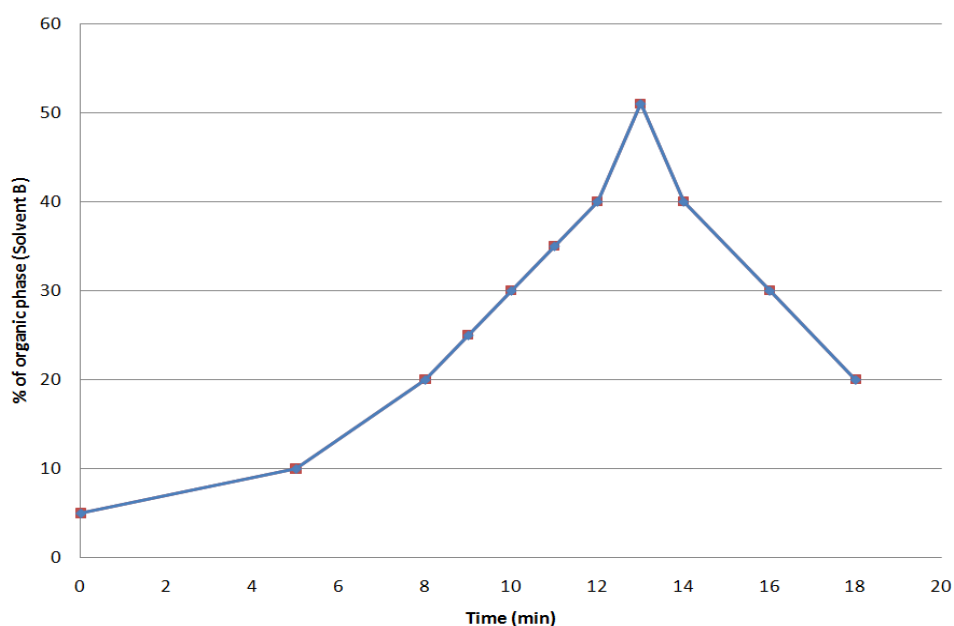


Figure 2-14 HPLC solvent profile

Solvent was passed over the column at 30°C with a flow rate of 1 ml.min⁻¹. 1 microlitre injections were taken from the sample. Compounds were analysed using a diode array detector at a UV wavelength of 254 nm. Chromatograms were produced containing peak areas and percentage compositions.

2.2.3.8 Calibrations

Calibrations were to be carried out after a successful reaction was completed. However after the first few reactions were carried out it was decided not to continue this work further, so no calibrations were completed.

2.2.4 Hydroformylation reactions

These reactions were carried out in the both the gas and liquid phase using a zirconium based catalyst.

2.2.4.1 Gas phase reactions

The gas phase hydroformylation reactions were carried out in a continuous flow system. Vaporised liquid consisting of 1,3,5-trioxane dissolved in isopropyl benzene was passed over the solid acid catalyst using a N₂ carrier gas.

2.2.4.1.1 Catalyst

A sulphated zirconia catalyst was required for these studies. The catalyst was prepared in the laboratory.

2.2.4.1.2 Preparation procedure

To prepare the catalyst, 2 g of zirconium hydroxide (MEL Chemicals, 99% purity) was placed in 30 ml, 0.5 mol L⁻¹ sulphuric acid. This solution was then left for 1 hour. This was filtered and dried in an oven at approximately 100°C.

2.2.4.1.3 Calcination

After drying, the catalyst was transferred to a glass calcination tube and inserted into a furnace. Calcination was carried out at 550°C, ramp rate of 10 degC.min⁻¹ for 8 hours in static air. Catalyst was allowed to cool to room temperature.

In the reactor the catalyst was dried at 300°C at a rate of 10 degC.min⁻¹ for 15 min with 50 ml.min⁻¹ of flowing N₂.

2.2.4.1.4 Reactor

The catalyst (0.5 g) was loaded into a reactor vessel and then placed in a furnace (LPC elements, 240 V, 1500 W), Figure 2-15. Gas flow rates were controlled using mass flow controllers (Brooks, maximum pressure 100 bar, flow range 0-700 ml.min⁻¹) and a flow controller (West controller Ltd). Prior to reaction, the catalyst was treated with nitrogen (300 ml.ml⁻¹) for 15 min at 300°C. After this the catalyst was cooled to reaction temperature. A pre-made solution of isopropyl benzene and 1,3,5-trioxane was pumped over the catalyst using HPLC pump (Gilson 307) at 2.2 ml.h⁻¹. The liquid was then converted into gas in a vaporiser and was then flown over the catalyst with N₂ gas at a rate of 50 ml.min⁻¹. Samples were collected from the knock out pot, which was kept cool by a chiller (thermo scientific chiller, approx 5°C). These samples were then analysed using GC-MS.

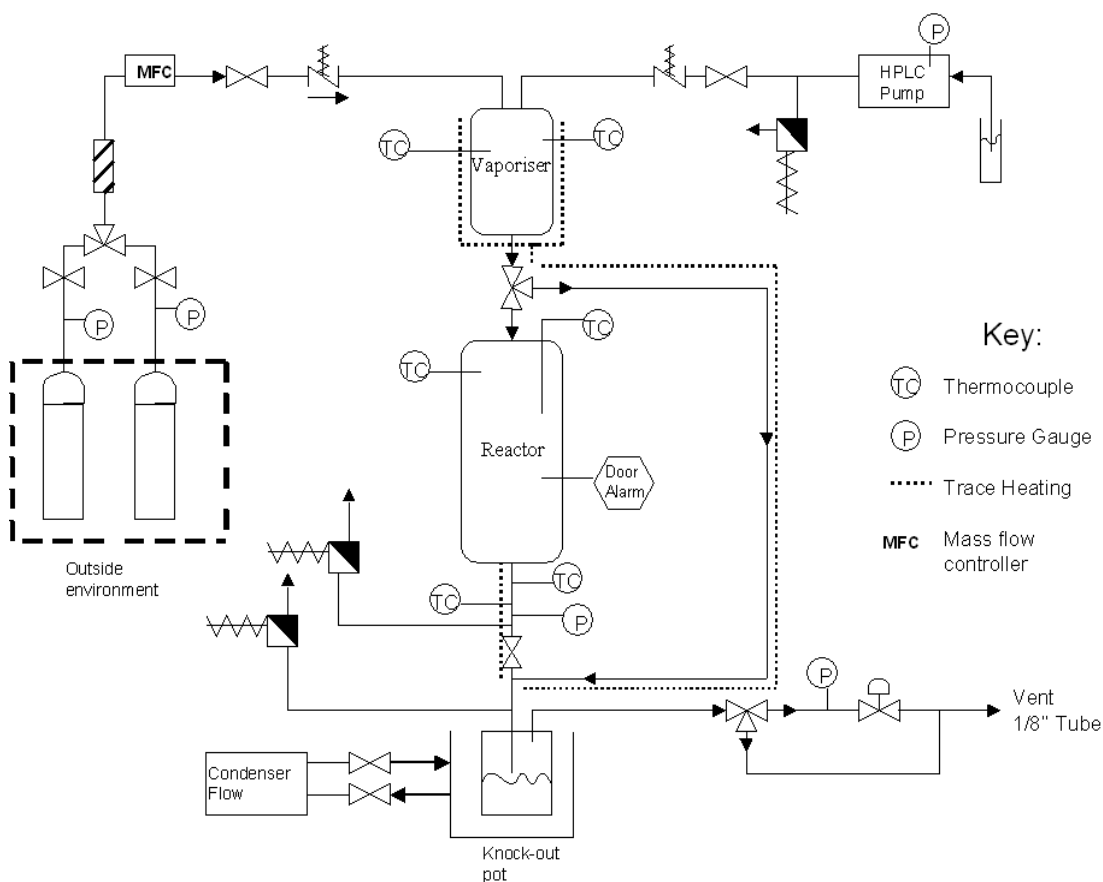


Figure 2-15 Gas phase reactor set-up for hydroformylation reaction

2.2.4.2 Reactions

Table 7 Hydroformylation vapour phase reactions

Isopropyl Benzene (IPB): trioxane ratio	Temperature
3.5: 1	300°C
10:1	300°C

2.2.4.3 Liquid phase

The hydroformylation reactions between 1,3,5-trioxane and Isopropyl benzene (Aldrich 98%) were carried out in a trickle bed reactor. This was a similar set up to the toluene oxidation (section 2.2.2.2). Figure 2-9 shows the reactor set up diagram

2.2.4.3.1 Catalyst

Commercial 7% sulphated zirconium hydroxide supplied from MEL chemicals was used for these studies.

2.2.4.3.2 Catalyst properties

Below are the properties of the catalyst as reported by MEL chemicals.

Table 8 7% Sulphated zirconia properties

Average Particle size (μm)	Surface area (m^2g^{-1})	Total pore volume (ml/g)
5	>300	>0.3

2.2.4.3.3 Catalyst activation

To achieve the active phase the catalyst was calcined in a furnace at 600°C at a ramp of 10 degC.min⁻¹ and held for 3 hours in static air. After this the catalyst was placed in the trickle bed reactor and re-calcined at 300°C for 1.5 hours with 10 ml.min⁻¹ of flowing N₂.

2.2.4.3.4 Reaction procedure

The trickle bed reactor was glass vessel, length 35 cm with an internal diameter of 2.5 cm. The catalyst once charged into the reactor, was held in place by a sinter 5 cm from the bottom of the reactor vessel. The liquid flow rate was controlled using an HPLC pump (Gilson model 302) and the gas flow was controlled using mass flow controllers (Brooks, maximum pressure 100 bar, flow range 0-100 ml.min⁻¹). Air and nitrogen were available as gas feeds when required. The liquid was pumped into the reactor where a 'shower head' distributor was employed at the exit of the fluid stream. This allowed a more dispersed fluid distribution over the catalyst. The reaction temperature was varied using a furnace with a temperature controller (Eurotherm 818P), accuracy ±1K. The temperature was measured outside of the reactor wall at half the catalyst bed height by a thermocouple. A needle valve at the exit stream was used to control the reactor pressure. Typically 3 g of catalyst was split into three equal portions. This first portion was loaded into the reactor, which was then gently tapped until the catalyst had settled. SiC (180<μm< 355) fines were then added until the majority of the catalyst was covered. The reactor was tapped again until the SiC filled the void space. This procedure was repeated three times (variation of Al-Dahhan and Duduković packing method (73)). The catalyst was then treated in flowing nitrogen (10 ml.min⁻¹) for 1.5 hours. A flow of material (1,3,5 trioxane and isopropyl benzene) was then passed over the catalyst at a rate of 1.5 ml.min⁻¹. Samples were taken at intervals from the outlet stream and analysed using GC (74).

2.2.4.3.5 Reactions

Table 9 Hydroformylation liquid reactions

IPB: Trioxane	Reaction Temperature
10:1	90°C
10:1	120°C

2.2.4.4 GC-MS

Liquid analysis was carried out on a Trace GC 2000 Series with an AS 3000 auto sampler. This is coupled to a Voyager MD800 mass spectrometer.

2.2.4.4.1 GC-MS conditions

Column- Chrompack DB-5 25m

Sample Volume 0.5 μL

Inlet temperature - 250°C

Carrier gas – helium at constant flow 2 $\text{ml}\cdot\text{min}^{-1}$

Ramp Rate –hold at 80°C for 5 minutes then ramp at 30°C /min to 240°C and hold for 177 minutes

2.2.4.4.2 Calibrations

Calibrations for the hydroformylation reactions were not carried out as the both liquid and gas phase reactions proved unsuccessful.

2.3 Results & Discussion

2.3.1 Toluene Oxidation

2.3.1.1 Catalyst Characterization

During catalytic testing, vanadium oxide supported on alumina was the chosen catalyst used. In this instance γ -alumina was the chosen support. γ -alumina is the most thermally stable transition alumina and hence used in high temperature applications (76). Supports are used instead of bulk V_2O_5 as they provide a higher catalytic activity and provide mechanical strength, increased surface area and thermal stability (77). It has also been found that bulk V_2O_5 can lead to the complete combustion of organic materials to CO_2 (78). Vanadium oxide can exist as isolated monomeric vanadium species, a one- or two-dimensional polyvanadate or as bulk V_2O_5 crystallites. Isolated monovanadates are the main surface species in low vanadium loading supported catalysts. As the vanadium oxide loadings increase, these monovanadate species condense into polyvanadates and finally into bulk V_2O_5 (75).

These catalysts have been the subject of extensive characterization by Jackson *et al* (75, 79-81). Three different loading weights of vanadium oxide support on alumina were studied, 1%, 3.5% and 8%. It was found that increasing the vanadium content caused a reduction in the surface area as shown in table 10. This is thought to be caused by a blockage of the pores by the VO_x species. Other studies have found that isolated VO_x species dominated at surface densities below $1 V/nm^2$, polyvanadates coexisted with monovanadates at surface densities of $1.24-4.4 V/nm^2$ and V_2O_5 formed at surface densities $>4.4 V/nm^2$ (75, 79, 81). Table 10 also shows the vanadia densities for the studied catalysts.

Table 10 Physiochemical characterisation of vanadium catalysts (75)

Catalyst	Surface area (m²/g⁻¹)	Vanadium Density (V/nm²)
Alumina support	105	n/a
1% VO _x /Al ₂ O ₃	103.5	1.1
3.5% VO _x /Al ₂ O ₃	93.6	3.7
8% VO _x /Al ₂ O ₃	76.6	10.4

XRD data analysis carried out on the catalysts suggested that at the lower vanadium loadings (1% and 3.5%), XRD peak positions and intensities were identical for that of the alumina support. This suggested that the vanadium oxide was well dispersed on the support. However a difference in the XRD pattern was visible for the 8% VO_x/Al₂O₃ and these peaks were characteristic of crystalline V₂O₅ (75). A simple XRD was measured to confirm reproducibility.

XRD patterns were obtained on fresh catalyst samples of 3.5% (figure 2-16) and 8% (figure 2-17) vanadium oxide supported on alumina. The pattern for 3.5% VO_x/Al₂O₃ showed only alumina. This suggested that the vanadium oxide was in an amorphous phase, and well dispersed on the support surface (75).

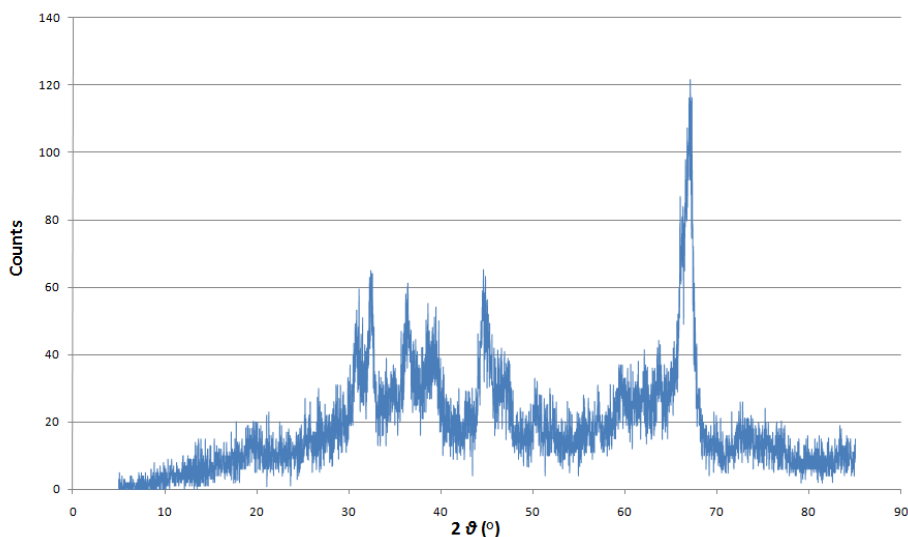


Figure 2-16 XRD 3.5% vanadium supported on alumina

It can be observed in figure 2-17 that there are two small additional peaks in the 8% $\text{VO}_x/\text{Al}_2\text{O}_3$ sample that are not in the 3.5%. These peaks (23.6°C and 34.6°C) correspond to crystalline V_2O_5 (75, 82, 83), in agreement with the literature findings.

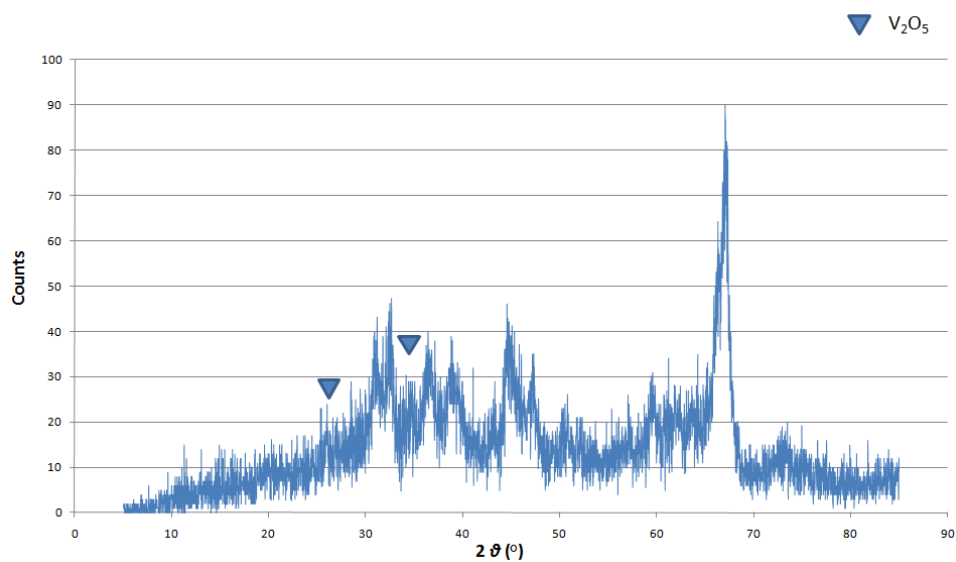


Figure 2-17 XRD 8% vanadium supported on alumina

2.3.1.2 Thermodynamics

The Gibbs free energy (ΔG°) for oxidation of toluene was calculated using reported enthalpy (ΔH°) and entropy values (S°) (84, 85). The calculations were calculated at room temperature (298 K).

The complete combustion of toluene involves the production of carbon dioxide and water. Figure 2-18 shows the general equation

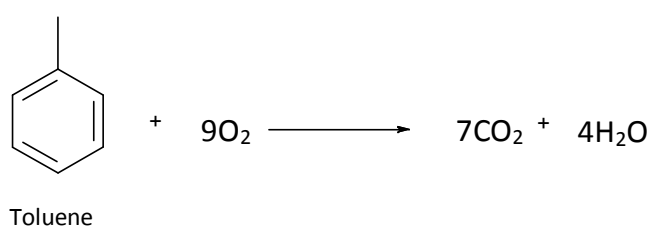
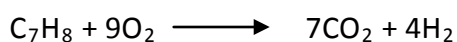


Figure 2-18 Complete combustion of toluene

Combustion reaction of toluene:



The combustion reaction is very heavily exothermic even at 298 K and hence the reaction had to be controlled by limiting the oxygen to prevent the potential for thermal runaway.

$$\Delta H^\circ_{\text{total}} = -3774.02 \text{ kJmol}^{-1} \quad \Delta S^\circ_{\text{total}} = 84.89 \text{ Jmol}^{-1}$$

$$\Delta G^\circ = -3799.3 \text{ kJmol}^{-1}$$

The thermodynamics were also calculated for the partial oxidation of toluene to benzaldehyde at 298 K.

Benzaldehyde production:



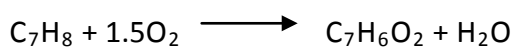
$$\Delta H^{\circ}_{\text{total}} = -328.73 \text{ kJmol}^{-1} \quad \Delta S^{\circ}_{\text{total}} = -1.23 \text{ Jmol}^{-1}$$

$$\Delta G^{\circ} = -328.363 \text{ kJmol}^{-1}$$

The thermodynamics indicate that at room temperature the partial oxidation of toluene will proceed as the value for the Gibbs free energy is negative. The effect of raising the temperature to 400 K on the value of the Gibbs free energy was also examined, and a similar value to the one calculated for room temperature was recorded ($\Delta G^{\circ} = -328.786 \text{ kJmol}^{-1}$). This suggested that increasing the temperature to 400 K would not have an effect on the equilibrium conversion, but it would enhance the speed of reaction (kinetics).

One of the main issues with the partial oxidation of toluene is the over oxidation to benzoic acid. Thermodynamics show that there is a significant difference in the Gibbs free energy between the two.

Benzoic acid production:



At 298 K

$$\Delta H^{\circ}_{\text{total}} = -582.83 \text{ kJmol}^{-1} \quad \Delta S^{\circ}_{\text{total}} = -70.48 \text{ Jmol}^{-1}$$

$$\Delta G^{\circ} = -561.317 \text{ kJmol}^{-1}$$

The thermodynamics show that the over oxidation is thermodynamically more favourable.

At 400 K, $\Delta G^{\circ} = -867.274 \text{ kJmol}^{-1}$.

There is a significant increase in ΔG° indicating that the higher the temperature the over oxidation to benzoic acid becomes more thermodynamically favoured.

2.3.1.3 Toluene reactions

In all of the reactions involving toluene no products were observed when analysed using GC. Samples were taken hourly. The mass balance of toluene was the same throughout the reaction proving that no other products were formed.

2.3.1.4 Benzaldehyde reaction

A standard reaction was carried out to make sure that benzaldehyde did not react with the catalyst to form any products. Pure benzaldehyde was pumped through the reactor at $1.5 \text{ ml}\cdot\text{min}^{-1}$ and $108.75 \text{ ml}\cdot\text{min}^{-1}$ of 5% O_2/Ar . The reaction was carried out at 100°C with 3.5% $\text{VO}_x/\text{Al}_2\text{O}_3$. Samples were taken hourly.

When the samples obtained were analysed using GC, no products were detected. However as expected, during the reaction benzaldehyde air oxidises to benzoic acid (86). This was detected, as a white solid formed in the reactor and the waste bottle.

2.3.1.5 Soxhlet extraction

A soxhlet extraction was carried out to see if any products had been retained by the catalyst.

The extraction was carried out on two of the catalyst samples. The reactions from which these were taken from are stated below:

- Reaction 2, 150°C , 3.5% $\text{VO}_x/\text{Al}_2\text{O}_3$
- Reaction 3, 100°C , 8% $\text{VO}_x/\text{Al}_2\text{O}_3$

The soxhlet extraction was carried out using 1 g of catalyst, with ethanol chosen as an appropriate solvent. The extraction was run for approximately 15 hours. From these extractions no products were obtained suggesting that there was no material on the catalyst surface.

An extensive literature search was carried out and no work was found on the liquid phase oxidation of toluene over a vanadium catalyst. This suggested that either work had never been undertaken or due to the reaction being unsuccessful had never been reported. At this stage it was decided to investigate a different route for the production of benzaldehyde.

2.3.2 Benzoic acid hydrogenation

2.3.2.1 Catalyst Characterisation

Catalytic testing was carried out using a ZrO_2 catalyst. This was due to its high selectivity for aldehydes in the hydrogenation of aromatic acids and its acid tolerant character (18).

XRD and TGA were used to study the catalyst before and after reaction. Figure 2-19 shows the XRD pattern obtained from fresh Zr(OH)_4 . It can be seen that the material is fairly amorphous in nature.

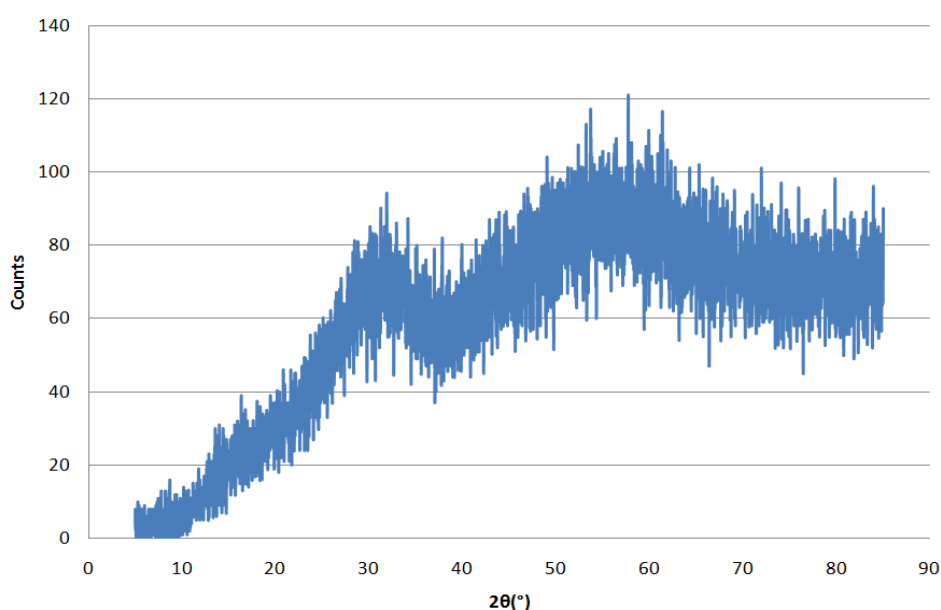


Figure 2-19 XRD fresh Zr(OH)_4 uncalcined

From the hot stage XRD analysis it is apparent that during activation the catalyst changes form with increasing temperature. Up to 300°C there are no major changes in the structure, however after 300°C zirconium hydroxide is converted to the oxide. The predominant peaks observed correspond to tetragonal zirconia (87).

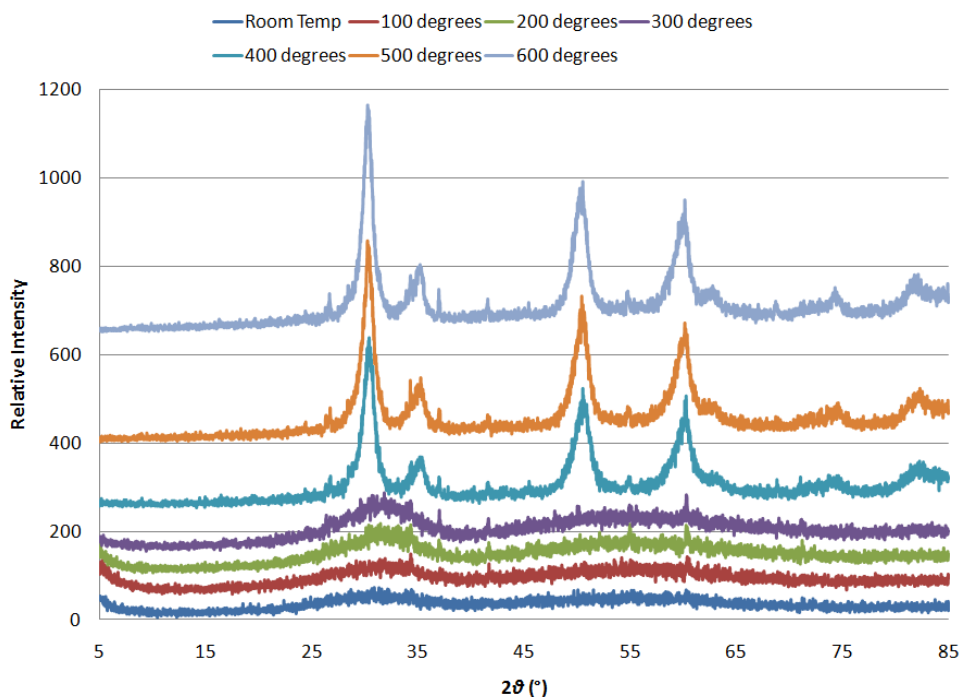


Figure 2-20 Hot stage XRD Zr(OH)_4 in N_2 atmosphere at room temperature, 100°C, 200°C, 300°C, 400°C, 500°C and 600°C

The Scherrer equation was used to calculate the zirconium oxide crystallite size from 400-600°C as shown in table 11.

Table 11 Crystallite size of hot stage XRD Zr(OH)_4

Temperature (°C)	Crystallite size
400	7.5 nm
500	8 nm
600	8.5 nm

It can be observed that crystallite size increases with temperature. This is due to the structural transformation. At 600°C the sample begins to change from the tetragonal to monoclinic phase. This is illustrated in figure 2-21. When this transformation takes place the crystallite size increases. Santos *et al* (88) carried out work studying the correlation

between thermal treatments and tetragonal/monoclinic nanostructured zirconia powder. They also reported an average crystallite particle of 8 nm. This small particle is thought to contribute to the stabilization of zirconia in the tetragonal phase (88).

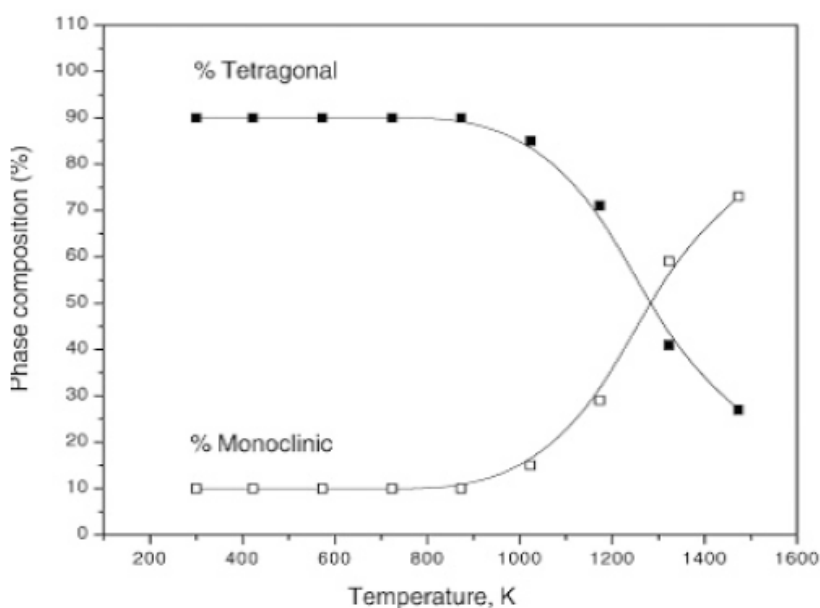


Figure 2-21 Variation of the relative phase of the polymorph mixture as a function of temperature (88)

A TGA was carried out to identify at what temperature zirconium hydroxide would form zirconium oxide. It can be seen in figure 2-22 that at approximately 90°C water is starting to be given off, this could be attributed to physisorbed water on the catalyst. Guo *et al* (89) also carried out thermal analysis on zirconium hydroxides and reported that the initial weight loss was due to coordinated water. After this there is a more gradual decline in weight which is postulated to be $Zr(OH)_4$ changing into ZrO_2 . In figure 2-20 the XRD data clearly shows that after 300°C a structural change occurs as crystalline zirconia is observed. This emphasises that the slow weight loss at around 300°C can be attributed to the dehydroxylation to form zirconia in the tetragonal phase. Overall there is a total weight loss of 28% which corresponds to work by Guo *et al* (89) who reported a total weight loss of 29%.

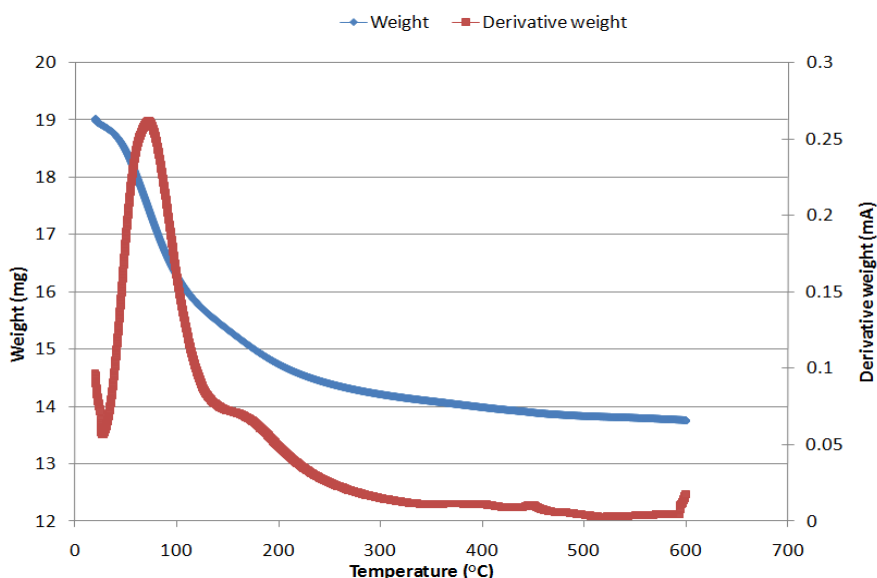


Figure 2-22 TGA weight and derivative weight profile of Zr(OH)_4 in N_2 from 25°C to 600°C

2.3.2.2 Reactions

2.3.2.2.1 Reaction 1

Reaction 1 was carried out using conditions stated previously. This pressure was not high enough and the benzoic acid blocked the upstream pipe. Subsequently the gas cut out after 30 min due to a build up in pressure and the reaction had stopped. The reactor was cleaned using ethanol to dissolve the solid acid which had formed. It was decided that the reactions in future would now be carried out at 5 barg pressure.

2.3.2.2.2 Reaction 2

Due to the problems in the previous reaction the saturator was opened up to 5 barg pressure. The reaction lasted 3 hours before a blockage occurred. This time however the blockage occurred in the ceramic wool plug at the bottom of the reactor. The benzoic acid had plated out and had formed a solid plug hence blocking the gas from flowing. This then caused a back pressure and the upstream pipe leading to the saturator then blocked again. Everything had to be once again cleaned out with ethanol including the reactor tube as the boiling chips had solidified due to the acid. Analysis on the catalyst was impossible due to this. However when the reactor tube was taken out of the oven the

smell of benzaldehyde was present, proving that the reaction was working. Subsequent reactions would be carried out using a metal sinter instead of a ceramic wool plug.

2.3.2.2.3 Reaction 3

This reaction was carried out for 114 hours. The system did not block, however the connection at the top of the saturator was found to be leaking. This was due to benzoic acid corroding the connection. The reaction was continued as H_2 and benzoic acid were still flowing over the catalyst but at a lower concentration of $0.002282 \text{ moles}\cdot\text{day}^{-1}$ (0.278 g). The samples that were obtained were analysed using HPLC. After 23 hours the first sample was taken. This following trace was produced (figure 2-23):

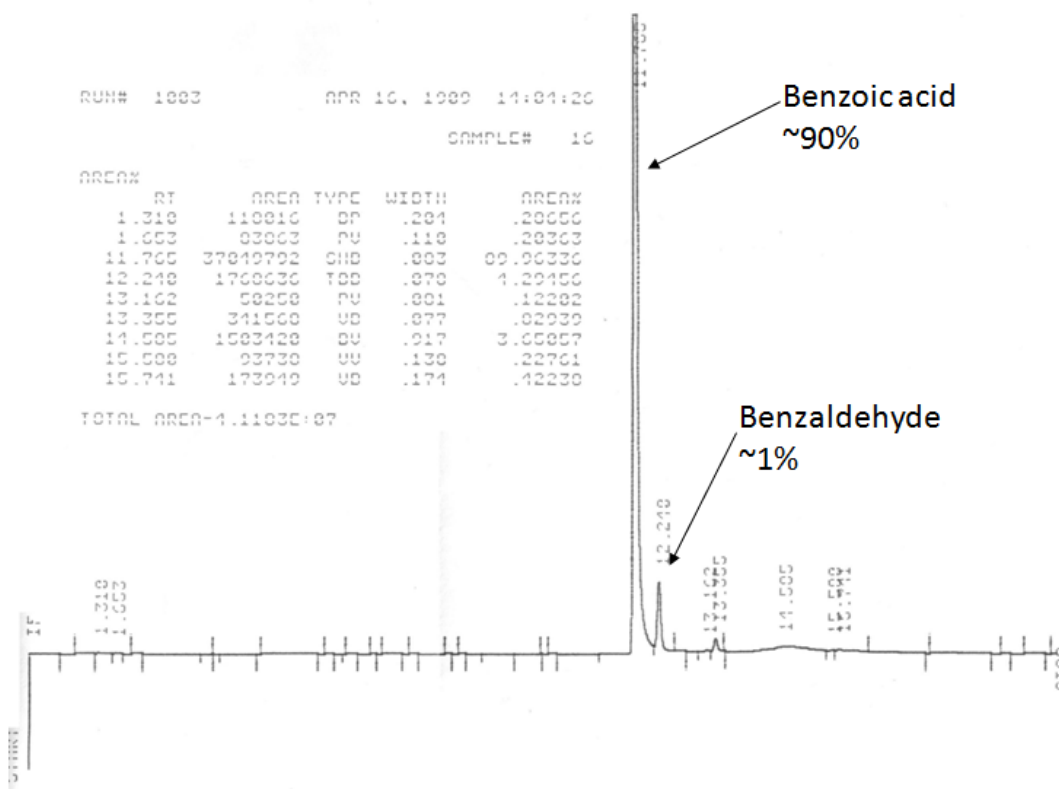


Figure 2-23 HPLC trace from benzoic acid hydrogenation reaction 3, after 23 hours

From the HPLC trace it can be seen that benzaldehyde was produced in small quantities, along with a second unidentified product. Previous work has shown toluene to be the main by-product formed at this temperature (90), and this was thought to be the product observed here. Benzyl alcohol formation was another possibility, although less likely.

Further calibration would be required to confirm the identity of the compound produced in our study.

Similar work carried out by De Lange *et al* (11) and Sakata *et al* (90) on the hydrogenation of benzoic acid showed excellent conversions (de Lange: 100%, Sakata: ~95%) and selectivity to the aldehyde (de Lange: ~95%, Sakata: ~94%) at 400°C. By-product formation was minimal at 400°C but became more apparent with increasing temperature. In this study comparable conversions with the literature were not achieved, however this could be due to the problems encountered. Benzoic acid was responsible for corroding the stainless steel reactor and leaks were formed as a consequence of this. Oxygen therefore would have been able to get into the system and subsequently oxidise benzaldehyde back to the acid. This could account for the low conversions produced.

The next sample was taken after 48 hours. However during this period the hydrogen flow cut out and only 13 ml.min⁻¹ of gas was flowing through the reactor and not the 40 ml.min⁻¹ intended. The problem was rectified and the reaction was continued. The HPLC trace showed reduced peak sizes. This was due to ethanol still pumping at the normal rate (100 ml/24h) even though the benzoic acid being introduced into the reactor was decreased. This resulted in the samples being less concentrated than previously. Figure 2-24 shows the trace produced from this.

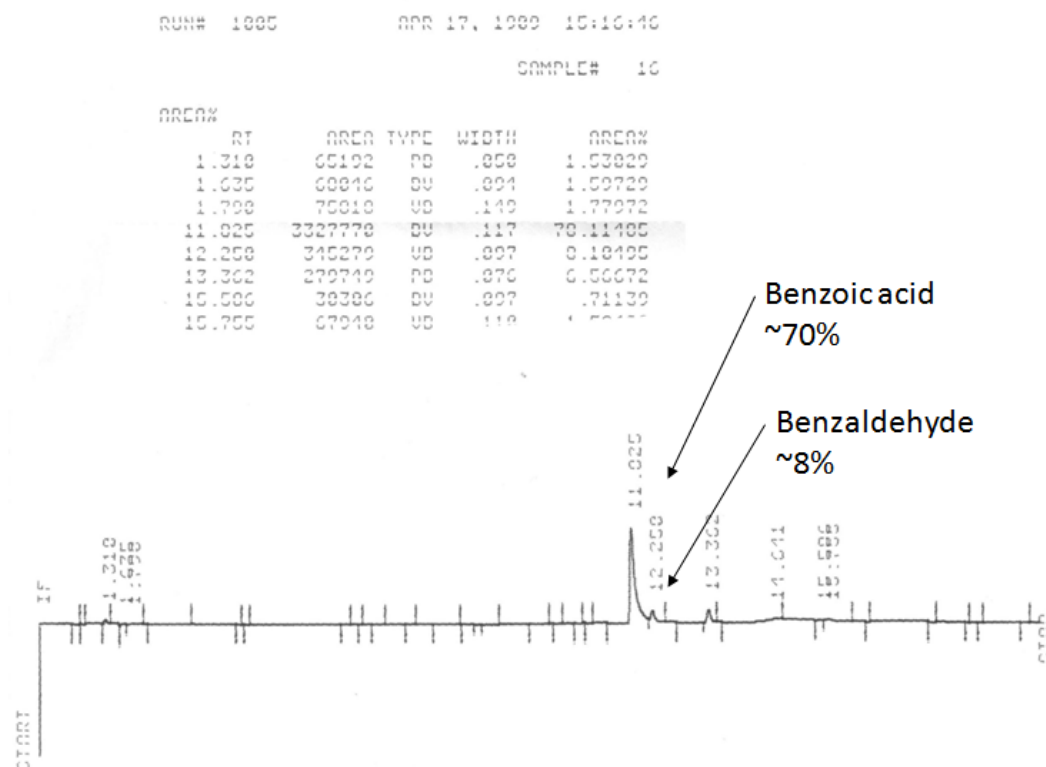


Figure 2-24 HPLC trace from benzoic acid hydrogenation reaction 3, after 48 hours

After 48 hours it can be seen that more benzaldehyde had been produced. The ratio of benzoic acid: benzaldehyde after 24 hours was 69:1 and after 48 hours this was 8.7:1 suggesting that more benzoic acid has been converted to benzaldehyde over time. Due to the increased contact time the starting material has with the catalyst, conversion is increased. This proved that the reaction was working even due to the technical issues experienced.

The last sample was taken after 114 hours. By this time the reaction was still proceeding but at a slower rate as the benzaldehyde concentration had started to decrease. The ratio had increased to 16.1:1 benzoic acid: benzaldehyde. This was subsequently due to the increase in the flow rate from $13 \text{ ml}\cdot\text{min}^{-1}$ to $40 \text{ ml}\cdot\text{min}^{-1}$. The contact time with the catalyst is once again reduced and subsequently conversion decreases.

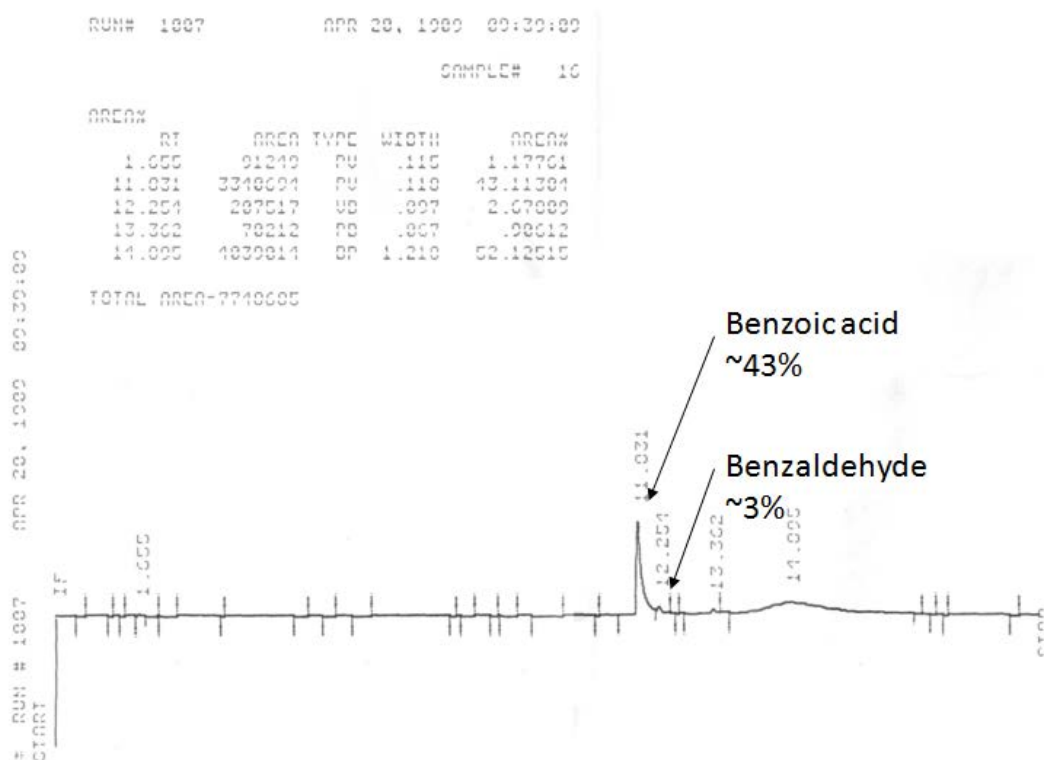


Figure 2-25 HPLC trace from benzoic acid hydrogenation reaction 3, after 114 hours

Although several problems were encountered throughout this experiment, benzaldehyde was produced. Pestman *et al* reported (91) work on the hydrogenation of acetic acid to acetaldehyde using oxide catalysts. The reaction was thought to have proceeded via a Mars and Van Krevelen mechanism. In this theory lattice oxygen plays an active role in two steps of the catalytic reaction. Firstly lattice oxygen reacts with a reducing adsorbate (hydrogen) to yield water, which desorbs to form an oxygen vacancy. Secondly this oxygen vacancy is refilled by an oxygen from the oxidant (acetic acid) and reacts to produce the aldehyde (91). Figure 2-26 shows a schematic of this process using acetic acid.

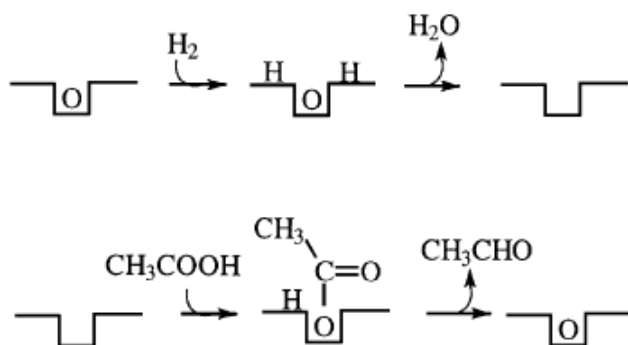
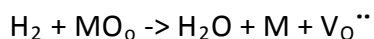


Figure 2-26 Selective hydrogenation of acetic acid to acetaldehyde (91)

From this work De Lange *et al* proposed the following mechanism for the hydrogenation of benzoic acid (11):

1. Activation of the catalyst by hydrogen:



2. Re-oxidation of the catalyst by benzoic acid yielding benzaldehyde



Throughout the experiment H_2 was continually supplied and hence oxygen vacancies were continuously created (11).

In the hydrogenation of benzoic acid, benzyl alcohol was not produced. Generally the following reduction would take place:



The lack of benzyl alcohol in by-products suggests that benzaldehyde is not being further reduced. This is thought to be due to the strong interaction of carboxylic acid with the catalyst. This consequently inhibits the consecutive reactions of the aldehyde, which maintains the high yield (18).

After this experiment was carried out further work on the hydrogenation of benzoic acid was ceased. This was due to all the technical issues that were encountered. Benzoic acid had corroded the inside of the rig and meant the apparatus would have to be re-built if work was to continue.

2.3.3 Hydroformylation reactions

A classic hydroformylation reaction involves the adding one equivalent of both CO and H₂ (synthesis gas) to an alkene to produce linear and branched aldehydes (51). The reaction proposed in this study was not a classic hydroformylation but used the basic concept. Formaldehyde was used as the “synthesis gas” and isopropyl benzene as the alkene. Formaldehyde is classified as a suspected human carcinogenic and is too self reactive to be isolated, shipped and stored in its pure form. For safety reasons an alternative was chosen. Several commercial forms of formaldehyde are available which include trioxane, formalin and methylal. Formalin is the cheapest out of the three options however it contains a large quantity of water which can cause problems throughout the reaction (92). For this reason 1, 3, 5-trioxane was used as the source of formaldehyde.

Hydroformylation reactions were studied to investigate if p-methylbenzaldehyde could be produced from isopropyl benzene and 1, 3, 5-trioxane over a solid acid catalyst. Figure 2-27 shows the possible products produced. These reactions were carried out in both the liquid and gas phase.

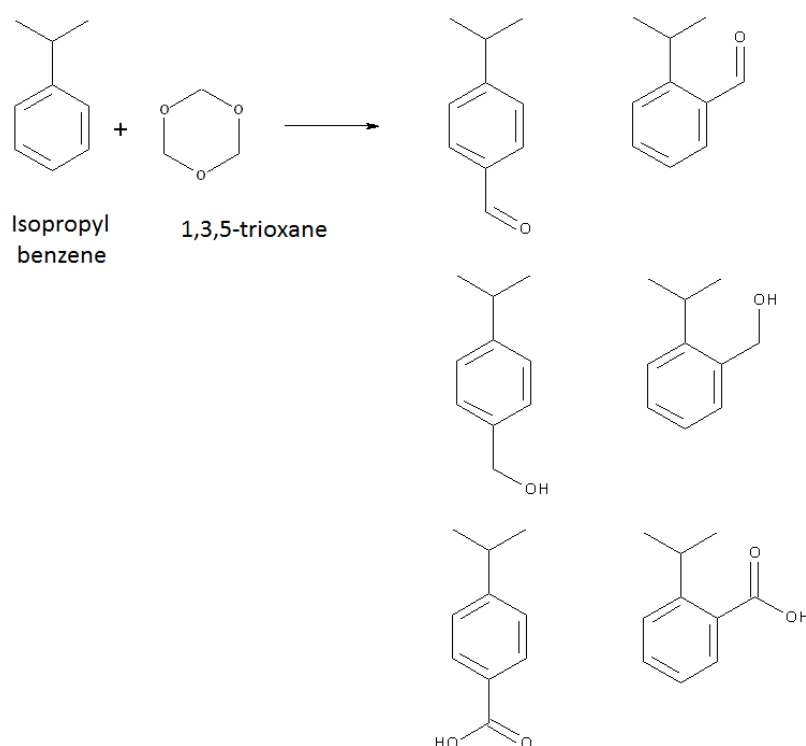


Figure 2-27 Schematic diagram of hydroformylation reaction

2.3.3.1 Gas phase reactions

Reactions were carried out in the gas phase using two different isopropyl benzene: 1, 3, 5-trioxane ratios.

2.3.3.1.1 Catalyst characterisation

XRD was used to look at the phases of the catalyst before and after calcinations had occurred. Figure 2-28 shows the zirconium sulphate prior to calcination. It can be seen that the material is amorphous.

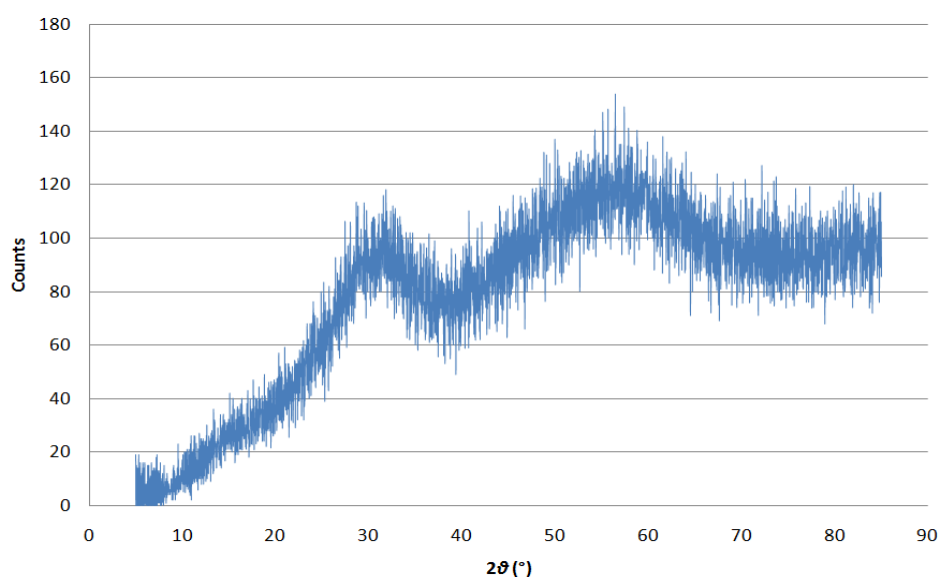


Figure 2-28 XRD uncalcined sulphated zirconia, laboratory prepared

Figure 2-29 shows the XRD pattern of the sulphated zirconia after calcination. The predominant peaks at 30, 50 and 60 2θ all signify tetragonal zirconia. Reddy *et al* suggested that the tetragonal phase which was observed was due to the impregnation of the sulphate ions, which show a strong influence on the phase modification of zirconia from thermodynamically more stable monoclinic to the metastable tetragonal phase (58).

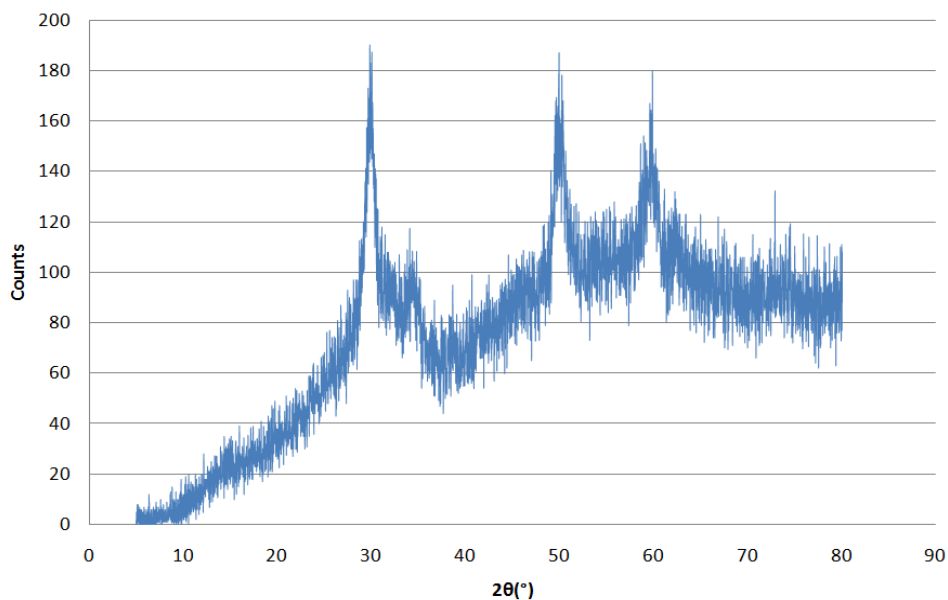


Figure 2-29 XRD calcined sulphated zirconia laboratory prepared, 550°C for 8 hours

2.3.3.1.2 Results

Reactions in the gas phase were carried out using different starting material ratios. The first reaction was carried out using a 3.5:1 ratio of isopropyl benzene: trioxane. This reaction proved unsuccessful. GC-MS analysis showed no products had been produced in the reaction.

After the reaction post analysis was carried out on the catalyst. The catalyst was visibly black suggesting that carbon lay down had occurred. A TPO was carried out on the used catalyst to examine this. Figure 2-30 shows the weight and derivative weight profile for this TPO.

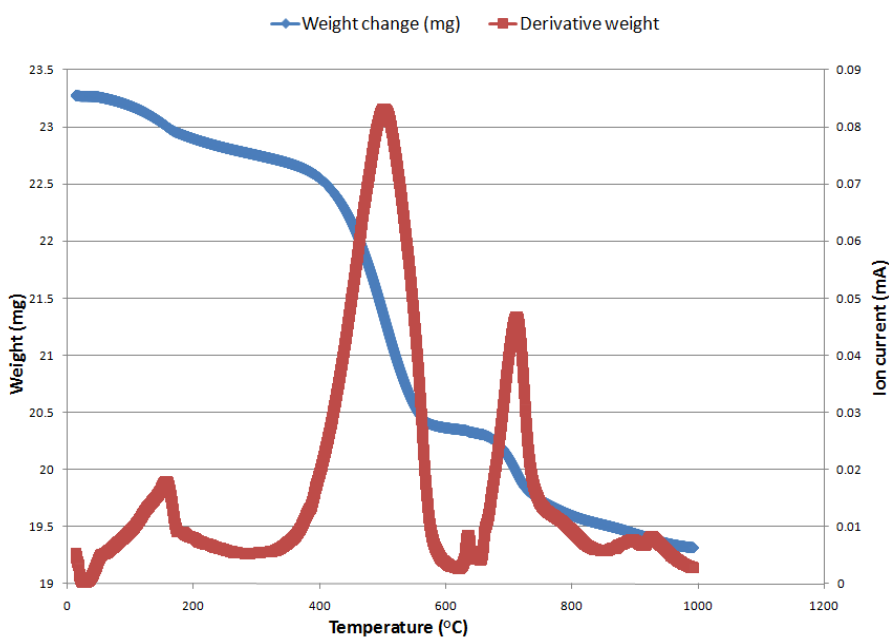


Figure 2-30 TPO weight and derivative weight profile: gas phase reaction between 3.5: 1 Isopropyl benzene: 1, 3, 5 trioxane, reaction conditions 300°C, 50ml.min⁻¹ N₂, feed rate 2.2ml.h⁻¹

It can be seen that there are 2 major weight losses occurring, one starting at approximately 400°C and the other at 630°C. There was also a small weight loss at the start of the analysis up to approximately 200°C. The catalyst is known to be hydroscopic and hence the weight loss at the start can be attributed to physisorbed water.

Figure 2-31 show clearly that the major weight loss at 400°C was due to formation CO₂ from the carbon on the surface burning off. Li and Gonzalez (93) studied work on the effect of deposition on the deactivation of sulphated zirconia catalysts and found that during TPO analysis in oxygen, the simultaneous elimination of CO₂ and SO₂ began to occur at 400°C reaching a maximum rate of elimination at 600°C. However when analysis was carried out in air it was found that SO₂ evolution occurred above 600°C and CO₂ evolution started at 300°C and was complete by 600°C. It was possible to selectively burn off the coke in air at temperatures of 450-500°C and then leave the sulphate species on the surface. The results from the literature were comparable with the data shown in this study. Analysis was carried out under a 5% O₂/Ar atmosphere so it was likely to produce similar results as to that Li *et al* (93) suggested when their analysis was carried out in air.

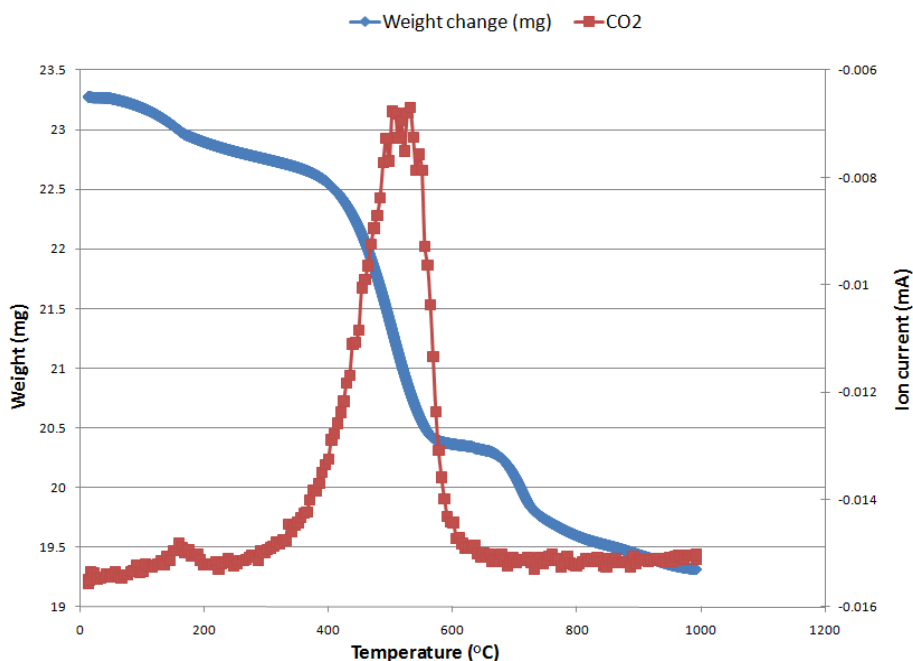


Figure 2-31 TPO weight and CO₂ mass profile: gas phase reaction between 3.5: 1 Isopropyl benzene: 1, 3, 5 trioxane, reaction conditions 300°C, 50ml.min⁻¹ N₂, feed rate 2.2ml.h⁻¹

The minor weight loss at approximately 600°C was thought to be produced by formaldehyde as shown in figure 2-32. Formaldehyde would have been produced when 1, 3, 5,-trioxane was broken down and subsequently desorbed from the catalyst. However this peak at 600°C could also correspond to the evolution of SO₂. Li *et al* (93) suggested that in air at temperatures above 600°C, SO₂ could be produced. Therefore it was possible that both formaldehyde and SO₂ were being formed at the same time and hence produce only one peak.

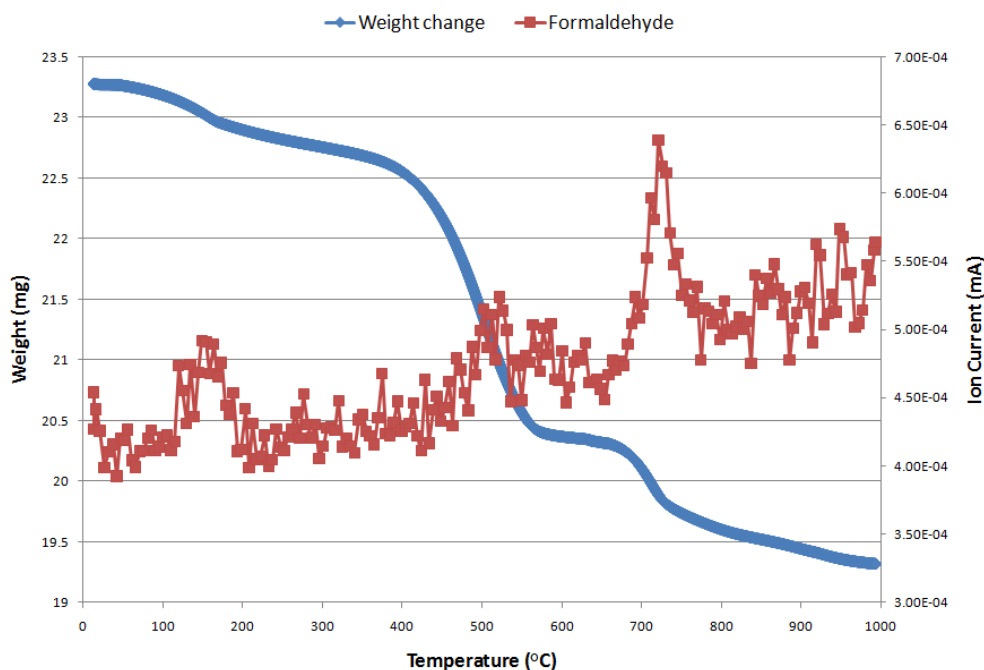


Figure 2-32 TPO weight and formaldehyde mass profile : gas phase reaction between 3.5: 1 Isopropyl benzene: 1, 3, 5 trioxane, reaction conditions 300°C, 50ml.min⁻¹ N₂, feed rate 2.2ml.h⁻¹

Due to the significant amount of carbon lay down the next reaction was carried out using a lower ratio of 10: 1 isopropyl benzene: trioxane. This allowed us to see if it was the trioxane or isopropyl benzene that was responsible for the build-up of material on the catalyst. This reaction once again proved unsuccessful. GC-MS analysis showed no products had been produced in the reaction.

As shown in figure 2-33 there is still a significant weight loss present starting at 400°C but the loss at 700°C has been significantly reduced. This was due to the reduced amount of trioxane producing formaldehyde.

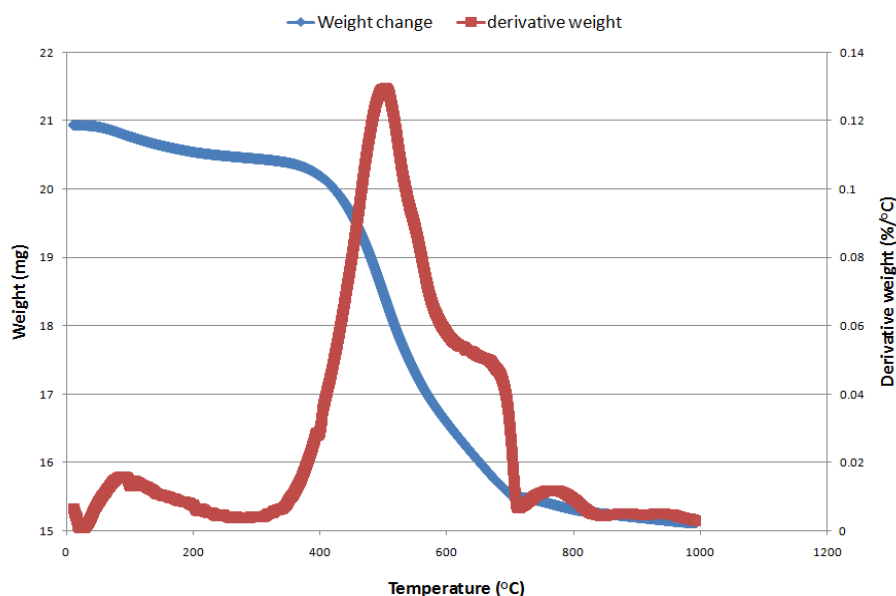


Figure 2-33 TPO weight and derivative weight profile: gas phase reaction between 10: 1 Isopropyl benzene: 1, 3, 5 trioxane, reaction conditions 300°C, 50ml.min⁻¹ N₂, feed rate 2.2ml.h⁻¹

The derivative weight profile in the figure above differs slightly from figure 2-30 (3.5:1 ratio). There was a visible shoulder peak present at 600°C which was not present in the thermal analysis profile of the previous reaction (10:1 ratio). This suggested that SO₂ may have started to be evolved at the same time as CO₂. The weight loss of CO₂ has increased from 17% with a 3.5: 1 ratio to 28% with the 10:1 ratio. Due to this increase this suggested that isopropyl benzene was laying down carbon on the catalyst and then being oxidized to form CO₂. Due to this increase in carbon laydown, the evolution of CO₂ may occur over a larger temperature range and subsequently as the production of CO₂ is coming to an end, SO₂ starts being evolved and produces a shoulder peak. As shown in figure 2-34 if CO₂ was produced above 600°C then both CO₂ and SO₂ peaks would converge slightly.

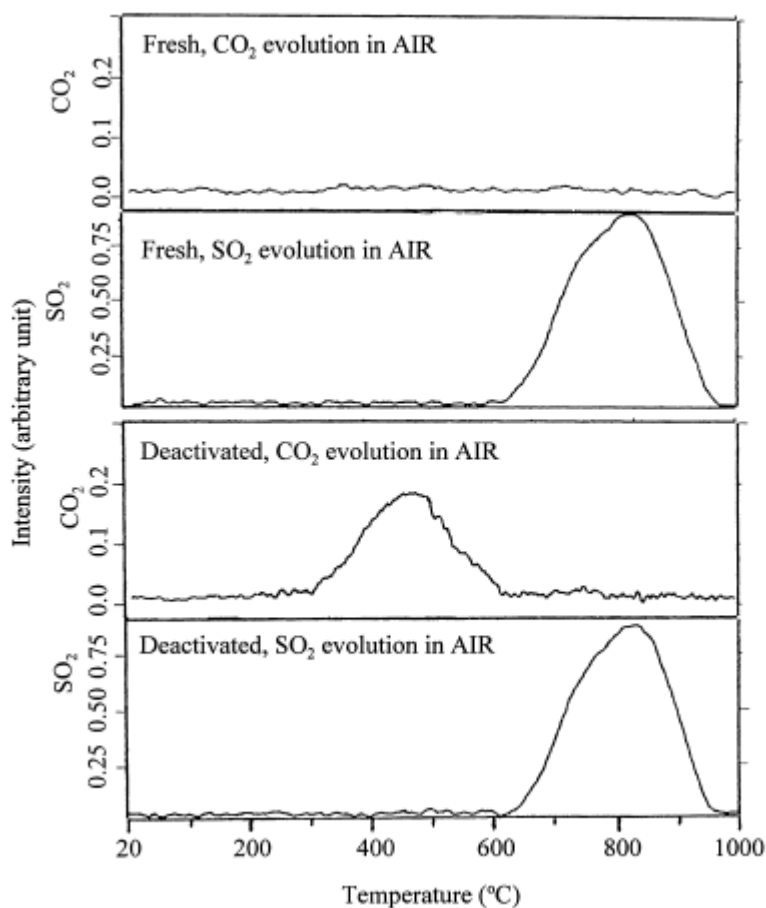


Figure 2-34 Chromatograms of CO₂ and SO₂ evolved from fresh and deactivated sulphates sol-gel process zirconia in TGA/FT-IR under air flow (94)

It was found that sulphated zirconia catalysts had a very low tolerance for coke formation. In the isomerisation of *n*-butane at 200°C, 0.04 wt% carbon reduced the catalytic activity to 10% of its initial value (93). It was also noticed that time on stream also plays an import role, as at 200°C carbon formation was linearly related to time on stream as shown in figure 2-35.

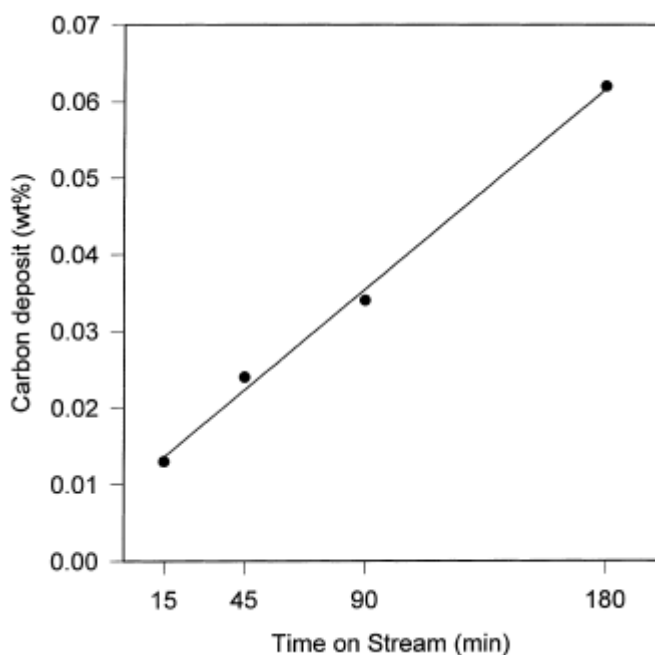


Figure 2-35 Carbon deposition on sulphated sol-gel zirconia in the isomerisation of *n*-butane at 200°C as a function of time (93)

The reactions studied within this section were carried out over a period of several days and at higher temperatures (300°C). From the data reported in the literature it was possible that the catalyst was deactivated rapidly. After an extensive literature search no work was reported suggesting that the reaction was ever carried out or unsuccessful and never published.

2.3.3.2 Liquid phase reactions

Both reactions that were carried out in the liquid phase used 10:1 isopropyl benzene: trioxane ratio. This was used to try and prevent any blockages from occurring.

2.3.3.3 Catalyst characterisation

Once again it can be seen from figure 2-36 that commercial uncalcined sulphated zirconium is amorphous in nature.

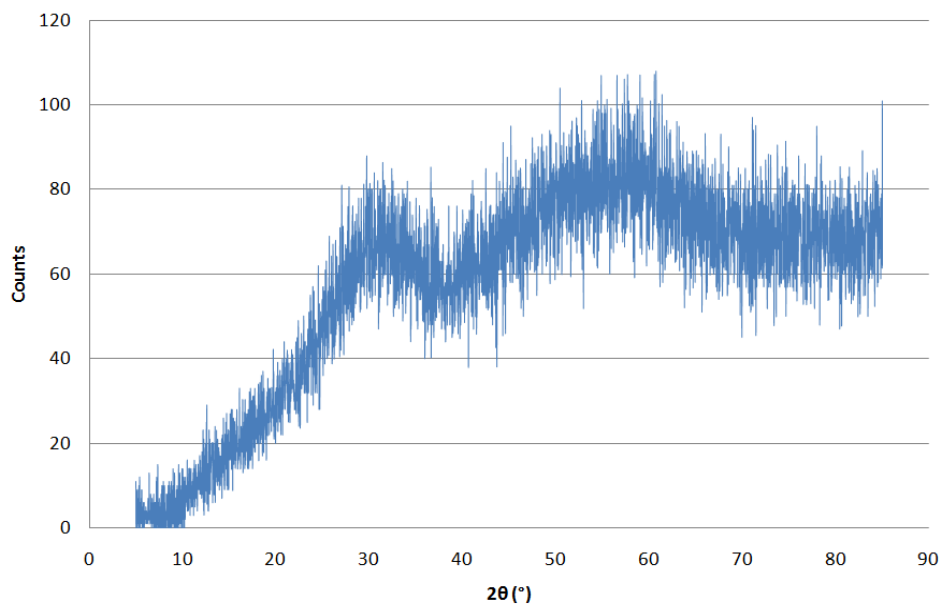


Figure 2-36 XRD commercial MEL chemicals 7% sulphated zirconium, uncalcined

However upon calcination, features corresponding to tetragonal zirconia become apparent (87).

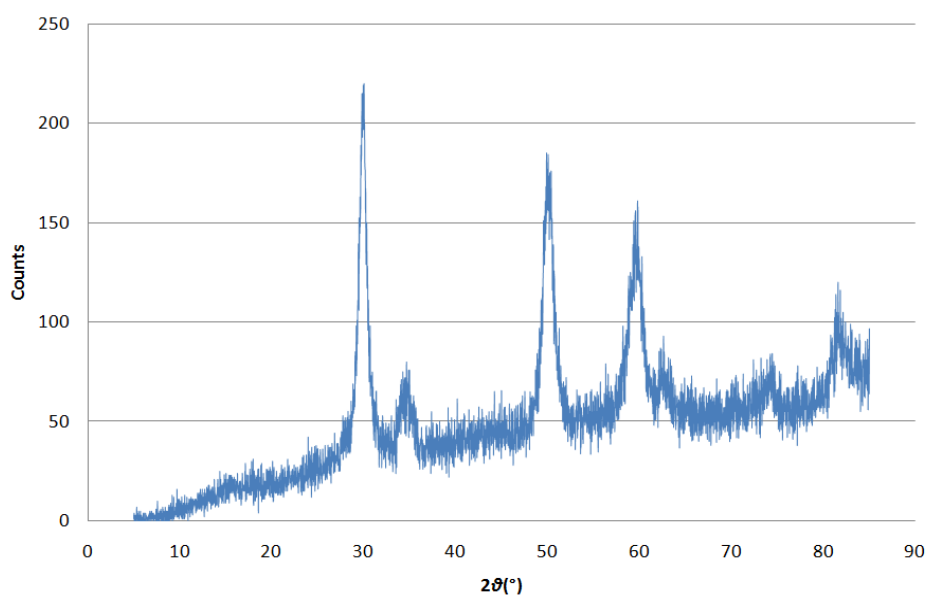


Figure 2-37 XRD commercial MEL chemicals 7% sulphated zirconia -calcined 600°C for 3 hours in static air

2.3.3.4 Reaction results

Both reactions carried out in the liquid phase proved unsuccessful due to a blockage within the reactor. Isopropyl benzene was refluxing and trioxane was coming out of solution and forming a solid layer within the catalyst and subsequently no material could pass through. Formaldehyde was responsible for the blockage within the catalyst as it was likely that polymerisation had occurred. The polymerization of trioxane to yield a high molecular weight polymer has been shown to take place over zirconium tetrachloride (95). After the reaction was stopped, the catalyst was allowed to dry out it and it was apparent that the catalyst had formed a solid layer and had to be removed using aqua regia acid. This however resulted in no post reaction analysis on the catalyst being carried out.

After this it was decided to cease work on the production of benzaldehyde after several failed attempts.

2.4 Conclusions

During the investigation into the production of benzaldehyde several routes were studied. The oxidation of toluene was carried out in the liquid phase using a vanadium oxide supported on alumina catalyst. Results suggested that no reaction had taken place, and work on this route was ceased. An alternative route was the hydrogenation of benzoic acid. This was carried out in the gas phase using a ZrO_2 catalyst. Analysis of results showed that hydrogenation of benzoic acid had taken place and benzaldehyde was produced. With reference to previous work in the literature, it was concluded that the reaction occurred via a Mars and Van Krevelen mechanism. However extensive corrosion to the rig had occurred and it was decided not to continue with this work as a full re-build would have to take place and this was not feasible. The last route for the production benzaldehyde studied was the hydroformylation reaction between isopropyl benzene and 1, 3, 5-trioxane in both the liquid and gas phase. Analysis of the products suggested that once again no products were produced. Liquid phase reactions had to be stopped prematurely as blockages occurred, possibly due to trioxane polymerization, and stopped the liquid from flowing. Gas phase reactions were carried out for several days but thermal analysis showed that severe coking of the catalyst had occurred.

After this it was decided not to continue work on the production of benzaldehyde. Several routes had been studied and no positive data had been obtained.

3 Liquid phase dehydrogenation

3.1 Introduction

3.1.1 Lilestralis

Lilestralis (α - Methyl-*p*-tert-butyl-phenyl propyl aldehyde) is also known by various different names such as lilal and lily aldehyde. In the fragrance industry it is of importance due to its pleasing odour. It has a fresh, floral note reminiscent of lily of the valley (96). Due to this pleasant odour it is used in soaps, detergents and cosmetic perfumes. It is a homologue of cyclamen aldehyde but is not found in nature. Lilestralis is classed as a muguet odourant. Flowers from the muguet (lily of the valley) plant are very small and difficult to extract oil from. This makes it impossible to produce commercially viable oil from this plant (97). Synthetic substitutes are available to the perfume industry and lilestralis (lilal) is one of those substitutes as shown in figure 3-1

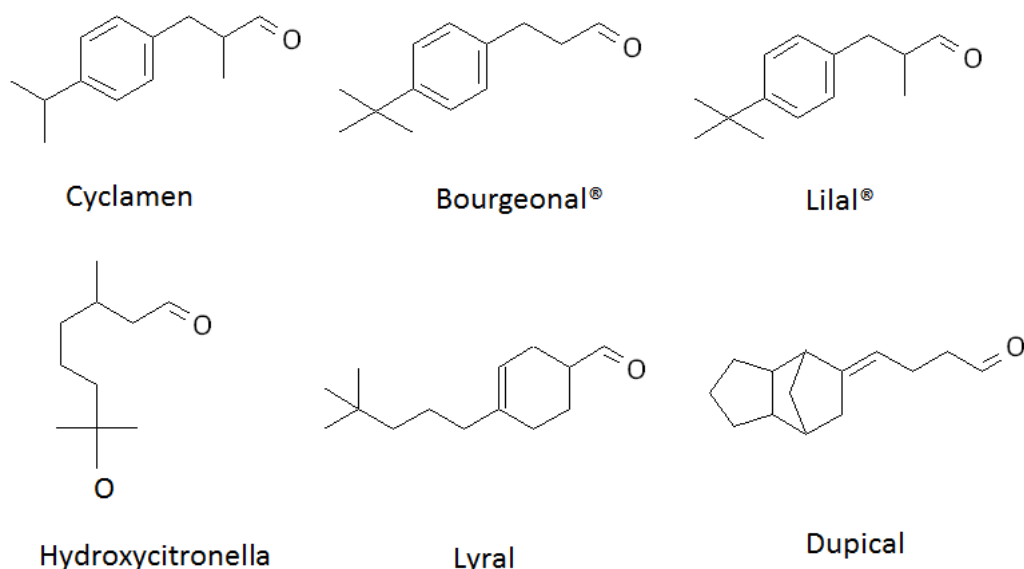


Figure 3-1 Synthetic aldehydic muguet odourants (97)

All of the early muguet odourants were known to be aldehydic and this was taken to be the functionality that was responsible for the smell, however it has now been found that

some alcohols can be also used (97). Figure 3-2 illustrates how muguet odourants differ in smell.

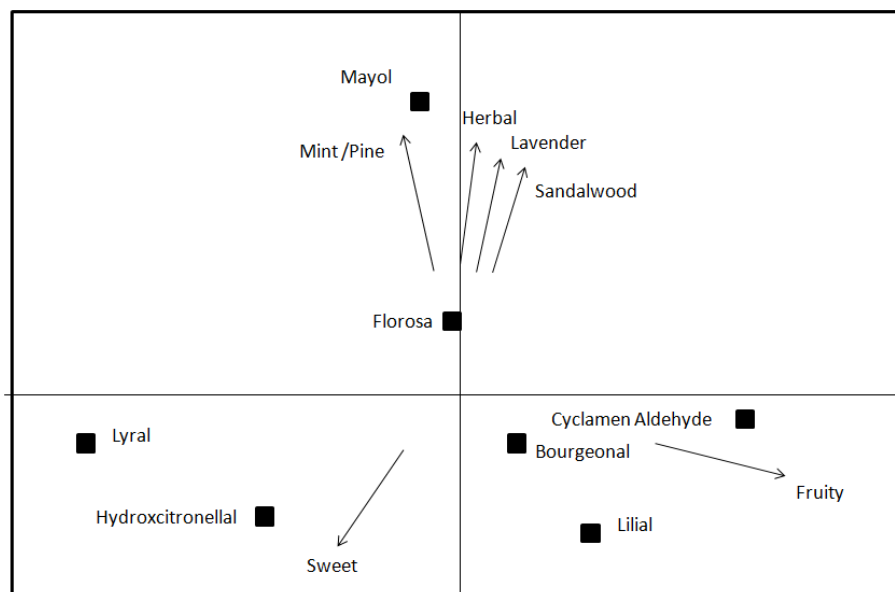


Figure 3-2 Differences in odour profiles of muguet odourants (97)

It can be seen from figure 3-2 that lillal, bourgeonal and cyclamen aldehyde are all classified as fruity whereas lyral and hydroxycitronellal produce sweet smells.

3.1.2 Possible methods

There are a few possible routes in which lilestralis and similar compounds can be produced, one of which is from benzene. Benzene can react with isobutene to produce *tert*-butylbenzene. This is followed by the addition of methacrolein to produce an intermediate which can then be hydrolysed to the corresponding hydrocinnamaldehydes (figure 3-3). Another method of production is from benzaldehyde which is also shown in figure 3-3 (4).

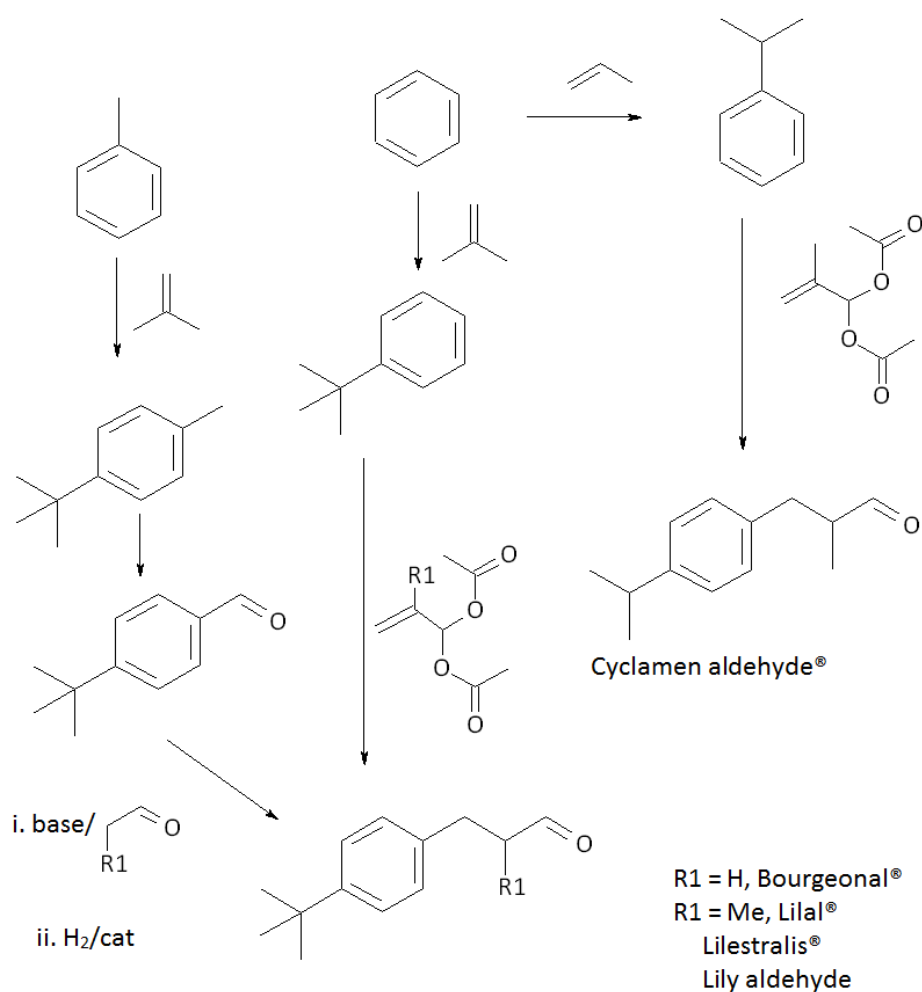


Figure 3-3 Production of hydrocinnamaldehydes (4)

3.1.3 Stability of lilestralis

Lilestralis displays a lack of stability, which is often seen in compounds in this class. As with benzaldehyde, oxidation to the carboxylic acid and lower homologues can occur. Lilestralis undergoes autoxidation to form a white crystalline solid which is the carboxylic acid.

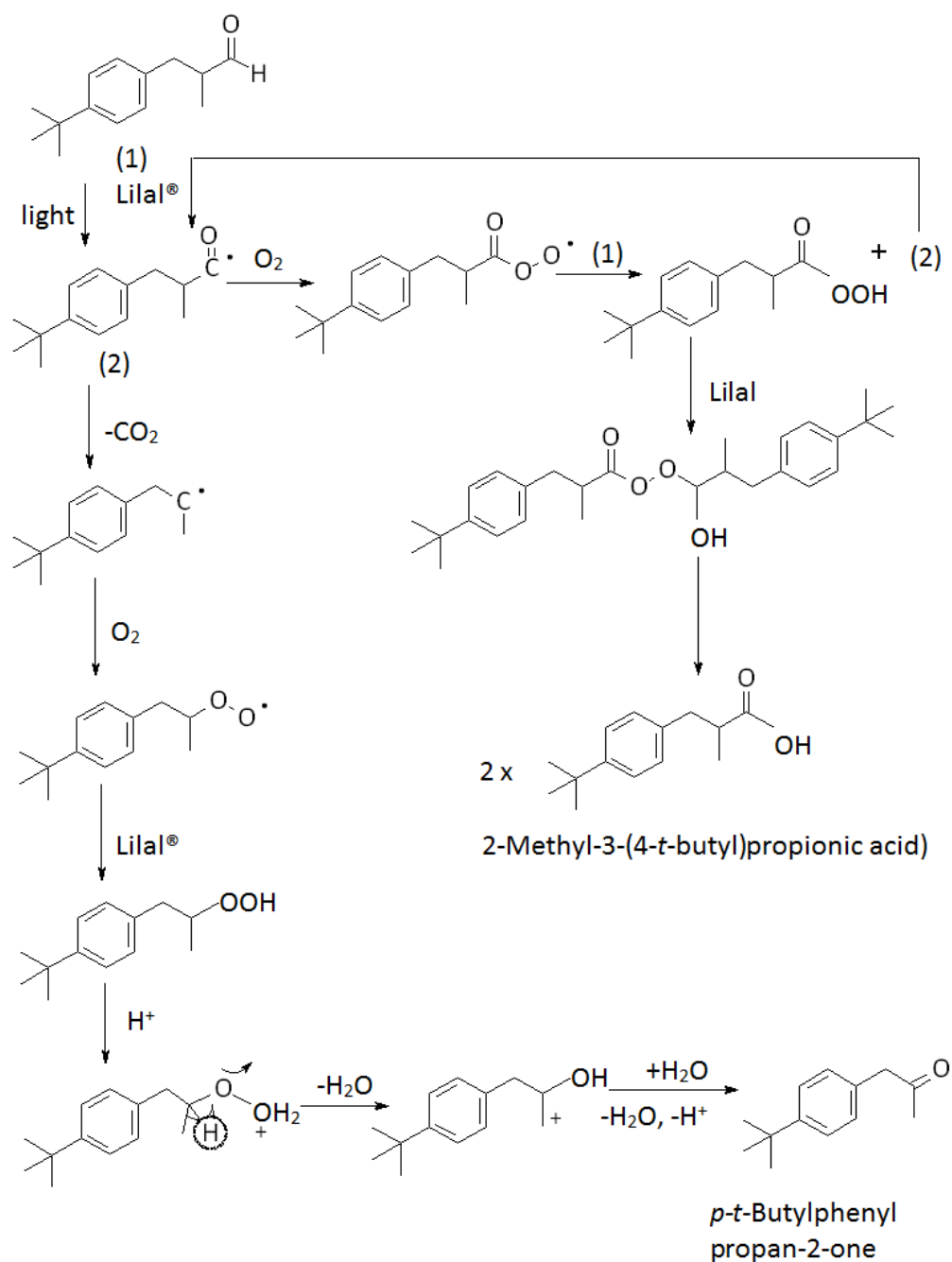


Figure 3-4 Autoxidation of lilestralis (4)

Figure 3-4 outlines the mechanism of autoxidation of lilestralis. The initial step of this mechanism is catalysed by light or the presence of metal ions that are capable of a one electron reduction transition. During this process there are two possible products: *p-t*-butylphenylpropan-2-one and 2-Methyl-3-(4-*t*-butyl)propionic acid. The major product formed is the acid in an approximate ratio of 20:1 (4).

3.1.4 Dehydrogenation Reactions

Dehydrogenation reactions are often used in industry to produce fine chemicals. The dehydrogenation of alcohols to aldehydes and ketones is a well known industrial process (98).



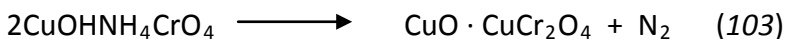
These types of reactions are endothermic and generally use a copper catalyst due to their high selectivity to the dehydrogenation product (98, 99). Copper chromite predominantly was the catalyst that was used to carry out these reactions. However due to new EPA restrictions, it is prohibited to dispose of chromite in landfills. For this reason alternative copper based catalysts without the presence of chromia are being examined for potential use.

3.1.5 Copper catalysts

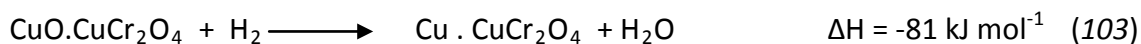
Over the years it has been found that copper is a good catalyst for the dehydrogenation of alcohols. It has been found to be the most active and widely used however its activity has been found to decrease within a few hours (100). For this reason catalysts containing promoters such as zinc oxide, chromium and magnesium oxide have been studied to try and prolong activity (101).

3.1.6 Copper chromite

Copper chromite is often used as the catalyst in many types of reactions such as dehydrogenation, hydrogenation, oxidation and alkylation. It was first reported by Adkins in 1908 (102, 103) and is often referred to as 'Adkins catalyst.' The most common route of preparation is by the calcination of the precipitated basic copper ammonium chromate in air (103)



To achieve the active phase, the catalyst is generally reduced using a H₂-N₂ mixture of varying compositions.



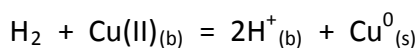
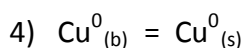
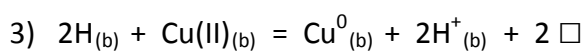
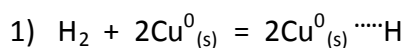
Both the calcination of the precursor and the reduction of the catalyst are highly exothermic processes and hence a great degree of care has to be taken to avoid overheating or uneven reduction of the catalyst. Sintering can be a problem during the reduction stage. To minimise this, the catalyst is reduced by heating slowly using a low concentration of hydrogen after being purged with an inert gas to remove any air (103).

However copper chromite is toxic and often a more environmentally replacement is sought after. In industry, dealing with the carcinogenic chromium (VI) compounds, the waste water formed in the production (which contains pollutants) and the disposal of the chromium catalysts are all things that want to be avoided (104)

Copper chromite catalysts have been known to exhibit high selectivity. This has been used to advantage in the hydrogenation of edible oils and fats where stronger hydrogenation catalysts, such as nickel, lead to excessive saturation and inferior nutritional quality of the final product (105). Copper chromite is used in hydrogenation reactions as they have been known to selectively hydrogenate carbonyl bonds while leaving unsaturated C=C bonds virtually untouched (98, 99).

Chromium is the most common additive in copper catalysts for the dehydrogenation of alcohols (106) and typically in the form of Cr_2O_3 or CuCr_2O_4 . Prasad and Shankar carried out work on the dehydrogenation of ethanol and found that the presence of chromia could prolong the activity and life of the catalysts (105). It was thought that chromia might act as a spacer between copper crystallites, hence inhibiting the sintering process throughout the period of use (107).

At high temperatures sintering can occur which can result in a loss of surface area and activity (103). In terms of reduction the following mechanism has been proposed (108) :



Here, $\text{Cu}^0_{(s)}$ and $\text{Cu}^0_{(s)} \cdots \text{H}$ correspond to a surface atom of metallic copper and a hydrogen adsorbed on the metallic copper atom respectively; $\text{Cu(II)}_{(b)}$ and $\text{Cu}^0_{(b)}$ are a copper atom in an oxidation state (II) and a metallic copper atom, which belong to the bulk of chromite, respectively; $\text{H}_{(b)}$ and $\text{H}^+_{(b)}$ are a hydrogen atom and a proton bound in the bulk of chromite, respectively; \square is an octahedral position in the chromite onto which the dissolved hydrogen is bound (108). It is suggested that step 3 is the rate determining step in the process with steps 1 and 2 near equilibrium.

3.1.7 Project outline

The main aim of this section of work was to maximise output for the production of lilestralis on the industrial scale and this was carried out by studying various aspects of the process. Currently the process employed by Innospec has several drawbacks. Firstly, the catalyst deactivates steadily over time, there are also problems with low conversions and formation of by-products. To study these issues a reactor was designed to mimic the conditions used on plant. In this work the dehydrogenation of lillol alcohol (p-LOL) to lilestralis (p-LAL) over a copper chromite catalyst was investigated. The reaction was carried out in a slurry reactor using a suspension referred to as the “inert bed.” The inert bed was a by-product of the reaction and recycled material from plant. Due to this there were a large number of impurities within the inert bed and over time this material increased in viscosity as the lights within the bed would boil off and leave a build up of the heavy components.

Within this thesis it was decided to study various aspects of the process to try and obtain better conversions. The following topics were studied:

1. Material investigation
2. Catalyst Activation and alternative catalysts
3. Concentration affects

3.2 Experimental

3.2.1 LPD Reactor

The liquid phase dehydrogenation of p-LOL was carried out in a slurry reactor using a copper chromite catalyst.

3.2.1.1 Specifications

A reactor had to be designed to mimic the set-up used on the industrial plant. It had to have the following specifications to carry out the reactions.

- Reach and maintain 230°C
- Pressure of 57 mbar
- Collect samples without opening reactor to atmosphere
- Stir reaction mixture
- Condense out products and starting materials
- Have both N₂ and a H₂ mixture gas readily available

The system was designed so that catalyst and all other materials could be placed in a round bottomed flask. This was positioned in a sand bath on top of a hot plate. A magnetic stirrer was used to keep the slurry of reactants and catalyst moving. Reactants could be introduced into the system via a dripping funnel. A double layered condenser allowed the condensation of materials that were then collected in flasks which could be rotated. To measure the slurry temperature a data logger and thermocouple was used. A solid CO₂ (cardice)/ ethanol trap was used before the vacuum to collect any materials not removed by the condenser. High vacuum grease was used to ensure a substantial seal at all glass connections. The reactor was lagged to minimise any heat loss.

3.2.1.2 Reaction procedure

Into the reactor 5 g of catalyst and 50 g of inert bed were placed. At this point the reactor was sealed and the system was purged with 20 ml.min⁻¹ N₂. This gas flow was consistent throughout the reaction. The system was then placed under a vacuum of 57 mbar and heated to 230°C. Once this temperature was maintained starting material (p-LOL) was added to the flask via a dripping funnel at a rate of 13 g (13.5 ml) in the 1st 10 min and then 5 g.h⁻¹ (5.5 ml) for the remainder of the reaction. Towards the end of the reaction,

no material was added for the last 20 min. Sample flasks were rotated every 2 hours to allow different samples over time to be taken. Figure 3-5 shows the reactor set-up

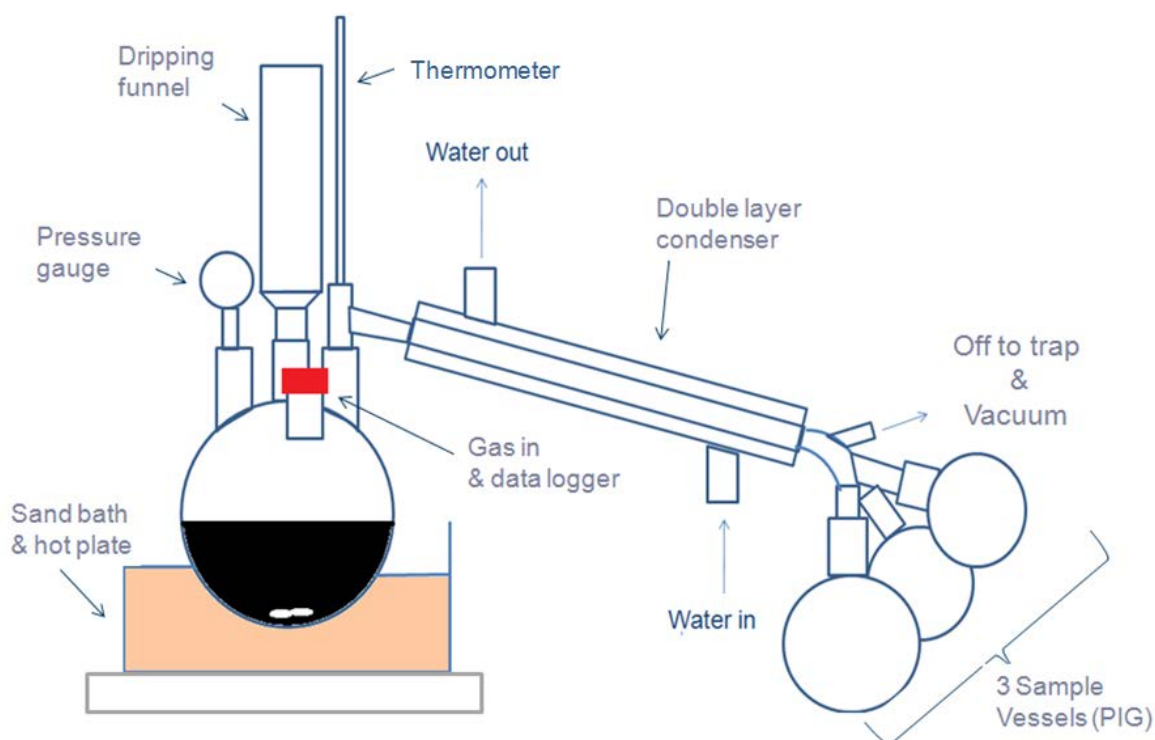


Figure 3-5 Schematic diagram of LPD reactor

3.2.2 GC method

Liquid analysis was carried out on a Thermo Finnigan focus GC with a thermo auto injector 3000 and auto sample 3000. A 30m Varian CP-Sil 5CB (0.25 mm x 0.25 μm) column was used to analyse all materials.

3.2.2.1 Column conditions

Inlet temp: 175°C

Carrier constant flow: 1 ml.min⁻¹

Detector Temp: 275°C

Ramp rate:

5 degC.min⁻¹

Initial 100°C → 230°C hold for 64 min.

3.2.3 Catalyst

Several catalysts were used in the dehydrogenation studies, including both laboratory prepared and commercial catalysts.

3.2.3.1 BASF Copper chromite catalyst

Several types of copper chromite catalysts were studied in catalyst testing reactions. The predominant one being supplied from BASF. Table 12 shows the weight percentage of the components.

Table 12 Percentage of components BASF copper chromite

Ingredient	Weight in Percentage
Copper chromite	71
Copper oxide	29
Chromium (VI) compound	0.5-2

Table 13 shows the properties of the copper chromite catalyst as reported by BASF.

Table 13 Properties of BASF copper chromite

Surface area, m²/g	30
Total pore volume, ml/g	0.5
Particle size (50th percentile), microns	20

3.2.3.2 Sud-Chemie copper chromite

Catalysts thought to contain less Lewis acid sites were tested to compare activity with the standard copper chromite. These were supplied from Sud-Chemie. Two catalysts were used: copper chromite modified with 120 ppm Na and copper chromite modified with 1600 ppm Na. The chemical compositions are shown in table 14.

Table 14 Percentage of components Sud-Chemie copper chromite

Component	Concentration
Copper oxide	40-50 %
Chromium (III) oxide	40-50 %
Manganese dioxide	<5 %
Barium chromate	3-4 %
Chromia (VI) compounds, with the exception of barium chromate	<0.2 %

3.2.4 Reduction of copper chromite catalysts

In reactions where reduction was required there were several methods by which this was achieved.

3.2.4.1 Reduction method 1

Reduction of the catalyst was carried out in the LPD reactor where catalyst and inert bed were placed and heated up to 230°C with bubbling 20 ml.min⁻¹ 5% H₂/Ar and held for 2 hours with stirring. This was carried out at atmospheric pressure.

3.2.4.2 Reduction method 2

This was carried out on a glass line to ensure that reduction had occurred. Approximately 2 g portions of catalyst were reduced at any one time. Figure 3-6 shows the glass line set up:

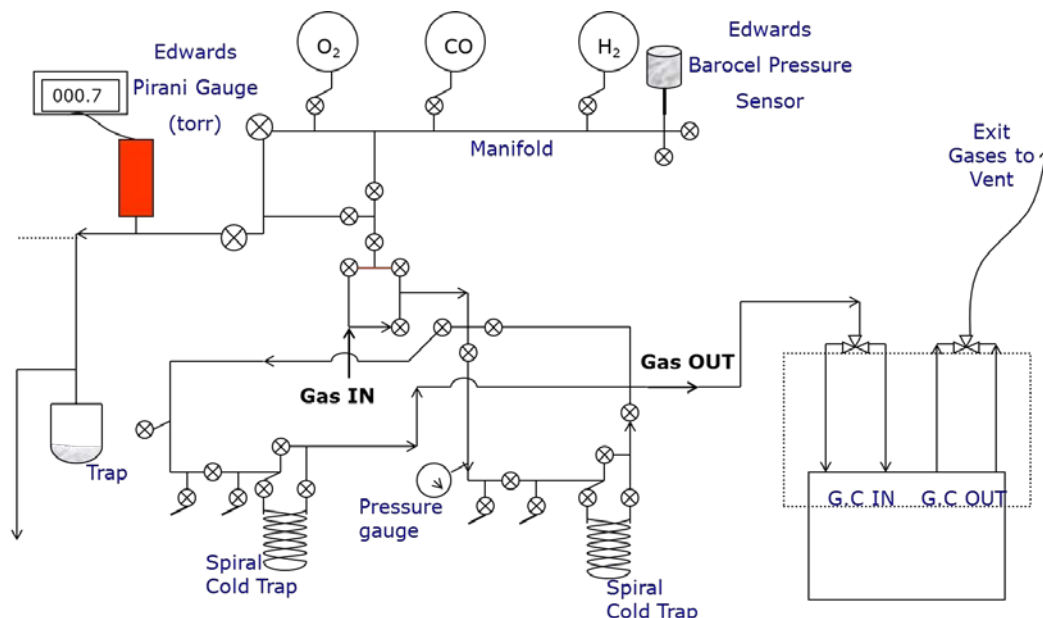


Figure 3-6 Glass line set-up for catalyst reduction

The catalyst was placed in the reactor and this was then connected to the glass line using wax to form a seal. Two thermocouples, one in the catalyst bed and one in the heater regulated and maintained the temperature. $25 \text{ ml} \cdot \text{min}^{-1}$ 5% H_2/N_2 was passed over the catalyst, the temperature ramped up to 270°C at a rate of 10 degCmin^{-1} and held for 3 hours. The gas was then switched to argon ($30 \text{ ml} \cdot \text{min}^{-1}$) and the catalyst allowed to cool. After this the reactor was sealed off, removed from the glass line and opened up in a N_2 glove box to avoid oxidation of the catalyst. The catalyst was placed in the reactor and a layer of inert bed was placed on top to avoid contact with air. The reactor was then removed from the glove box and set-up using the normal procedure.

3.2.4.2.1 Reduction method 3

Reduction of the catalyst was also carried out in a tube reactor. $25 \text{ ml} \cdot \text{min}^{-1}$ 5% H_2/Ar was flown over the catalyst at 270°C for 3 hours with a ramp of 10 degCmin^{-1} . Approximately 1 g of catalyst was reduced at a time. The reactor was then sealed off and placed in the glove box to avoid oxidation of the catalyst. The catalyst was placed in the reactor and a

layer of inert bed was placed on top to avoid contact with air. The reactor was then removed from the glove box and set-up using the normal procedure.

3.2.4.3 CuO/ZnO/Al₂O₃ catalyst

A commercial methanol synthesis catalyst was also used in the dehydrogenation studies. The typical weight percentage in a standard CuO/ZnO/Al₂O₃ catalyst is shown in table 15.

Table 15 Typical weight % of each component in copper methanol synthesis catalysts (72)

Component	Weight (%)
CuO	40-80
ZnO	10-30
Al ₂ O ₃	5-10

3.2.4.4 Copper/silica Preparation

10% Cu/SiO₂ catalyst was prepared in the laboratory using spray impregnation. To obtain a 10% loading of copper, 18.875 g of Cu(NO₃).3H₂O (99.5%, BDH Limited) was dissolved in 45 ml of water. The support used was silica beads (Caricat Q10 supplied from Fuji Sylisia) and to obtain an even coverage, they were placed in a tumbling bed. Table 16 shows the support properties. The copper solution was placed in an air driven spray gun and a continuous spray of solution was directed at the moving silica beads. Catalyst was allowed to dry out in an oven at approximately 100°C overnight to remove any water.

Table 16 Silica Q10 support properties

Surface area, m ² /g	300
Pore volume, ml/g	0.1
Average pore diameter (nm)	10

3.2.4.4.1 Calcination

To achieve the metallic oxide, the catalyst was placed in a glass calcination tube and glass wool was used as a plug at either end. The tube was then placed in the centre of a furnace. The catalyst was calcined at 250°C, ramp rate of 5 degCmin⁻¹ and held for 6 hours with flowing air and then allowed to cool to room temperature. To obtain the particle size required the catalyst was ground up using a mortar and pestle. This was then sieved to obtain a particle size of <250 µm.

3.2.4.4.2 Reduction

Reduction of the catalyst was carried out using the glass line set up described in section 3.2.4.2. 2.5 g portions of catalyst were reduced at any one time. This was carried out by heating the reactor to 250°C, 10 degC⁻¹ min ramp rate with 25 ml.min⁻¹ flowing 5% H₂/N₂ and held for 3 hours. Catalyst was then removed from reactor in a N₂ glove box to avoid oxidation of catalyst.

3.2.5 Extraction methods

Spent catalysts were supplied by Innospec. They were taken from the lilestralis production plant, Widnes at three different stages in the reaction. The catalysts came suspended in the inert bed. To obtain catalyst samples they had to be extracted from this suspension. Two extraction methods were employed using centrifuging.

3.2.5.1 Centrifugation

3.2.5.1.1 Method 1

To separate the catalyst from the suspension material the catalyst was centrifuged. The samples are spun at high rotation speeds and high centrifugal force. A MSE Centraur 2E was used to carry out this procedure. Samples were spun at a speed of 5000 rev/min until separation had occurred. Catalyst material formed a black solid in the bottom of the tube

3.2.5.1.2 Method 2

This method involved centrifuging with acetone to allow easier separation and reduce viscosity. The oil layer was continually removed and replaced with acetone. This was carried out to try and remove the entire oil layer. Black catalyst was produced in the bottom of the centrifuge tube with just enough acetone to cover it to avoid oxidation.

3.2.6 Air sensitive XRD

Air sensitive XRD was used to produce XRD patterns of material that had not been exposed to air and allowed to oxidise.

3.2.6.1 Preparation of samples

Using catalyst samples produced from extraction method 2, XRD samples were prepared in an inert atmosphere to avoid oxidation of the catalyst. The catalyst in acetone was placed in a glass line reactor tube and then sealed off. The reactor was attached to the glass line and the connections sealed with wax to prevent exposure to air. A flow of argon was passed through the glass line for 30 minutes to remove trace air before the reactor tube valves were opened and the argon flow passed over the sample. To evaporate off the acetone the reactor was heated to 56°C using a tubular furnace and held for 2 hours in flowing Ar. To remove any remaining oil on the catalyst the sample was then heated to 260°C for 1 hour. After this a dry solid catalyst was visible in the reactor. The reactor was then sealed off under inert atmosphere and placed in an N₂ atmosphere glove box. Catalyst was removed from the reactor and placed in a 0.5 mm capillary. This was then sealed under inert gas and XRD was carried out.

3.2.7 Lewis acid site determination

Testing of the catalysts to determine number of Lewis acid sites was carried out on the glass line. 0.5 g of copper chromite was placed into the reactor and reduced with 90 ml.min⁻¹ of flowing 5% H₂/N₂ at 270°C for 3 hours. The flow was then switched to Ar and the catalyst allowed to cool in of flowing argon (90 ml.min⁻¹). Pyridine was then introduced into the system via a bubbler. The vapour was passed over the catalyst for 3 hours until saturation had occurred. At this stage the pyridine bubbler was by-passed and physisorbed pyridine was removed by flowing argon. Chemisorbed pyridine was then removed by ramping the temperature to 230°C at a rate of 10 degCmin⁻¹. Mass spectrometry was used for analysis. The mass fragments of pyridine were followed during the desorption (m/z = 52,79).

3.2.8 Calibrations

Calibrations were carried out to calculate the number of moles produced in each reaction. Due to the viscosity of the materials, calibrations were carried out using weight rather than volume. To obtain a total weight of material produced each sample flask was weighed before and after reaction, and hence weight of material could be calculated.

Calibrations for both p-LOL and p-LAL were carried out. Different known weights of each material were dissolved in 1.5 ml of acetone and ran through the GC. Each weight produced a different peak area (figure 3-7 and 3-8). From the weights used, the concentration for each sample could be calculated and plotted against the corresponding peak area. The number of moles and concentration could be calculated and related to this peak area.

A known weight was then taken from the reaction samples and dissolved in 1.5 ml acetone. This produced a peak area for the amount of p-LOL and p-LAL in the sample. Using the graph the weight of component could be attained.

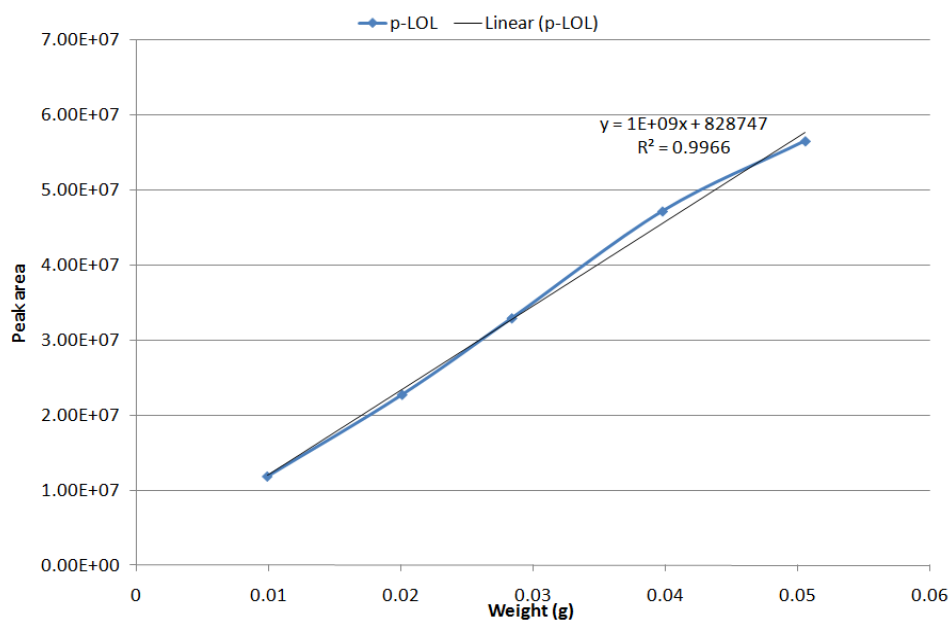


Figure 3-7 p-LOL weight calibration

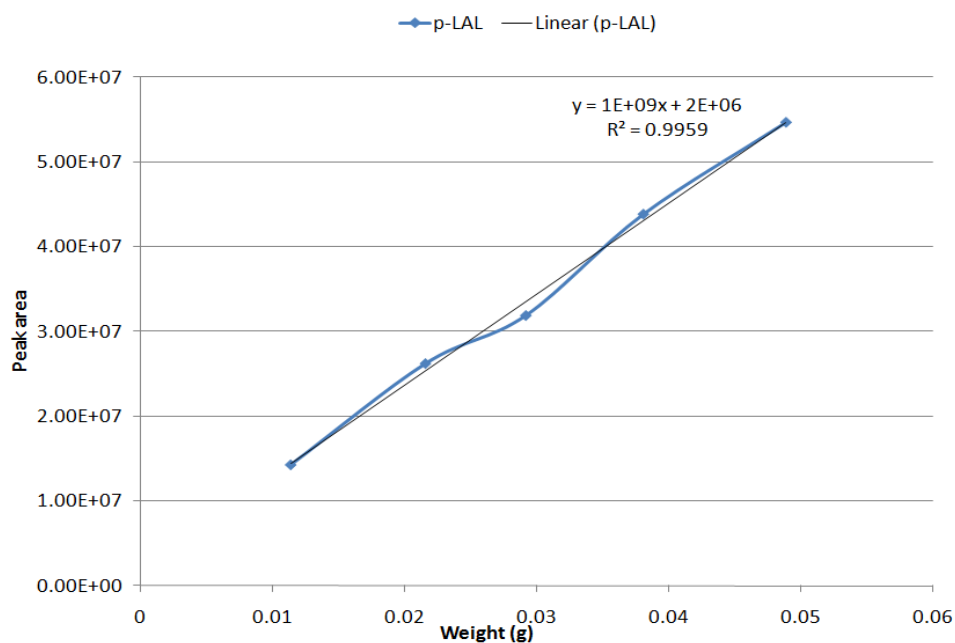


Figure 3-8 p-LAL weight calibration

From the weight of both p-LAL and p-LOL the concentration of the both could be obtained using figures 3-9 and 3-10. From this concentration, the number of moles in the known

weight of sample analysed could be calculated. This was then used to work out the total number of moles produced in the whole sample.

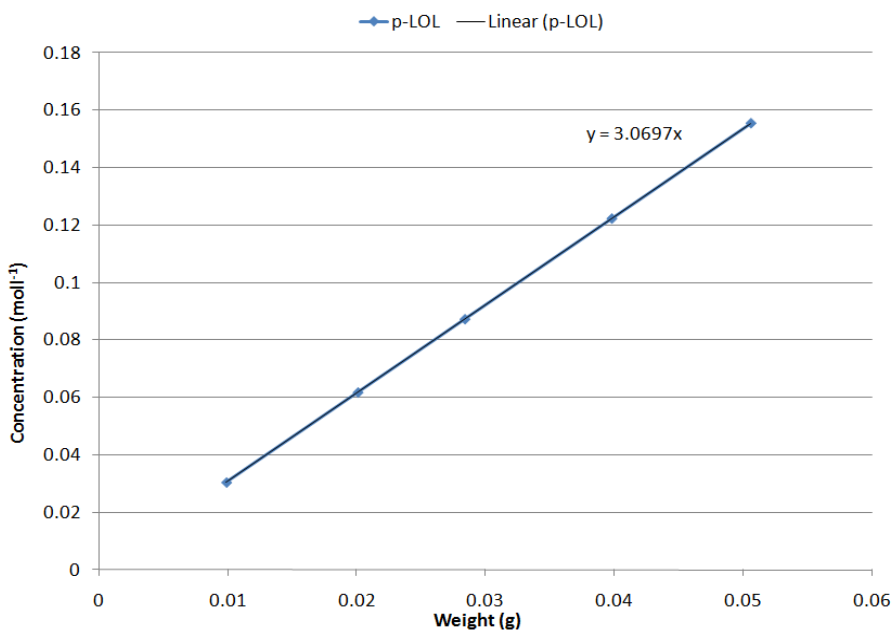


Figure 3-9 p-LOL concentration calibration

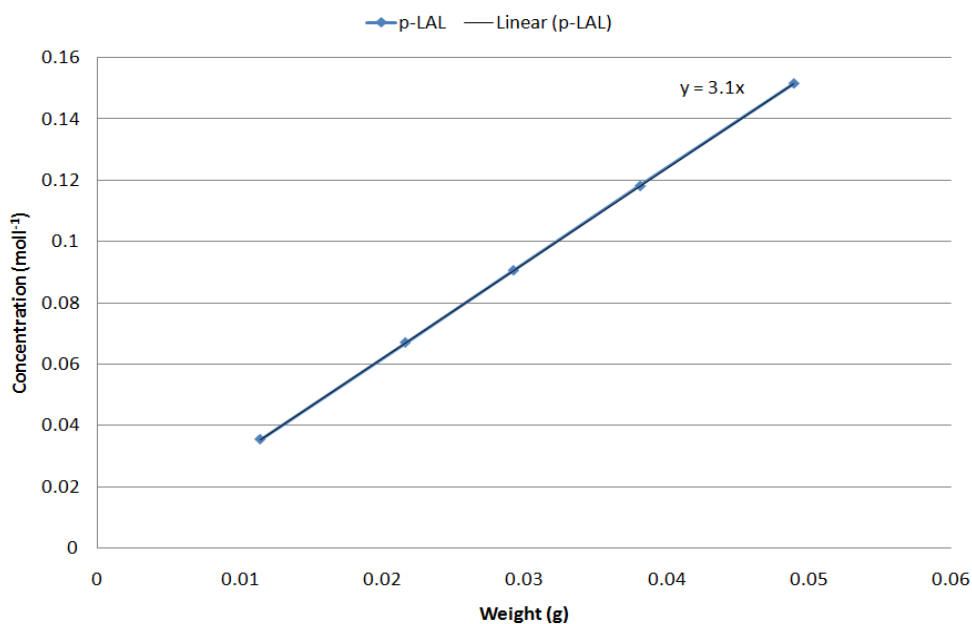


Figure 3-10 p-LAL concentration calibration

3.2.9 Product analysis

During the reaction many by-products were produced. In any one trace approximately 120 peaks were detected. All of the reaction data was studied and it was decided that only the most abundant by-product peaks and starting material peaks would be studied. The peaks chosen for analysis were those with retention times of: 4.6, 4.71, 7.02, 7.21, 7.53, 7.7, 8.19, 9.13, 10.94, 11.1, 11.94, 12.7, 13.46, 14.3, and 16.03.

3.2.9.1 GC-MS

GC-MS analysis was carried out at Widnes to obtain structures for some of the possible compounds in the samples. This was carried out on a HP 6890A Gas Chromatograph System equipped with HP7683A Series Autosampler and Agilent Technologies 5973 Network Mass Selective Detector

3.2.9.2 GC conditions

Temperature program: Starting temperature: 60°C final temperature: 240°C at a ramp rate of 3°C/ min.

Run time: 60 mins

Column Flow: 1 ml.min⁻¹ He

Column: HP 5MS 0.25 mm i.d. x 30 m x 0.25 µm thickness

Injection: 0.1 mm (4 drops in 2 mls acetone)

3.2.9.3 Mass spectrometry conditions

EM Voltage 506

Scanning range 15 – 550

Scans / second 2.76

3.2.9.4 Analysis

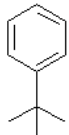
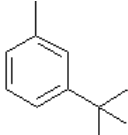
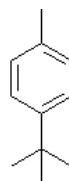
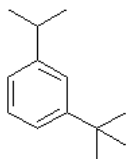
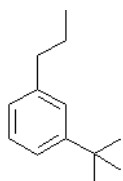
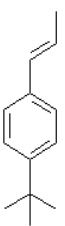
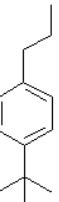
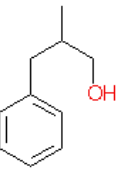
Various samples containing a large variety of materials were analysed. However most of the compounds in the samples were not available in the mass spectrometry library. To gain information on each compound the mass spec fragmentation pattern was obtained for each sample. From this pattern, structures could be worked out by deriving all the possible fragments present. To distinguish between isopropyl and propyl groups the patterns of isopropyl benzene and propyl benzene were studied to look at the

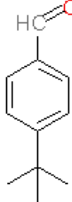
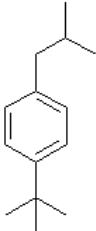
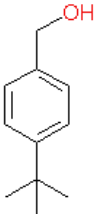
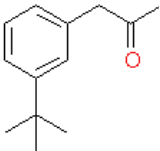
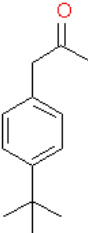
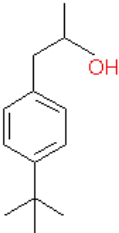
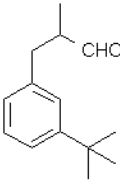
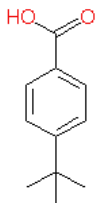
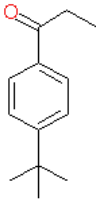
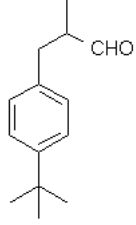
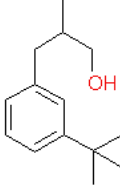
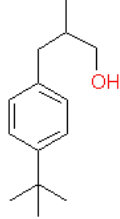
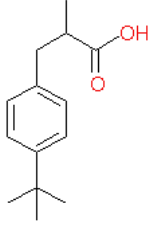
differences. Propyl benzene has major fragments at m/z : 120, 91 and 78 where as isopropyl benzene m/z : 120, 105, 91 and 77. This allowed any similar species to be identified due to the difference in the patterns.

3.2.9.5 Products obtained

From the mass spec data all of the following compounds could be attained as shown in table 17.

Table 17 Possible products

RT (min)	Name	Structure	RT (min)	Name	Structure
3.35	tert-butylbenzene		4.5	1-tert-butyl-3-methyl-benzene	
4.7	1-tert-butyl-4-methyl-benzene		7.02	1-tert-butyl-3-isopropyl-benzene	
7.20	1-tert-butyl-3-propyl-benzene		7.5	1-tert-butyl-4-prop-1-enyl-benzene	
7.7	1-tert-butyl-4-propyl-benzene		8.08	2-methyl-3-phenyl-1-propan-1-ol	

8.18	4-tert-butyl benzaldehyde		8.51	1-tert-butyl-4- isobutylbenzene	
9.12	(4-tert- butylphenyl) methanol		9.4	1-(3-tert- butylphenyl)prop an-2-one	
10.92	1-(4-tert- butylphenyl)prop an-2-one		11.1	3-(4-tert- butylphenyl)-1- methyl-propan- 1-ol	
11.935	3-(3-tert- butylphenyl)-2- methyl-propanal (m-LAL)		12.15	4-tert- butylbenzoic acid	
12.39	1-(4-tert- butylphenyl)prop an-1-one		12.7	3-(4-tert- butylphenyl)-2- methyl-propanal (p-LAL)	
13.4	3-(3-tert- butylphenyl)-2- methyl-propan- 1-ol (m-LOL)		14.3	3-(4-tert- butylphenyl)-2- methyl-propan- 1-ol (p-LOL)	
16.03	3-(4-tert- butylphenyl)-2- methyl- propanoic acid (LAL acid)				

3.2.10 Materials

All of the reactants used were supplied from Innospec. The table below shows all materials used in reactions and reductions.

Table 18 Material suppliers and purity

Material	Purity	Supplier
Lilol	95%	Innospec
Lilestralis	95%	Innospec
Inert bed	unknown	Innospec
Ethanol (absolute)	99.99%	Fischer Scientific
Acetone	100%	BDH Limited
Nitrogen Gas (oxygen free)	99.998%	BOC gases
5% H ₂ /Ar		BOC gases
Argon		BOC gases
5% H ₂ /N ₂		BOC gases

3.2.11 Calculations

Conversion = (total product peak area / total material peak area) x 100

Selectivity = (peak area of product/ total peak area) x 100

3.3 Results & discussion

3.3.1 Catalyst characterisation

3.3.1.1 Spent catalyst

Spent copper chromite catalysts supplied from Innospec were analysed. The catalysts were taken from the industrial plant in which lilestralis was produced. Three samples were taken from the industrial reactor pot at the beginning of reaction, before shutdown and after shutdown respectively and were designated high, low and minimal activity. The catalysts provided were suspended in inert bed, which is composed principally of lillol liliate. To separate the catalyst from the suspension material the catalysts were centrifuged using method 1. High activity catalyst centrifuged well due to the low viscosity. However both low and minimal activity did not centrifuge well due to the increase in viscosity of the inert bed. The oil layer that was obtained above the catalyst was sent for CHN analysis.

3.3.1.1.1 CHN analysis

CHN analysis was carried out on the three oil samples obtained. Table 19 shows the results

Table 19 CHN analysis results for spent Innospec catalysts

	C (%)	H (%)	N (%)	O (%)
High activity	83.57	9.99	0	6.44
Low Activity	83.64	10.03	0	6.32
Minimal Activity	82.24	9.48	0	8.28

Results from the three samples produced almost identical percentage compositions. All of the samples produced a ratio of $C_7H_{10}O_{0.5}$ which when doubled produces $C_{14}H_{20}O$. This was the formula for lilestralis which was the product in the reaction. When $C_{14}H_{20}O$ is doubled again this produced $C_{28}H_{40}O_2$. The formula obtained was the same as that of lillial liliate which is the main component of the inert bed.

3.3.1.1.2 Air sensitive XRD

To produce viable samples for XRD from the spent catalyst extraction method 2 was used. Air sensitive XRD was carried out to produce the diffraction patterns of spent catalysts that had not been allowed to oxidise. Both high and low activity catalysts were analysed using this method.

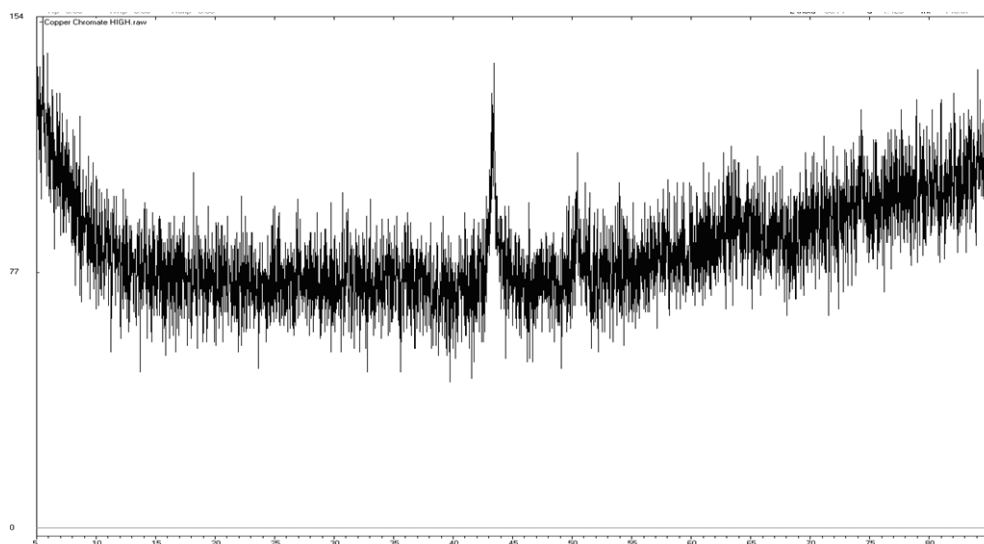


Figure 3-11 XRD pattern spent high activity catalyst from production plant

Figure 3-11 shows that peaks corresponding to Cu^0 are present in the sample at approximately 45, 50 and 60°, suggesting that the catalyst had been reduced slightly.

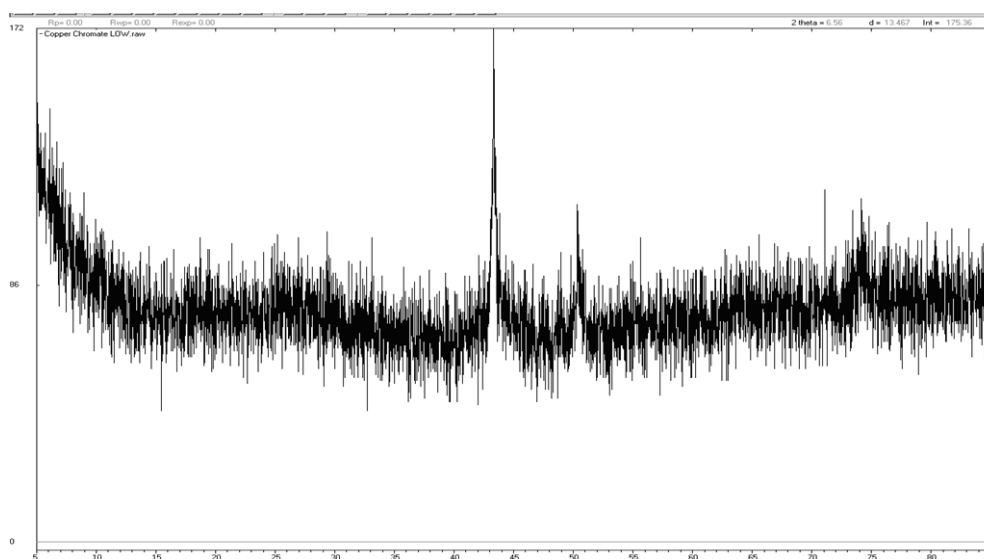


Figure 3-12 XRD pattern of spent low activity catalyst from production plant

Figure 3-12 shows that once again there are peaks corresponding to Cu^0 in the sample. However the peaks are slightly larger suggesting that more of the catalyst has been reduced. Figure 3-13 shows the difference in the samples more clearly.

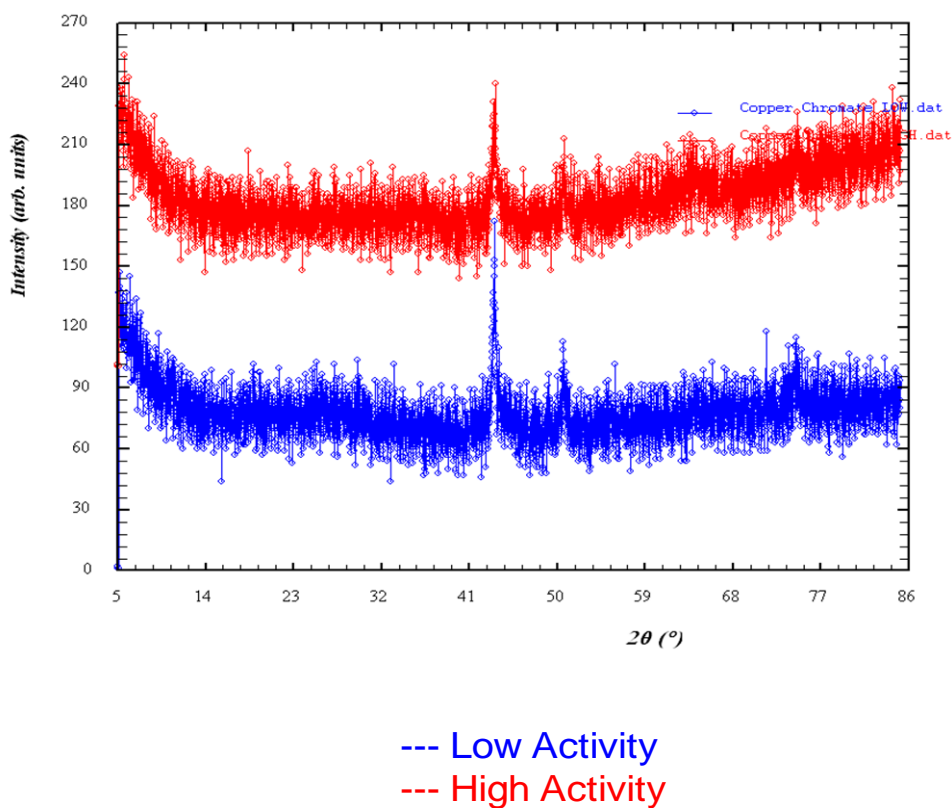


Figure 3-13 XRD pattern of spent low and high activity catalyst from production plant

Figure 3-13 clearly illustrates that the low activity catalyst contained more intense metallic copper peaks than the high activity, suggesting that the catalyst was in a more reduced state. Prior to plant start up the catalyst was not reduced. When the reaction was started the catalyst starts to reduce and hence in the XRD of the high activity catalyst, metallic copper peaks appear. During the reaction the catalyst has continued to slowly activate and hence the copper peaks are more prominent and larger.

3.3.1.1.3 Temperature programmed oxidation (TPO)

The catalyst samples that were obtained from extraction method 2 were also used to carry out TPO. Oxygen uptake was the point of interest in this analysis. Samples were analysed up to 500°C in 100 ml.min⁻¹ 2% O₂/Ar with a ramp rate of 10 degC.min⁻¹.

3.3.1.1.4 High activity Catalyst

TPO of high activity was carried out as shown in figure 3-14

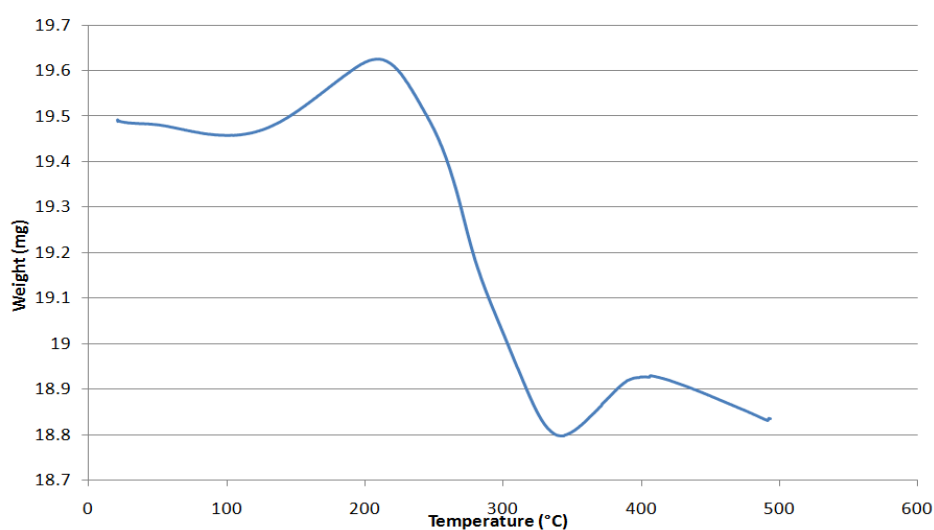


Figure 3-14 TPO high activity spent catalyst (30-1000°C, 10 degC.min⁻¹, 2% O₂/Ar)

As show, at approximately 100°C copper starts to reoxidise and a weight gain is observed. After 200°C a decrease in weight was shown suggesting that any remaining organic material was starting to oxidise off the catalyst surface. However at this point both copper oxidation and the oxidation of organic material was occurring. Burning of the organics however was more favourable and hence a decrease was observed. After this had taken place, copper oxidation was more favourable again and an increase in weight was shown at 335°C.

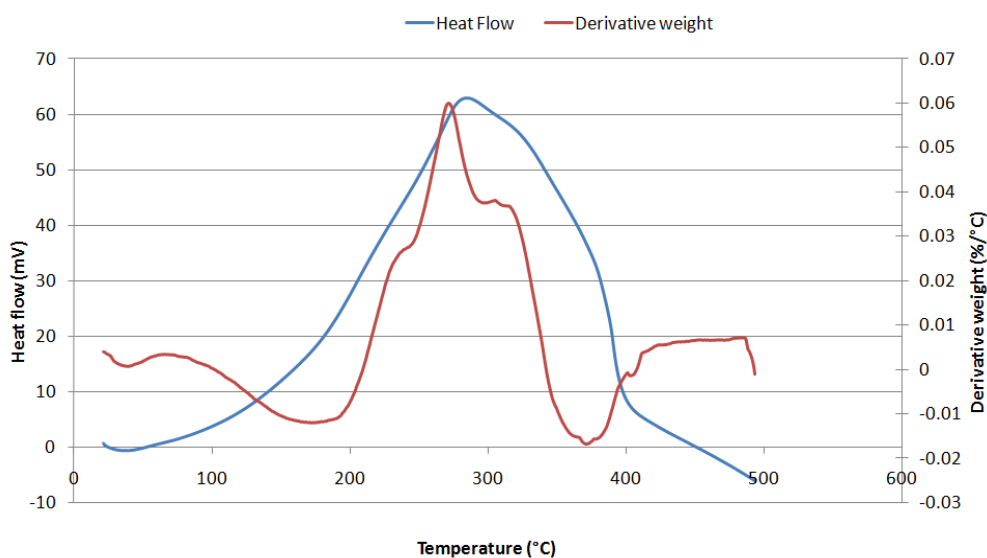


Figure 3-15 TPO derivative weight and heat profile for high activity catalyst (30-1000°C, 10 degC.min⁻¹, 2% O₂/Ar)

It can be seen from figure 3-15 that this was a highly exothermic process. The burning of the carbon occurs in several stages suggesting that there was more than one type of carbon species present. The species of carbon cannot be identified as it will burn off the surface to produce CO₂.

3.3.1.1.5 Low activity catalyst

Low activity catalyst was analysed as a comparison to the high activity in terms of oxidation.

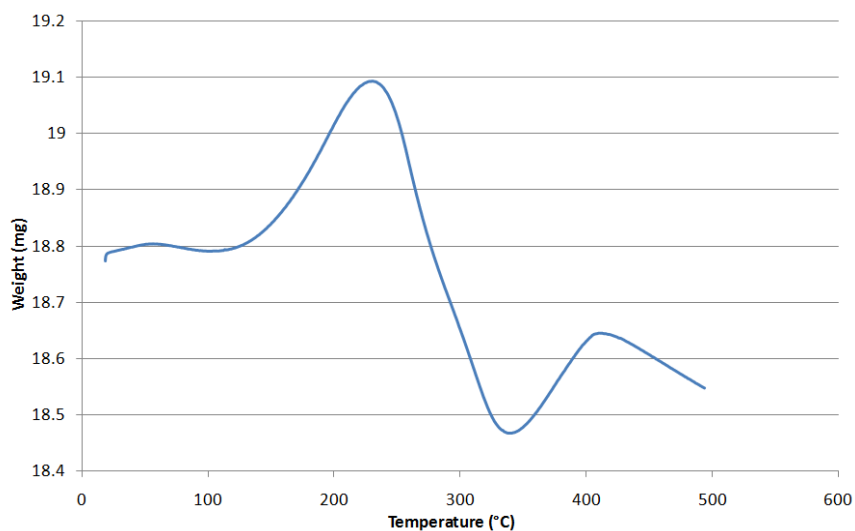


Figure 3-16 TPO Low activity spent catalyst profile (30-1000°C, 10 degC.min⁻¹, 2% O₂/Ar)

As shown in figure 3-16 the low activity catalyst has a similar profile to the high activity. Burning of organics however occurred at a higher temperature due to the increase in viscosity of the catalyst slurry.

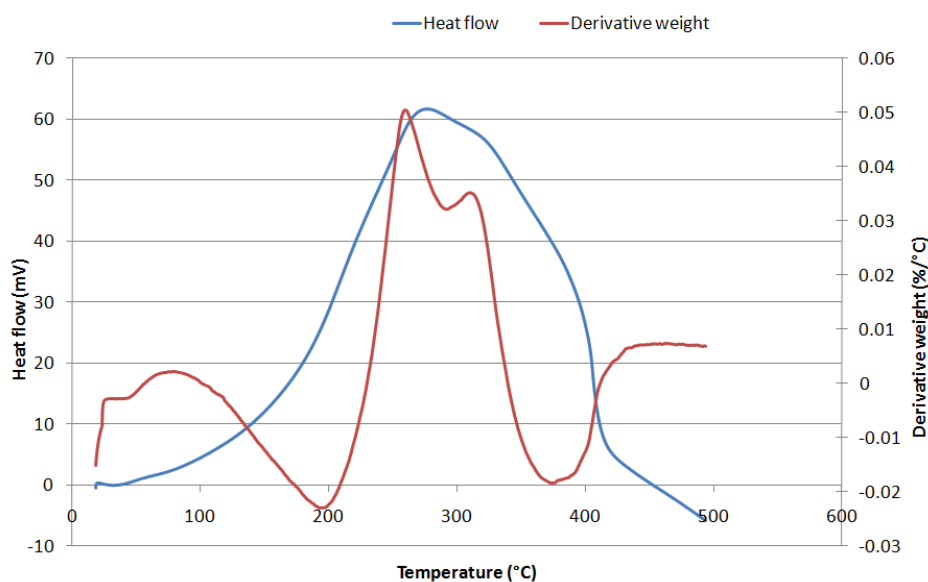


Figure 3-17 TPO derivative weight and heat profile for low activity catalyst (30-1000°C, 10 degC.min⁻¹, 2% O₂/Ar)

It can be seen that more than one species of organic was present. It too was also an exothermic process.

It can be noticed by the thermal analysis that organic material was still present on the catalyst surface as a consequence of the reaction being carried out in a slurry reactor.

Christopher *et al* (109) suggested that the oxidation of metallic copper always leads initially to the formation of Cu_2O followed on by CuO and that the oxidation of the latter does not take place until the oxidation of Cu_2O was completed. Work carried out on metallic copper by Lupu (110) also reported a similar trend. As shown in figure 3-18 the oxidation of metallic copper starts at approximately 100°C and ends at $600\text{--}700^\circ\text{C}$.

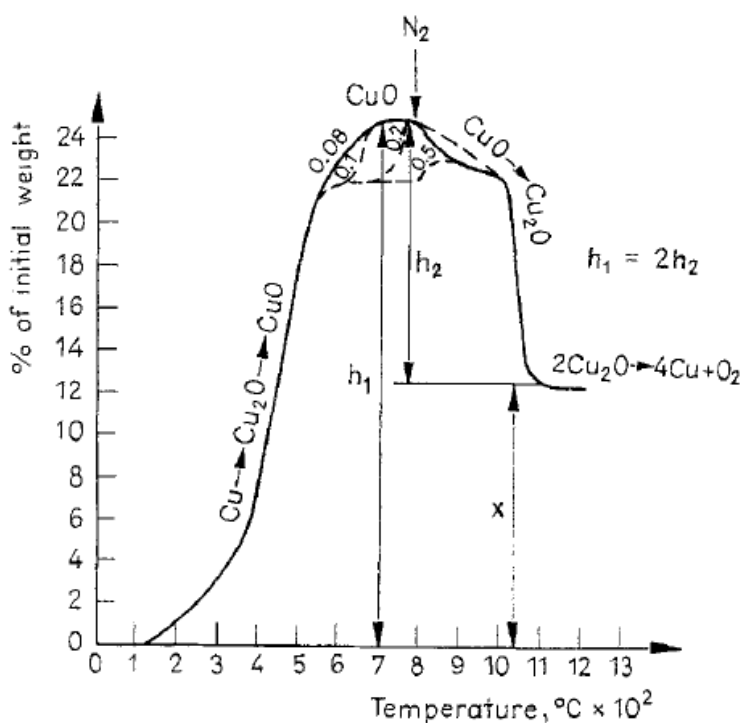


Figure 3-18 TG of metallic copper (ramp rate 5degCmin^{-1}) (110)

Both TPO analyses in the current study also suggested that oxidation of metallic copper started at approximately 100°C and was still continuing at 500°C . However slight variations may occur as the data reported in the literature was tested on pure metallic copper where as the samples analysed in figure 3-16 and 3-17 are copper chromite catalysts.

In the case of copper chromite, Plyasova *et al* (111) studied the reduction-reoxidation process of copper chromite and reported that rapid oxidation of metallic copper on the surface ($2\text{Cu}^0 + \text{O}_2 \rightarrow 2\text{CuO}$) occurred first. Subsequently copper ions do not return into the spinel structure and cation-deficient spinel passes into CuCrO_2 (111, 112). In this case Cu^+ was not oxidised first due to its location in the tetrahedral holes within the spinel structure. Therefore Cu^0 on the surface was reported to be oxidised primarily to Cu_2O and/ or CuO (111).

Shreiber *et al* (113) reported work on the dehydrogenation of methanol over a copper chromite catalyst using a slurry reactor and found that if the catalyst was not washed properly with acetone residual slurry material was responsible for the loss in surface area when carrying out a BET (113). In our study this residual material represents that primary loss of weight during the TPO and due to this the oxidation of copper chromite may differ slightly from fresh catalyst reduction-oxidation processes. A higher temperature may be required to oxidise the catalyst as the residual material may have to be “burned off” first to expose the metallic sites of the catalyst before oxidation can occur.

3.3.1.2 Fresh catalyst

Analysis was carried out on fresh copper chromite catalyst to study the reduction and oxidation processes.

3.3.1.2.1 Hot Stage XRD

Hot stage XRD was carried out to investigate how the catalyst reduces with respect to metallic copper peaks. Figure 3-19 shows the hot stage XRD that was carried out in 5% H_2/N_2 .

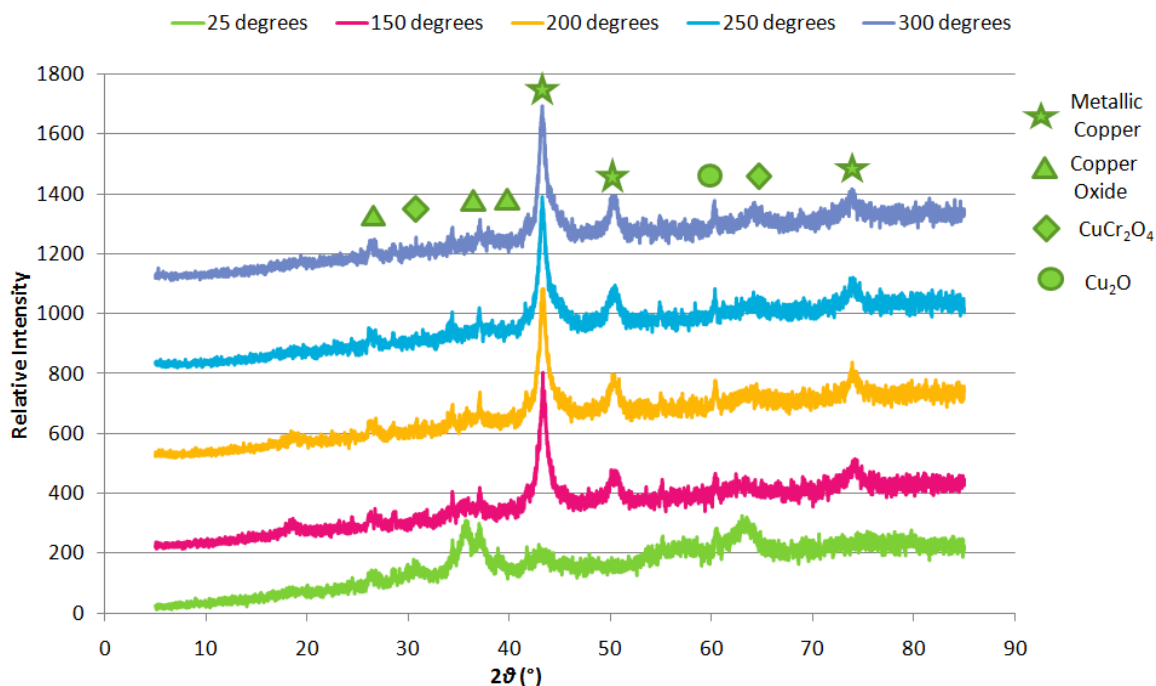


Figure 3-19 Hot stage XRD of fresh BASF copper chromite catalyst, carried out under 5% H_2/N_2 atmosphere. Scans recorded at 25°C, 150°C, 200°C, 250°C and 300°C

It can be noticed from the XRD pattern at 25°C that copper oxide (35.6°, 38.8° and 48.7°) and CuCr_2O_4 (30.4°, 35.6° and 63.2°) are present (114). When increasing the temperature metallic copper features more apparent suggesting that the catalyst was reducing. Peaks at 43, 51 and 73° are characteristic of metallic copper (115). However there are also small peaks for Cu_2O (36.4°, 42.2° and 60.5°) suggesting that Cu^+ may also be present (116). At 300°C some copper oxide was still present suggesting that not all the copper oxide was being reduced.

3.3.1.2.2 Scherrer equation

The Scherrer equation was used to calculate the crystallite size from the main metallic copper peak at increasing temperatures. It was found that at all temperatures between 150°C- 300°C the crystallite size was 10 nm. Yuan-Jen Tu *et al* (106) also reported reduced copper particles with a crystalline size of 110 Å.

3.3.1.2.3 BET analysis

BET analysis was carried out to look at the surface area.

Table 20 BET analysis Copper chromite

Catalyst	Surface Area (m ² / g)	Pore Diameter (Å)
Copper chromite	32	283

3.3.1.2.4 Temperature programmed Reduction (TPR)

TPR was carried out to look at the reduction stages of fresh copper chromite. It was studied up to 500°C in 5% H₂/N₂ at a ramp of 10 degC.min⁻¹.

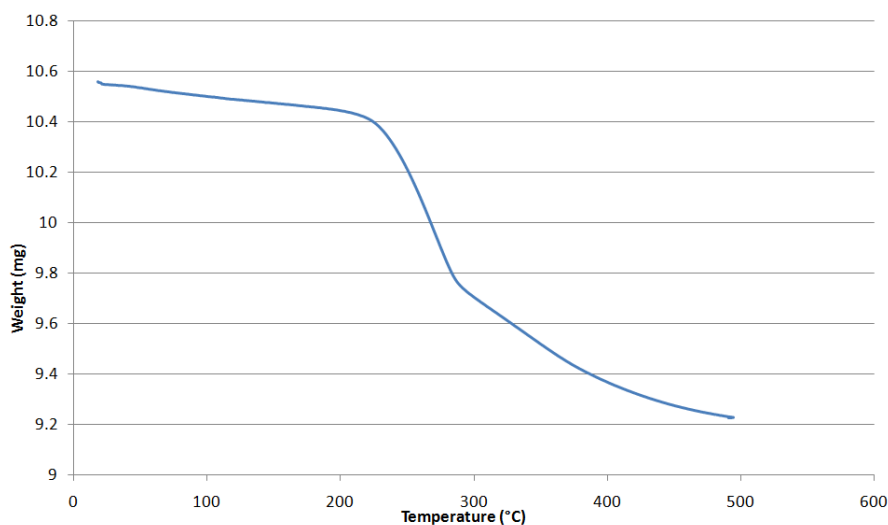


Figure 3-20 TPR fresh copper chromite weight loss profile (30-500°C, 5%H₂/N₂, ramp rate of 10 degC.min⁻¹)

It can be seen from figure 3-20 that there was a change in weight due to the copper reducing. Oxygen would be released in the form of water when the oxide was converted into the metal. This is known to be an autocatalytic process, which was mediated by dissociative hydrogen adsorption on the released Cu⁰ atoms (117). There are two reduction bands in this process as illustrated clearly in figure 3-20. The major weight loss occurs at 274°C and the minor starts at 350°C. Figure 3-21 shows this more clearly. The

first weight loss was attributed to the reduction of CuO to Cu metal. The second, more gradual weight loss was due to the reduction of copper in the spinel to metallic copper (117).

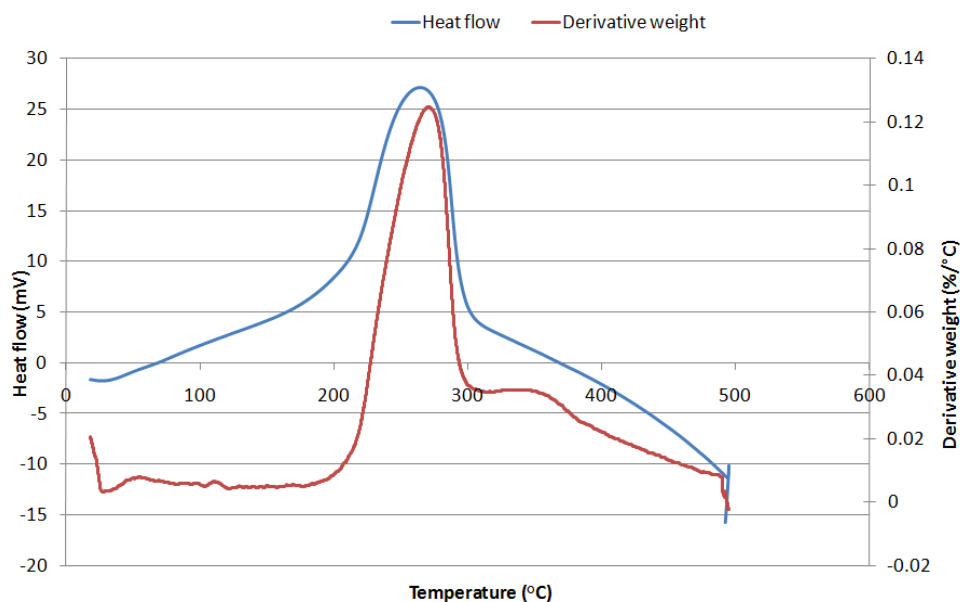


Figure 3-21 TPR derivative weight and heat profile fresh copper chromite (30-500°C, 5% H_2/N_2 , ramp rate of 10 degC.min $^{-1}$)

During the reduction of the copper chromite, various changes occur within the spinel. Firstly oxygen on the surface reacts with hydrogen to yield water and reduced copper metal (Cu^0 or Cu^+) on the chromite surface. Due to these copper species, a homolytic rupture of the bond within a hydrogen molecule occurs. These hydrogen atoms then penetrate into the free octahedral holes and copper containing tetrahedral positions. Protons are generated in the tetrahedral positions due to an exchange interaction between the copper ions and hydrogen atoms. Cu^0 is the released onto the surface of the spinel after interacting with two hydrogen atoms where they form a flat build-up of particles bonded epitaxially to the spinel. When only one hydrogen atom reacts with the copper ions, Cu^+ is formed and moves towards the tetrahedral holes (118). Figure 3-22 shows a schematic of this process.

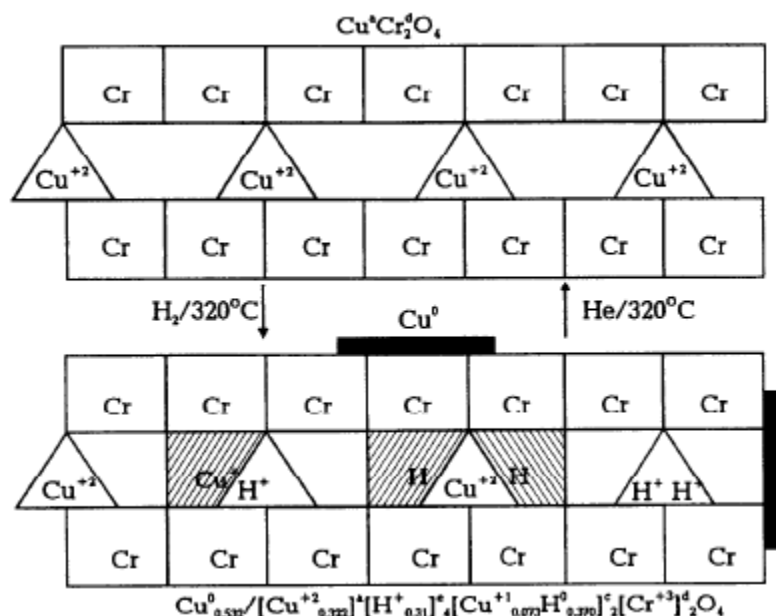
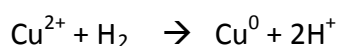


Figure 3-22 The scheme of the reversible reduction of copper chromite. Triangles indicate (a) tetrahedral positions; squares indicate (d) octahedral positions; hatched areas indicate (c) octahedral positions (119)

Previous work carried out by Khassin *et al* (120) suggested that when the reduction of copper chromite was carried out using a hydrogen pressure of 7-800 Pa, the amount of water produced was much less than the amount of hydrogen consumed for the copper reduction. For example in the initial step (reduction of less than 1.5 monolayers of copper chromite), the amount of water makes up only 40% of reacted hydrogen and this percentage decreases significantly with deeper reductions (reduction of more than 7 monolayers, 4% of hydrogen react with copper chromite to yield water) (120). This was thought to proceed via the following redox mechanism



Copper cations react with the hydrogen which is then absorbed in the oxidised state (protons) by the oxide structure (120). Thermal analysis carried out by Khassin *et al* (120) suggested that in the range of 250-400°C there is a weight gain of the sample (approximately +0.3-/+0.7%) due to this absorption. However this does not correspond to the data obtained in this study as copper oxide was also present (29% wt). The reduction of copper oxide occurs at the same temperature as the weight gain would appear and hence is masked by the large reduction weight loss.

3.3.1.2.5 Reduction- reoxidation process

To examine the reduction- reoxidation process a series of thermal analysis measurements were carried out. The catalyst was firstly subjected to a reducing environment (5% H₂/N₂, final temperature 500°C) where CuO was converted to Cu. After this the catalyst was cooled and left to stabilise for 20 minutes in argon before being exposed to an oxidising atmosphere (5% O₂/Ar, 500°C). The catalyst was once again cooled and stabilised in argon. This whole process was repeated three times to investigate the reduction/oxidation profile of the copper oxide.

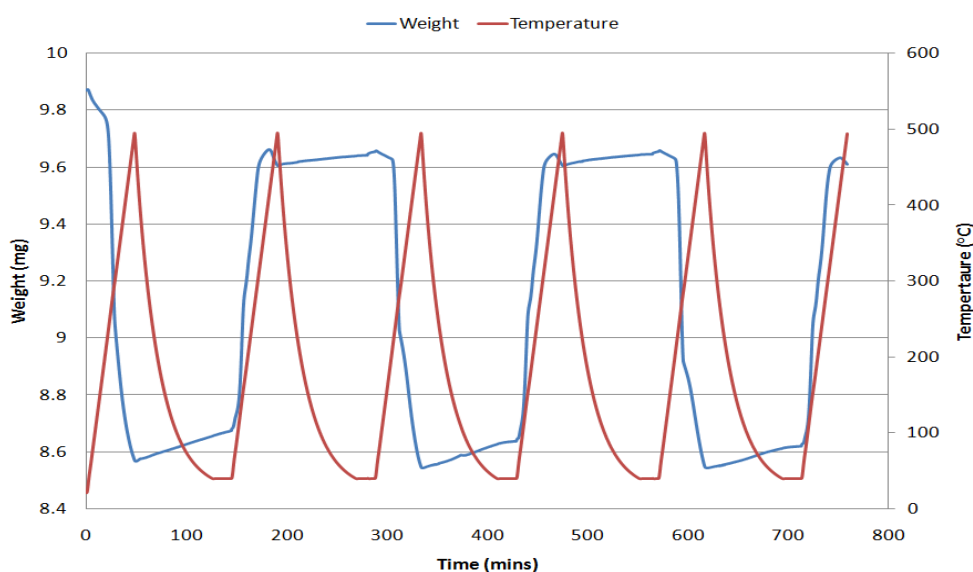


Figure 3-23 TPR-TPO process of copper chromite a) Reduction: 30-500°C, 5%H₂/N₂, ramp rate of 10 degC.min⁻¹ then allowed to stabilise in Argon for 20minutes b) Oxidation: 30-500°C, 2% O₂/Ar, ramp rate of 10 degC.min⁻¹ then allowed to stabilise in Argon for 20minutes

As shown in figure 3-23 the first reduction that occurs was the largest and when the catalyst undergoes oxidation it does not return to its initial weight. There are two explanations as to why the initial weight loss was larger than in the subsequent reductions. Firstly, physisorbed water was present on the catalyst surface and was removed during the first reduction. Secondly, more copper was reduced during the first reduction than in the subsequent reductions. Plyasova *et al* (111) studied the reduction-reoxidation process of copper chromite and reported that rapid oxidation of metallic copper ($2\text{Cu}^0 + \text{O}_2 \rightarrow 2\text{CuO}$) occurred. Subsequently copper ions do not return into the spinel structure and cation-deficient spinel passes into CuCrO₂ (111, 112).

As shown in figure 3-24 the first reduction occurs at approximately 220°C. This was the reduction of CuO to Cu⁰. The second reduction, which starts at 300°C, was thought to be the reduction of the spinel. The reduction was an exothermic process as shown in the equation below (103)

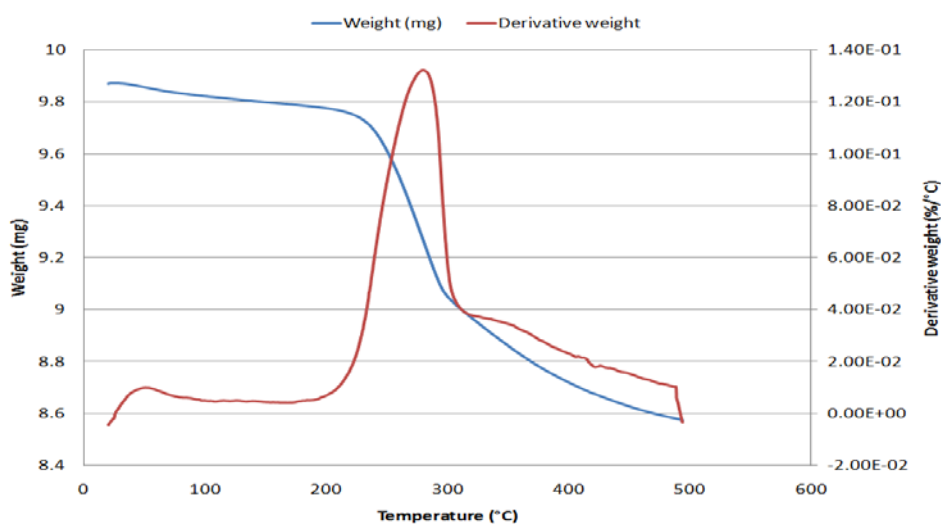
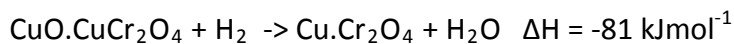


Figure 3-24 TPR weight and derivative weight profile from 1st reduction in reduction/oxidation process of fresh copper chromite (30-500°C, 5% H₂/N₂, ramp rate of 10 degC.min⁻¹)

Lee *et al* (114) also studied copper chromite in terms of thermal analysis using similar conditions (ramp: 7.5 degC.min⁻¹, 4% H₂/N₂) and the TPR data obtained was almost identical to the data observed in this study. Figure 3-25 illustrates this. Both samples lose approximately 14% of the initial weight of the sample during analysis (114).

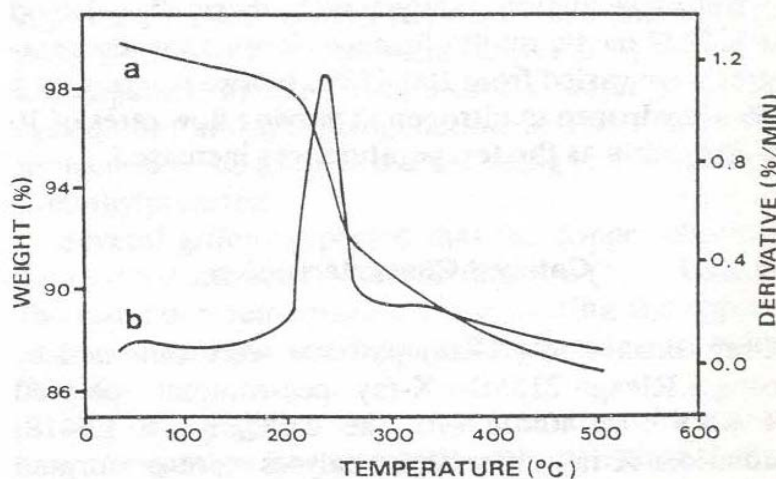


Figure 1. Thermogravimetric spectra of fresh copperchromite catalyst: (a) weight loss denoted in %, and (b) differential weight loss.

Figure 3-25 Thermal analysis of copper chromite comparison (114)

The data from the TPR was used to calculate how much copper was being reduced in the 1st reduction of the catalyst. The composition for this catalyst is: 29% CuO and 71% CuCr₂O₄.

Starting weight of sample: 0.009773976 g

End weight of sample: 0.00858836 g

Weight lost: 0.001185616 g

Weight lost attributed to oxygen: $0.001185616/32 = 3.705 \times 10^{-5}$ moles of O₂

Therefore 7.4101×10^{-5} moles of water were produced

To determine how much water would be produced if all the copper oxide and copper chromite in the sample was reduced to Cu⁰ the following calculation was performed:



Starting weight of sample: 0.009773976 g

29% CuO: 0.00283445 g = 3.565×10^{-5} moles of CuO

71% CuCr₂O₄: 0.00693952 g = 2.998×10^{-5} moles of CuCr₂O₄

Total moles of Cu in sample: 6.563×10^{-5} moles

Moles of water produced: 6.563×10^{-5} moles

Moles of oxygen: 3.282×10^{-5} moles

From this calculation it was evident that the number of moles of oxygen removed in the reduction was greater than what was required to reduce all the copper in the sample. This suggested that chromium was also being reduced. Previous work carried out by Khasin *et al* and Yurieva *et al* suggested that when reduction of copper chromite was carried out between 200-400°C, approximately 60% of Cu(II) atoms of copper chromite transformed to metallic copper (118, 121). It can be assumed that all of the CuO will reduce to Cu⁰. However from previous work in the literature it was suggested that only 60% of the copper chromite spinel would be reduced. From this the following assumption could be made:

29% CuO: 3.565×10^{-5} moles

60% of the 71% CuCr₂O₄ present in the sample: 1.798×10^{-5} moles

Total number of moles of Cu in sample reduced: 5.363×10^{-5} moles

Moles of oxygen required: 2.682×10^{-5} moles

From the previous calculation it can once again be observed that the number of moles of oxygen required was considerably lower.

Oxygen removed in actual TPR: 3.705×10^{-5} moles

Oxygen removal required to reduce copper in sample: 2.682×10^{-5} moles

Difference in oxygen: 1.023×10^{-5} moles

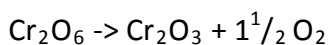
The excess of oxygen could be attributed to the reduction of chromium. The catalyst was thought to contain 0.5-2% Chromium (VI) compounds. Chromium (VI) is a strong oxidising agent and therefore would be susceptible to reduction to chromium (III). This could account for the excess of oxygen removed during reduction.

If it was assumed that 2% of the sample was Cr(VI) compounds and in the form of chromium (VI) oxide (CrO₃), then:

Starting weight of sample: 0.009773976 g

Weight of 2% Cr₂O₆ (CrO₃): 0.000195479 g

Moles of potentially Cr₂O₆ available: 9.77×10^{-7} moles



If all of the chromium (VI) was reduced to chromium (III) then 1.466×10^{-6} moles of oxygen would be removed from the catalyst.

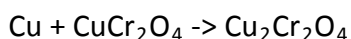
Moles of oxygen remaining: 8.764×10^{-6} moles

After all of the copper oxide, 60% of the copper chromite and all of the chromium (VI) was reduced, 8.764×10^{-6} moles of oxygen remained. This could be attributed to the reduction of the chromium within the spinel. Tonner *et al* (122) suggested that reduction of the spinel to cuprous chromite could occur via the following two routes:

- 1) Direct reduction of CuCr₂O₄



- 2) Reverse disproportionation reaction between Cu metal and CuCr₂O₄



However if all of the copper in copper chromite within the sample was reduced the final number of moles of excess oxygen would be lower. Yurieva *et al* (118) also suggested that above temperatures of 450°C, almost 100% of copper would be reduced.

Oxygen removed in actual TPR: 3.705×10^{-5} moles

Oxygen removal required to reduce copper in sample: 3.282×10^{-5} moles

Difference in oxygen: 4.23×10^{-6} moles

Moles of oxygen required for the reduction of Cr(VI) to Cr(III): 1.466×10^{-6} moles

After the complete reduction of copper oxide, copper chromite and Cr(VI), 2.764×10^{-6} moles of oxygen remain. This once again could only be attributed to the reduction of chromium within the spinel.

Throughout the reduction of copper chromite the calculations have been worked out on the assumption that Cu^{2+} will reduce to only Cu^0 . This however will not be the case as it has been found that Cu^{2+} will also reduce to Cu^+ (119) as previously described. From the data obtained it was not possible to distinguish between both of these reductions.

3.3.1.3 Post hot stage

The catalyst that was used for the hot stage XRD was allowed to oxidise for approximately one week then analysed again. This was to check if after one week how much of the copper metal had oxidised to copper oxide. XRD and TGA's were carried out to see what the effect was.

3.3.1.3.1 XRD

XRD was carried out in order to distinguish if any reduced copper was still present in the oxidised sample. This is illustrated in figure 3-26

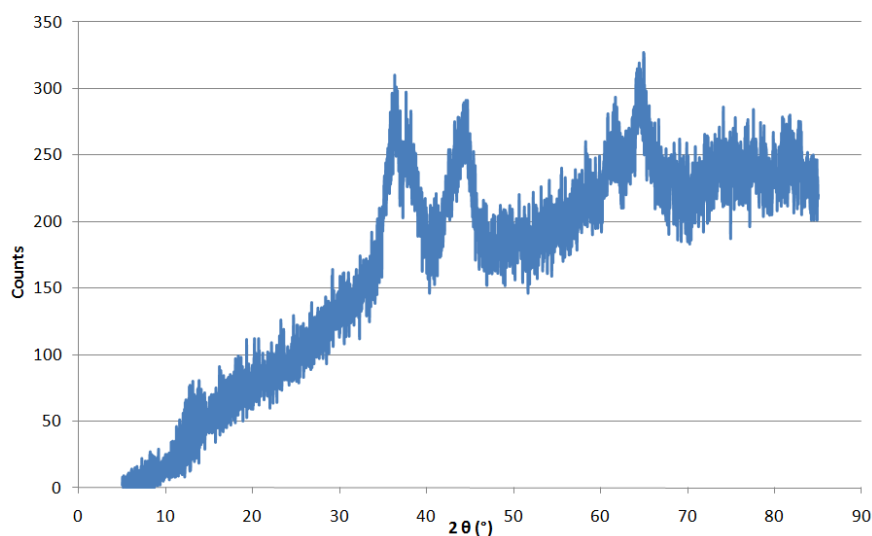


Figure 3-26 XRD of post hot stage copper chromite (reduced: 25-300°C, 5% H_2/N_2) after 1 week of air exposure

It can be seen that a reduced copper peak was still present at 45° suggesting that not all of the copper was oxidised. This once again suggests that due to quick oxidation of the

surface layers, metallic copper was still present within the spinel (112). Figure 3-27 shows this more clearly.

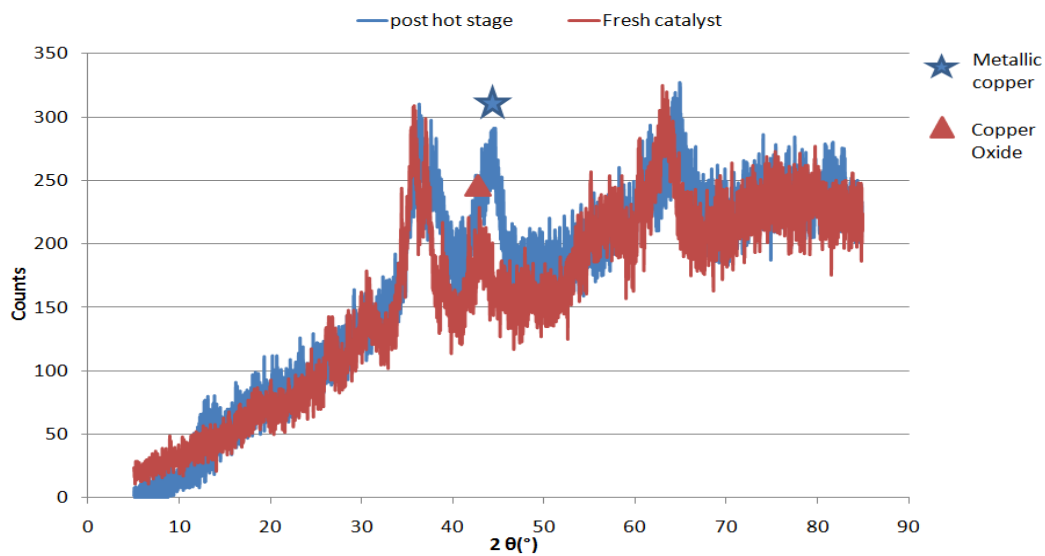


Figure 3-27 Comparison of a) fresh copper chromite and b) post hot stage XRD catalyst (reduced: 25-300°C, 5% H₂/N₂) allowed to oxidise in air for 1 week

3.3.1.3.2 TPR

TPR was carried out to see if the already reduced and oxidised sample could be reduced once again as shown in figure 3-28

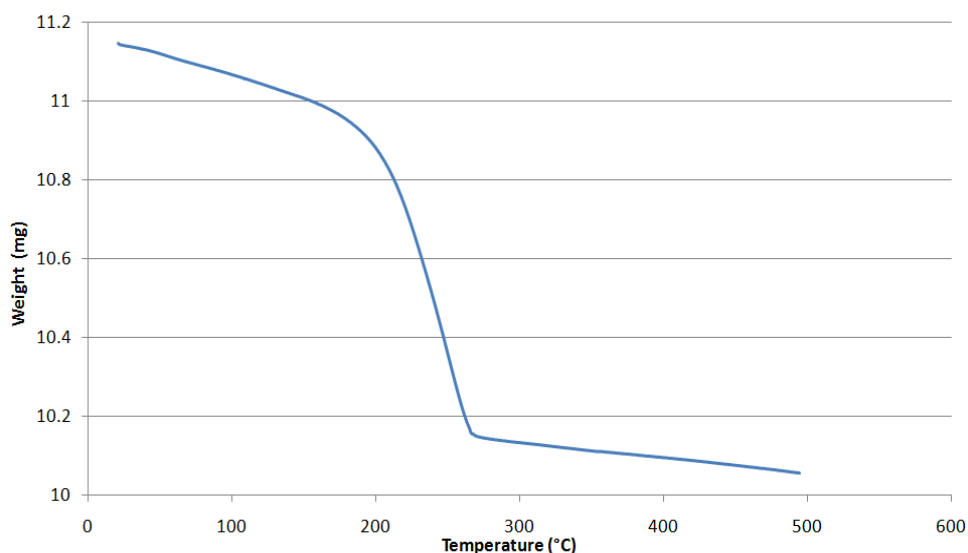


Figure 3-28 TPR weight profile of reduced copper chromite sample allowed to oxidise for 1 week then re-analysed (25-500°C, 5% H₂/N₂)

It can be seen that the catalyst will reduce for a second time after prior reduction-oxidation has taken place. The weight profile indicated however that only one large reduction stage was present this time unlike the first reduction. In the initial reduction the first weight loss was attributed to the reduction of CuO to Cu metal. The second, more gradual weight loss was due to the reduction of copper chromite in the spinel to metallic copper (117). The loss of the second stage can be attributed to the copper within the spinel already being in the metallic phase. When the catalyst was exposed to air the surface layers of metallic copper oxidise very quickly and forms an oxide layer. Subsequently Cu⁰ within the bulk does not get oxidised and remains in the metallic phase. This also agrees with the XRD obtained as metallic copper peaks were apparent after oxidation.

3.3.1.4 Acid Sites determination

Lewis acid sites on the catalyst play an important role in the reaction. They are responsible for carrying out the Tishchenko reaction. This will be discussed later in section 3.3.2.4.1. This involves converting the product, lilestralis into inert bed. Pyridine was used to determine this as it has been found to adsorb onto acid sites (123, 124). The

advantage to this method was that it allows the catalyst to be studied under conditions nearly the same as reaction conditions. Cr_2O_2 was known to exhibit some acidity (122).

To determining the quantity of Lewis acids sites on the catalyst a temperature programmed desorption was carried out. This entailed passing a flow of pyridine over the catalyst and allowing saturation to occur. Physisorbed pyridine was then removed with flowing argon and chemisorbed pyridine was removed using a temperature programmed ramp rate. The results from this were analysed using mass spectrometry following the pyridine fragments (m/z : 52, 79).

It was seen from the TPD/mass spectrometry results that the catalyst contained Lewis acid sites.

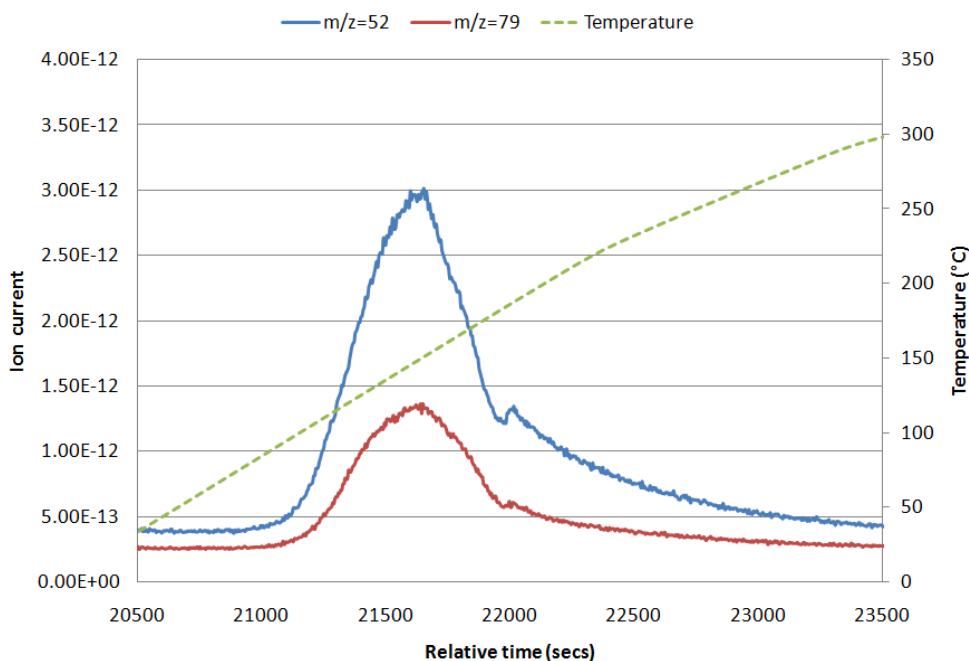


Figure 3-29 TPD profile of BASF copper chromite post pyridine adsorption ($m/z= 52, 79$). Conditions: 25-300°C, ramp rate of 10 degC.min⁻¹, 90 ml.min⁻¹ Ar

As shown in figure 3-29 a peak was obtained when the temperature ramp rate was started. This corresponded to the chemisorbed pyridine suggesting that pyridine was desorbing from the Lewis acid sites on the catalyst.

3.3.1.5 Sud-chemie Copper chromite

Catalysts supplied from Sud-chemie were also studied as a comparison to the copper chromite supplied from BASF. Two catalysts were used: copper chromite modified with 120 ppm Na and copper chromite modified with 1600 ppm Na.

3.3.1.5.1 Copper chromite 120 ppm Na

3.3.1.5.1.1 XRD

An XRD was carried out on the copper chromite 120 ppm Na catalyst (figure 3-30). It can be seen from the XRD pattern that copper oxide and CuCr_2O_4 were present as the visible peaks correspond to this.

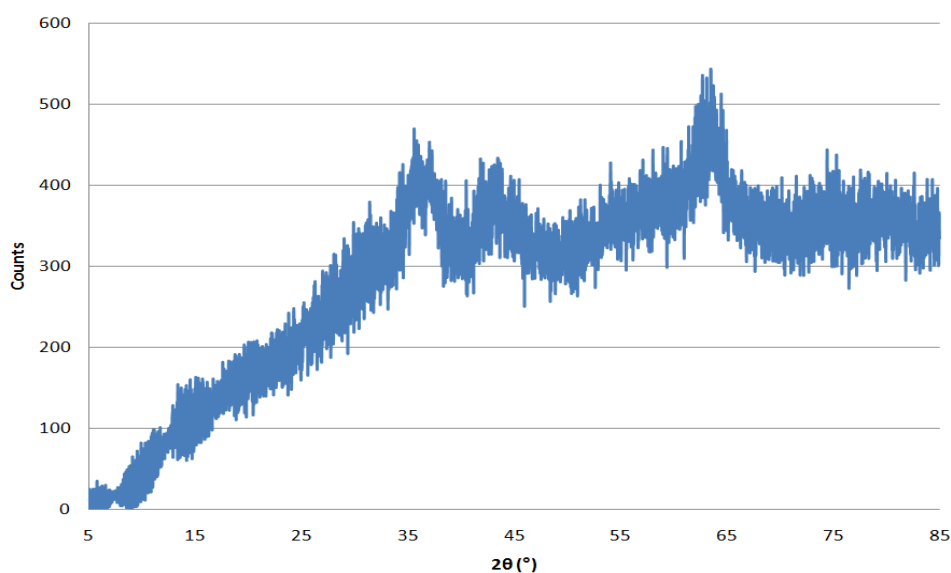


Figure 3-30 XRD of fresh copper chromite 120 ppm Na

3.3.1.5.1.2 TPR

A TPR was carried out to study the reduction profile of the catalyst. Figure 3-31 shows this profile. The profile shows CuO and CuCr_2O_4 reducing to form reduced copper (Cu^0 and Cu^+). Once again it can be seen that there are 2 stages of reduction as previously mentioned with the BASF copper chromite.

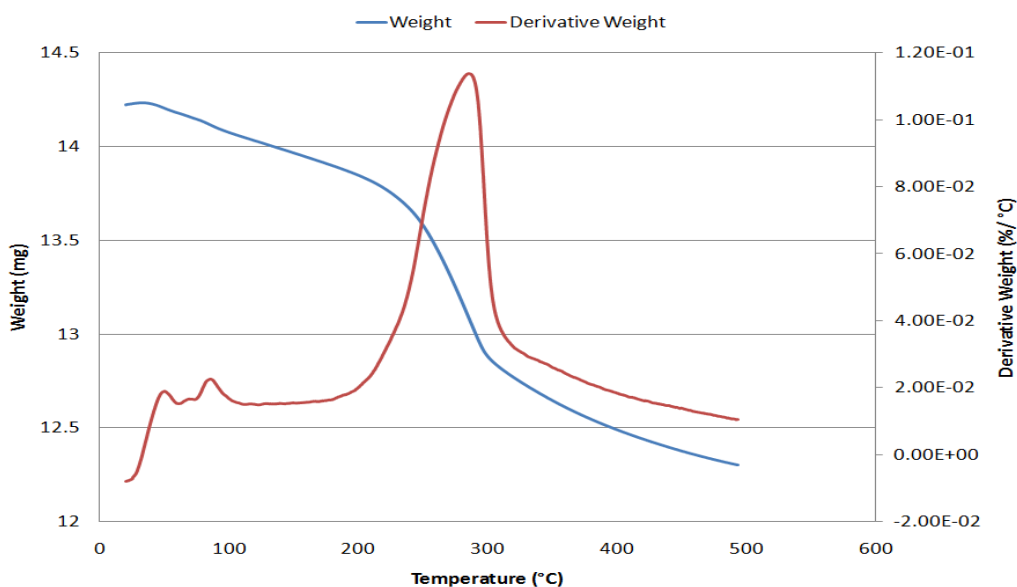


Figure 3-31 TPR of fresh copper chromite 120 ppm Na (30-500°C, ramp rate 10 degC.min⁻¹, 5% H₂/N₂)

3.3.1.5.1.3 BET analysis

Table 21 BET analysis 120 ppm Na Copper chromite

Catalyst	Surface Area (m ² / g)	Pore Diameter (Å)
Copper chromite 120 ppm Na	72.6	71.7

3.3.1.5.1.4 Acid sites determination

A TPD was carried out to investigate the Lewis acid sites present on the catalyst. This was calculated using the same method as before. Figure 3-32 shows the profile produced.

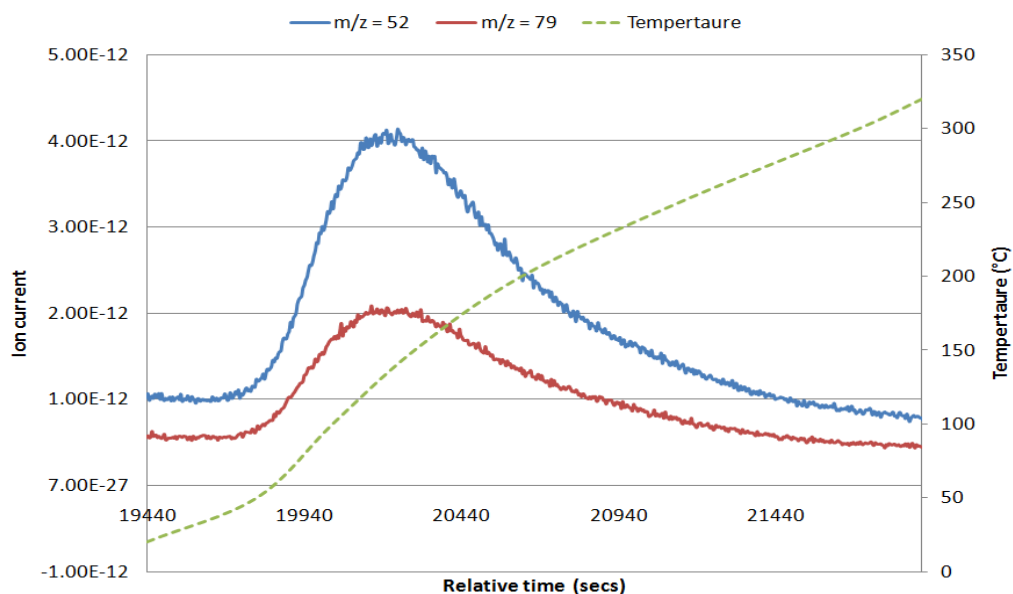


Figure 3-32 TPD profile of Sud chemie copper chromite 120 ppm Na post pyridine adsorption ($m/z = 52$, 79). Conditions: 25-300°C, ramp rate of 10 degC.min⁻¹, 90 ml.min⁻¹ Ar

From this the following could be calculated:

Total number of moles desorbed = 1.79×10^{-4}

Molecules of pyridine desorbed = 1.08×10^{20}

Lewis acid sites per gram = 2.13×10^{20}

3.3.1.5.2 Copper chromite 1600 ppm Na

3.3.1.5.2.1 XRD

An XRD was carried out on the copper chromite 1600 ppm Na catalyst (figure 3-33). It can be seen from the XRD pattern that copper oxide and CuCr_2O_4 was present as the visible peaks correspond to this.

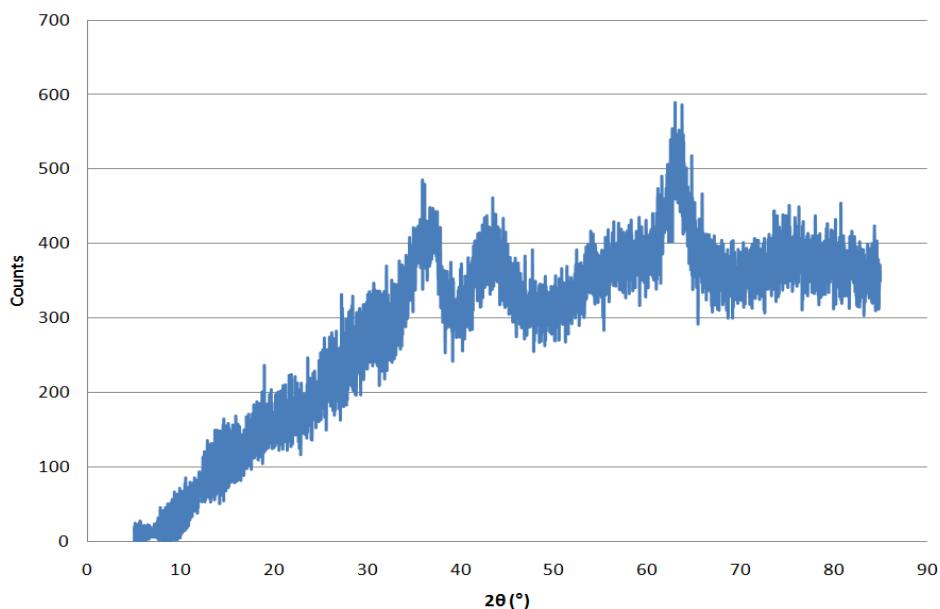


Figure 3-33 XRD of fresh Copper chromite 1600 ppm Na

3.3.1.5.2.2 TPR

To confirm that the reduction profile of both Sud-Chemie copper chromite catalysts were the same a TPR was carried out. A similar reduction profile was produced (figure 3-34) showing CuO and CuCr_2O_4 being converted to Cu . Once again it can be seen that there are 2 stages of reduction as previously mentioned with the BASF copper chromite.

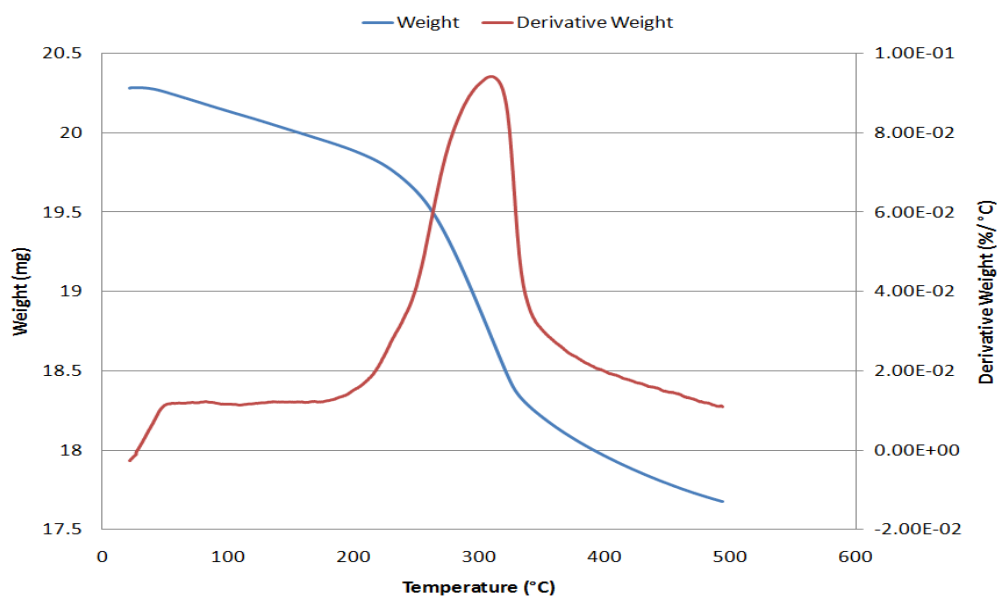


Figure 3-34 TPR of fresh copper chromite 1600 ppm Na (30-500°C, ramp rate 10 degC.min⁻¹, 5% H₂/N₂)

3.3.1.5.2.3 BET analysis

Table 22 BET analysis 1600 ppm Na Copper chromite

Catalyst	Surface Area (m ² / g)	Pore Diameter (Å)
Copper chromite 1600 ppm Na	55.6	126

3.3.1.5.2.4 Lewis acid sites determination

A TPD was used to calculate the number of Lewis acid sites present on the catalyst. This was carried out using the same method as before. Figure 3-35 shows the mass profile when subjected to a temperature ramp.

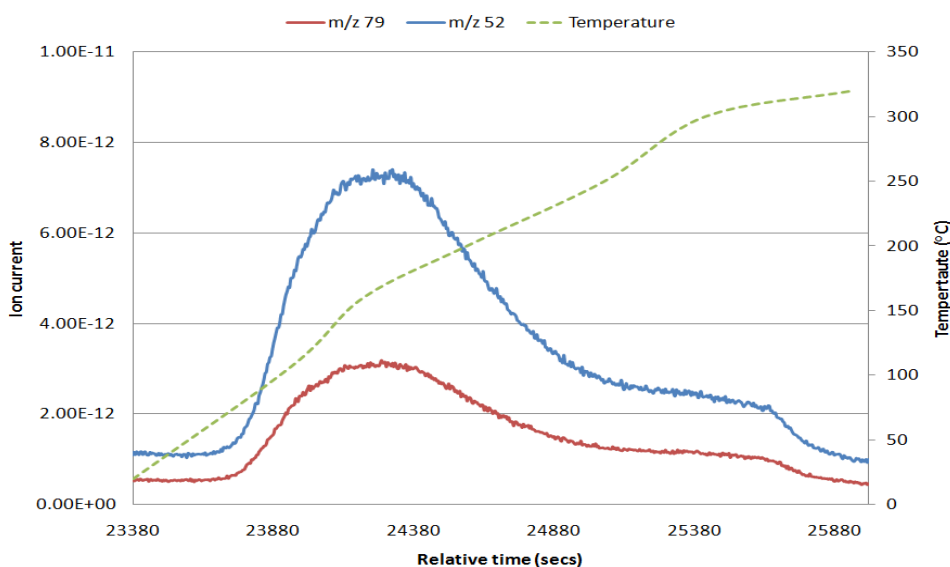


Figure 3-35 TPD profile of Sud chemie copper chromite 1600 ppm Na post pyridine adsorption (m/z= 52, 79). Conditions: 25-300°C, ramp rate of 10 degC.min⁻¹, 90 ml.min⁻¹ Ar

From this data the following could be calculate:

Total number of moles desorbed = 2.22×10^{-4}

Molecules of pyridine desorbed = 1.34×10^{20}

Lewis acid sites per gram = 2.66×10^{20}

3.3.1.6 CuO/ZnO/Al₂O₃

3.3.1.6.1 TPR

The CuO/ZnO/Al₂O₃ catalyst used during the study was commercially produced, and as such was sold pre-calcined. All that remained to do was activate the catalyst. A TPR was carried out to study the reduction in terms of weight loss (figure 3-36).

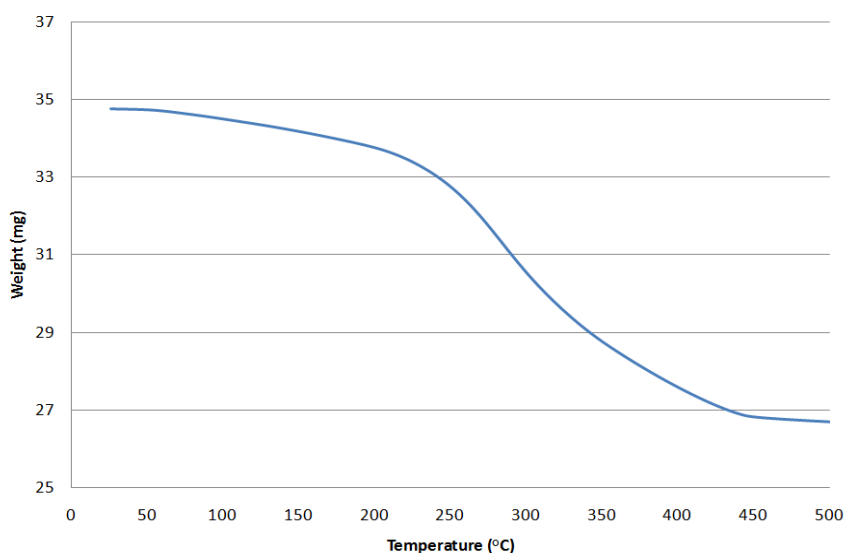


Figure 3-36 TPR weight loss profile of fresh Cu/ZnO/Al₂O₃ (30-500°C, ramp rate 10 degC.min⁻¹, 5% H₂/N₂)

The weight loss observed is mainly due to the loss of water when CuO is reduced to Cu metal. However, a small amount of methane was also detected, indicating incomplete decomposition of the precursor carbonates during the calcination step.

3.3.1.6.2 Hot stage XRD

Hot stage XRD was carried out on the CuO/ZnO/Al₂O₃ catalyst to look at the reduction process. This was done using the hot stage XRD with 2% H₂/N₂.

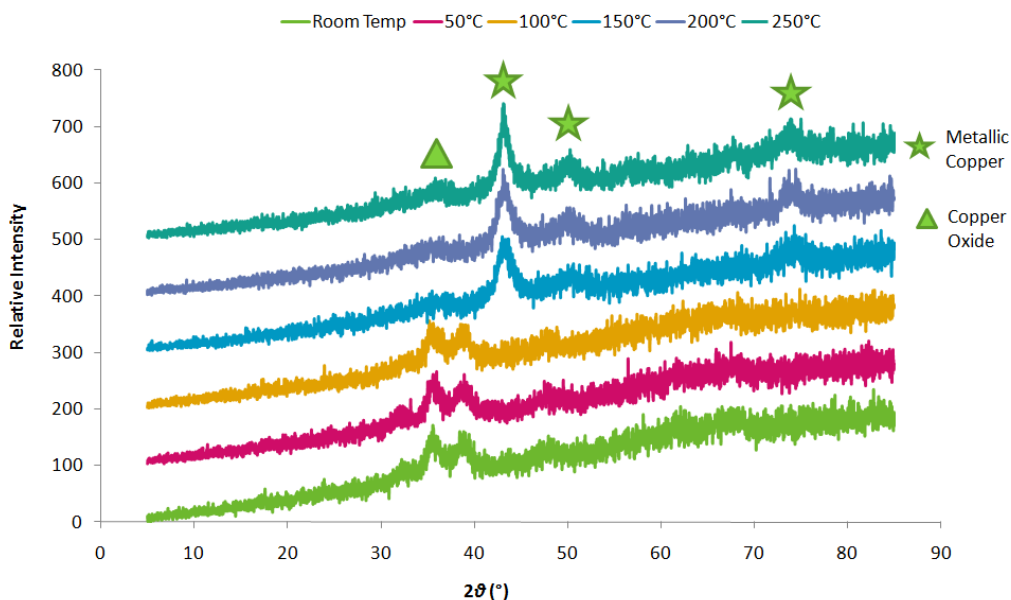


Figure 3-37 Hot Stage XRD CuO/ZnO/Al₂O₃ carried out under 5%H₂/N₂ atmosphere. Scans recorded at 25°C, 50°C, 100°C, 150°C, 200°C and 250°C

It can be seen from figure 3-37 that at room temperature copper oxide was present but with increasing temperature, metallic copper features become apparent. The fact that the XRD pattern did not show any ZnO or Al₂O₃ peaks suggested that these materials were amorphous.

3.3.1.6.3 BET Analysis

BET analysis was carried out on the catalyst as shown in table 23.

Table 23 BET analysis CuO/ZnO/Al₂O₃

Catalyst	Surface Area (m ² / g)	Pore Diameter (Å)
CuO/ZnO/Al ₂ O ₃	89	37

3.3.1.7 Copper Silica

Analysis was carried out on copper silica before and after calcinations to compare the changes that had occurred.

3.3.1.7.1 XRD

XRD was carried out on both the silica support and the prepared catalyst. The pattern obtained from the silica support showed that it was an amorphous material. Figure 3-38 shows this.

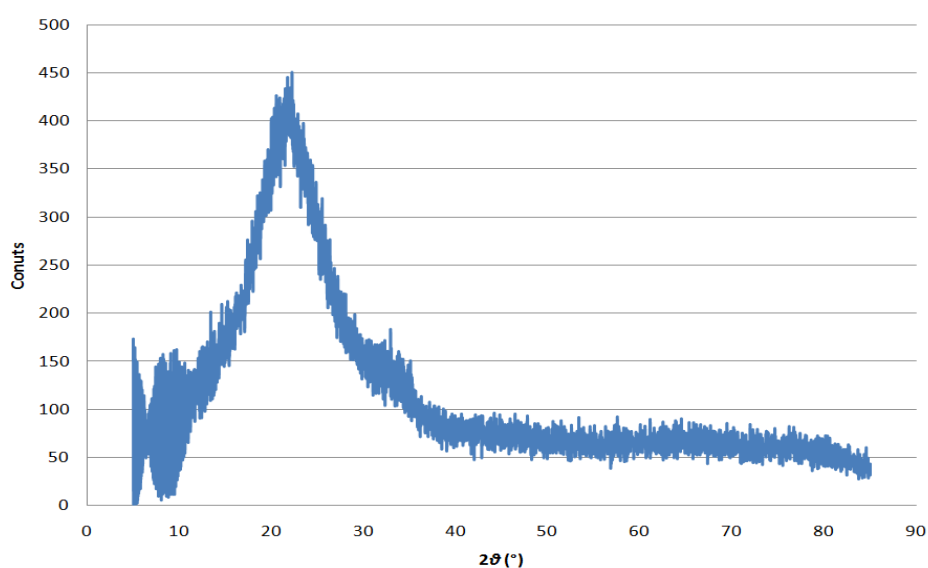


Figure 3-38 XRD of fresh silica support (Caricat Q10)

The pattern obtained from 10% Cu/SiO₂ (figure 3-39) contained copper oxide peaks with the two main predominant peaks around 35° and 38° (126).

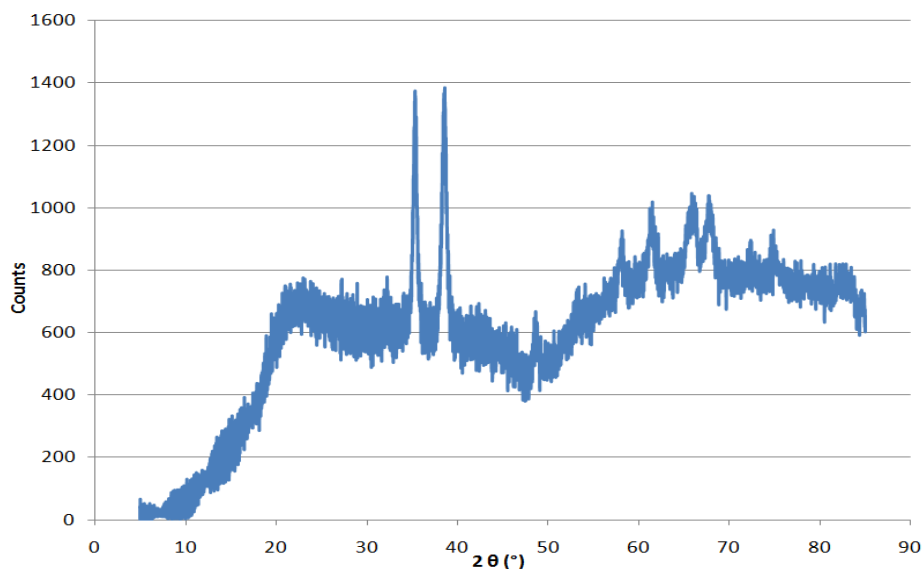


Figure 3-39 XRD of calcined 10% copper silica catalyst

3.3.1.7.2 Thermal analysis

Thermal analysis was carried out on both the uncalcined and calcined copper silica. The uncalcined sample was subjected to an argon atmosphere.

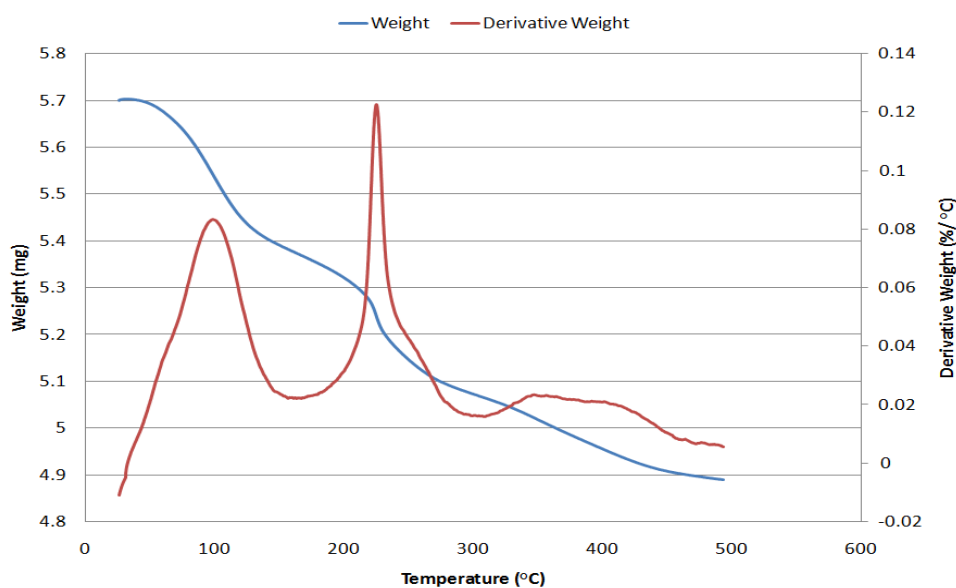


Figure 3-40 TGA uncalcined 10% Cu/SiO₂ (30-500°C, ramp rate 10 degC.min⁻¹, Ar)

As shown in figure 3-40 the decomposition of 10% Cu/SiO₂ occurs at various stages. The first weight loss at approximately 100°C is due to the loss of any water remaining from

the preparation. The sharp peak in the derivative weight profile at 224°C corresponds to the loss of the nitrate from the precursor. Work by Moura *et al* (127) also reported thermal analysis data on Cu/ SiO₂ and suggested that from 30-200°C was characteristic of physisorbed water and weight loss at 200-350°C to be decomposition of the copper salts.

Temperature programmed reduction was also carried out on the calcined copper silica as shown in figure 3-41.

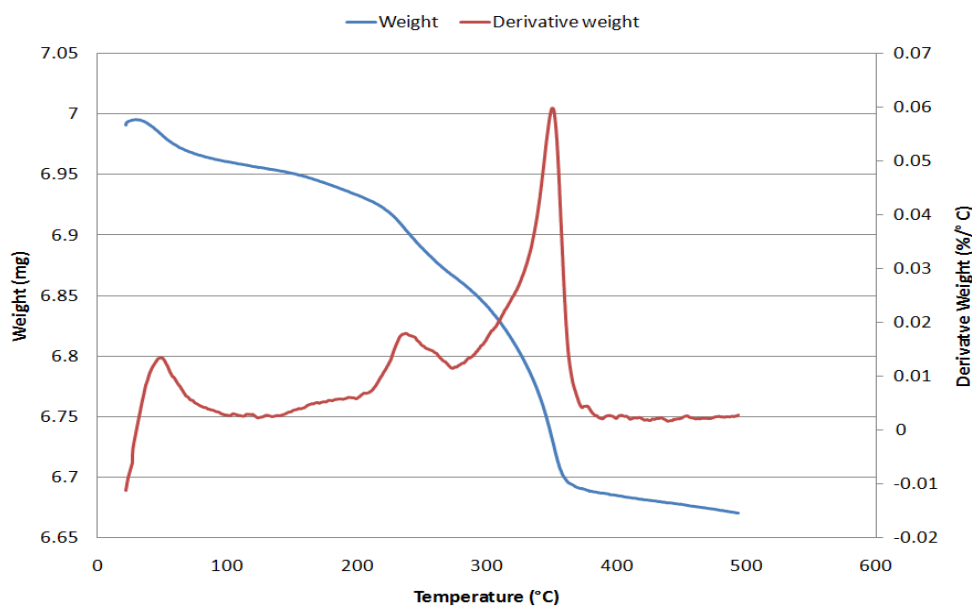


Figure 3-41 TPR of calcined 10% Cu/SiO₂ (30-500°C, ramp rate 10 degC.min⁻¹, 5% H₂/N₂)

It can be seen in figure 3-41 that during the reduction of 10% Cu/SiO₂ there are various stages in which this occurs by. The first weight loss at approximately 100°C is due to the loss of physisorbed water and the second peak (~240°C) corresponds to the loss of any remaining nitrate from the precursor after calcination. The major weight loss starting at ~275°C can be attributed to the reduction of CuO to Cu⁰.

3.3.1.7.3 BET analysis

BET was carried out on calcined copper silica as shown in table 24. It can be noticed that the surface area was significantly larger than with copper chromite and Cu/ZnO/Al₂O₃ due to the silica support. Shiau *et al* reported a surface of 241.5 m² / g for a 10% Cu/SiO₂ catalyst (128) which was within experimental error of the data obtained within this study.

Table 24 BET analysis 10% Cu/SiO₂

Catalyst	Surface Area (m ² / g)	Pore Diameter (Å)
10% Cu/SiO ₂	259	145

3.3.2 Material investigation

To investigate the materials and how they interact with each other, a series of experiments were carried out in an attempt to obtain a clearer picture of what was taking place during catalytic testing.

3.3.2.1 Inert bed only

The inert bed which contains principally lillol liliate was used as a solvent for the reaction. The bed was a by-product from the reaction and hence was recycled. The material however was not pure (as illustrated by figs 3-42 and 3-43). Roberts *et al* (129) studied work on methanol dehydrogenation in a slurry reactor to investigate different suspension materials. It was found that the composition of the slurry had a pronounced effect on the performance of the catalyst. In some studies by the end of the reaction, the slurry had either disappeared (129) or had reacted further (92).

An experiment was carried out using inert bed only, to determine if the composition of the inert bed changed over time. No catalyst or starting material present. Inert bed was placed in the reactor on its own and held for 6.5 hours under normal conditions (230°C, 57 mbar). A small amount of sample was collected from the flask at the end of the experiment and was analysed by GC along with a sample from the reactor pot. The sample from the reactor showed some impurities but was significantly purer than fresh inert bed. This was due to the impurities boiling off over time as they have a lower boiling point than the lillol liliate. In figure 3-42 and 3-43 the GC traces that were obtained are shown. The sample that was collected in the flask contained all the impurities that had boiled off from the inert bed and hence was very impure.

Due to the inert bed being recycled material there was a great degree of inconsistency between samples used during the current study. Inert bed was provided from plant production and the colour often varied from orange to yellow as shown in figure 3-44. It was unclear what compound or mixture was responsible for the colour. There were so many unknown components present that it was impossible to distinguish which particular compound was responsible.



Figure 3-44 Inert bed from production plant

3.3.2.2 Inert bed & catalyst

As the inert bed contained so many impurities, it was unclear as to how actually “inert” it would be. To ascertain how reactive the material was an experiment was performed to determine if the bed had an effect on the catalyst and whether in the absence of hydrogen would the catalyst be reduced. Both materials were placed in the reactor and subjected to normal reaction conditions. After 6.5 hours the experiment was stopped and the catalyst analysed.

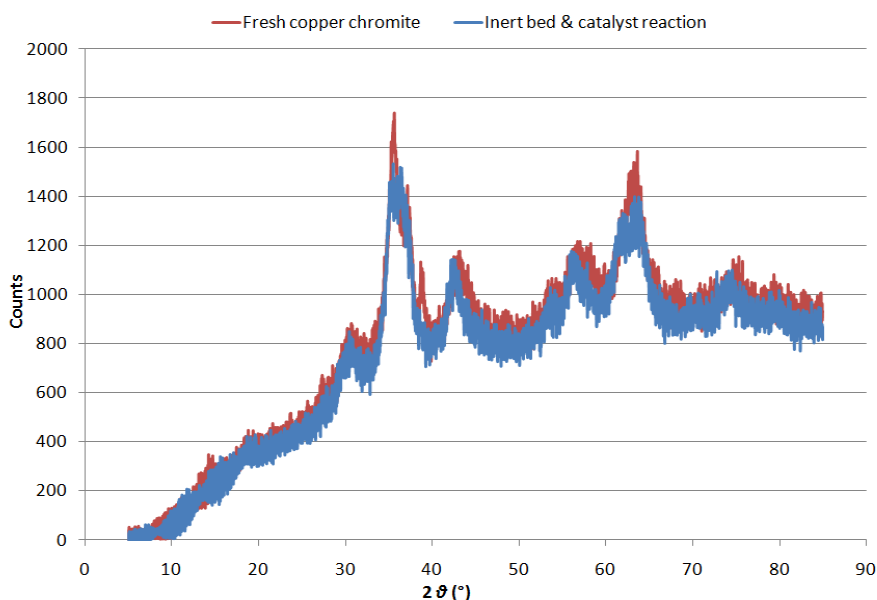


Figure 3-45 Post reaction XRD comparison between a) fresh and b) used copper chromite from reaction between inert bed and catalyst (230°C, 57 mbar)

As shown in figure 3-45 the XRD that was obtained from the post reaction catalyst indicated that the inert bed played no role in the reduction of the catalyst, as no metallic copper peaks were present. Metallic copper peaks would be apparent at 43, 51 and 75° if present (115). The catalyst remained in its original form. This further suggested that it was the hydrogen produced from the dehydrogenation of p-LOL that is responsible for the reduction of copper oxide to the metal.

3.3.2.3 Inert bed & p-LOL

Copper species, both metallic and monovalent, are thought to be the active species in dehydrogenation reactions (100, 130). To ensure that the inert bed does not play any role in the dehydrogenation an experiment involving no catalyst was carried out. The samples produced were analysed using GC.

230°C and 57 mbar the inert bed was not at boiling point and remains in liquid form. However when the inert bed was not present these conditions could not be achieved as both p-LOL and p-LAL have lower boiling points. P-LOL boils at approximately 250°C at 1atm. When subjected to 57mbar this value will decrease as equilibrium is maintained. Hence in the reaction with p-LOL and catalyst, when the temperature reached 203°C at 57mbar, p-LOL was at boiling point. To allow the temperature to rise, the pressure had to be increased as this would allow the boiling point of p-LOL to increase slightly. Table 25 describes the conditions used during the reaction.

For the first two hours the pressure was achieved but not temperature, after this the vacuum was reduced to allow the temperature to rise. 5 g copper chromite: 50 g starting material was used at the start.

Table 25 p-LOL & catalyst material addition

Time (hours)	Material Added (g/h)	Temperature(°C)	Pressure (mbar)
0-2	20	203	57
2-3	50	230	270
3-6.5	20	230	270

The conversion observed during reaction revealed that without inert bed present p-LOL would still react. When the temperature was at 203°C the conversion was reduced and it was not until the temperature was increased that the conversion subsequently improved (figure 3-47). After 6.5 hours the conversion was as high as 49% however the yield to p-LAL was only 19%, revealing substantial by-product formation.

Post reaction an XRD of the catalyst revealed conversion of Cu^{2+} to Cu metal. This revealed that the hydrogen produced in the reaction does reduce the catalyst *in-situ*.

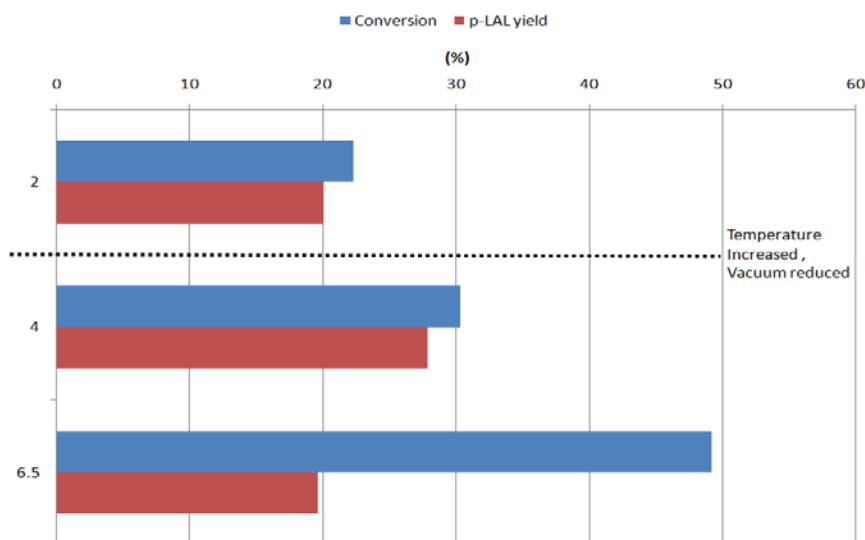


Figure 3-47 Conversion of p-LOL and p-LAL yield in the reaction between p-LOL & copper chromite (0-2 hours: 203°C, 57 mbar, starting material rate addition 20g/h then 2-6.5 hours: 230°C, 270 mbar, rate of addition of p-LOL 50g/h)

The selectivity to by-products is shown in figure 3-48. A significant increase in the selectivity was observed as the temperature and pressure changed. As the temperature increased, the by-product formation also increased. This though could be due to the increase in pressure. The material is subsequently in contact with the catalyst for longer and hence has a greater probability to react again. Mechanistic aspects of the formation of by products will be reviewed at the end of the chapter.

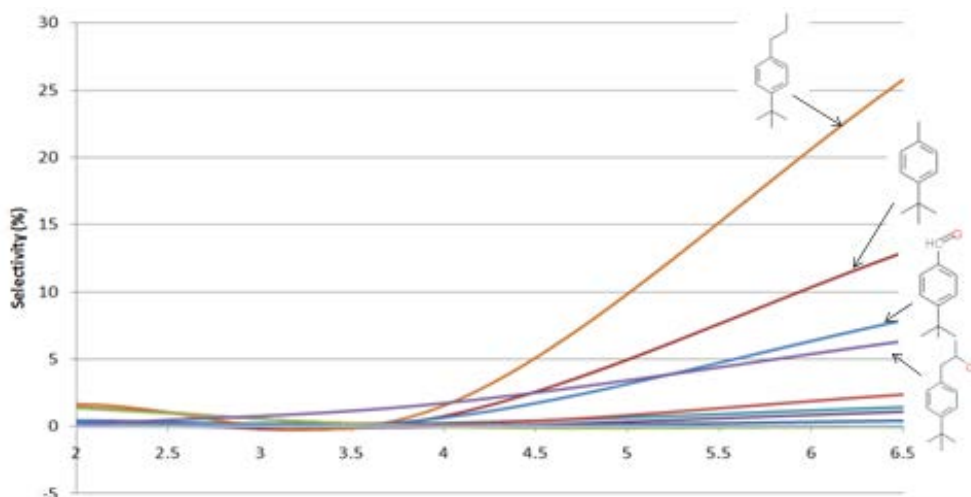


Figure 3-48 Selectivity for all other by-products for reaction between p-LOL and copper chromite (0-2 hours: 203°C, 57 mbar, starting material rate addition 20g/h then 2-6.5 hours: 230°C, 270 mbar, rate of addition of p-LOL 50g/h)

The effect of the temperature in the production of p-LAL was significant. When the temperature was only 17°C below normal reaction temperature, a significant negative effect on the conversion was observed, suggesting that the reaction was very temperature sensitive.

The samples that were obtained from the reaction had a slight yellow colouration. The first sample obtained was clear, the second was a pale yellow and the third was a stronger yellow. Both the starting material and products are colourless but the inert bed is yellow. It was evident that there were trace amounts of species contained in the inert bed in the samples produced and had been produced during the experiment. The samples were all analysed using GC and all contained inert bed peaks confirming its presence in the sample.

3.3.2.4.1 Inert bed production

Components of the inert bed had clearly been produced in the previous experiment. The inert bed is a by-product of the liquid phase dehydrogenation of liliol to lilestralis, believed to be produced through a Tishchenko reaction.

3.3.2.4.2 Tishchenko reaction

The Tishchenko reaction is a disproportionation reaction that allows the preparation of esters from 2 equivalents of an aldehyde (132).

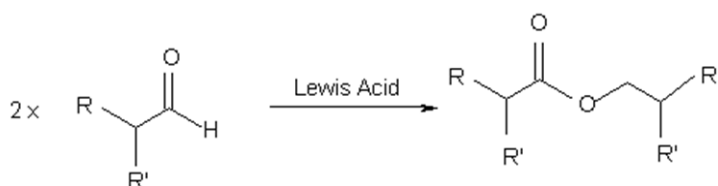


Figure 3-49 Tishchenko reaction mechanism

It can be seen from figure 3-49 that for a Tishchenko reaction to proceed, a Lewis acid and an aldehyde are required. In the experiment with no inert bed present it was shown that lilestralis was produced. This indicated that a Lewis acid was present in the system, allowing the Tishchenko reaction to proceed. The Tishchenko reaction has been shown to take place over heterogeneous catalysts, specifically mixed metal oxides (133) Figure 3-50 shows the Tishchenko reaction scheme of lilestralis to inert bed:

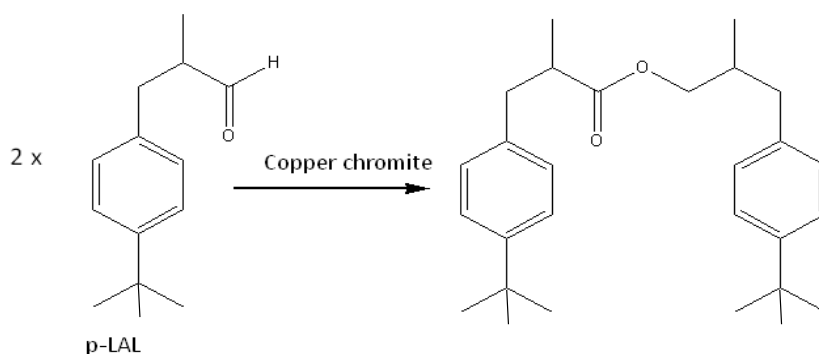


Figure 3-50 Inert bed production

If copper chromite contained Lewis acid sites then production of inert bed through a Tishchenko reaction was possible (figure 3-50). A literature search revealed only one previous investigation into Lewis acid sites in copper chromite. Rajeev *et al* (125) investigated the Lewis acid site density for various samples of copper chromite using a

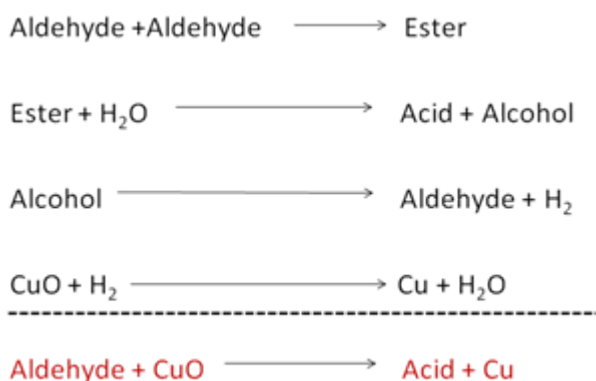


Figure 3-51 Reaction equations

Figure 3-51 illustrates all the individual equations of what was potentially taking place inside the reactor vessel. The final equation illustrates that in the presence of unreduced catalyst, p-LAL can be destroyed to produce LAL acid and reduced catalyst. To minimise the destruction of the desired product, water would have to be eliminated.

3.3.2.5 P-LOL and catalyst direct comparison

A direct comparison with respect to temperature with only p-LOL and catalyst was carried out. Therefore it was decided to carry out the reaction at 230°C and increase the pressure to 270mbar. P-LOL was added at the standard rate.

From the GC analysis it revealed that there was a reasonably high conversion of p-LOL. In the first two hours there was a conversion of around 52% which then increased to approximately 70% for the latter 4.5 hours. However only about 10% of this was converted to and remained as p-LAL as shown in figure 3-52.

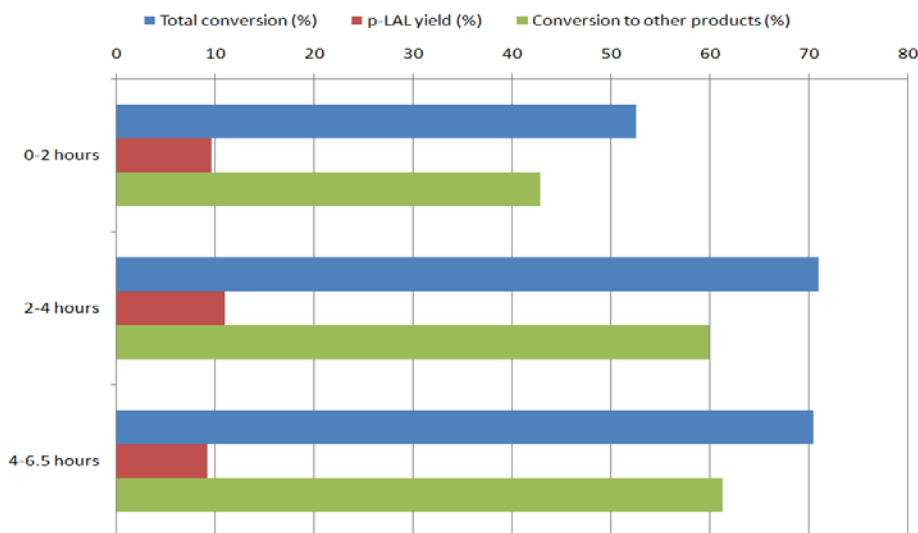


Figure 3-52 Conversion of p-LOL and p-LAL yield for the reaction between p-LOL and copper chromite (230°C, 270 mbar, rate of addition of p-LOL: 13.5g/10 min then 5g/h)

Figure 3-53 shows the selectivity for the other by-products that were produced. It can be observed that the two major by-products are 1-tert-butyl-3-methyl-benzene and 1-tert-butyl-4-propyl-benzene. It can be seen that as the selectivity of 1-tert-butyl-3-methyl-benzene increases, 4-tert-butyl benzaldehyde decreases respectively suggesting that the aldehyde was being hydrogenated due to prolonged exposure on the catalyst surface with adsorbed hydrogen.

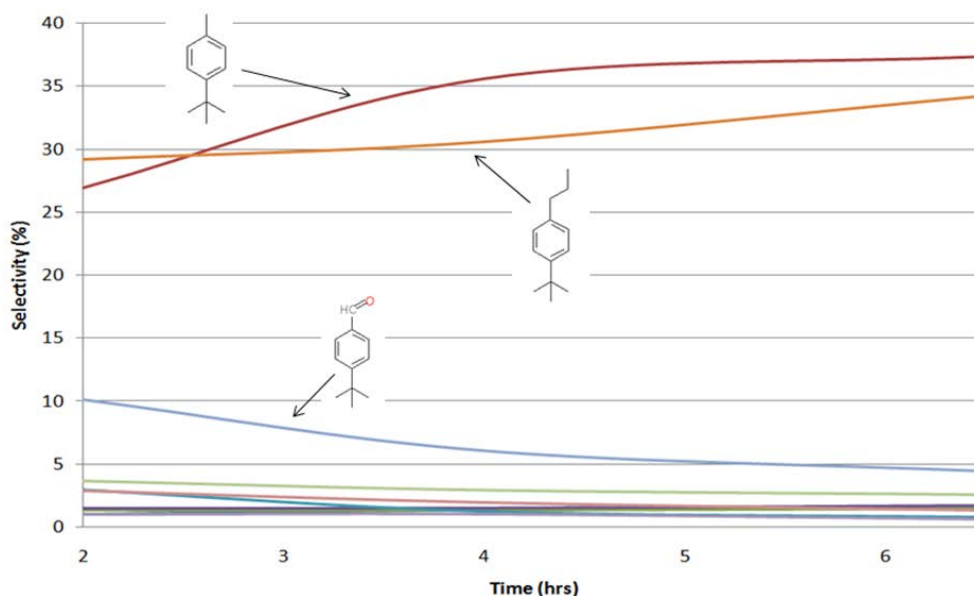


Figure 3-53 Selectivity for all other by-products for the reaction between p-LOL and copper chromite (230°C, 270 mbar, rate of addition of p-LOL: 13.5g/10 min then 5g/h)

Due to the high conversion to other by-products it is thought that when p-LOL has a long contact time with the catalyst, further reactions can take place. When the inert bed is present the alcohol can enter into the reaction medium, react and then leave quickly due to the high vacuum. The increase in pressure would have meant that the material was not being pulled out of the slurry just as fast. This suggested that inert bed had to be present to avoid further reactions taking place.

The presence of the inert bed in the standard reaction will also introduce a dilution effect which could also lower the contact time of the active material.

3.3.2.6 P-LAL & unreduced catalyst

Reactions involving p-LAL and copper chromite were studied. This was to investigate if the product reacted further with the catalyst. It was observed in previous experiments that by-products were formed; it was unknown however if they had been produced from the reactant, or product further reacting. The aim of these experiments was to identify which component was responsible.

3.3.2.6.1 N₂ atmosphere

During a standard reaction no H₂ was fed into the system. The H₂ that was consumed during the catalyst reduction was produced from the dehydrogenation reaction. To investigate what effect p-LAL had on the catalyst a reaction was carried out under an inert atmosphere.

50 g p-LAL was placed into the reactor alongside 5 g copper chromite. The reaction was carried out at 230°C and 400 mbar pressure. When the reactor reached temperature p-LAL was added. In the 1st hour 10 g was added then this was reduced to 5 g/h for the next two hours. After this no more material was added as there was no sample being collected so the reactor was subsequently just filling up. At the end of the reaction a very small sample was produced (~0.6-0.9 g) and this was analysed using GC.

It can be seen in figure 3-54 and 3-55 that p-LAL (RT: 12.713) has been converted to other products. The two main by-products that are produced are 1-tert-butyl-3-methyl-benzene (RT:4.685) and 1-tert-butyl-4-propyl-benzene (RT:7.715). These are the same by-products that were formed in the reaction with p-LOL and catalyst. This would suggest that it was not p-LOL that was responsible for their formation but p-LAL.

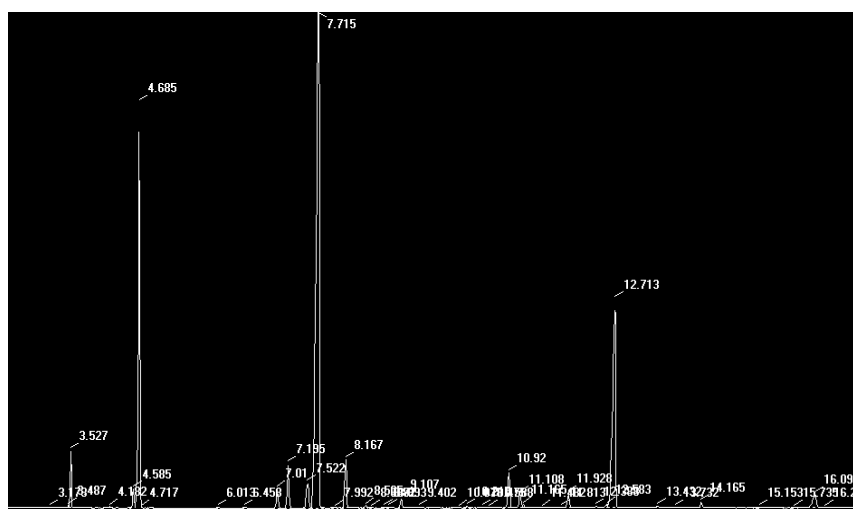
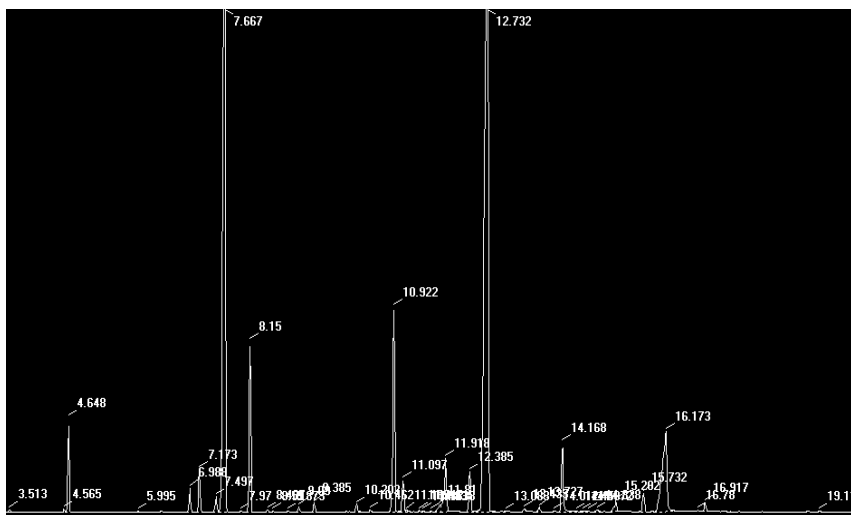


Figure 3-54 GC trace p-LAL and catalyst flask sample



products, H_2 was evolved hence reducing copper oxide to metallic copper. Another possibility as shown in figure 3-50, was the interaction of the aldehyde over copper oxide to produce LAL acid and reduced copper. As the aldehyde and copper oxide were the starting materials, this was the most likely route to produce a reduced catalyst.

Peaks consistent with the d-spacing of Cu metal are present at $43, 51$ and 75° (115). A small amount of copper oxide was still present indicating that full reduction did not take place.

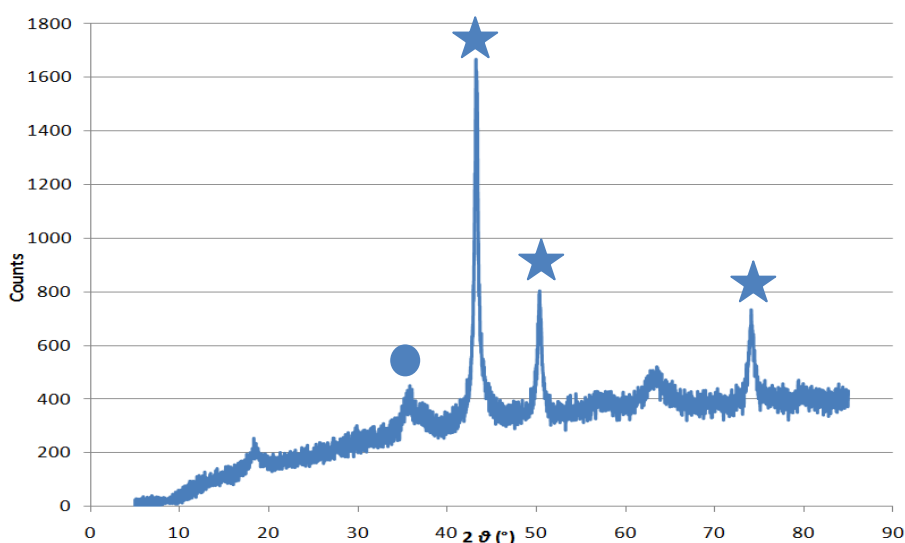


Figure 3-56 Post reaction XRD from reaction between p-LAL, copper chromite & N_2 ($230^\circ C$, 400 mbar)
(Key: star – Cu^0 , Circle – CuO)

3.3.2.6.2 H_2 atmosphere

Throughout the reaction the reactants and products are subjected to an atmosphere of hydrogen which was being constantly produced from the dehydrogenation. An experiment with p-LAL, catalyst and H_2 was carried out to see if there was any change in the product distribution from the reaction upon changing from an inert to reducing atmosphere. 50g of p-LAL was placed into reactor with 5 g copper chromite. P-LAL was added in at a rate of 10 g/hr. The reaction was carried out at $230^\circ C$, 400mbar and under a continual flow of 5% H_2/Ar . Samples were collected in the three collecting flasks and analysed using GC. Figure 3-57 illustrates that p-LAL was readily converted to other products with conversions as high as 70%.

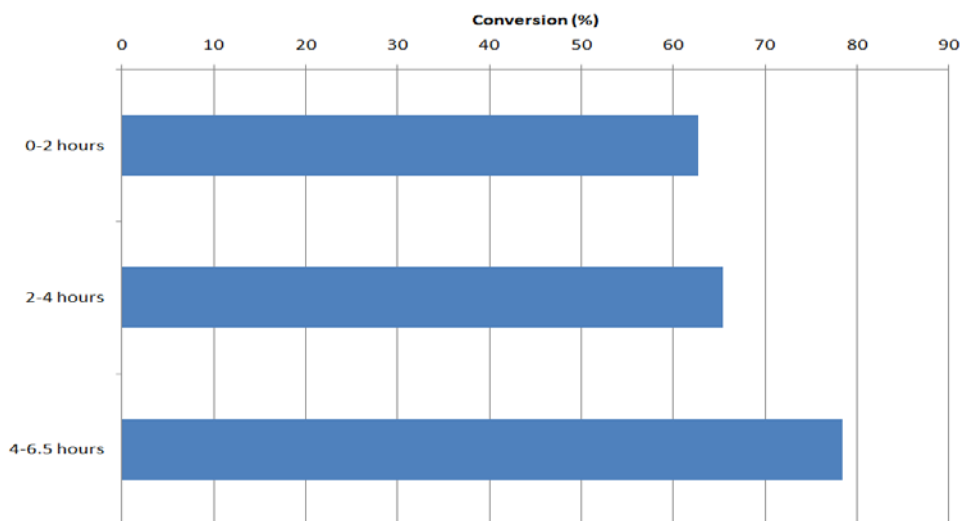


Figure 3-57 Conversion of p-LAL in reaction between p-LAL, copper chromite & H₂ (230°C, 400 mbar, 20 ml.min⁻¹ 5%H₂/Ar)

The selectivity of the by-products shown in figure 3-58 once again highlights the main product as 1-tert-butyl-4-propyl-benzene. This was the case in all of the previous reactions where by-products were formed. The absence of p-LOL was unusual as the hydrogenation of carboxylic acids over copper chromite has been found to result in a high yield of the alcohol instead of the aldehyde (16). Due to the absence of inert bed being present, the high concentration of reactants on the catalyst surface could have led to the conversion of the alcohol to other side products.

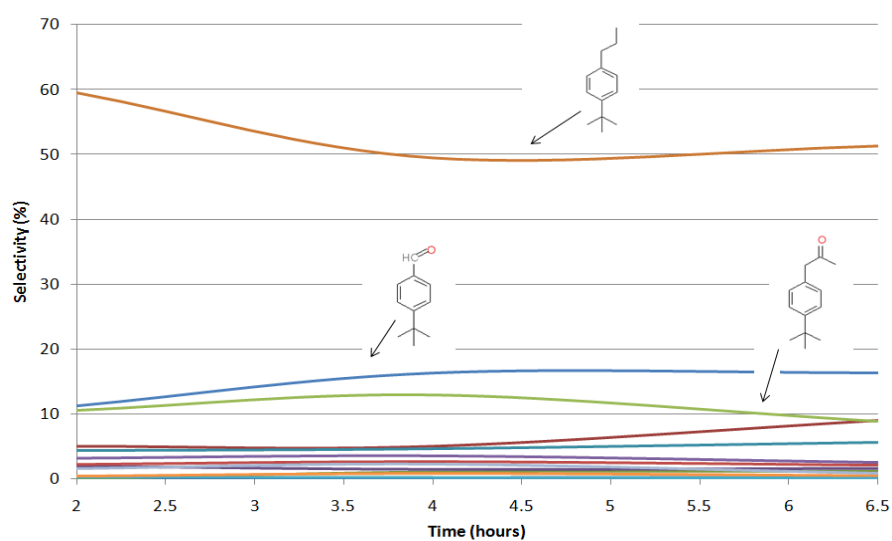


Figure 3-58 Selectivity of reaction between p-LAL, copper chromite & H₂ (230°C, 400 mbar, 20 ml.min⁻¹ 5%H₂/Ar)

3.3.2.7 Standard reaction involving p-LAL & unreduced catalyst

A standard reaction including inert bed was carried out using p-LAL instead of p-LOL to examine the effects if any that the catalyst had on the product when inert bed was present. All conditions were kept the same except p-LAL was added throughout the reaction at the standard rate (13 g in 1st 10 min then 5 g/hr)

GC analysis revealed that conversion of p-LAL did proceed throughout the experiment. However conversion of p-LAL was reduced when the inert bed was present as shown in figure 3-59. This suggests that when the inert bed was present in the system it reduces the chances slightly of p-LAL further reacting as the solution was more dilute.

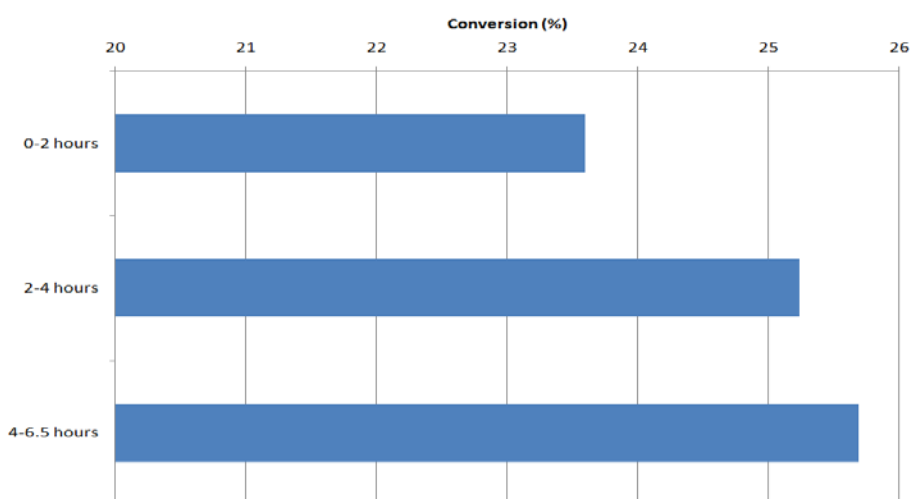


Figure 3-59 Conversion of p-LAL in standard reaction between p-LAL and copper chromite (230°C, 57 mbar)

The selectivity of the by-products (figure 3-60) was similar to that of the previous p-LAL reactions. P-LOL was produced this time but could be due to some of the material being present in the inert bed and it boiling out of solution. However, the presence of the inert bed would also yield a dilution effect and this could also affect the product distribution.

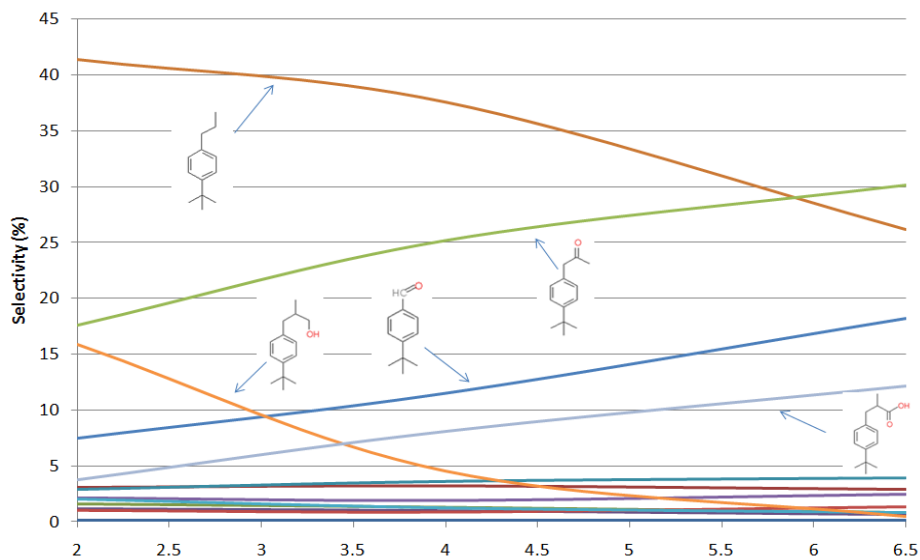


Figure 3-60 Selectivity of by-products in standard reaction between p-LAL and copper chromite (230°C, 57 mbar)

Post reaction XRD analysis (figure 3-61) indicated that the catalyst was in the reduced state at the end of the reaction.

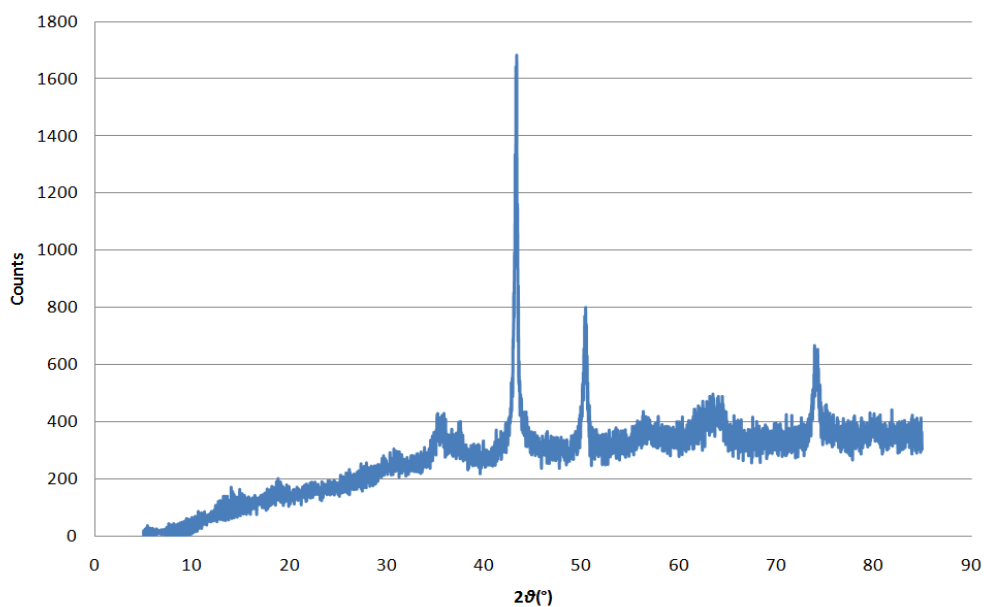


Figure 3-61 Post reaction XRD standard reaction between p-LAL and unreduced copper chromite (230°C, 57 mbar)

During a standard reaction the catalyst was reduced using evolved hydrogen from the dehydrogenation reaction, however p-LOL was not the feedstock in this reaction. By-product analysis suggested that the selectivity to p-LOL was relatively high within the first four hours. However analysis carried out on the inert bed suggested the p-LOL was present in fresh bed material. The amount present within the bed would have been enough to cause the dehydrogenation reaction to occur and yield hydrogen (113), this in turn would have reduced the catalyst.

3.3.2.8 Standard reaction involving p-LAL & reduced catalyst

It can now be concluded that p-LAL, when in the presence of unreduced copper chromite will further react to produce other products. It was decided to investigate the effect of pre-reduced copper chromite on p-LAL. The conversion and by-products were studied to examine if there were any changes observed between unreduced and a reduced catalyst. The conditions used to carry out this experiment were the standard conditions. Catalyst was reduced prior to the reaction in a furnace at 270°C for 3 hours. This was then transferred into a glove box where it was placed into the reactor along with inert bed to avoid oxidation. P-LAL was added into the slurry throughout the reaction at a rate of 13 g in the first 10 min then 5 g/h.

GC analysis revealed that p-LAL reacted when in the presence of reduced copper chromite as shown in figure 3-62. However the conversion to by-products was lower than with the reaction with p-LAL and unreduced catalyst.

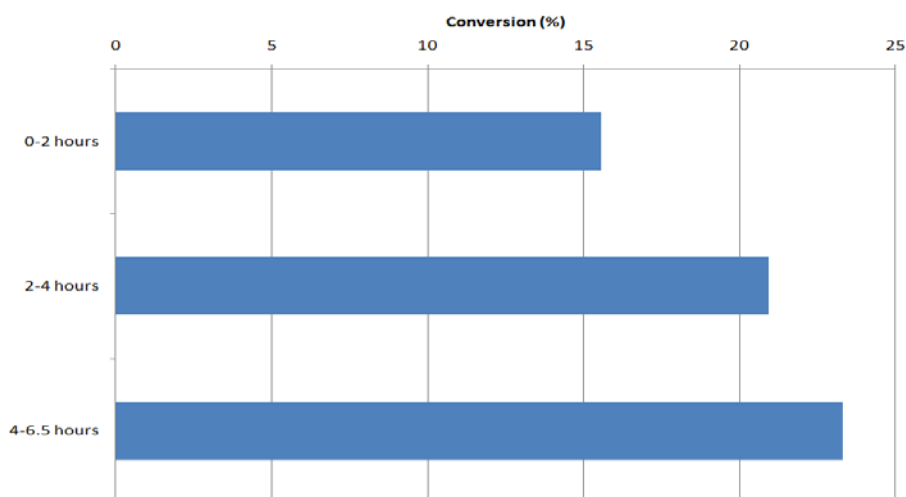


Figure 3-62 Conversion of p-LAL in a standard reaction between p-LAL & reduced copper chromite (230°C, 57 mbar)

All of the experiments that were carried out using p-LAL instead of p-LOL may have differing conversions but they all follow the same trend. As time progresses the conversion increases. This suggests that the longer that p-LAL was in contact with the catalyst the more likely it is to further react. Figure 3-63 shows the selectivity's to the by-products that were produced.

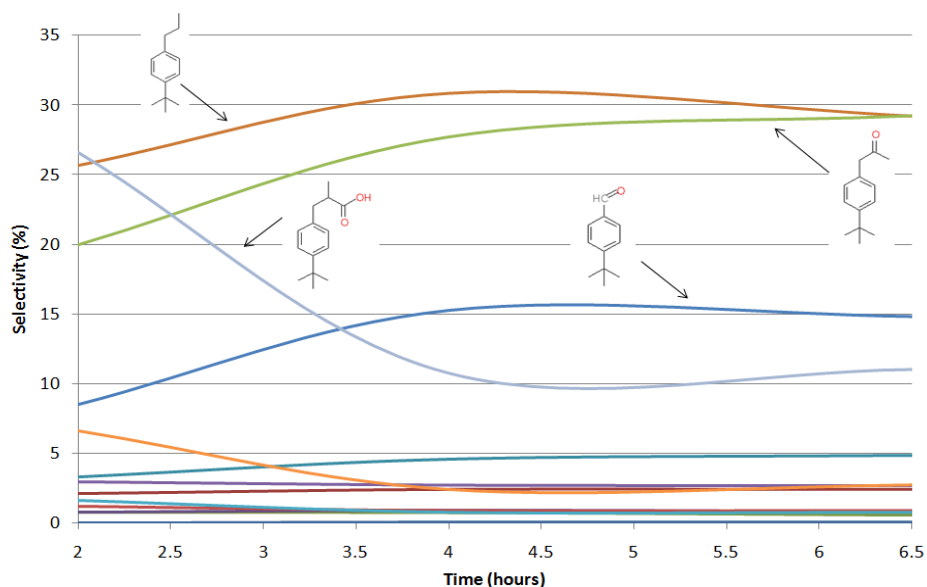


Figure 3-63 Selectivity of by-products in a standard reaction between p-LAL & reduced copper chromite (230°C, 57 mbar)

From these studies it can be concluded that p-LAL will further react with the catalyst to produce other products. However in the presence of inert bed this occurrence was dramatically reduced due to the increased vacuum and the solution being more dilute as shown in figure 3-64. In the case of pre-reduced catalyst once again the conversions of p-LAL was minimised further. This may suggest that the water produced from the catalyst reduction could have been playing a role in p-LAL further reacting.

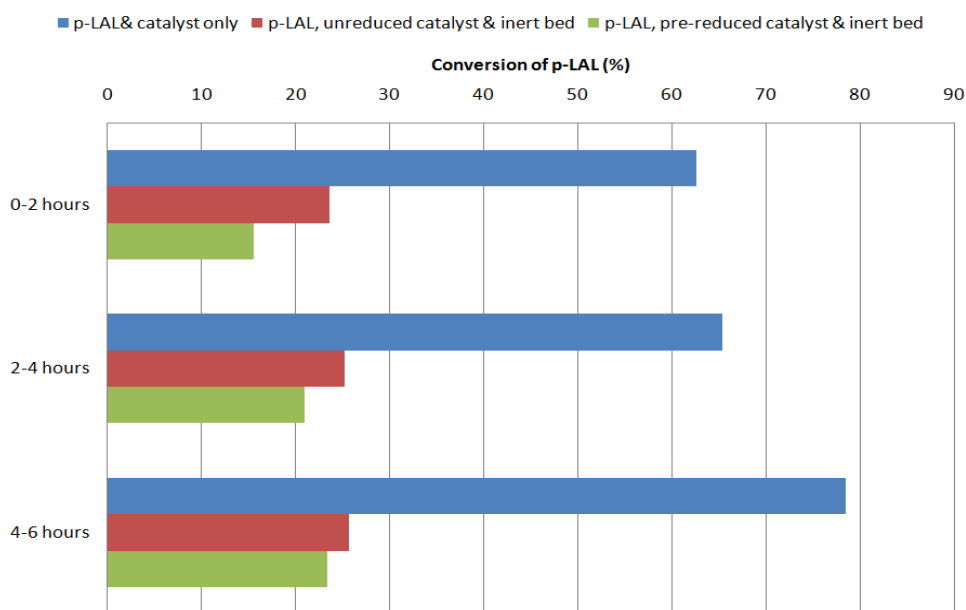
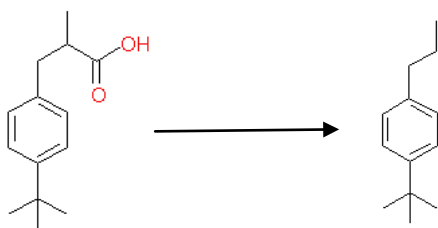


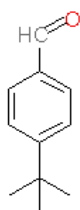
Figure 3-64 Conversion of p-LAL in the reaction between p-LAL and a) unreduced copper chromite & no inert bed b) unreduced copper chromite & inert bed and c) pre-reduced copper chromite & inert bed

3.3.2.9 By-product formation

Throughout all of the experiments studied there were six main by-products that occur in the greatest yields. LAL acid was one of those products and there are two possible routes how this could have occurred. Although the reaction was carried out in an oxygen free atmosphere, water was produced from the reduction of the catalyst and could subsequently oxidise p-LAL. Another possible route could occur via the hydrolysis of the inert bed into p-LOL and LAL acid. 1-tert-butyl-4-propyl-benzene could possibly be produced from the decarboxylation of LAL acid.



Another main by-product produced was 4-tert-butyl benzaldehyde as shown below.



It may be possible that this could have been formed by some form of a cyclisation reaction involving m-LAL where the aldehyde group would react at the para position on the benzene ring. This however was found not to occur as a reaction involving m-LAL was carried out using standard conditions and 4-tert-butyl benzaldehyde was not one of the by-products produced. This ruled out this option of production. Hence we are currently unable to suggest a credible mechanism as to how 4-tert-butyl benzaldehyde was produced. Another by-product produced was the corresponding alcohol, (4-tert-butylphenyl)methanol. This suggested that maybe it was the alcohol that was produced first and then this was dehydrogenated to the aldehyde. The reaction conditions are set up to carry out dehydrogenation reactions so this was feasible. This would also correlate with the results produced from the reactions as the aldehyde always shows a higher selectivity than the alcohol.

1-tert-butyl-4-methyl-benzene was another by-product. This was thought to be produced from the hydrogenation of 4-tert-butyl benzaldehyde. Although the system was set up to carry out dehydrogenation reactions, copper catalysts has also been reported to carry out hydrogenation reactions (135). Hydrogen produced from the dehydrogenation of p-LOL would be available to perform these hydrogenations. Figure 3-65 shows a proposed scheme.

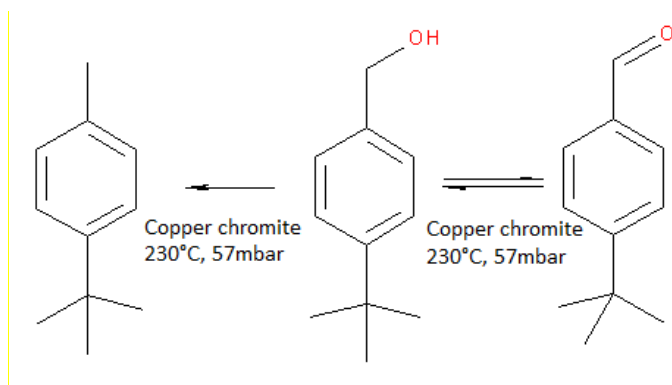


Figure 3-65 By-product formation

The last major by product was 1-(tert-butylphenyl) propan-2-one. Once again there was uncertainty as to how this was produced during the dehydrogenation of p-LAL. However it was found that during the auto-oxidation of p-LAL, 1-(tert-butylphenyl) propan-2-one was one of the products produced (4). Figure 3-66 shows the mechanism for this.

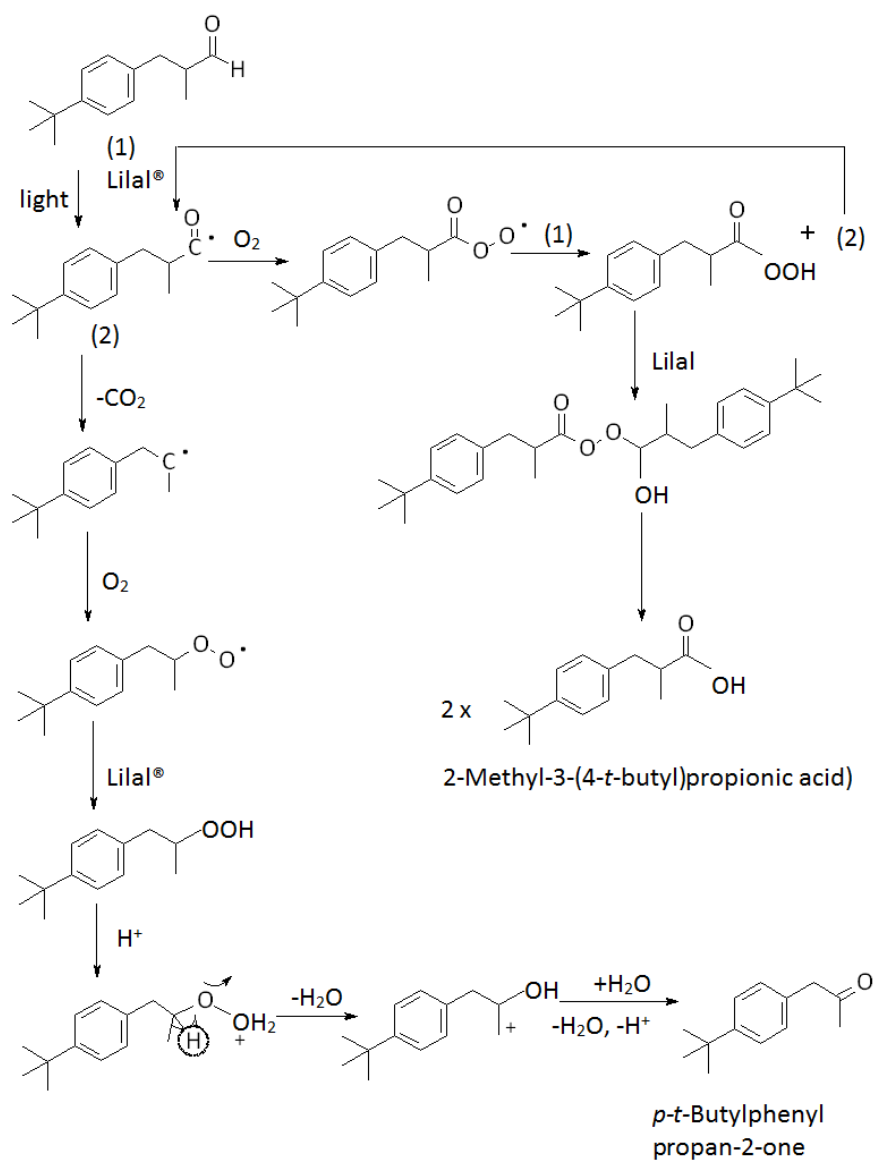


Figure 3-66 Autoxidation of lilestralis (4)

Although this route seems unlikely, it was not impossible. The initial step of the reaction involves light. The set-up used within this study was a glass reactor which would easily allow the passage of light and hence initiate the first step. The oxygen and water that was required further on once again may come from the *in-situ* reduction of the catalyst.

3.3.3 Catalyst activation

To investigate the effects of catalyst activation, a series of experiments were carried out. Currently at Innospec no catalyst activation is carried out prior to reaction. Several different methods of activation were studied.

3.3.3.1 Plant ratio

Firstly it was undecided if the Innospec plant ratio or plant rate of addition of p-LOL would be studied. The plant ratio corresponded to the ratio of catalyst: inert bed: p-LOL at the end of a reaction (which lasts for 10 days). After this time the ratio is 1 g catalyst: 10 g inert bed: 490 g p-LOL. A reaction was carried out to see if this ratio could be achieved over a 6.5 hour period. 1 g of catalyst was used and 10 g of inert bed. . The copper chromite catalyst was present in the oxidised form prior to reaction. The conditions used mimicked the plant, 230°C and 57 mbar. P-LOL was added in at a rate of 90 g in the 1st 10 min then 65 g/hr thereafter. GC analysis suggested that no reaction had taken place. To investigate as to why no reaction had taken place, data from the data logger (which monitored reaction temperature during the experiment) was examined. As shown in figure 3-68 there was a significant decrease in temperature when the initial material is added. After this point the temperature began to increase slightly but the desired reaction temperature (230°C) was never achieved.

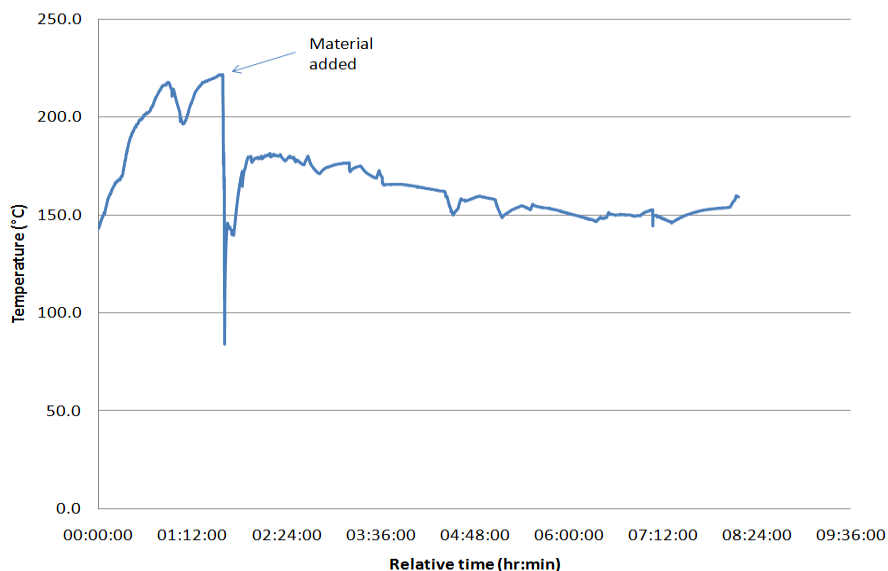


Figure 3-67 Data logger temperature profile from reaction where plant ratio studied (ratio used: 1 g catalyst: 10 g inert bed: 490 g p-LOL, conditions: 230°C, 57 mbar)

The rate of addition of p-LOL was too great for the reactor to maintain a steady temperature. Due to reaction temperature not being achieved the reaction did not proceed. Dehydrogenation reactions are extremely temperature sensitive (136) and hence the reaction did not take place.

3.3.3.2 Plant rate

It was then decided to study the rate of addition of p-LOL used on plant instead of the ratio of catalyst: inert bed: p-LOL and at the end of the reaction. The rate of addition mimicked the rate from the lilestralis production plant. When scaled down the following composition was used for all future reactions: 5 g catalyst: 50 g inert bed: 13 g p-LOL in the 1st 10 min then 5 g/hr. Analysis was carried out for a period of 6.5 hours. Liquid samples were analysed using GC.

Figure 3-69 shows the total conversion of p-LOL and the yield of p-LAL produced in the standard reaction.

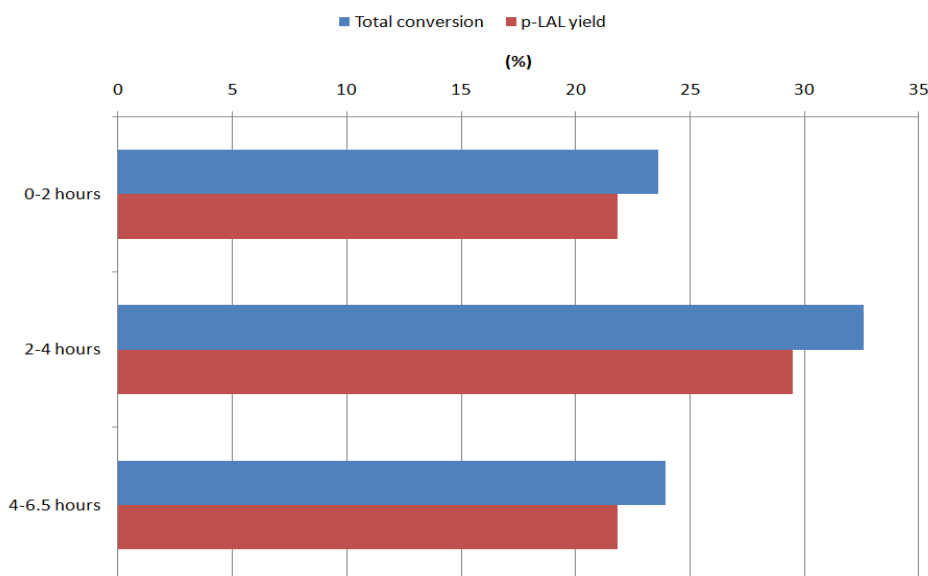


Figure 3-68 Conversion of p-LOL & p-LAL yield for reaction between p-LOL and non activated copper chromite: short reaction (230°C, 57 mbar)

It can be observed from figure 3-68 that the conversion of p-LOL increased after the first 2 hours and then began to decrease. Previous work by Pillai *et al* (137) observed that fresh copper chromite (not prerduced) required an induction period to gain maximum activity. This agreed with the data that was obtained in the reaction between p-LOL and unreduced catalyst. However after this point a decrease in conversion was observed, this was due to the catalyst starting to deactivate. Tu *et al* (106) suggested that the predominant decay of copper catalysts in dehydrogenation reactions was due to sintering rather than coking. Sintering is the loss of active catalyst surface area due to crystallite growth of either the support or supported metals (138). Sintering has been found to be strongly temperature dependant (139). It has been suggested that the higher the temperature, the greater the rate of sintering. Sintering of metal particles can be reduced by the addition of a second higher melting point metal (140). In the case of copper chromite, chromium is responsible for the reduction in sintering due to its higher melting point (Cu mpt: 1084°C, Cr mpt: 1907°C).

Another explanation for the initial low activity of the catalyst could be due to the oxidation state of the copper catalyst. At the beginning of the experiment, the copper in the catalyst is fully oxidised i.e in the Cu^{2+} state. However, evidence from the literature suggests that the active phases of the copper for dehydrogenation reactions are Cu^{+1} , Cu^0

or a combination of both. Cunningham *et al* (141) have shown, using high purity Cu^0 , CuO , and Cu_2O powders, that the activity for IPA dehydrogenation is dependent upon the Cu oxidation state, and Cu_2O and CuO display dehydrogenation activity only after a significant induction period which is dependent on the extent of prior reduction, suggesting that Cu^0 is the active phase. However Fridman *et al* (130) studies into the active phase of copper catalysts in the dehydrogenation of cyclohexanol revealed that Cu^{1+} was more active than Cu^0 .

In either case, Cu^{2+} has been shown not to be the active phase. Therefore at the beginning of the current experiment, the majority of the copper in the catalyst was inactive, and hence only a small conversion was observed. However as the dehydrogenation reaction proceeds, hydrogen is evolved as a by-product and can reduce the copper to the active phase(s). It can therefore be seen that as the reaction proceeds, the conversion increases as inactive copper is converted to the active phase. This initial induction period for copper catalysts in dehydrogenation reactions has been observed previously in the literature (98, 141).

Although the *in-situ* reduction has the effect of increasing the activity, the selectivity to the desired product actually decreases over time and can also possibly be linked to the formation of metallic copper. A recent study into copper based catalysts has revealed the presence of two distinct active sites, Cu^+ and Cu^0 . Fridman *et al* (130) examined the dehydrogenation of cyclohexanol to cyclohexanone over copper based catalysts and found that metallic copper, whilst active for dehydrogenation, was not selective towards the desired product. Monovalent copper (Cu^+) was found to be more selective, and 15 times more active for the dehydrogenation reaction.

The author's explanation (130) for the difference in selectivity between the two active sites was related to the species adsorbed on each site. In their studies they found that over monovalent copper, cyclohexanol was adsorbed onto the site to form cyclohexanol alcoholate (precursor species for cyclohexanone, the desired product). Over metallic copper however, adsorption of cyclohexanol yielded two species, the cyclohexanol alcoholate and a phenolate species. The existence of the two adsorbed species may explain the low selectivity of this active site.

In the present study, the catalyst was reasonably selective at the beginning of the reaction but as time progressed became less selective. As the catalyst was not pre-reduced prior to use, at the beginning of the reaction the majority of the copper would be in the fully oxidised state, with a small amount of Cu^+ present and even less copper metal. Fully oxidised copper does not catalyse the reaction, therefore the main active species in the catalyst would be the small amount of monovalent copper. As discussed, Cu^+ is highly selective, and this accounts for the low production of side products that was observed. Over time, the evolution of by-product hydrogen would result in the inactive Cu^{2+} being converted to copper metal, and yield an increase in conversion. This was observed in the current experiment, along with a drop in selectivity (consistent with Fridman *et al's* (130) observation that copper metal is active but not selective)

The data logger profile (figure 3-70) highlighted that using the Innospec rate instead of the ratio allowed a more consistent temperature throughout. There was still a slight decrease when the initial material is added in the first 10 minutes but after that it is fairly constant. There are several small dips in temperature but it is unsure if these are due to cold material being added or the endothermic nature of the reaction. However reaction temperature was still achieved.

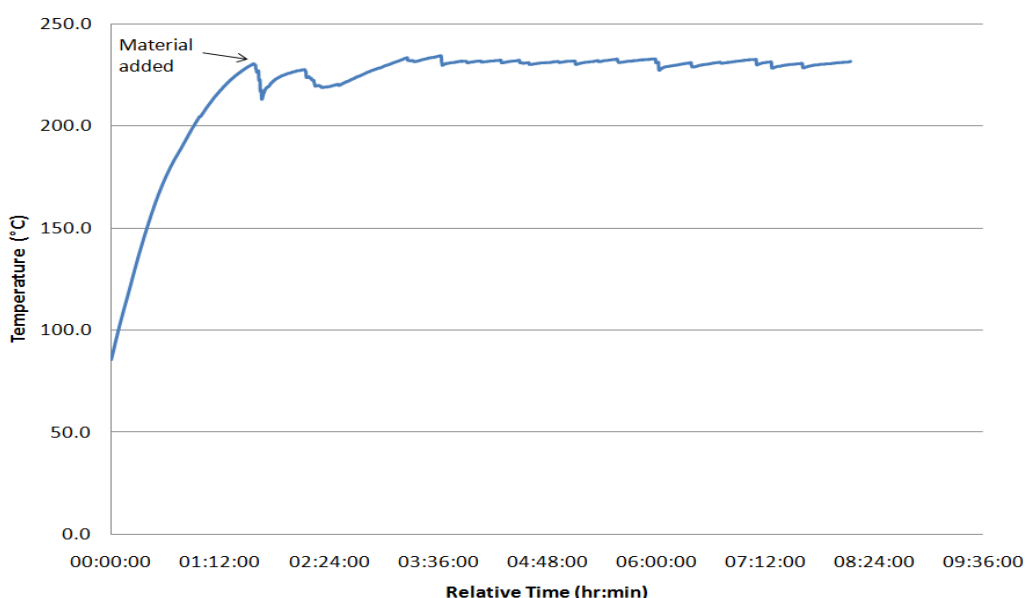


Figure 3-69 Data logger temperature profile from plant rate of addition of p-LOL (13.5g in 1st 10 minutes then 5g/h, conditions: 230°C, 57 mbar)

Post reaction, the catalyst was centrifuged with acetone and allowed to air oxidise for 1 hour before analysis was carried out. A post reaction XRD pattern was obtained (figure 3-71) and revealed that peaks with 2θ values consistent with Cu^0 were present. This indicated that the hydrogen produced from the dehydrogenation of p-LOL reduces the catalyst as the reaction proceeds. As well as this, the presence of Cu metal could also explain the low selectivity towards the desired product (130).

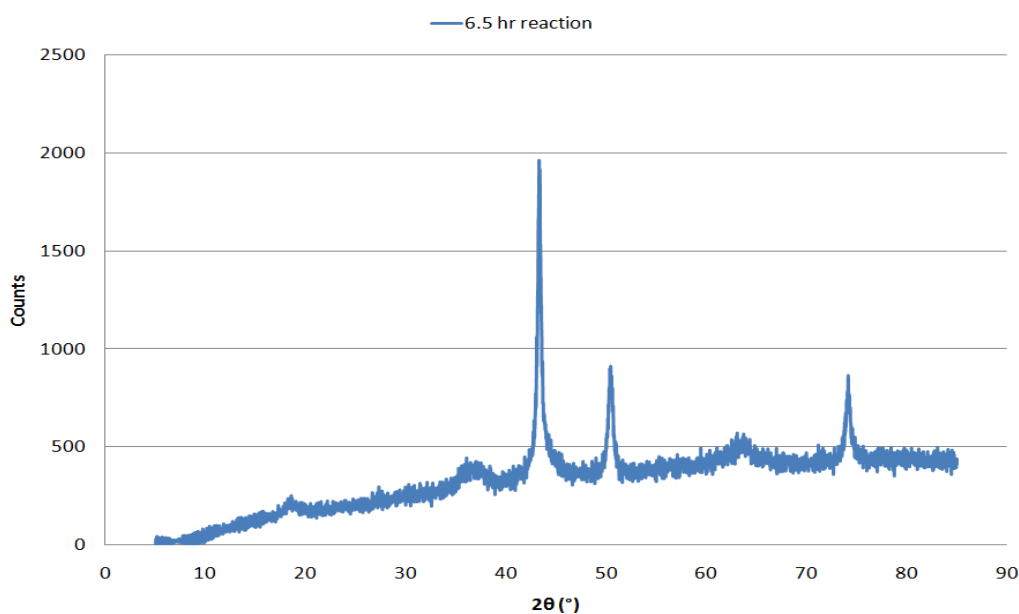


Figure 3-70 Post reaction XRD from standard reaction between p-LOL and copper chromite (230°C, 57 mbar)

To determine if during the reaction, sintering of the catalyst had occurred, the Scherrer equation was used to calculate crystallite size.

Table 27 Crystallite size comparison between hot stage XRD and 6.5 h reaction

Catalyst	Crystallite size
Hot stage XRD	10 nm
6.5 hour post reaction XRD	17 nm

It can be illustrated from table 27 that there is an increase in crystallite size between the two samples. The hot stage XRD was a fresh reduced catalyst sample. This emphasises that during the reaction sintering had occurred as the crystallite size had increased (106).

To investigate the reproducibility of the dehydrogenation of p-LOL, the reaction was repeated twice more. Figure 3-72 shows that a degree of variation was present throughout these three reactions. The greatest variation in the samples is within the first 4 hours, the start-up period. After this time the reaction begins to “settle down” and produce similar conversions. In the initial period there are various reactions taking place at once as described in section 3.3.2.4.3. P-LOL will dehydrogenate into p-LAL yielding hydrogen. This in turn will reduce the catalyst. Inert bed will be produced via the Tishchenko reaction and destroyed by ester hydrolysis. It was therefore likely that small variations in the start-up procedure between the experiments could lead to the appreciable differences observed.

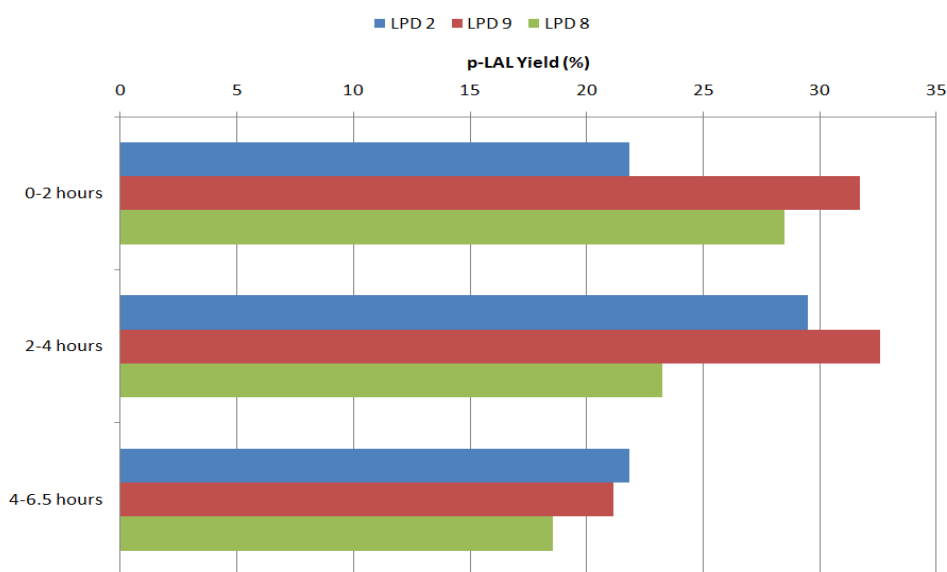


Figure 3-71 P-LAL yield comparison for standard reaction involving p-LOL and copper chromite (230°C, 57 mbar)

An average of p-LAL yield was taken from the three sets of data as shown in figure 3-73. It can be illustrated that after 4 hours deactivation was starting to occur.

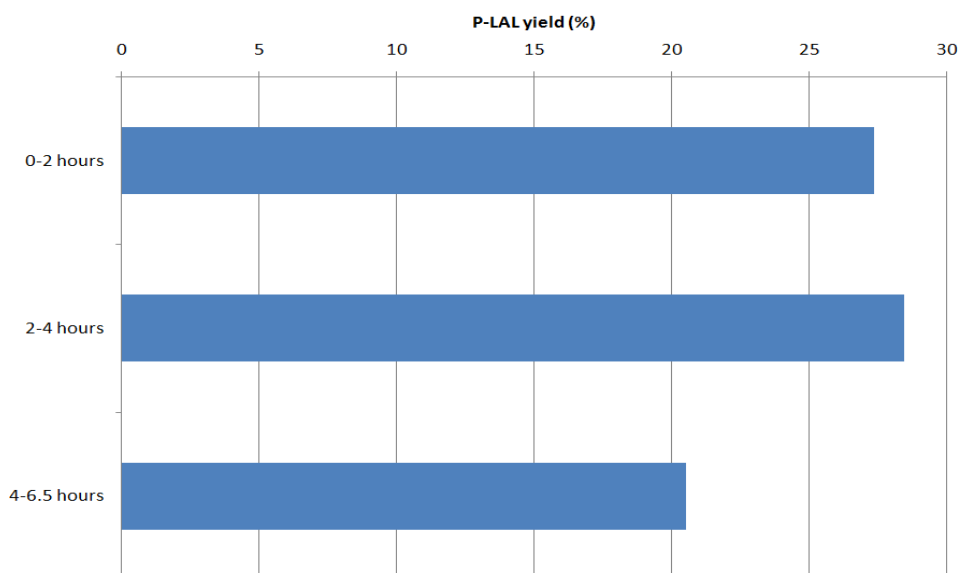


Figure 3-72 p-LAL average yield for standard reaction involving p-LOL and copper chromite (230°C, 57 mbar)

3.3.3.3 Catalyst reduction

During the standard reaction no prior catalyst activation was carried out. However at the end of the reaction the catalyst was in the active phase (metallic). As stated in the previous section, the *in-situ* activation of the catalyst was achieved through reaction with evolved hydrogen (113). Elemental copper was thought to be an active form of copper for the dehydrogenation (122) and this meant that during the reaction the catalyst was reducing. To investigate what form (inactive or active) the catalyst was in after 2 hours, a short reaction was carried out. All conditions were the same as the standard reaction.

Figure 3-74 shows the XRD pattern of sample that was obtained after the 2 hours and peaks consistent with metallic copper were apparent.

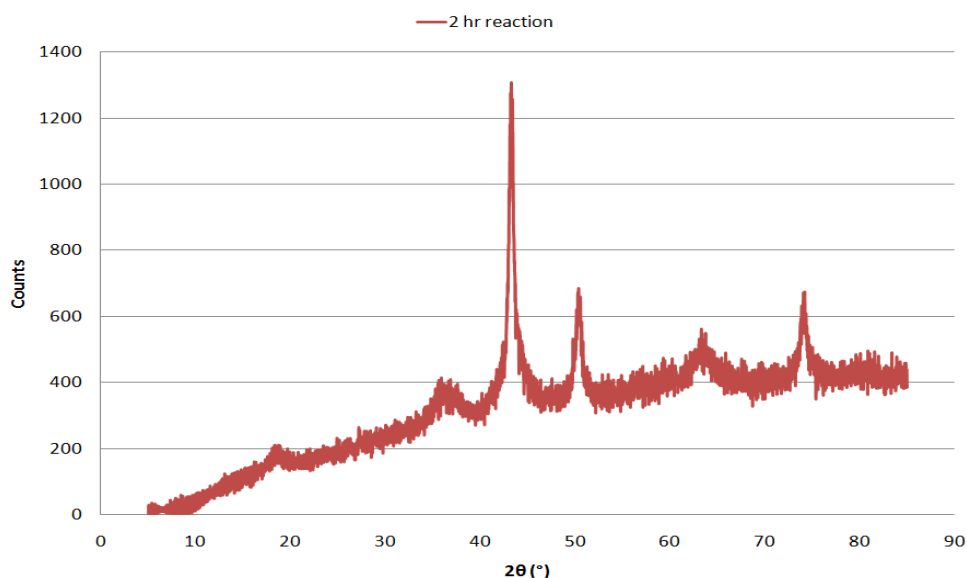


Figure 3-73 Post reaction XRD 2hour reaction between p-LOL and copper chromite (230°C, 57 mbar)

When this XRD pattern was compared to a post reaction XRD it was clear there was a difference as shown in figure 3-75. The longer reaction showed higher intensity copper peaks suggesting that more oxidised copper is now in the active state of metallic copper. This highlights that during the reaction the catalyst was reducing with time. However the catalyst had also started to deactivate at this point, possibly due to the growth of copper crystallites (sintering).

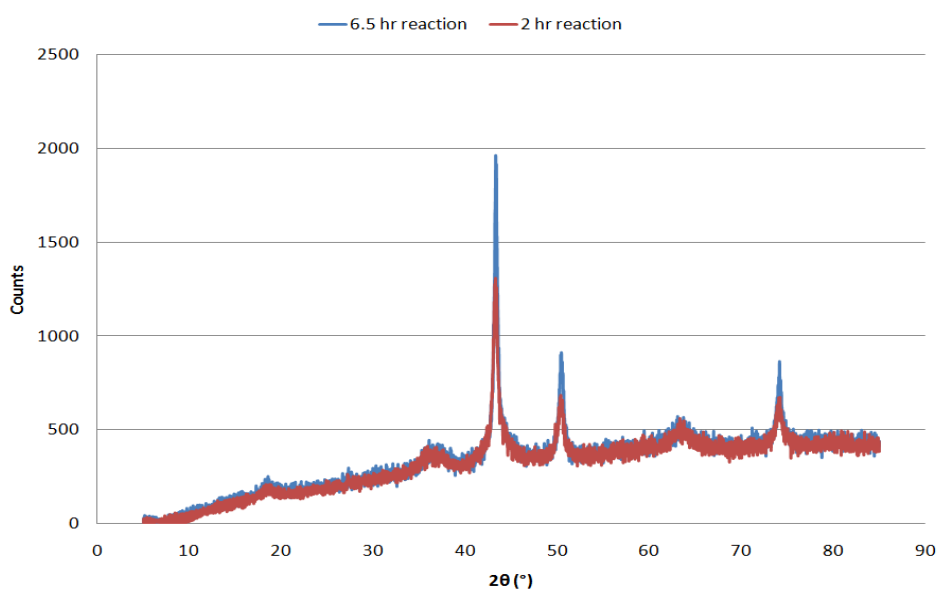


Figure 3-74 Post reaction XRD comparison of a) 2hr and b) 6.5hr reaction between p-LOL and copper chromite

From the above XRD the Scherrer equation was used to calculate the crystallite size of the copper crystallites in the post reaction catalyst. Table 28 shows the results obtained. It can be observed that over time the crystallite size increases, suggesting that sintering was taking place and hence the catalyst was deactivating.

Table 28 Crystallite size comparison between 2 h reaction and 6.5 h reaction

Catalyst	Crystallite size
2 hour post reaction XRD	15 nm
6.5 hour post reaction XRD	17 nm

3.3.3.4 Sequential addition

Throughout the standard reaction the catalyst was found to continually deactivate. To overcome this deactivation it was decided to carry out sequential catalyst additions during the reaction to prolong the activity. The first part of the reaction was run for 10 hours using the standard conditions. After this the reactor was opened and the second batch of catalyst and inert bed was added into the system and continued for another 6 hours. Figure 3-76 shows the conversion for the first part of the reaction.

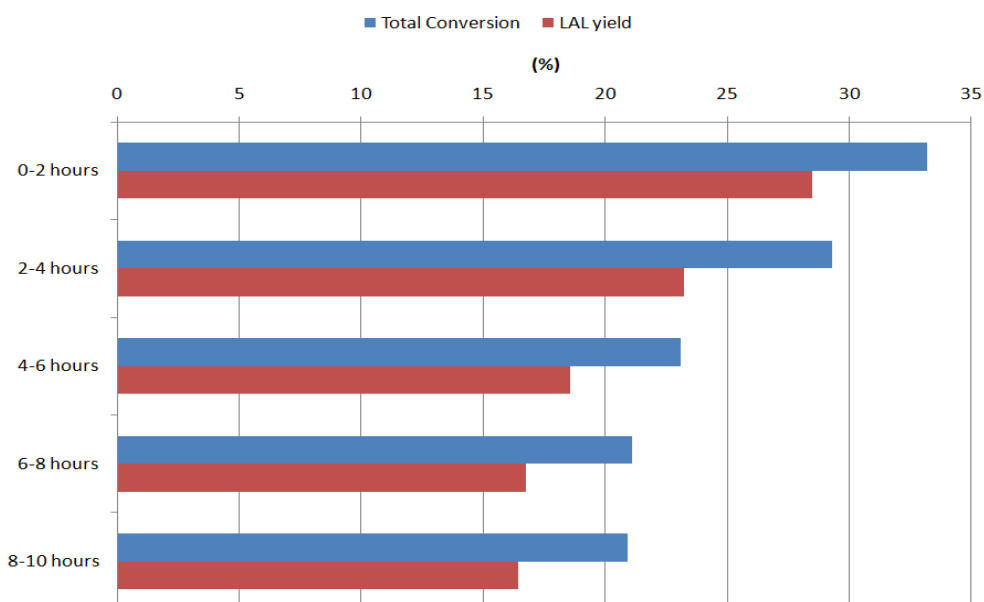


Figure 3-75 Conversion of p-LOL & p-LAL yield for part 1 of sequential addition involving p-LOL and copper chromite (230°C, 57 mbar)

As illustrated in figure 3-76 that deactivation does occur as expected and as a result of this, p-LAL yield decreases.

Figure 3-77 shows the second part of the reaction after the second catalyst addition. Some of the catalytic activity is regained but also deactivates over time as before.

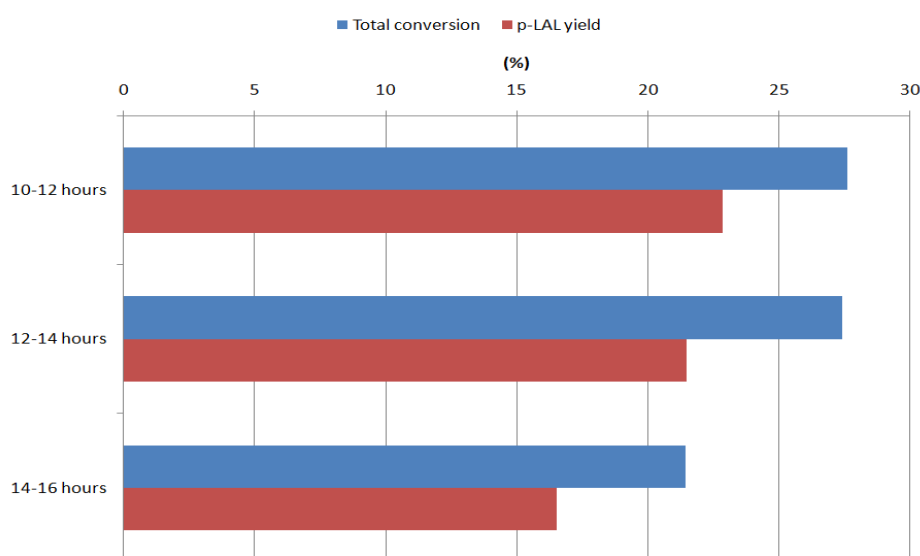


Figure 3-76 Conversion of p-LOL & p-LAL yield for part 2 of sequential addition involving p-LOL and copper chromite (230°C, 57 mbar)

It can be observed in figure 3-78 that despite the second addition of catalyst, the initial conversion that was produced in the first 2 hours it is not regained. The conversion after the addition is similar to that of the 2-4 hour sample. This implies that adding in sequential catalyst additions will not produce the high initial conversion that was produced at the start of a reaction.

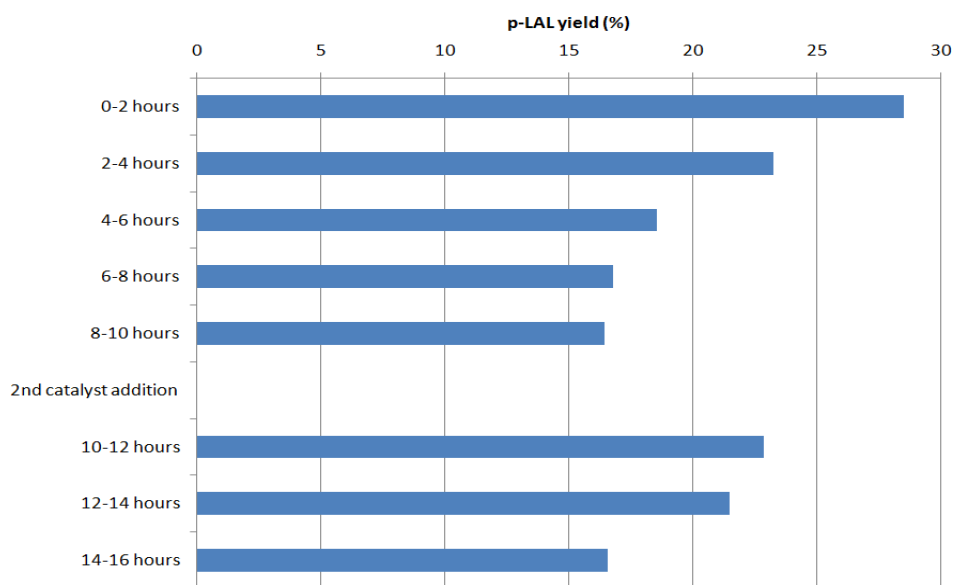


Figure 3-77 Conversion of p-LOL & p-LAL yield for sequential addition reaction involving p-LOL and copper chromite (230°C, 57 mbar)

3.3.3.5 Activation effect

During the standard reaction, no prior catalyst activation was carried out. To examine if activating the catalyst to the active state has an effect on the conversion, a series of experiments involving pre-reduced catalyst was carried out.

3.3.3.5.1 In-situ activation

In-situ reduction involved activating the catalyst within the reactor and was carried out by charging both the inert bed and catalyst into the reactor as in a standard reaction. The system was purged with nitrogen to create an inert atmosphere. The reactor was then brought up to reaction temperature with 20 ml.min⁻¹ 5% H₂/Ar bubbling into the slurry and held for 2 hours. During this *in-situ* activation, water was produced (142). After this reduction p-LAL was introduced into the system and the reaction began as normal.

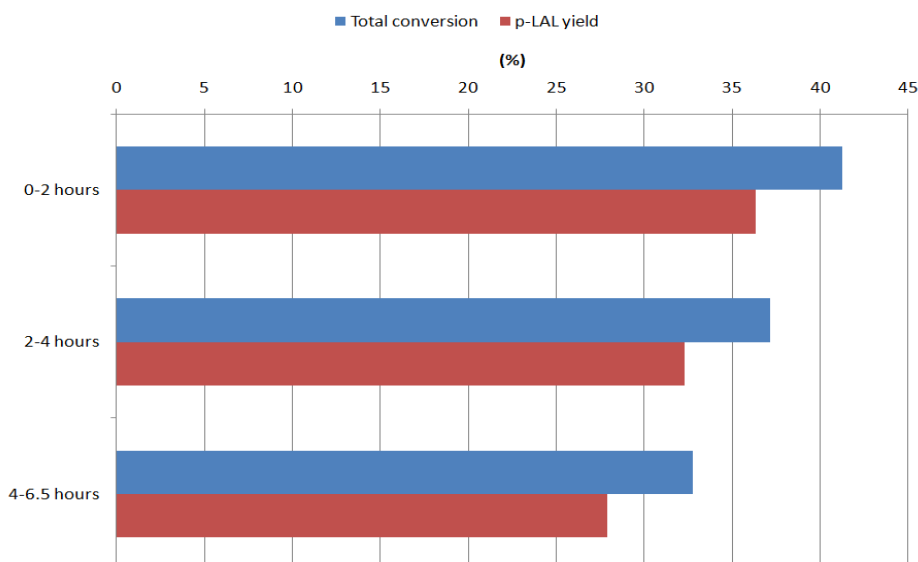


Figure 3-78 Conversion of p-LOL & p-LAL yield for reaction involving p-LOL and *in-situ* activation of copper chromite: short reaction (230°C, 57 mbar)

As shown in figure 3-79, both the p-LAL yield and conversion of p-LOL is increased from the standard reaction (figure 3-69). This signifies that activating the catalyst has had a positive effect on the reaction. Tu *et al* (106) suggested that the dehydrogenation activity is proportional to metallic copper surface area. Hence activating the catalyst prior to reaction will ensure that the dehydrogenation will occur more readily. Other studies also reported that no induction period occurred when the catalyst was pre-reduced (137, 143). This was evident in these studies as the highest conversion was produced at the start of the reaction and was significantly larger than the reaction involving unreduced catalyst .

3.3.3.5.2 Ex-situ activation

To ensure that the catalyst is in the active form, it was reduced *ex-situ*. Transition metals of the first row are easily oxidised by exposure to air, hence they should be reduced and protected from air exposure (144). Copper chromite was activated on a glass line at 270°C for 3 hours with 20 ml.min⁻¹ 5% H₂/N₂. The reactor was allowed to cool in an inert gas and then sealed to avoid the catalyst being exposed to air. This was then placed into a N₂ purged glove box where the catalyst was removed and placed into the LPD reactor. The catalyst was covered with a layer of inert bed to avoid oxidation when removed from

the glove box and then setup as normal. The system was purged with nitrogen before the mixture was stirred.

Figure 3-80 shows the conversion and p-LAL yield produced. It can be observed from the results that once again there was an increase in both from the standard reaction (fig 3-69), signifying that activation of the catalyst plays a positive role in the dehydrogenation reaction.

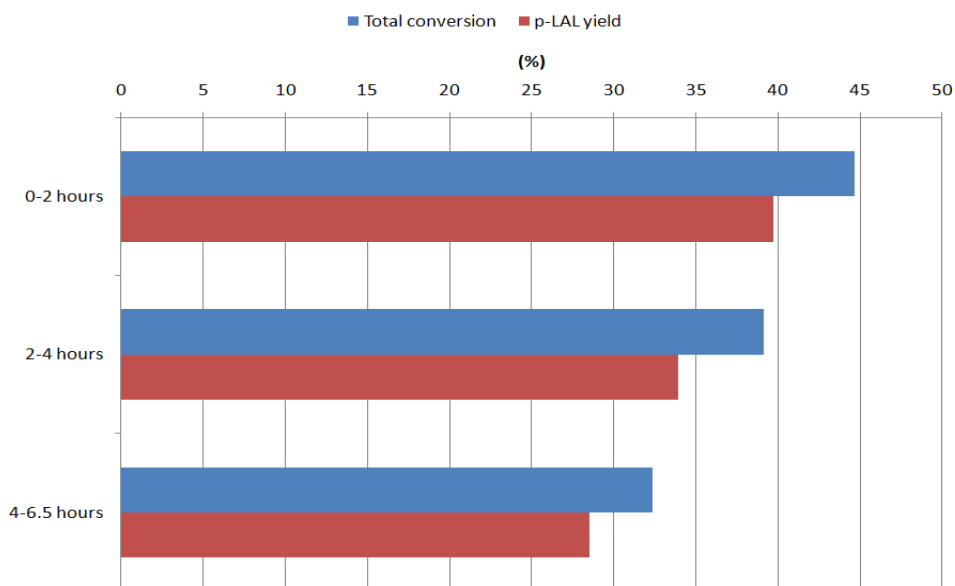


Figure 3-79 Conversion of p-LOL & p-LAL yield for reaction involving p-LOL and *ex-situ* activation of copper chromite: short reaction (230°C, 57 mbar)

Once again both conversion and p-LAL yield are increased due to activation. Pillai studied the preactivation of copper chromite (active phase: Cu^+) and its effect on the alkylation of aniline (137). It was noticed that fresh catalyst (not prereduced) showed an activity of 52% due to *in-situ* reduction of Cu^{2+} to Cu^+ . However the catalyst pretreated at 300°C for 4 hours showed the maximum initial activity (76.8%). Results within this study may have showed lower conversions due to the nature of the reaction but followed the same trend.

3.3.3.6 Activation Comparison

It was clear that activating the catalyst had a positive effect on the p-LAL yield. A comparison was made to distinguish how much of a variation there was, as illustrated in figure 3-81.

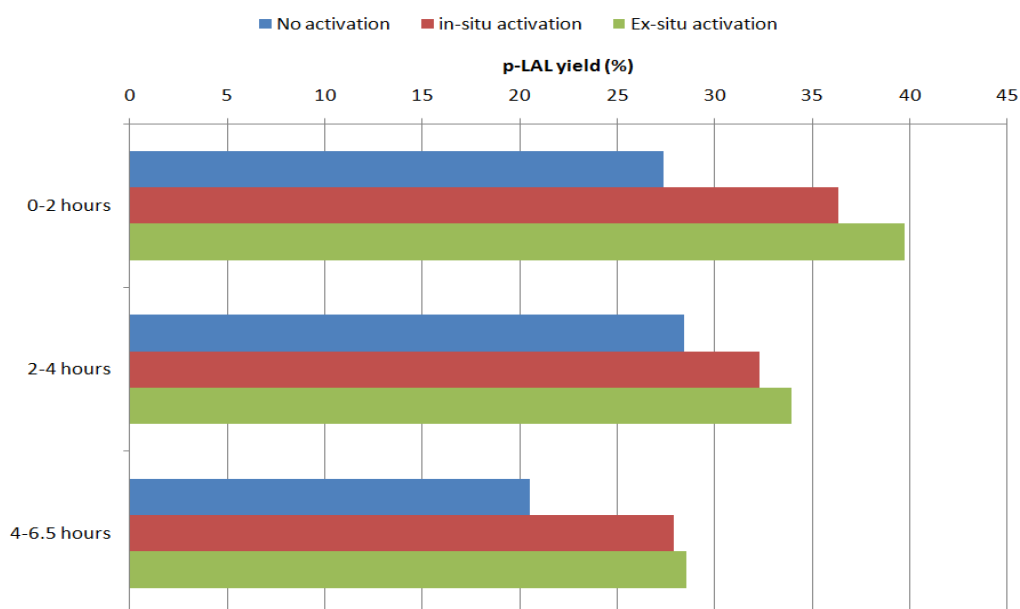


Figure 3-80 p-LAL yield activation comparison between reaction involving a) no catalyst activation b) *in-situ* activation and c) *ex-situ* activation of copper chromite

It can be observed that activating the catalyst increases the p-LAL yield. Work carried out on dehydrogenation of aromatic alcohols over a supported palladium catalyst, suggested that the alcohol can reduce the oxidised metal but the process was slower than pre-reducing the catalyst, which accelerated the reaction (145). This was concurrent with the results produced in this study. Both types of activation produced an increased yield but *ex-situ* activation was slightly more beneficial. This was due to the fact that the catalyst will reduce more efficiently in the glass line rather than *in-situ* with inert bed. However it can be observed that deactivation still occurs with reduced catalyst. At the temperature employed throughout the reactions, it was most likely that the deactivation would be due to agglomeration of metallic copper (sintering).

Although *ex-situ* activation gave the greatest conversions and p-LAL yields, it is not a realistic option for working on plant. Transporting large amounts of activated catalyst

requires special conditions to avoid oxidation. Consequently *in-situ* activation was the most suitable and feasible option.

3.3.3.7 Extended reactions

The data obtained over a period of 6.5 hours revealed that deactivation occurred and to study this over a longer period of time, reactions were carried out for a period of 10 hours.

3.3.3.7.1 No activation

A non activated reaction was carried out using the standard conditions. Samples were taken every 2 hours. Figure 3-82 shows the conversion and p-LAL yield.

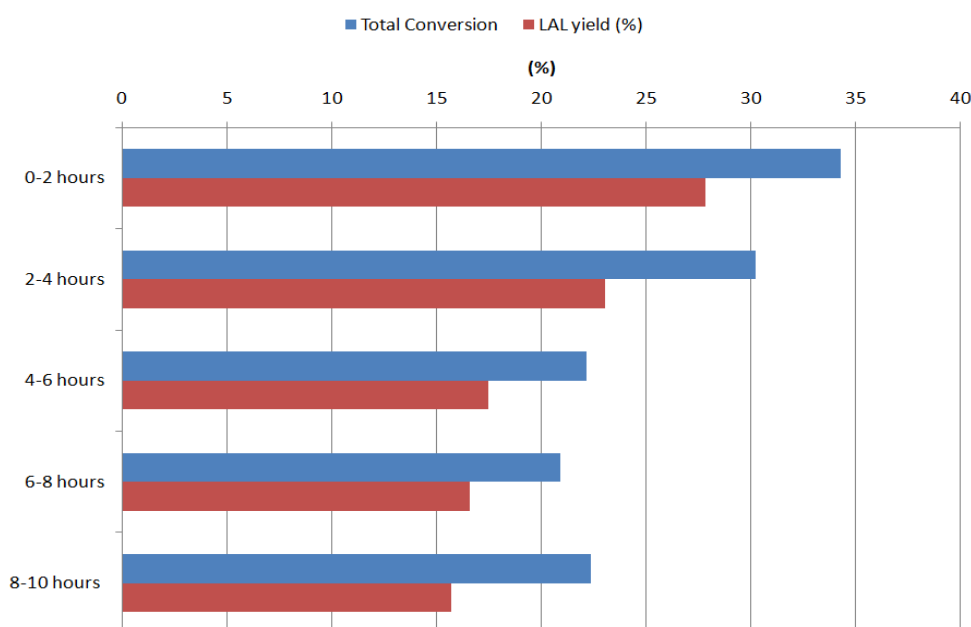


Figure 3-81 Conversion of p-LOL & p-LAL yield for reaction involving p-LOL and non activated copper chromite: extended reaction (230°C, 57 mbar)

Deactivation was clearly taking place throughout this reaction. Growth of copper crystallites (sintering) in the catalyst was thought to be responsible for the reduction in activity. Figure 3-83 shows the by-product selectivity. It was clear that there were several main by-products produced. LAL acid may have been produced through the hydrolysis of the inert bed or oxidation of p-LAL. As described previously 1-tert-butyl-4-propyl-benzene

may be produced from the decarboxylation of LAL acid. From figure 3-83 it can be seen that after 6 hours the selectivity to LAL acid decreases and 1-tert-butyl-4-propyl-benzene increases suggesting that this was taking place.

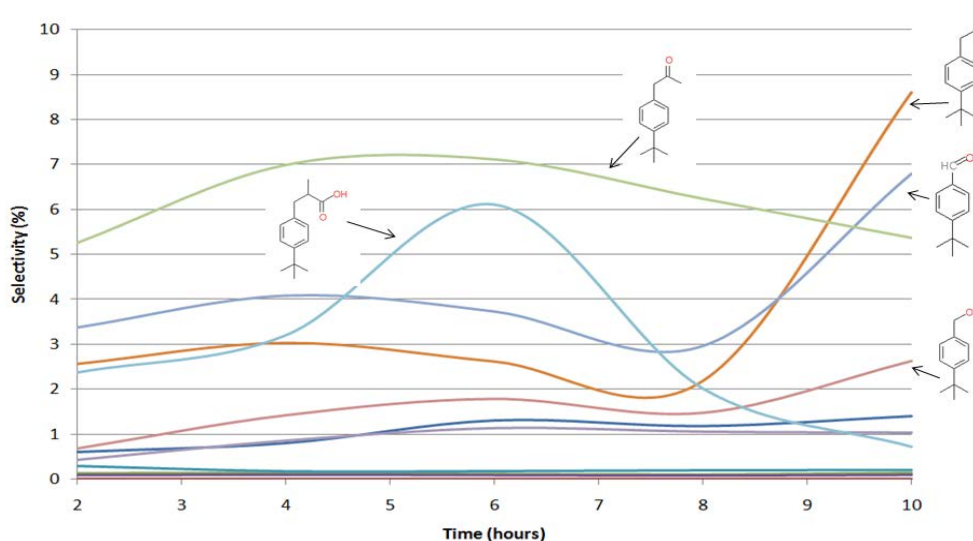


Figure 3-82 Selectivity for all other by products for reaction involving p-LOL and non activated copper chromite: extended reaction (230°C, 57 mbar)

An XRD was obtained from the post reaction catalyst. It can be observed in figure 3-84 that metallic copper peaks were present.

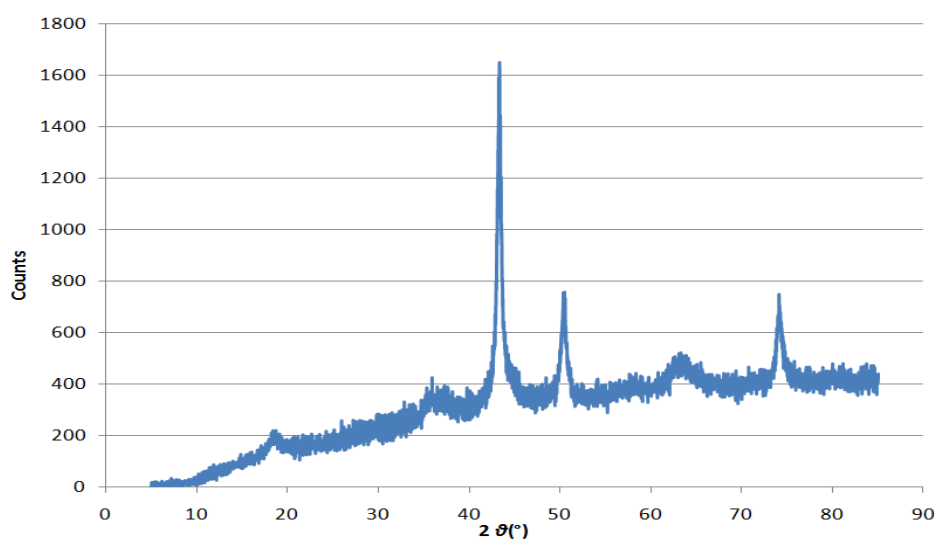


Figure 3-83 Post reaction XRD from reaction involving p-LOL and no activated copper chromite: extended reaction (230°C, 57 mbar)

The Scherrer equation was used to calculate the crystallite size for the post reaction catalysts. Table 29 emphasises that sintering was taking place as the crystallite size increased with reaction duration.

Table 29 Crystallite size comparison between hot stage, 2 h, 6.5 h and 10 h reaction

Catalyst	Crystallite size
Hot stage Sample	10 nm
2 h post reaction	15 nm
6.5 h post reaction	17 nm
10 h post reaction	19 nm

3.3.3.7.2 In-situ activation: N₂

An extended reaction was carried out involving *in-situ* activation (figure 3-85). The catalyst was reduced for 2 hours with 20 ml.min⁻¹ 5% H₂/Ar bubbling into the slurry. After this the gas was switched to N₂ and the reaction began as normal.

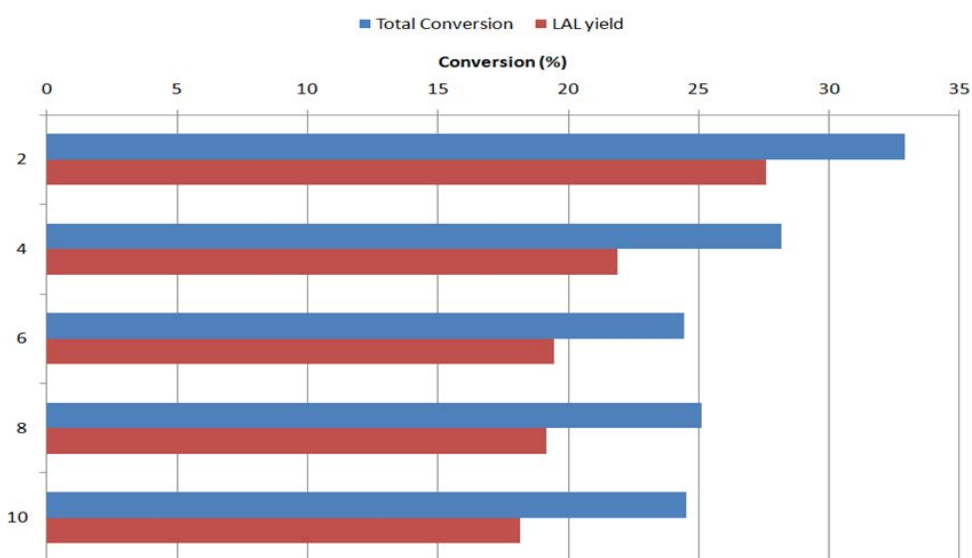


Figure 3-84 Conversion of p-LOL & p-LAL yield for reaction involving p-LOL and *in-situ* activation of copper chromite: extended reaction (230°C, 57 mbar, N₂)

Work reported by Keresszegi *et al* (145) on the dehydrogenation of aromatic alcohols on supported palladium suggested that the alcohol reactant can reduce the oxidised metal but this process was much slower than using pre-reduced catalysts. It was found that pre-reduction of Pd by hydrogen accelerated the reaction at low conversions but yields after several hours were barely affected compared to the reaction without pretreatment. In this study, reactions involving reduced catalysts produce greater initial p-LAL yields. After 10 hours it was shown that the p-LAL yield was approximately 17.5% for the reaction involving *in-situ* activation and 16% for the reaction with no activation. Both these yields are similar suggesting that like the work by Keresszegi *et al* (145), the yields produced in the dehydrogenation of p-LOL are barely affected after several hours. After a prolonged period both catalysts will be in the same reduced state and hence produce similar yields.

Figure 3-86 shows the selectivity of the by-products during the reaction between p-LOL and *in-situ* reduced catalyst.

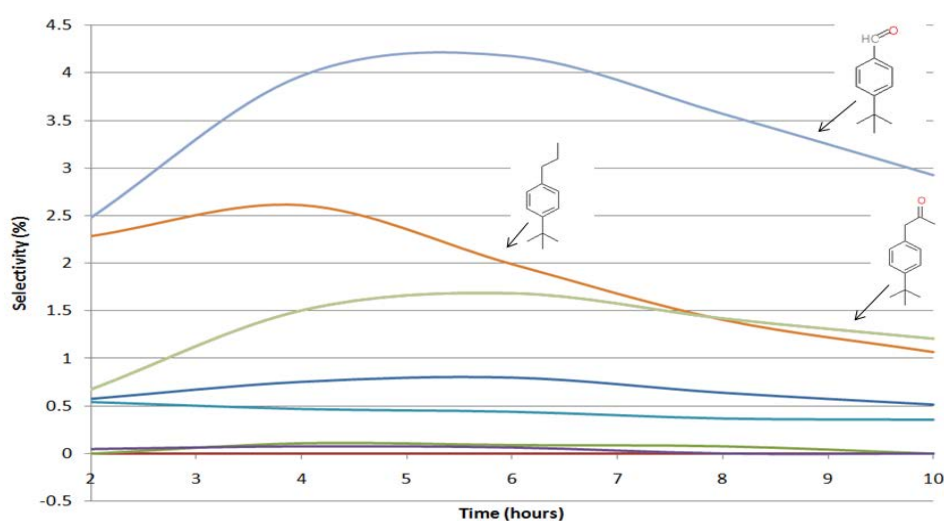


Figure 3-85 Selectivity for all other by products for reaction involving p-LOL and *in-situ* activation of copper chromite: extended reaction (230°C, 57 mbar, N₂)

3.3.3.7.3 In-situ activation: 5% H₂/Ar

Once again *in-situ* activation was carried out to activate the catalyst. However after this the reaction was carried out under a 5% H₂/Ar atmosphere. This was to examine if continually feeding hydrogen into the system had an effect on the conversion and yield.

As shown in figure 3-87 both the conversion and p-LAL yield were reduced from the previous reaction where N₂ was fed into the system.

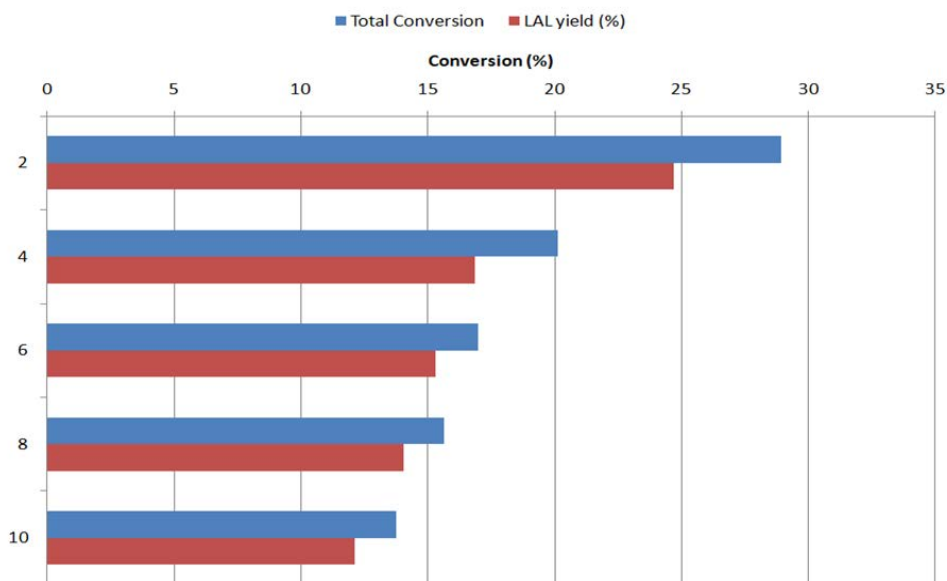
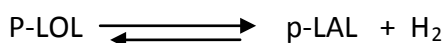


Figure 3-86 Conversion & p-LAL yield for reaction involving p-LOL and *in-situ* activation of copper chromite: extended reaction (230°C, 57 mbar, 5% H₂/Ar)

During the dehydrogenation of p-LOL, H₂ is a by-product of the reaction.



In a standard reaction under N₂, the evolved H₂ will react with copper chromite to activate the catalyst. Product water will be removed from the system via distillation. However if H₂ was continually fed into the reactor it will push the equilibrium of the dehydrogenation in favour of the reverse reaction, hence converting p-LAL back to p-LOL. It has been suggested, through work on the dehydrogenation of cyclohexane, that the conversion was increased beyond the equilibrium by removing generated hydrogen from the feed side (146). This highlights that removing the hydrogen from the system is a vital part of the reaction to attain the dehydrogenation product. The only positive aspect of continually feeding in H₂ was a lower yield of by-products. As the reaction proceeds, by-product formation decreases with time. Normally this does not take place. In the previous chapter it was suggested that p-LAL was responsible for the further reaction to produce by-products. As shown in figure 3-88 there are three main by-products produced similar

to that in the reaction with *in-situ* activation carried out under a N₂ atmosphere. It was unusual that under a H₂ atmosphere oxygenated products were formed. However during the catalyst reduction water was produced and will be present in the slurry until it is removed via distillation.

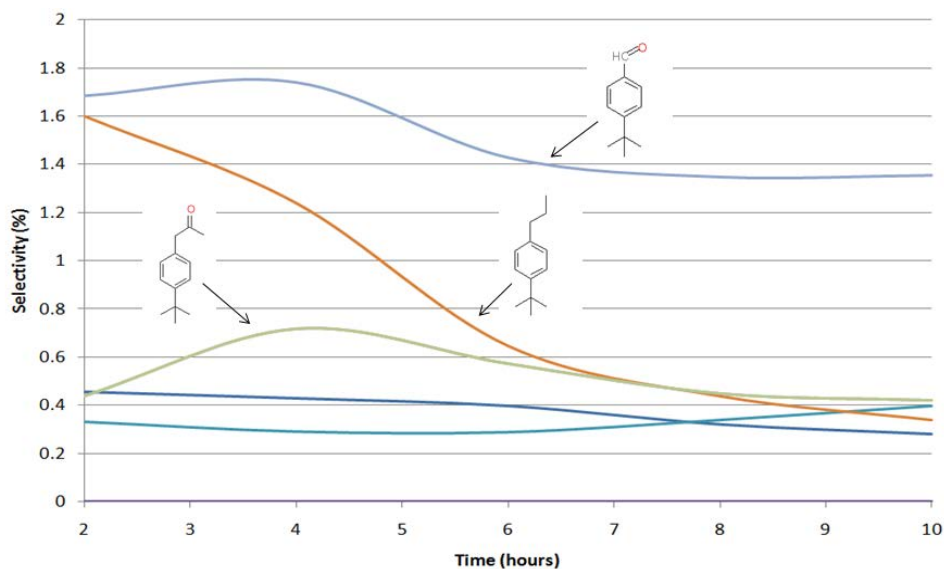


Figure 3-87 for all other by products for reaction involving p-LOL and *in-situ* activation of copper chromite: extended reaction (230°C, 57 mbar, 5% H₂/Ar)

3.3.3.8 Deactivation

Throughout all of the experiments deactivation was observed. This deactivation however may not have occurred at the same rate in all instances. Deactivation plots were prepared using the experimental data from the 10 hour reactions. Figure 3-89 shows the first of these comparisons.

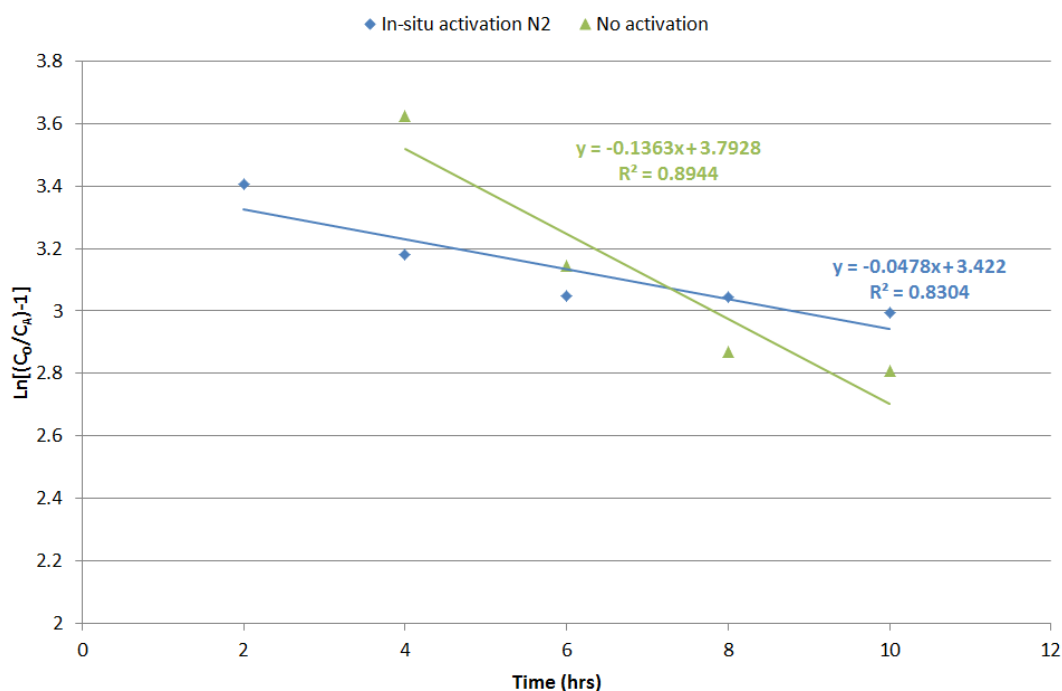


Figure 3-88 Deactivation comparison of 10 hour reaction between p-LOL and copper chromite with a) no activation b) *in-situ* activation then reaction carried out under N₂

It can be clearly illustrated from figure 3-89 that the rate of deactivation for the un-activated catalyst is greater than for *in-situ* activation (reaction carried out under N₂). This suggests that once the catalyst has been activated it deactivates at a slower rate, emphasising the view that pre-reducing the catalyst has a beneficial effect. Table 30 also suggests that less sintering had occurred during the *in-situ* reduction compared to the un-activated catalyst.

Table 30 Crystallite size comparison between 10 h no activation reaction and *in-situ* activation N₂

Catalyst	Crystallite size
10 h no activation post reaction	19 nm
10 h <i>in-situ</i> activation post reaction N ₂	17 nm

It has been previously reported that copper particle size and shape as well as the support can significantly influence the activity. Work carried out on methanol synthesis suggested

that the catalyst with the smaller copper crystallite size gave better performance (147).

Figure 3-90 highlights this.

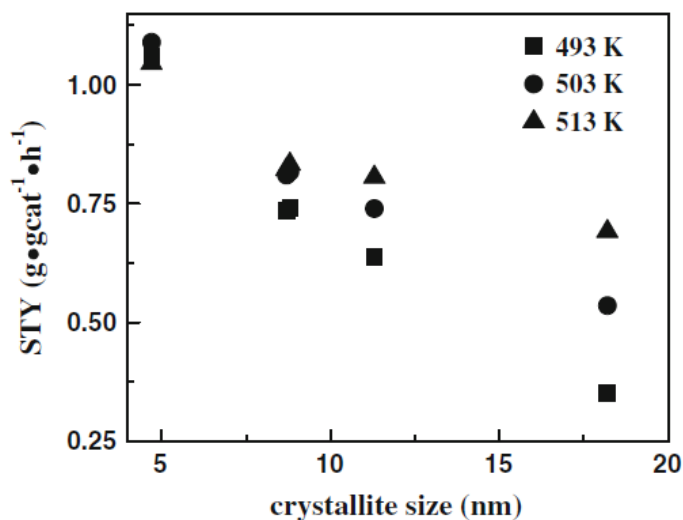


Figure 3-89 Methanol synthesis activities on Cu based catalysts with different metallic copper crystallite sizes (147)

Work also carried out on the dehydrogenation of methanol (148) and propan-2-ol (149) over a Cu/SiO₂ catalyst revealed the mechanisms to be structure sensitive (150). This suggested that over copper chromite, the dehydrogenation of p-LOL may be sensitive to changes in structure. When the level of sintering was increased, copper particles will be larger and hence the surface area will be reduced.

A comparison was also made between both cases of *in-situ* activation. As observed in figure 3-91, the reaction carried out in H₂ deactivates at a quicker rate than under N₂. Sintering does not take place when the catalyst is in the oxidised form, it only occurs when metallic species are present (138). In the instance when H₂ is being continually fed into the reaction, the catalyst will be kept in the metallic form. However this will also increase the extent of sintering.

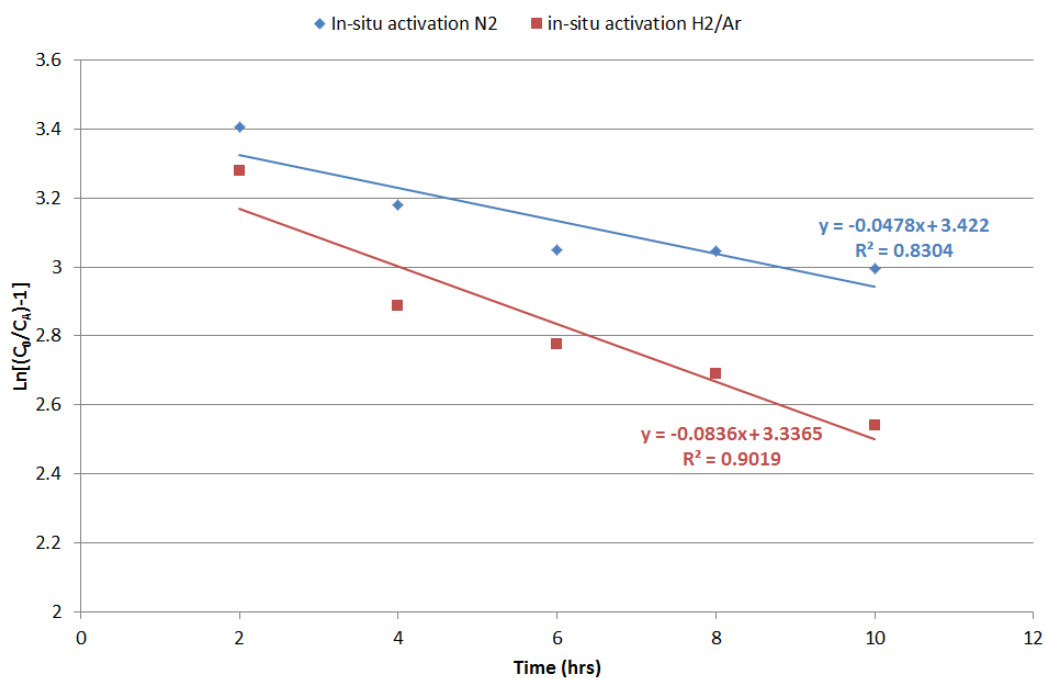


Figure 3-90 Deactivation comparison of 10 hour reaction between p-LOL and copper chromite with a) *in-situ* activation then reaction carried out under N₂ b) *in-situ* activation then reaction carried out under 5% H₂/Ar

Table 31 illustrates that reaction carried out under a 5% H₂/Ar atmosphere has a greater degree of sintering occurring than the reaction carried out under N₂.

Table 31 Crystallite size comparison between 10 h reaction carried out in N₂ and 5% H₂N₂

Catalyst	Crystallite size
10 h <i>in-situ</i> activation post reaction N ₂	17 nm
10 h <i>in-situ</i> activation post reaction 5% H ₂ /Ar	21 nm

3.3.4 Concentration variation

In the liquid phase dehydrogenation of p-LOL, certain ratios of materials were chosen and used for all reactions. In a standard reaction, the ratio studied was: 5 g catalyst: 50 g inert bed: 13 g p-LOL in 1st 10 min then 5 g/hr. Investigation into the effects of concentration was studied by varying these ratios.

3.3.4.1 Reduced mass of catalyst

To study the effects that the catalyst mass had on dehydrogenation, an experiment was carried out using half the normal amount of catalyst. Catalyst (2.5 g) was charged into the reactor along with 50 g inert bed and 13 g p-LOL in 1st 10 min the 5 g/hr. Standard reaction conditions were used (230°C, 57 mbar). It can be seen from figure 3-92 that both the total conversion and p-LAL yield was lower than that of the standard reaction.

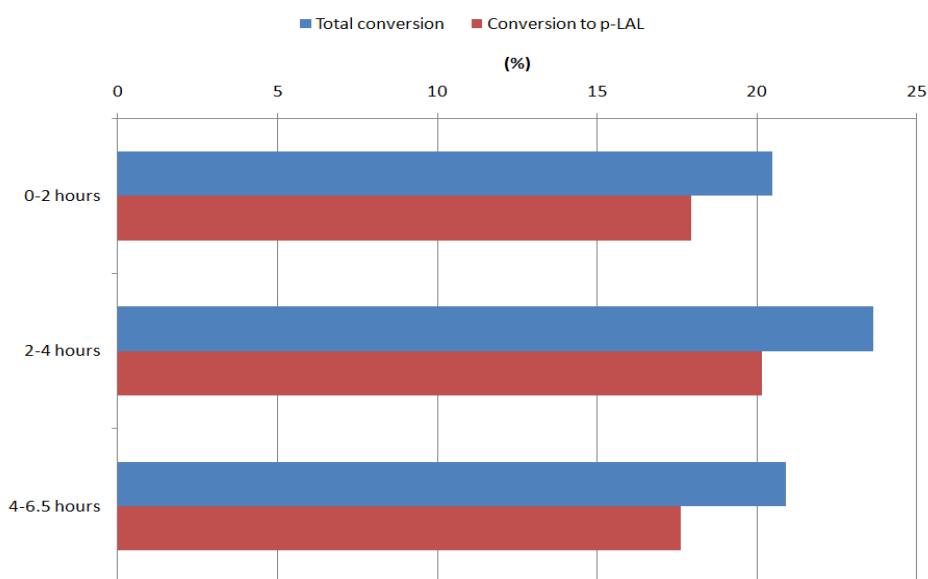


Figure 3-91 Conversion of p-LOL and p-LAL yield for 2.5 g catalyst: 50 g inert bed: 13 g p-LOL in 1st 10min then 5 g/h (230°C, 57 mbar)

The loss in conversion is due to the reduced amount of catalyst. P-LOL is still being added in at the standard rate, but there is half the amount of catalyst particles to react with. Dilution of the catalyst could also contribute to the loss in conversion.

To study this further an experiment was carried out using only 1 g of catalyst. It can be illustrated from figure 3-93 that both conversion and p-LAL yield was reduced suggesting that once again it was due to the reduction in catalyst mass. In both experiments the induction period in catalyst activity was observed, consistent with previous results.

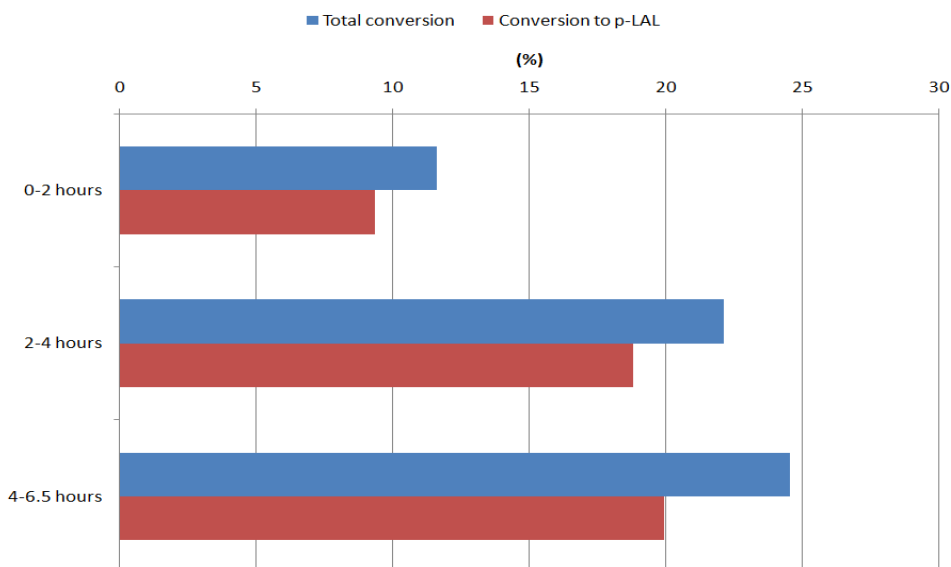


Figure 3-92 Conversion of p-LOL and p-LAL yield for 1 g catalyst: 50 g inert bed: 13 g p-LOL in 1st 10min then 5 g/h (230°C, 57 mbar)

In theory, if the system was reacting at thermodynamic equilibrium, and conversion was limited by availability of active sites on the catalyst surface, decreasing the catalyst mass by 50% would result in a reduction of the p-LAL yield by 50%. However in this instance it can be observed from figure 3-94 that when the mass of catalyst charged into the reactor was halved, p-LAL yield did not reduce by 50%. The yield reduced by approximately 35% in the first 2 hours. When the catalyst mass was further reduced to 1g there was a 50% reduction in yield in the first two hours from the reaction with 2.5 g. In all three instances after 4-6.5 hours the p-LAL yield is similar.

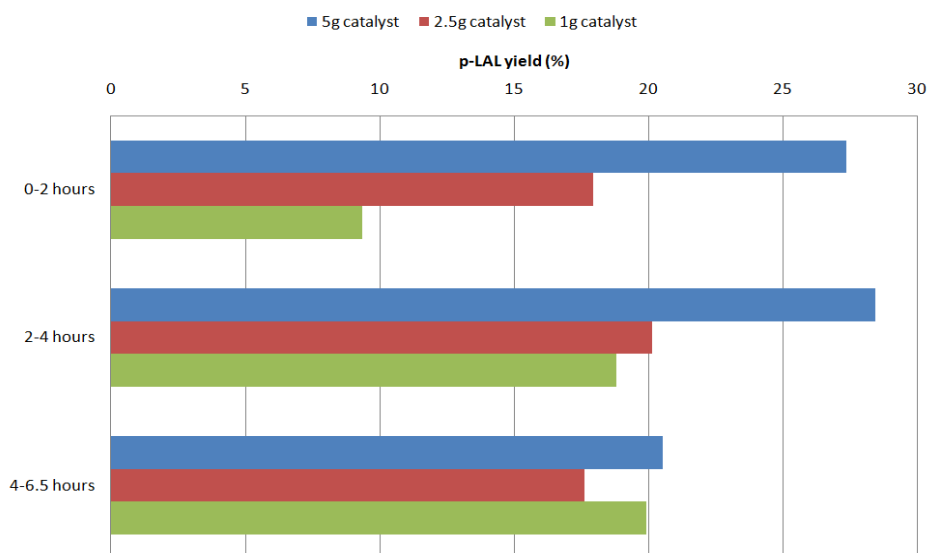


Figure 3-93 p-LAL yield comparison for catalyst mass a) 5 g b) 2.5 g c) 1 g , reaction conditions: 230°C, 57mbar

3.3.4.2 Dilution effect

To study the effect of dilution the previous experiment was repeated, however the mass of inert bed was halved (25 g). This would indicate as to whether dilution contributed to the drop in conversion observed in the previous experiment.

The results of the catalytic testing (figure 3-95) revealed that dilution was not a significant factor in the conversion decrease. Considering the variability of the starting materials, the small increase in conversion observed was well within reasonable experimental error.

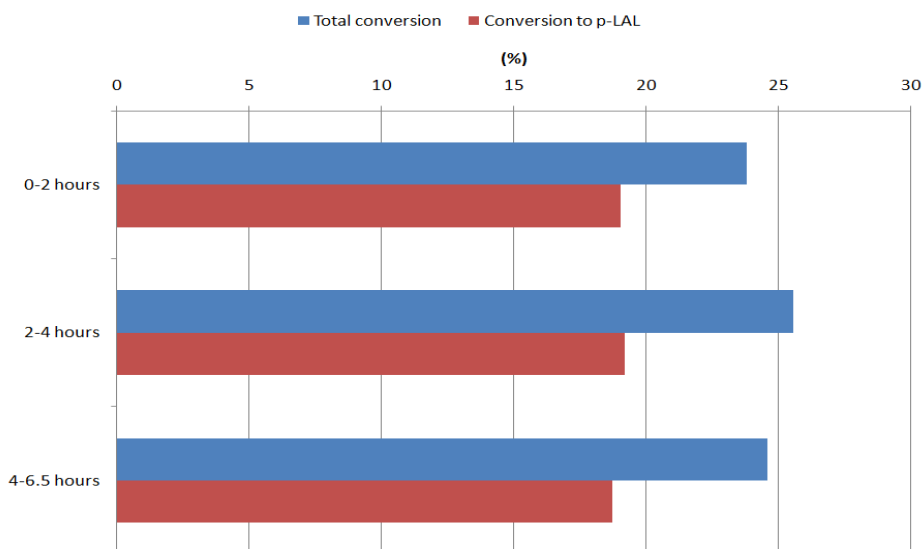


Figure 3-94 Conversion of p-LOL and p-LAL yield for 2.5 g catalyst: 25 g inert bed: 13 g p-LOL in 1st 10min then 5 g/h (230°C, 57 mbar)

3.3.4.3 Rate of addition

Throughout the dehydrogenation of p-LOL deactivation of the catalyst occurs and the yield of p-LAL decreases over time. To examine if altering the rate of addition has an effect on conversion a comparison was made. All conditions used mimicked that of the standard reaction however p-LOL was added in a rate of 10 g in the 1st 10 min then 10 g/hr. As illustrated in figure 3-96 both the conversion and p-LAL yield are reduced.

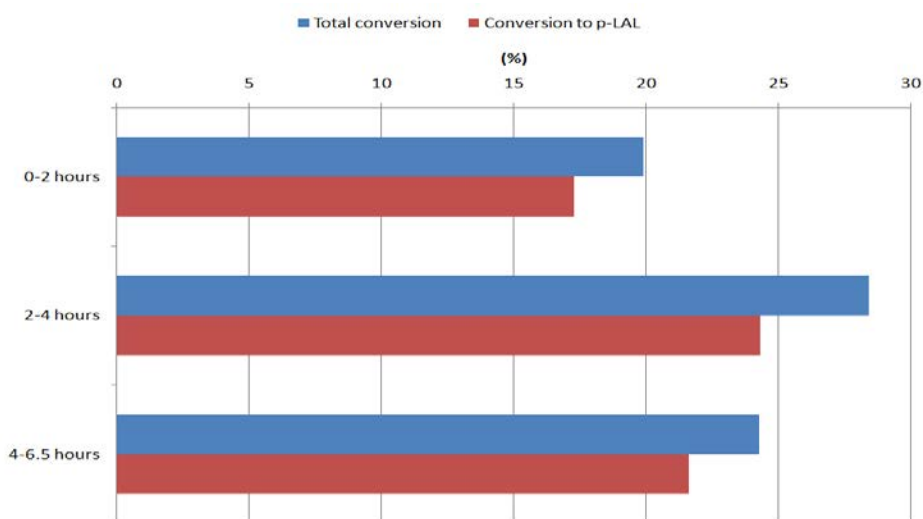


Figure 3-95 Conversion of p-LOL and p-LAL yield for 5 g catalyst: 50 g inert bed: 10 g in 1st 10 min then 10 g/h p-LOL

This was due to a temperature effect. During a standard reaction 5 g/h of p-LOL was added, however in this instance the rate of addition was doubled to 10 g/h. As a result of this reaction temperature could not be achieved and subsequently the reaction did not reach its potential. Figure 3-97 Illustrates the temperature profile.

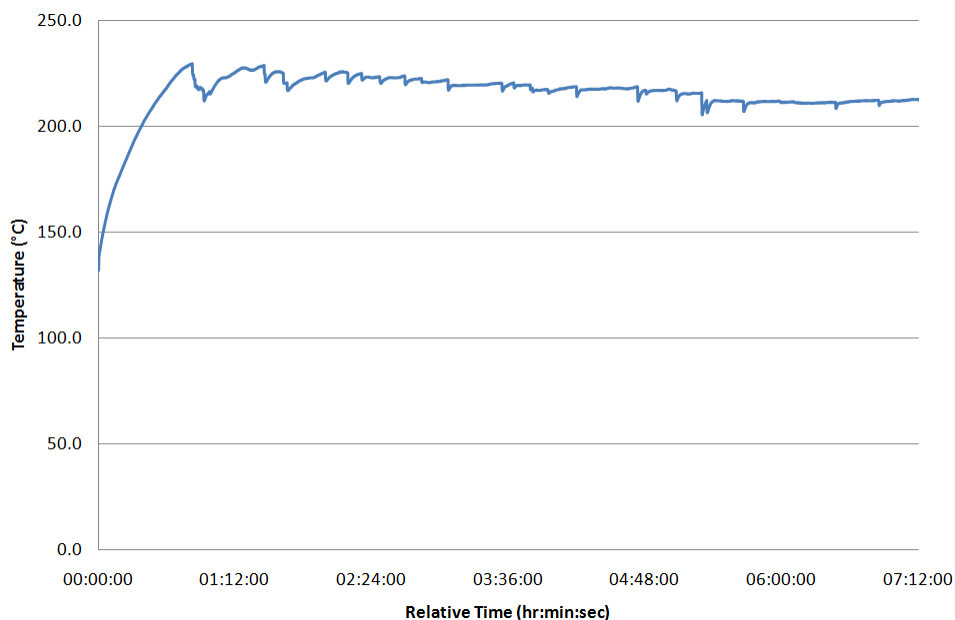


Figure 3-96 Data logger temperature profile from reaction involving increased feed rate: 5 g catalyst: 50 g inert bed: 10 g in 1st 10 min then 10 g/h p-LOL (230°C, 57 mbar)

The reduction in temperature may be due to cold material being added into the system or consequently due to the endothermic nature of the reaction or a combination of both. This resulted in lower conversions and p-LAL yields. As a general rule a 10°C rise in temperature doubles reaction rate. This suggested that even a slight change in temperature would significantly affect the reaction kinetics.

3.3.5 Alternative copper chromite

The standard copper chromite supplied from BASF is the main catalyst tested in the current study. However the catalyst was found to contain Lewis acid sites which may facilitate side reactions. It was decided to investigate alternative copper chromite catalysts to study the differences in conversion and selectivity.

Catalysts supplied from Sud-Chemie were chosen as alternatives. Two catalysts were tested: copper chromite modified with 120 ppm Na and copper chromite modified with 1600 ppm Na. These were thought to have reduced Lewis acid site content.

3.3.5.1 Copper chromite 120 ppm Na unreduced

To determine the number of Lewis acid sites present, a TPD was carried out on copper chromite 120 ppm Na using pyridine as an adsorbate, and the data analysed using mass spectrometry. As shown in table 32, results revealed that fewer Lewis acid sites were present when compared with the standard BASF catalyst.

Table 32 Catalyst comparison for Lewis acid sites

Catalyst	Lewis acid sites (per gram of catalyst)
BASF copper chromite	2.3×10^{20}
Sud-Chemie copper chromite 120 ppm Na	2.13×10^{20}

Catalytic testing was then carried out on copper chromite 120 ppm Na in the unreduced form. The conditions that were used mimicked the standard reaction (230°C, 57 mbar). This comparison in catalytic testing was carried out to investigate if the reduction in Lewis acid sites enhanced the conversion and / or selectivity. The results are illustrated in Figure 3-98.

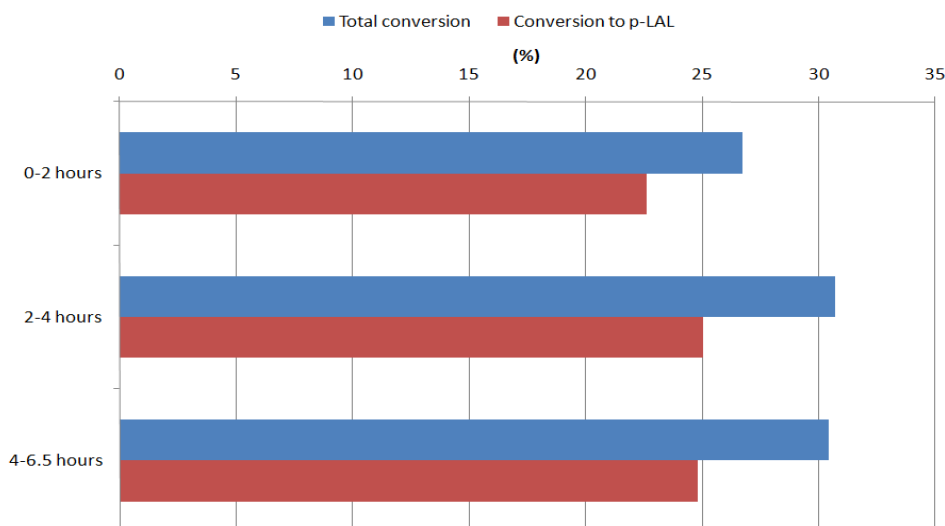


Figure 3-97 Conversion of p-LOL & p-LAL yield for reaction between p-LOL and non activated copper chromite 120 ppm Na (230°C, 57 mbar)

GC analysis suggested that deactivation did not occur as readily as with the BASF copper chromite. This may be due to the presence of barium in the catalyst. Both sud-chemie catalysts contain approximately 3-4% of barium chromate. It has been found that barium chromate inhibits the sintering process of the copper chromite and hence reduces deactivation. This is thought to occur due to the separation of the crystals brought about by the presence of barium chromate (151). Barium chromate is also known to stabilise the copper chromite against the reduction of Cu(II) to Cu(I) (152, 153). The sud-chemie catalysts also contain <5% manganese dioxide. Capece *et al* (154) found that when a manganese additive was added to copper chromite it had a stabilising effect with respect to Cu(I) species on the surface layer. It has also been suggested that the manganese additive retards the reduction of Cu(I) to Cu(0). From this it can be suggested both additives are playing an active role in reducing the deactivation of the catalyst.

As shown in figure 3-99 the selectivity of the by-products is similar to that of the standard copper chromite catalyst (fig 3-83 from previous chapter). There was however less conversion to by-products. In the first two hours conversion to by-products was only 4% with this catalyst and 6.5% with the original copper chromite.

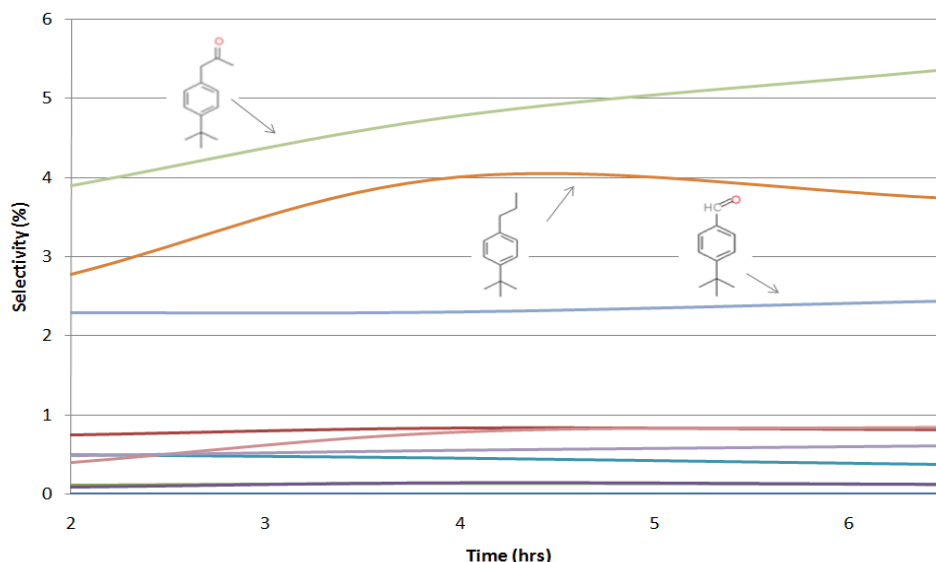


Figure 3-98 Selectivity for all other by products for reaction involving p-LOL and non activated copper chromite 120 ppm Na (230°C, 57 mbar)

The reduced quantity of by-products formed could be attributed to the reduction in Lewis acid sites available. Sodium has been known to poison Lewis acids on the catalyst. Dehydrogenation catalysts often facilitate side reactions (such as cracking, isomerisation and polymerisation), which are catalysed by acid centres. To minimise the occurrence of by-products these sites must be inhibited (155). This can be achieved during the preparation of the catalyst, as alkali metal ions can be used to poison the acid sites. Previous work by Pines and Haag (156) suggested that alkali metal ions poison the Lewis acid sites on alumina and Jiratová and Beranek (157) also reported selective poisoning of the support when alumina was doped with sodium ions. Sachett *et al* (158) studied the effect of sodium doping (140 ppm and 1600 ppm Na) and suggested that one sodium atom is able to poison one acid site (158, 159). Bocanegra *et al* (155) studied work on the dehydrogenation of butane over Pd/Al₂O₃ and Na- Pd/Al₂O₃ catalysts. Studies were carried out on a pulse system and they found that after the first pulse conversion was lower with the doped catalyst than the undoped catalyst, however there was an increase in selectivity with all of the doped catalysts.

Lewis acid sites on the catalyst facilitate the Tishchenko reaction (132). This involves the inert bed reacting with water to produce p-LOL and LAL acid. As described previously, LAL

acid is likely to further react and produce by-products. If Lewis acid sites are not available on the catalyst, subsequently by-product formation will be reduced.

The effects of sodium and other alkali metals on selectivity/deactivation aspects of various catalytic systems have been documented in the literature. The effect of Na addition to silica-supported copper (Cu/SiO₂) catalysts has been studied in the gas-phase catalytic oxidation of benzyl alcohol(160). The addition of alkali metal was found to promote the oxidation activity, particularly the partial oxidation activity. Co-ordination and redox properties of the Cu/SiO₂, catalysts, with and without alkali metal, were investigated using diffuse reflectance (DR) spectroscopy and temperature-programmed reduction (TPR) measurements. It was suggested, based on the diffuse reflectance DR spectra, that the alkali-metal added to the Cu/SiO₂, catalysts decreases the electronegativity of the supported Cu species; this decrease makes dissociative oxygen adsorption easier. The other role of the added alkali metal was thought to be to remove the oxidic Cu species which do not have catalytic activity for the partial oxidation.

In the steam reforming of ethanol over sodium doped Co catalysts, when the catalysts were operated at low conversion values (< 10%), at 523 K and initial reaction times, only H₂ and acetaldehyde (ca. 1:1 molar basis) were produced due to the dehydrogenation of ethanol(161). For these catalytic systems this is the first step in the ethanol steam-reforming reaction. The initial activity at 523 K for the dehydrogenation of ethanol decreased with decreasing sodium content of the catalyst, and was probably related to the high sodium segregation on the surface, as determined by XPS. Sodium species were postulated to block surface cobalt active sites in accordance with results of CO chemisorption followed by FTIR. However, for higher conversion values at 573 K, when the reforming of acetaldehyde takes place, an increase of sodium content in the catalyst produces a decrease in the residual acetaldehyde. As well as this the introduction of sodium resulted in a decrease in deactivation. Analysis of the catalysts revealed a retardation of carbonaceous deposit formation, and was attributed to be due to sodium's ability to aid CH_x species evolution from the catalyst surface.

Under the current system it is likely that the addition of sodium to the catalyst would yield a change in the interaction of the reactant with the surface, therefore leading to a change in activity/selectivity. This was observed along with an increase in stability.

3.3.5.2 Copper chromite 120 ppm Na reduced

To investigate the affect if any reduction had on the catalyst, a comparative reaction was carried out. Prior to the reaction the catalyst was reduced *in-situ* at 230°C for 2 hours. This was then transferred into a N₂ purged glove box to avoid oxidation. Standard conditions were used during the reaction (230°C, 57 mbar).

Analysis of the samples produced showed very little difference from that of the unreduced catalyst (figure 3-100 and 3-101).

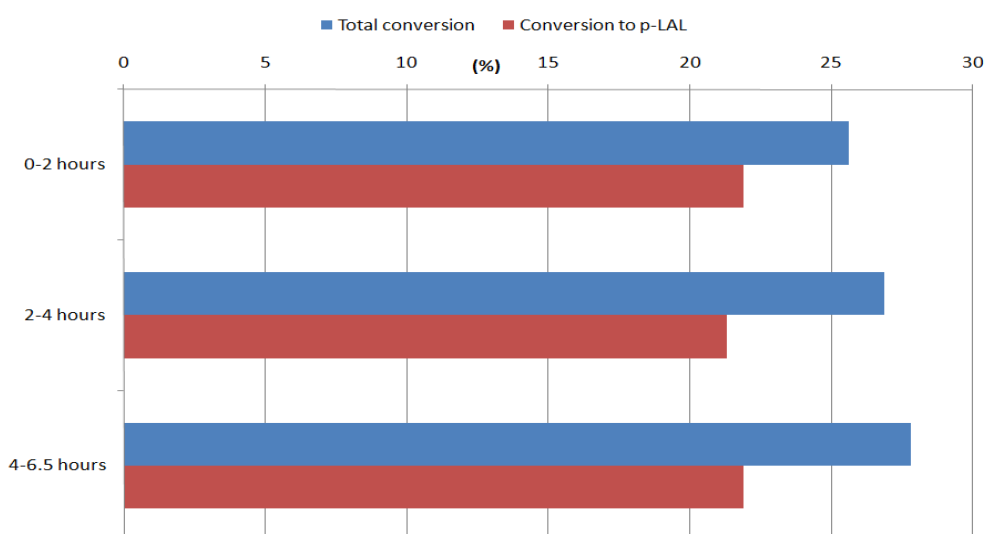


Figure 3-99 Conversion of p-LOL & p-LAL yield for reaction between p-LOL and *in-situ* copper chromite 120 ppm Na (230°C, 57 mbar)

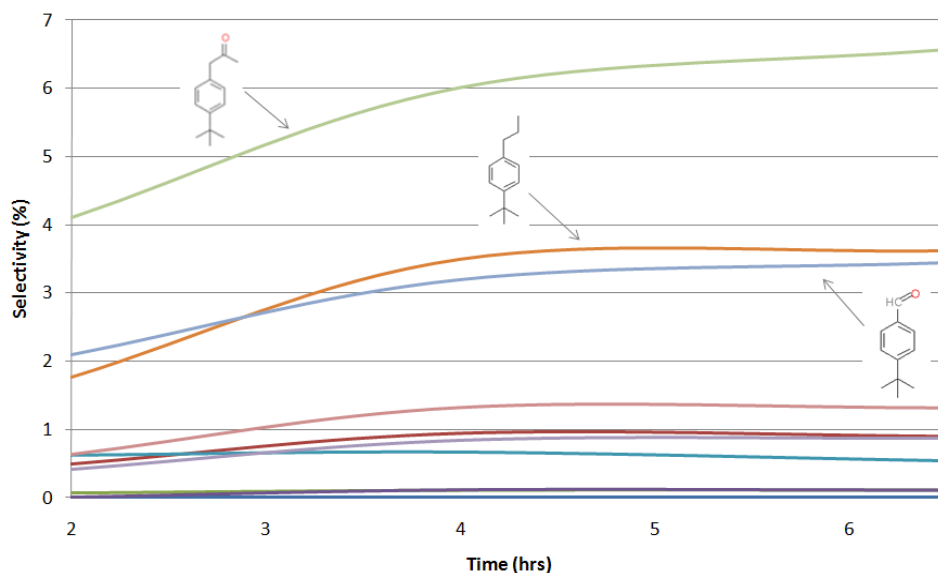


Figure 3-100 Selectivity for all other by products for reaction involving p-LOL and *in-situ* activated copper chromite 120 ppm Na (230°C, 57 mbar)

3.3.5.3 Copper chromite 1600 ppm Na unreduced

Another catalyst supplied from Sud-Chemie was copper chromite 1600 ppm Na. This contained more sodium than the previous catalyst and hence should have had less Lewis acid sites. However, a TPD carried out on the catalyst revealed an increase in the number of acid sites present when compared with the standard BASF catalyst (table 33).

Table 33 Catalyst comparison for Lewis acid sites 2

Catalyst	Lewis acid sites (per gram of catalyst)
BASF copper chromite	2.3×10^{20}
Sud-chemie Copper chromite 1600 ppm Na	2.66×10^{20}

Catalytic testing was carried out to study the effect of the increased Lewis acid sites on conversion. GC analysis showed that the conversion of p-LOL was approximately 28% within the first two hours (figure 3-102).

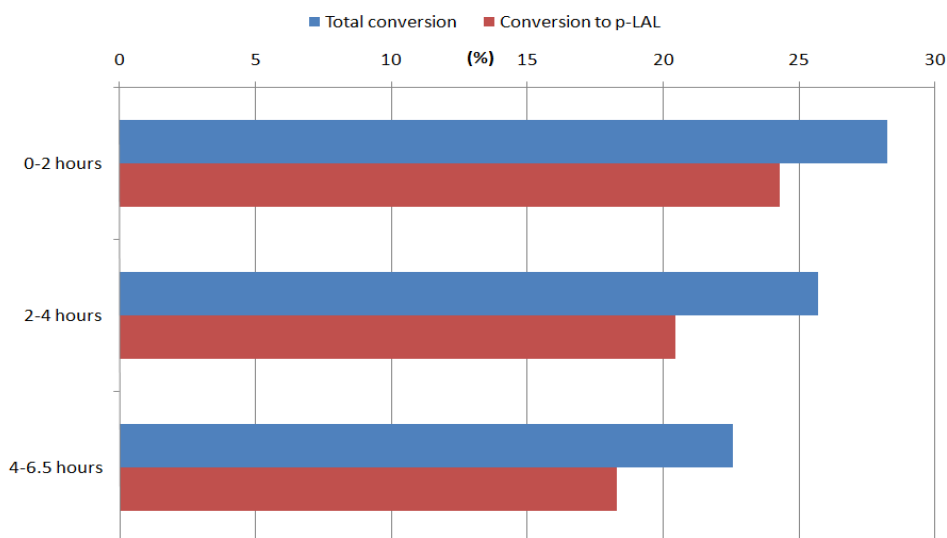


Figure 3-101 Conversion of p-LOL & p-LAL yield for reaction between p-LOL and non activated copper chromite 1600 ppm Na (230°C, 57 mbar)

After this time, deactivation was apparent and the p-LAL yield began to decline. The reason for this could be that the catalyst contains too much sodium, and the sodium is having a negative effect on the catalytic activity. US Patent 3,935,128 stated that sodium and other monovalent ions severely lower catalyst activity (162). Work carried out on the dehydrogenation of benzyl alcohol to benzaldehyde also suggested that the reaction was generally retarded with an increase in the amount of a sodium compound which is adsorbed on the catalyst during the modification process (163). This is illustrated in figure 3-103.

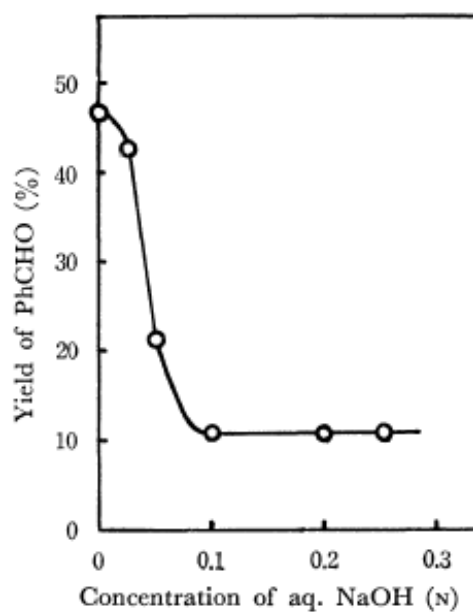


Figure 3-102 Relation of relative ratio of the dehydrogenation of benzyl alcohol vs concentration of aq. NaOH (163)

By- product formation shown in figure 3-104 is similar to that of copper chromite 120 ppm.

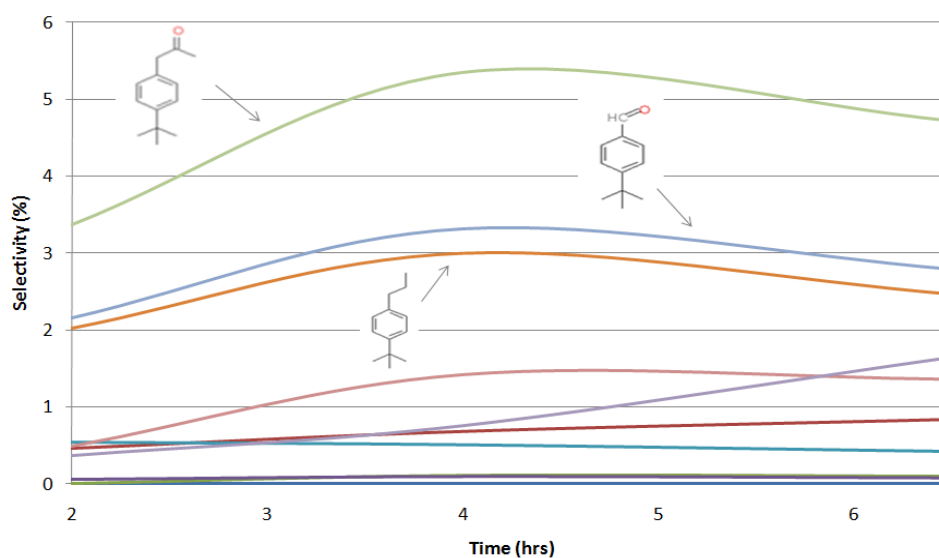


Figure 3-103 Selectivity for all other by products for reaction involving p-LOL and non activated copper chromite 1600 ppm Na (230°C, 57 mbar)

3.3.5.4 Catalyst comparison

A comparison has been made of all three copper chromite catalysts in the unreduced form. As illustrated in figure 3-105 BASF copper chromite shows the greatest yield of p-LAL in the first two hours but then deactivates very quickly. A similar trend is followed by copper chromite 1600 ppm Na. The deactivations in catalytic activity observed for both catalysts could possibly be attributed to the increased number of Lewis acid sites present. In contrast, very little deactivation over the course of the experiment was observed for copper chromite 120 ppm Na, which contained the lowest number of Lewis acid sites.

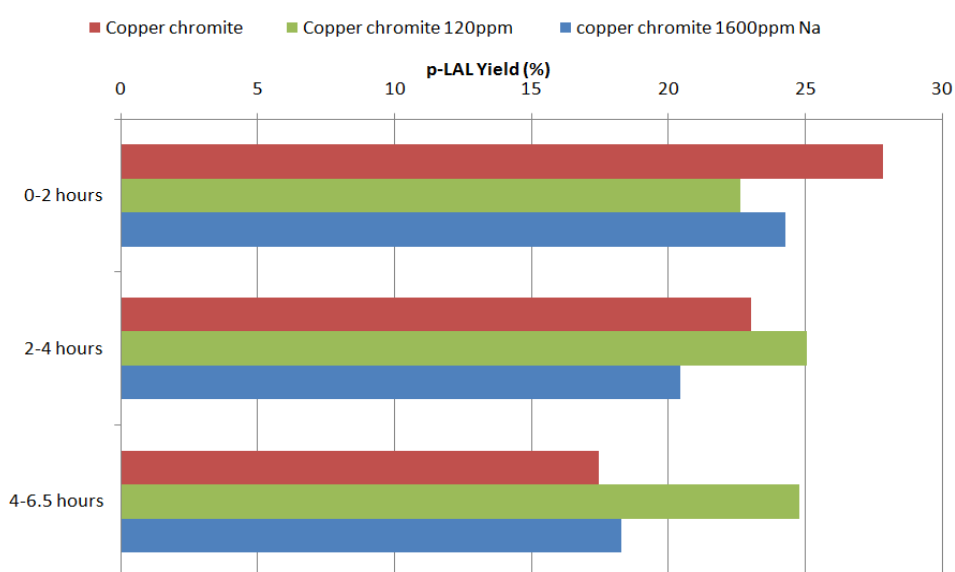


Figure 3-104 Comparison of p-LAL yield for unreduced catalysts for a) BASF copper chromite b) copper chromite 120 ppm Na and c) copper chromite 1600ppm Na

By-product yield was also compared as shown in figure 3-106. Once again BASF copper chromite shows the greatest yield of by-products. Both sud-chemie catalysts show similar percentage yields when averaged over time. In the first 4 hours their by-product yield is noticeably lower.

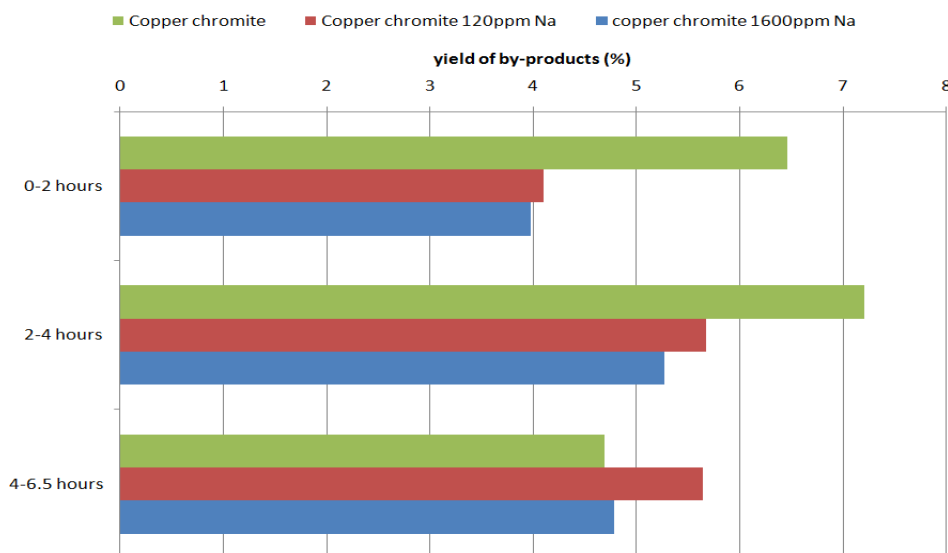


Figure 3-105 Comparison of by-product yield for unreduced catalysts a) BASF copper chromite b) copper chromite 120 ppm Na and c) copper chromite 1600ppm Na

These results suggested that the BASF copper chromite may not be the most suitable catalyst employed when carrying out the dehydrogenation of p-LOL. Copper chromite 120 ppm Na shows good conversion, less deactivation and less by-product formation. The reduction in deactivation can be related to the additives within the catalyst that are thought to reduce sintering (151). Catalytic testing of copper chromite 1600 ppm Na however revealed a deactivation similar to that observed for the BASF, and this could be attributed to the increased number of Lewis acid sites present in the catalyst, as well as the negative effect of high concentrations of sodium ions.

3.3.6 Alternative catalysts

Due to the low conversion and deactivation of copper chromite for the dehydrogenation of p-LOL it was decided to investigate the effect of different catalysts. Also due to the toxicity of copper chromite, a more environmentally friendly alternative would be beneficial. In industry, dealing with the carcinogenic chromium (VI) compounds, the waste water formed in the production (which contains pollutants) and the disposal of the chromium catalysts are all things that want to be avoided (104). Two catalysts were tested in both a reduced and unreduced form.

3.3.6.1 CuO/ZnO/Al₂O₃

A commercial methanol synthesis catalyst was selected for use in the dehydrogenation reaction. This catalyst was chosen due to its high copper loading, making it comparable with the conventional copper chromite. In general commercial CuO/ZnO/Al₂O₃ catalysts are usually made up of the following composition (table 34):

Table 34 Typical weight % of each component in copper methanol synthesis catalysts (72)

Component	Weight (%)
CuO	40-80
ZnO	10-30
Al ₂ O ₃	5-10

In these catalysts the zinc oxide and alumina phases were added to disperse the active copper phase, as well as stabilising the copper particles to prevent sintering (164). The zinc oxide has also been found to act as a promoter in the methanol synthesis reaction (165).

These types of catalysts have been previously studied in dehydrogenation reactions (166) and as a replacement for copper chromite catalysts (104). It was found that like the

copper chromite catalysts, metallic copper was the active species (167, 168). However CuO/ZnO/Al₂O₃ will reduce to form both Cu⁰ and Cu⁺, with Cu⁰ being the predominant species (168). It is well established that surface species of copper can be estimated quantitatively with carbon monoxide adsorption measurements. Klier (169) reported that reversibly adsorbed or physisorbed CO is a measure of metallic copper and Cu⁺ species corresponds to the irreversible CO uptake, whereas Cu²⁺ is totally inactive for both. Following on from this Sivaraj *et al* (168) carried out work on the dehydrogenation of cyclohexanone using CuO/ZnO/Al₂O₃ and found that maximum conversion was obtained when the reversible CO uptake was at its highest, confirming that metallic copper was the active species.

3.3.6.1.1 Unreduced CuO/ZnO/Al₂O₃

A reaction was carried out using unreduced catalyst as a direct comparison to a standard copper chromite reaction. All the conditions were kept the same as before (230°C, 57 mbar).

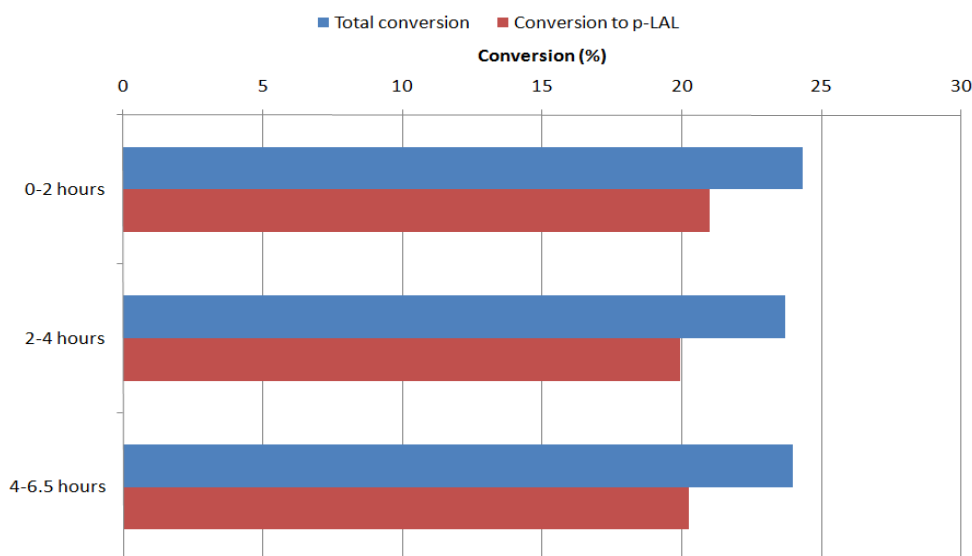


Figure 3-106 Conversion of p-LOL & p-LAL yield for reaction between p-LOL and non activated CuO/ZnO/Al₂O₃ (230°C, 57 mbar)

It can be seen from figure 3-107 that both the conversion and p-LAL yield was reduced compared to the copper chromite (p 170 , figure 3-69). Deactivation does not occur as rapidly however, only a gradual decline in activity was observed. Post reaction analysis

revealed the catalyst was in a reduced state as peaks corresponding to Cu^0 were present (figure 3-108).

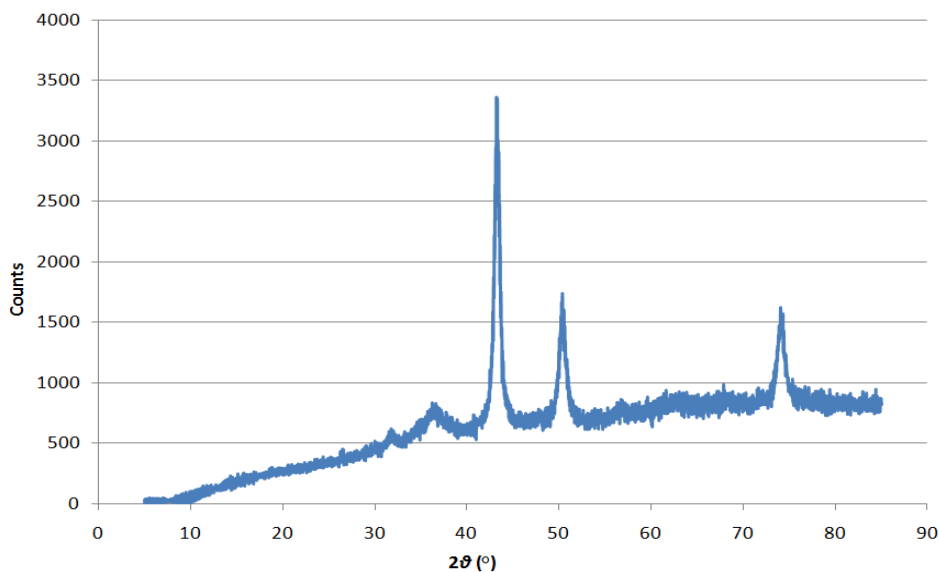


Figure 3-107 Post reaction XRD from standard reaction between p-LOL and $\text{CuO}/\text{ZnO}/\text{Al}_2\text{O}_3$ (230°C, 57 mbar)

At the end of the reaction when the catalyst and material was removed from the reactor it was visible that there was a metallic film present at the bottom. Due to its colour it was assumed to be metallic copper. Onda *et al* (170) reported that copper oxide catalysts show deactivation due to the leaching of copper caused by the catalyst being exposed to an aqueous acid solution. Figure 3-109 illustrates this. It can be noticed that when the concentration of water-soluble organic compounds (WSOCs) was at its highest, the pH was low. This confirmed that much of the WSOCs were organic acids and that due to this, the concentration of copper ions that had leached out was at its highest.

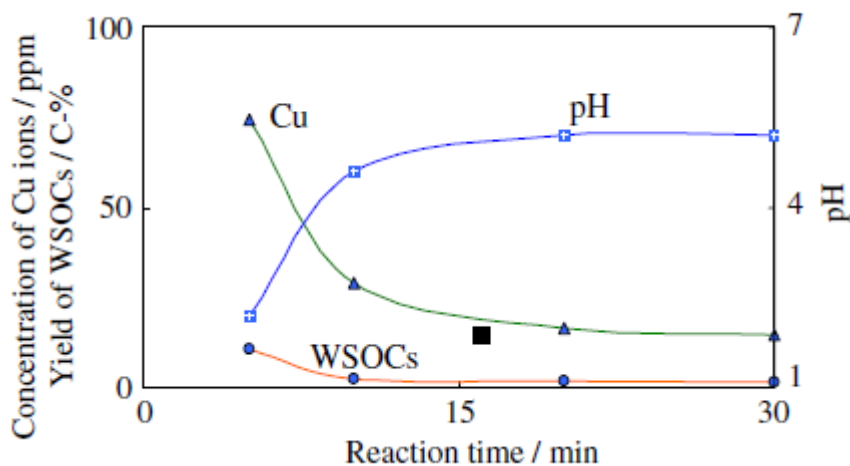


Figure 3-108 Leaching of Cu species. Naphthalene 10 mg; 1.0M H_2O_2 aqueous solution, 10 ml; $\text{CuO}/\text{Al}_2\text{O}_3$, 20 mg; reaction temperature 100°C (170)

Santos *et al* (171) also confirmed this in the wet oxidation of phenol, as it was observed that copper could be extracted from the $\text{Cu}/\text{Al}_2\text{O}_3$ catalyst by intermediate organic acids. However as the reaction proceeded and pH increased, the copper was subsequently precipitated.

In the current system there was a strong possibility that LAL acid could be formed. The GC analysis of the samples extracted during reaction revealed that the acid was present. It was therefore possible that it was the presence of the organic acid in solution that was leaching the copper out of the catalyst. As the reaction proceeded and the acid was reacted, the copper would precipitate onto the reactor wall, as observed previously by Santos *et al* (171). To confirm that copper leaching was taking place, 1 g of catalyst was placed in p-LAL and left for a few days. Due to the autoxidation process that p-LAL undergoes producing the acid, the catalyst was subjected to an acidic environment. After several days the solution had turned blue suggesting that $\text{Cu}(\text{II})$ ions were present. UV was carried out on this sample to confirm this as illustrated in figure 3-110.

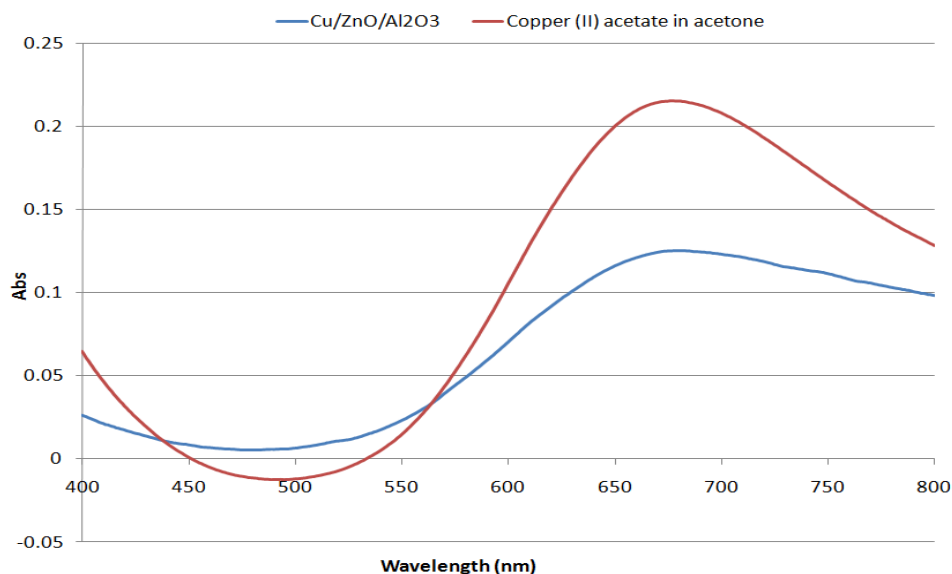


Figure 3-109 Liquid UV analysis of a) p-LAL after exposure to Cu/ZnO/Al₂O₃ b) copper (II) acetate in acetone

The band at approximately 650 nm is characteristic of the Cu²⁺ species hence proving that copper had leached out of solution.

In the current catalyst, the presence of a small amount of alumina is thought to act as a stabiliser (164). However, copper was clearly able to be extracted from the catalyst. In copper chromite, the chromia component is thought to have the same effect as alumina, and stabilise the copper component (106). Chromite has been shown to be more effective for this purpose, and could explain the high stability of the copper chromite under reaction conditions.

3.3.6.1.2 Reduced CuO/ZnO/Al₂O₃

After the reaction with unreduced catalyst it was decided to compare this to a reduced catalyst. The catalyst was reduced in a furnace for 3 hours at 270°C with 20 ml.min⁻¹ 5% H₂/N₂. To avoid oxidation the reactor tube was transferred to an inert atmosphere glove box where the catalyst was removed and placed in the reactor. A layer of inert bed was then placed over the catalyst to minimise oxidation. Standard conditions were used.

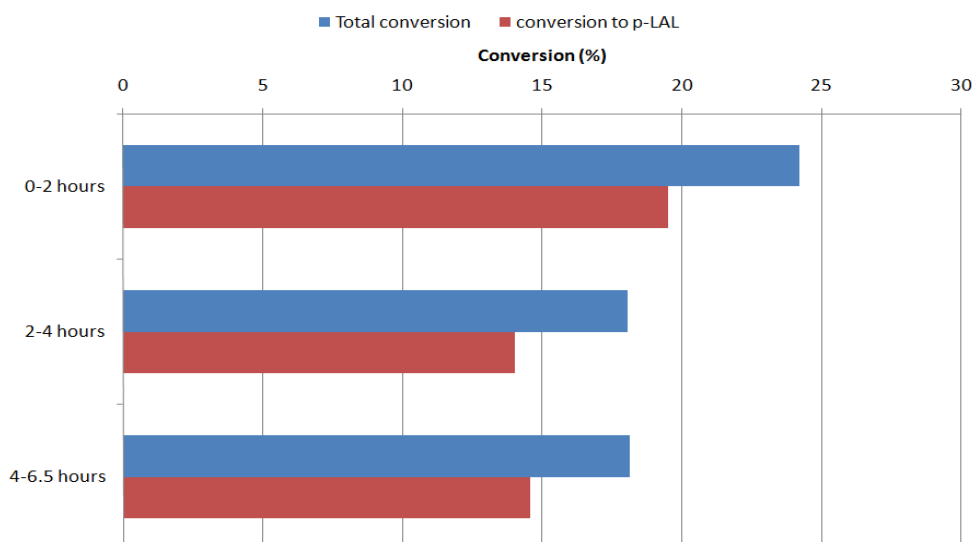


Figure 3-110 Conversion of p-LOL & p-LAL yield for reaction between p-LOL and *in-situ* activated CuO/ZnO/Al₂O₃ (230°C, 57 mbar)

During this reaction the deactivation occurred faster than previously observed using unreduced catalyst (figure 3-111). This could be due to the leaching of the copper and sintering. At the end of the reaction involving *in-situ* activation the amount of leached copper was greater than the reaction involving no activation. After the catalyst had been centrifuged it was apparent that a colour change had occurred (catalyst changed from black to brown) suggesting metallic copper was present.

SEM images were taken to see if there were any changes between fresh and used catalysts (figure 3-112). The post reaction sample from the unreduced reaction showed that the particles were a lot smaller than the fresh catalyst.

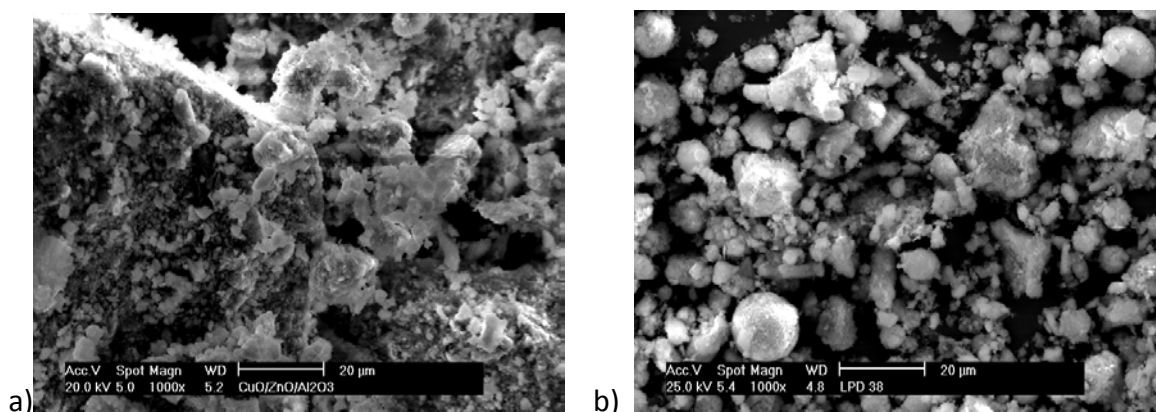


Figure 3-111 SEM images of a) fresh and b) post reaction sample from reduced CuO/ZnO/Al₂O₃ reaction

Table 35 BET CuO/ZnO/Al₂O₃

Catalyst	Surface area (m ² /g)	Pore volume (cm ³ /g)	Pore Diameter (Å)
Fresh CuO/ZnO/Al ₂ O ₃	87	0.22	99
Post reaction reduced	46.3	0.13	115

BET analysis showed that there was a reduction in the surface area (table 35). Due to the leaching that occurred the results obtained cannot be compared as this may have an effect. Due to this reason no further work on CuO/ZnO/Al₂O₃ was carried out.

3.3.6.2 Copper supported on silica

A 10% Cu/SiO₂ catalyst was prepared for catalytic testing as it was another possible alternative to copper chromite used in industry and had also previously been studied for dehydrogenation reactions (172). Once again copper is used to provide the active phase due to its high activity and selectivity. As the equilibrium constant of dehydrogenation reactions is high at high temperature due to its endothermic character, the dispersion of copper at these temperatures is important in industry. Therefore to improve thermal stability and dispersion the copper catalysts are prepared using an inert support (172) such as alumina and silica. Supports can be acidic, basic or both. The acidity determines whether the dehydration or the dehydrogenation reaction will be favoured. Basic supports favour the dehydrogenation whereas acidic supports favour the dehydration (173). Alumina however has strong acidic properties and can often facilitate side reactions. For this reason silica (which is basic) was the chosen support.

3.3.6.2.1 Unreduced 10% Cu/SiO₂

Copper silica was studied in both reduced and unreduced forms. Standard conditions were used to carry out these tests. Analysis of the data showed a reduction in the conversion (figure 3-113) from the standard copper chromite reaction (p 170, figure 3-69). Work carried out on the dehydrogenation of 2-butanol showed that increasing the

temperature and exposed copper atoms increased reaction rate (174), suggesting that the reduced rate was attributed to the low copper loading on the catalyst. The trend produced is similar to copper chromite with the deactivation starting to occur after 4- 6 hours.

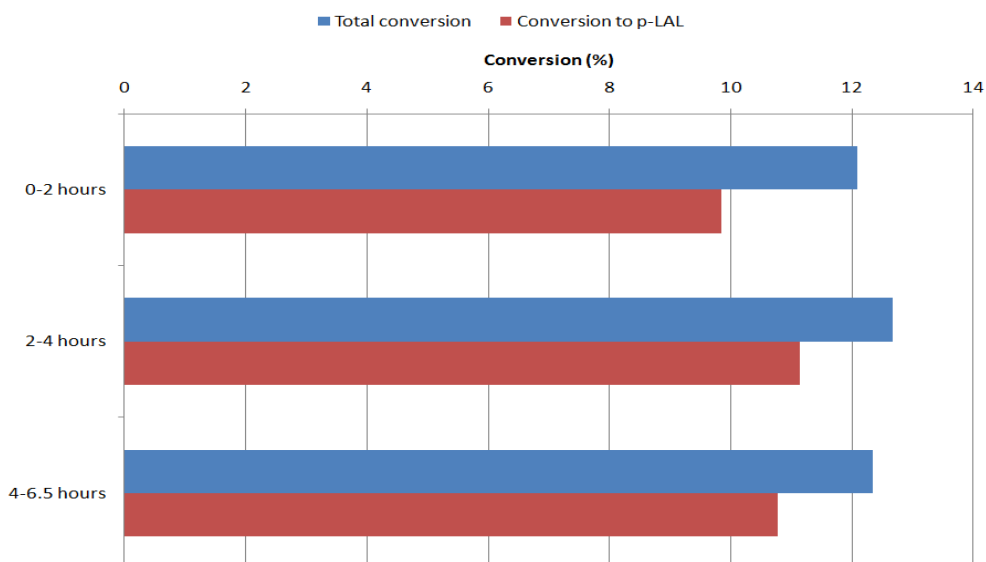


Figure 3-112 Conversion of p-LOL & p-LAL yield for reaction between p-LOL and non activated 10% Cu/SiO₂ (230°C, 57 mbar)

Shiau *et al* (128) also reported work on the liquid phase dehydrogenation of *n*-butanol at 270°C using several weight loadings of copper supported silica. It was found that significant deactivation occurred especially with the 5% Cu/SiO₂. Conversion was found to decrease from 43% to approximately 18% over a period of 8 hours using a 10% Cu/SiO₂ catalyst (128). In this study conversion was significantly lower than the work carried out on *n*-butanol. However this could be due to the lower temperature required for the dehydrogenation of p-LOL (230°C) and as previously mentioned temperature has a significant effect on dehydrogenation reactions.

After the reaction however copper was present in the reactor suggesting that leaching had occurred similar to the reactions with CuO/ZnO/Al₂O₃. Once the catalyst had been centrifuged it was apparent that the colour had changed. XRD also proved that metallic copper was present (figure 3-114) in the sample suggesting that reduction of the catalyst had occurred during the reaction.

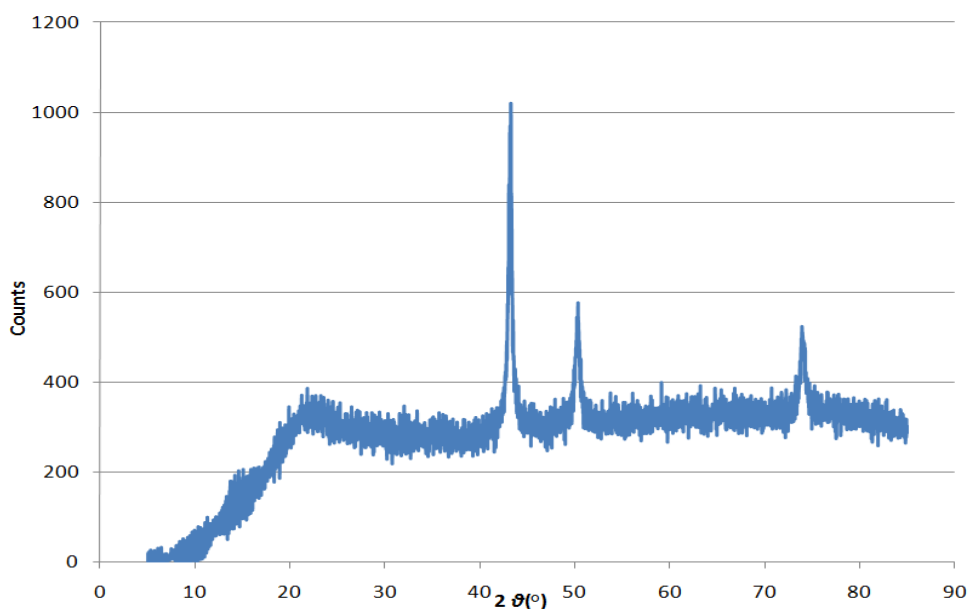


Figure 3-113 Post reaction XRD from standard reaction between p-LOL and non activated 10%Cu/SiO₂ (230°C, 57 mbar)

3.3.6.2.2 Reduced 10%Cu/SiO₂

To investigate the effects of reduction, the catalyst was reduced at 250°C for 3 hours prior to reaction and then placed into the reactor. An XRD was carried out to ensure that the catalyst was in a reduced state prior to reaction. The results from the catalytic testing revealed a slightly reduced conversion in comparison with the unreduced catalyst (figure 3-115). This once again may be due to copper leaching and sintering.

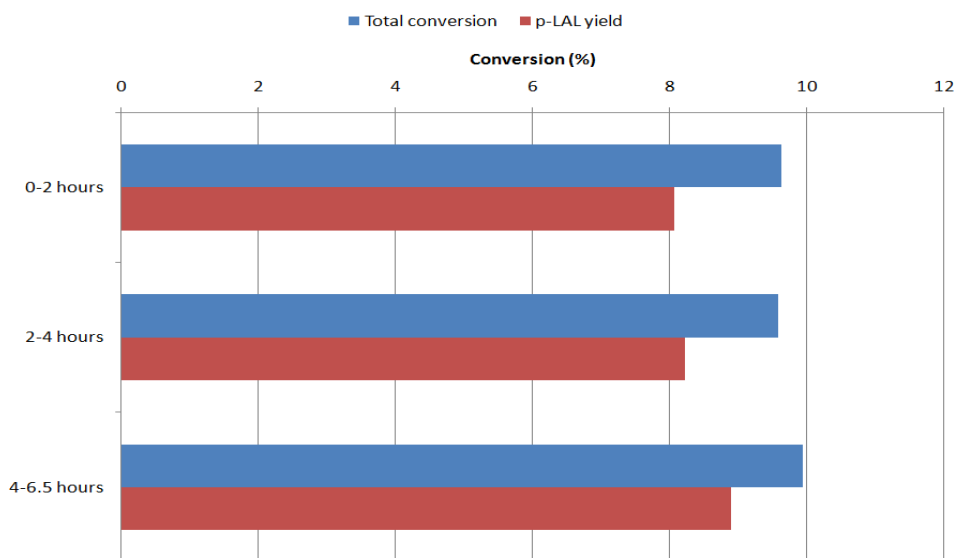


Figure 3-114 Conversion of p-LOL & p-LAL yield for reaction between p-LOL and *ex-situ* activated 10% Cu/SiO₂ (230°C, 57 mbar)

The catalyst was pre-reduced and in the metallic form at the start of the reaction. It would be reasonable to have expected a greater conversion than that of the unreduced reaction, however this did not occur. To investigate why this was the case, post reaction analysis was performed.

After the reaction the catalyst was centrifuged to allow analysis to be carried out. When the catalyst was allowed to dry it was visible that the catalyst had once again changed colour. Shiny copper coloured metallic particles were visible in the brown/red solid. This colouration has been found to be characteristic of metallic copper (175). XRD analysis confirmed that metallic copper was present as shown in figure 3-116.

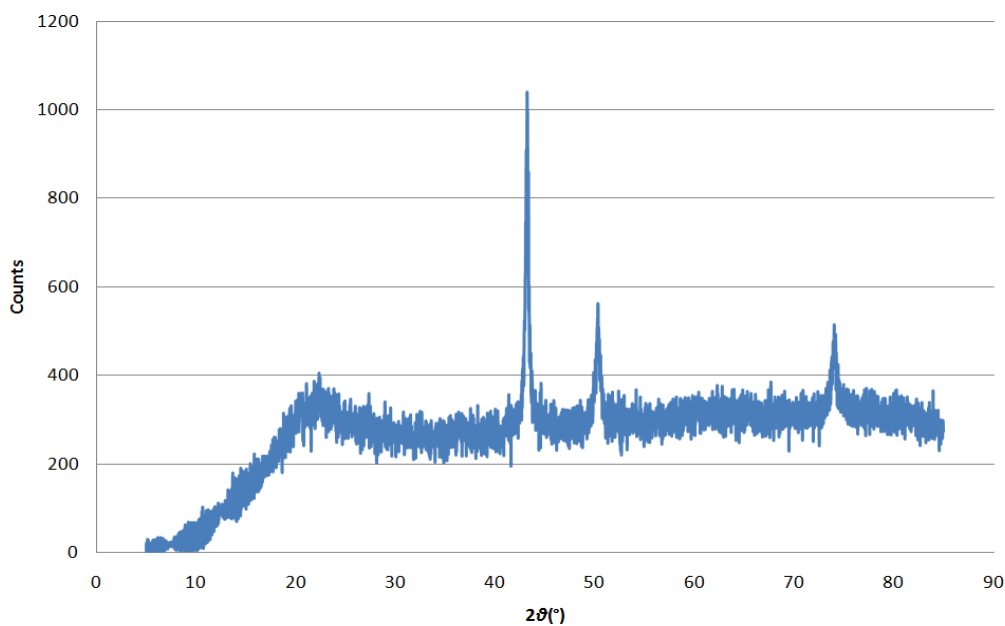


Figure 3-115 Post reaction XRD from standard reaction between p-LOL and *ex-situ* activated 10%Cu/SiO₂ (230°C, 57 mbar)

From the XRD data the Scherrer equation was used to calculate average crystallite size of the both post reaction reduced and unreduced catalysts. It can be seen from table 36 that there is a significant increase in crystallite size between the two samples. The pre reduced catalyst has a much larger crystallite size suggesting that sintering has occurred.

Table 36 Crystallite size Cu/SiO₂

Sample	Crystallite size
Post reaction unreduced	21 nm
Post reaction reduced	31 nm

SEM and BET were used to examine the catalyst surface area and form. SEM images showed that the catalyst from the unreduced reaction and the fresh catalyst looked fairly similar. However the sample from the reduced reaction was completely different. It can be seen from figure 3-117 that the particles are a lot larger, indicating that sintering had taken place. This agreed with the particle size data obtained from the XRD analysis.

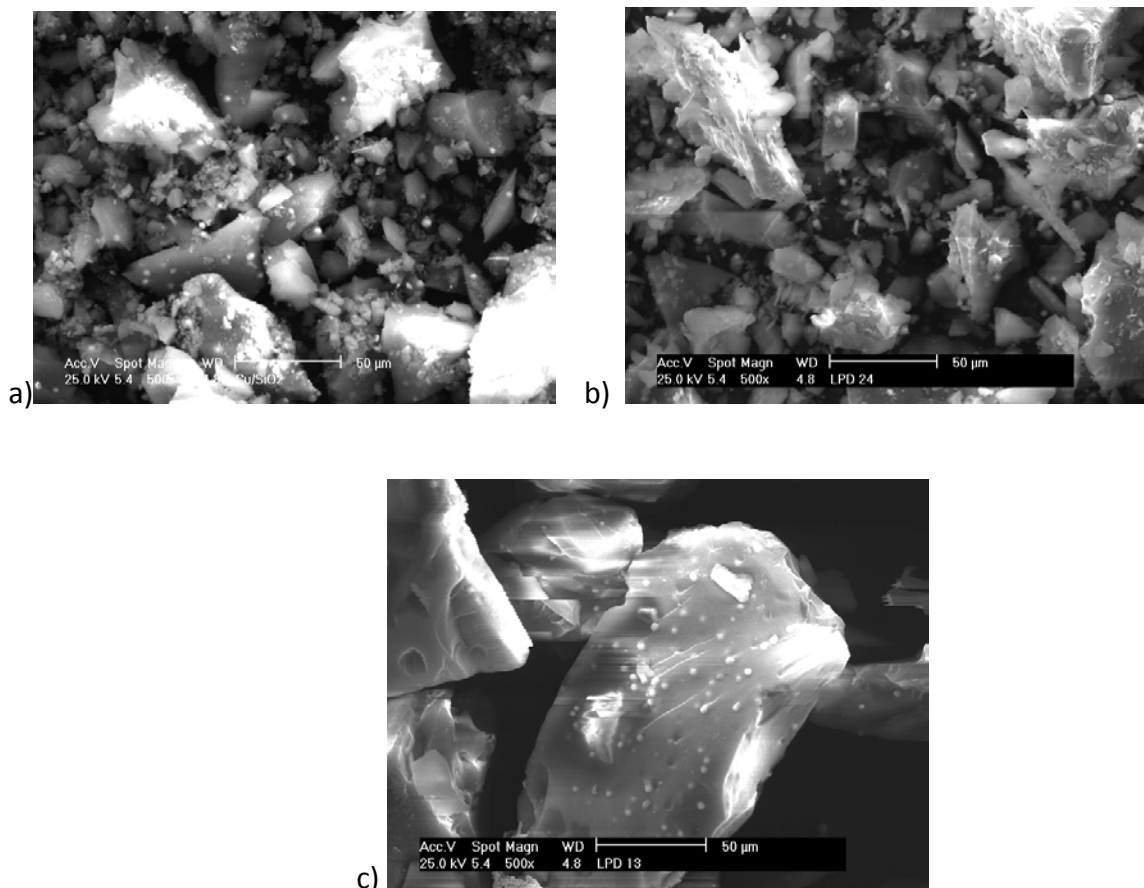


Figure 3-116 SEM images of a) fresh 10%Cu/SiO₂ b) post reaction unreduced c) post reaction reduced

Post reaction BET analysis of the catalysts (table 37) revealed also that sintering had occurred, as a loss of approximately 22 m²/g surface area was observed between the unreduced catalyst and the reduced catalyst. Work reported in the literature using Cu/SiO₂ catalysts for dehydrogenation reactions also observed a loss of surface area and report it to be caused by sintering (128). However, the loss of surface area could also have attributed to more extensive copper leaching.

Table 37 BET 10% Cu/SiO₂

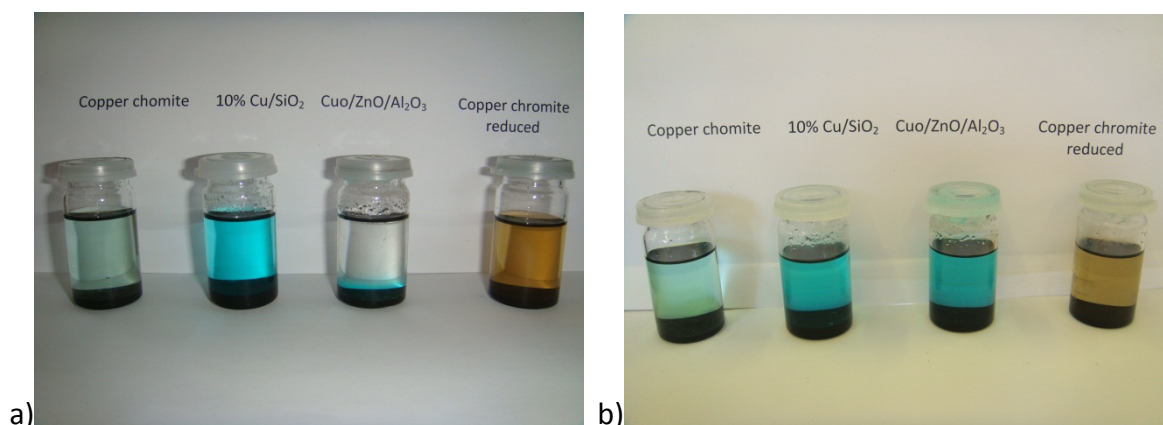
Catalyst	Surface area (m ² /g)	Pore volume (cm ³ g)	Pore Diameter (Å)
Fresh 10%Cu/SiO ₂	259	0.94	145
Post reaction unreduced	203	0.66	130

Post reaction	181	0.659	129
reduced			

This loss of surface area due to sintering is greater with Cu/SiO₂ than with both copper chromite and CuO/ZnO/Al₂O₃ due to the latter two having textural stabilisers present to minimise the occurrence of sintering. Cu/SiO₂ however does not possess this property and makes it more susceptible to sintering.

3.3.6.3 Acid leaching

Leaching of copper out of the catalyst was found to be a problem throughout reactions involving 10% Cu/SiO₂ and CuO/ZnO/Al₂O₃ but not with copper chromite. To investigate the effects of acid leaching on the various different catalysts, 1 g of each catalyst was placed into p-LAL and left for several weeks. A sample of pre-reduced copper chromite was also tested to examine if leaching occurred in this instance. The samples were left under an air atmosphere. This allowed air oxidation of p-LAL to occur and form LAL acid. It was visible in the sample that acid had been formed as a white solid was present at the top of the vial. It can be seen from figure 3-118 that copper silica was the first sample to leach out copper after 10 days. This was concurrent with the results obtained from liquid phase dehydrogenation reactions. Copper silica experiments showed the most leaching over the 6.5 hours.



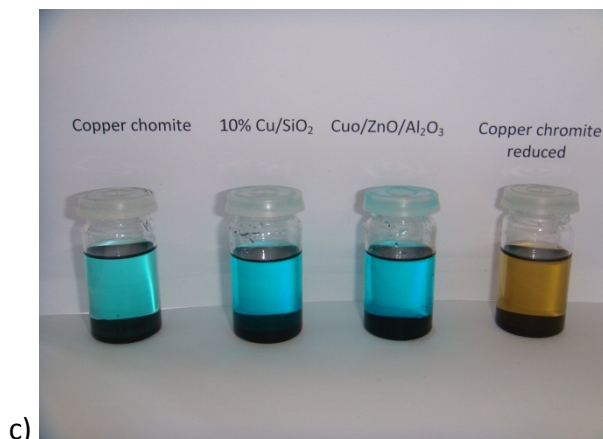


Figure 3-117 Catalyst & p-LOL experiment after a) 10 days, b) 20 days and c) 40 days

After 20 days the three unreduced catalysts all showed signs of leaching (figure 3-118). However copper chromite showed the least amount of leaching among the unreduced catalysts suggesting that it was more resistant to acidic conditions. After 40 days all of the unreduced catalysts have leached copper as they are all clearly blue. The solution with pre-reduced copper chromite produced a brown colouration suggesting that metallic copper may be in suspension.

No further work was carried out on both alternative catalysts due to the extensive leaching and sintering problems occurred.

3.4 Conclusions

Throughout this section of work, the experimental data focussed on several aspects. The main objective was to try and optimise the process by which lilestralis was produced. Several methods were used to try and achieve this. The project was split into several sections: (i) catalyst characterisation, (ii) material investigation, (iii) catalyst activation and (iv) alternative catalysts.

For catalytic testing, a reactor was designed to mimic the plant reactor and conditions used at Innospec. A commercial copper chromite catalyst was used in these studies. Characterisation into spent (catalyst from plant) and fresh catalyst was carried out. It was found that the spent catalyst was in the reduced form, suggesting that activation was occurring during the reaction. Analysis on fresh catalyst suggested that the reduction of copper chromite was not a simple process. Hot stage XRD suggested that subjecting the catalyst to a reducing environment, the catalyst was subsequently reduced from oxidised copper chromite to metallic copper. Thermal analysis was also used to study this further and it was seen that several stages occurred during this process. Acid site determination also suggested that the catalyst contained acid sites which were responsible for carrying out several reactions.

Investigation into the materials used within this study was carried out to obtain a clearer picture of what was occurring during a reaction. It was found that the inert bed (which is recycled material) contained a lot of impurities. Several reactions were carried out to see the effect of having bed material present had on the dehydrogenation. It was found that when the inert bed was not present there was an increased conversion of p-LOL (~70%) but the selectivity to p-LAL was very low (~10%). A reaction with only p-LAL and catalyst suggested that p-LAL may be responsible for the production of a lot of the by-products. When inert bed was present this conversion was reduced to approximately 25% suggesting that the bed material was required to minimise further reaction of p-LAL. When reduced catalyst was used in a reaction with p-LAL, the conversion once again decreased, suggesting that the water produced from the reduction could be having an effect on the reaction.

During a standard reaction no prior catalyst activation takes place. To investigate what effect activated catalyst had on the reaction a series of experiments with *in-situ* and *ex-situ* activation were carried out. The results highlighted that activating the catalyst had a positive effect on the reaction and conversion was increased. Deactivation plots suggested that reactions involving *in-situ* activation of the catalyst deactivated at a slower rate than no activation.

Throughout the dehydrogenation of p-LOL, copper chromite was known to deactivate over time due to sintering. To study if this deactivation could be reduced, alternative copper chromite catalysts were studied. These catalysts were modified with sodium and found to contain additives (barium chromate and manganese dioxide) to reduce the occurrence of sintering. The catalyst with the lowest sodium content showed very little deactivation and was suggested as a possible alternative to the standard catalyst. Different types of catalysts were also studied: CuO/ZnO/Al₂O₃ and 10% Cu/SiO₂. Both these catalyst were found to be unsuitable replacements for the copper chromite as sintering and extensive leaching of the copper occurred.

4 References

1. http://www.leffingwell.com/top_10.htm.
2. H. Ziegler, *Flavourings: Production, composition, application, regulations*. (Wiley-VCH, ed. 2nd).
3. R. R. Calkin, J. S. Jellinek, *Perfumery: Practice & principles*. (Wiley Interscience).
4. C. S. Sell, *The chemistry of fragrances, From perfumer to consumer*. (RSC, ed. 2nd).
5. H. Surburg, J. Panten, *Common fragrance & flavor materials*. (Wiley-VCH, ed. 5th).
6. P. Z. Bedoukian, *Perfumery & flavouring synthetics*. (allured publishing corporation, ed. 3rd revised edition).
7. J. A. B. Satrio, L. K. Doraiswamy, *Chemical Engineering Journal* **82**, 43 (2001).
8. Y. Y. Yu *et al.*, *Chemical Engineering Journal* **162**, 738 (Aug 15, 2010).
9. C. Y. Ma *et al.*, *Applied Catalysis B: Environmental* **92**, 202 (2009).
10. D. Cheng, C. Hou, F. Chen, X. Zhan, *Journal of Rare Earths* **27**, 723 (2009).
11. M. W. de Lange, J. G. van Ommen, L. Lefferts, *Applied Catalysis A: General* **220**, 41 (2001).
12. B. M. Choudary *et al.*, *Patent EP 1,088,810* (2004).
13. *Institut Francias de petrole des carburants et lubrinants*, *US Patent 3,579,589*, (1971).
14. P. C. Van Geem, A. J. J. Teunissen, *US Patent 4,137,259* (1979).
15. T. Kondow, K. Okazaki, Y. Katshara, K. Matsuoka, *US Patent 4,450,298* (1984).
16. T. Yokoyama, N. Yamagata, *Applied Catalysis A: General* **221**, 227 (2001).
17. T. Maki, T. Yokoyama, *US Patent 4,613,700*, (1986).
18. T. Yokoyama *et al.*, *Applied Catalysis A: General* **88**, 149 (1992).
19. C.-C. Guo, Q. Liu, X.-T. Wang, H.-Y. Hu, *Applied Catalysis A: General* **282**, 55 (2005).
20. <http://www.icas.com/v2/chemicals/9076550/toluene/uses.html>.
21. V. Augugliaro *et al.*, *Applied Catalysis B: Environmental* **20**, 15 (1999).
22. B. Grzybowska-Swierkosz, *Applied Catalysis A: General* **157**, 263 (1997).
23. A. Martin, B. Lücke, *Catalysis Today* **57**, 61 (2000).
24. H. Ge, G. Chen, Q. Yuan, H. Li, *Catalysis Today* **110**, 171 (2005).
25. F. Wang *et al.*, *Advanced Synthesis & Catalysis* **347**, 1987 (2005).
26. H. V. Borgaonkar, S. R. Raverkar, *Industrial & Engineering Chemistry Product Research & Development* **119**, 7 (1984).

27. D. A. Bulushev, L. Kiwi-Minsker, V. I. Zaikovskii, A. Renken, *Journal of Catalysis* **193**, 145 (2000).
28. Z. Hui-Liang, Z. Wei, D. Xiang, F. Xian-Cai, *Journal of Catalysis* **129**, 426 (1991).
29. T. Zhang, L. Mao, W. Liu, *Journal of Natural gas chemistry* **13**, 238 (2004).
30. F. M. Bautista, J. M. Campelo, D. Luna, J. Luque, J. M. Marinas, *Applied Catalysis A: General* **325**, 336 (2007).
31. U. Scharf, M. Schraml-Marth, A. Wokaun, A. Baiker, *Journal of the Chemical Society, Faraday Transactions* **87**, 3299 (1991).
32. A. Corma, J. M. L. Nieto, N. Paredes, M. Pérez, *Applied Catalysis A: General* **97**, 159 (1993).
33. G. Martra, F. Arena, S. Coluccia, F. Frusteri, A. Parmaliana, *Catalysis Today* **63**, 197 (2000).
34. M. L. Ferreira, M. Volpe, *Journal of Molecular Catalysis A: Chemical* **184**, 349 (2002).
35. I. E. Wachs, Y. Chen, J.-M. Jehng, L. E. Briand, T. Tanaka, *Catalysis Today* **78**, 13 (2003).
36. M. Xue, J. Ge, H. Zhang, J. Shen, *Applied Catalysis A: General* **330**, 117 (2007).
37. <http://science.irank.org/pages/825/Benzoic-Acid.html>.
38. <http://www.inchem.org/documents/cicads/cicads/cicad26.htm#SectionNumber:4.3>.
39. D.-G. Cheng, M. Chong, F. Chen, X. Zhan, *Catalysis Letters* **120**, 82 (2008).
40. W. J. Zhao, X. Z. Jiang, G. L. Zhuo, *Journal of Molecular Catalysis A: Chemical* **225**, 131 (2005).
41. C. Keresszegi, D. Ferri, T. Mallat, A. Baiker, *The Journal of Physical Chemistry B* **109**, 958 (2004).
42. W. F. Hölderich, J. Tjoe, *Applied Catalysis A: General* **184**, 257 (1999).
43. M. W. de Lange, J. G. van Ommen, L. Lefferts, *Applied Catalysis A: General* **231**, 17 (2002).
44. F. Dury, V. Misplon, E. M. Gaigneaux, *Catalysis Today* **91-92**, 111 (2004).
45. F. Dury, D. Clément, E. M. Gaigneaux, *Catalysis Today* **112**, 130 (2006).
46. Y. Sakata, V. Ponec, *Applied Catalysis A: General* **166**, 173 (1998).
47. C. Doornkamp, V. Ponec, *Journal of Molecular Catalysis A: Chemical* **162**, 19 (2000).

48. J. Kondo, Y. Sakata, K. Domen, K.-i. Maruya, T. Onishi, *Journal of the Chemical Society, Faraday Transactions* **86**, 397 (1990).
49. C. T. Campbell, C. H. F. Peden, *Science* **309**, 713 (July 29, 2005, 2005).
50. M. Chong, D.-g. Cheng, L. Liu, F. Chen, X. Zhan, *Catalysis Letters* **114**, 198 (2007).
51. S. Bektesevic, A. M. Kleman, A. E. Marteel-Parrish, M. A. Abraham, *The Journal of Supercritical Fluids* **38**, 232 (2006).
52. A. M. Trzeciak, J. J. Ziolkowski, *Coordination Chemistry Reviews* **190-192**, 883 (1999).
53. I. Kani, R. Flores, J. P. Fackler, A. Akgerman, *The Journal of Supercritical Fluids* **31**, 287 (2004).
54. A. R. Tadd, A. Marteel, M. R. Mason, J. A. Davies, M. A. Abraham, *The Journal of Supercritical Fluids* **25**, 183 (2003).
55. W. J. Zhao, X. Z. Jiang, G. L. Zhuo, *Journal of Molecular Catalysis A: Chemical* **225**, 131 (2005).
56. Clingenpeel.T.H, A. I. Biaglow, *Journal of the American Chemical Society* **119**, 5077 (1997).
57. X. Wu, R. G. Anthony, *Journal of Catalysis* **184**, 294 (1999).
58. B. M. Reddy, P. M. Sreekanth, P. Lakshmanan, *Journal of Molecular Catalysis A: Chemical* **237**, 93 (2005).
59. X. Li *et al.*, *Journal of Catalysis* **230**, 214 (2005).
60. B. H. Davis, R. A. Keogh, R. Srinivasan, *Catalysis Today* **20**, 219 (1994).
61. G. D. Yadav, J. J. Nair, *Microporous and Mesoporous Materials* **33**, 1 (1999).
62. X. Song, A. Sayari, *Catalysis Reviews: Science and Engineering* **38**, 329 (1996).
63. S. X. Song, R. A. Kydd, *Journal of the Chemical Society, Faraday Transactions* **94**, 1333 (1998).
64. N. Katada *et al.*, *The Journal of Physical Chemistry B* **104**, 10321 (2000).
65. A. Corma, A. Martinez, C. Martinez, *Journal of Catalysis* **149**, 52 (1994).
66. T.-K. Cheung, B. C. Gates, *Journal of Catalysis* **168**, 522 (1997).
67. Hino.M, Arata.K, *Chemistry Letters*, 1671 (1981).
68. Tanabe.K *et al.*, *In proceedings of the 8th International catalysis congress; Verlag Chemie; Weinheim* **5**, 601 (1984).
69. T. H. Clingenpeel, T. E. Wessel, A. I. Biaglow, *Journal of the American Chemical Society* **119**, 5469 (1997).
70. A. S. C. Brown, J. S. J. Hargreaves, *Green Chemistry* **1**, 17 (1999).

71. C. J. Norman, P. A. Goulding, P. J. Moles, M. M. Hideshi Hattori, O. Yoshio, in *Studies in Surface Science and Catalysis*. (Elsevier, 1994), vol. Volume 90, pp. 269-272.
72. C. N. Satterfield, *Heterogenous Catalysis in Industrial Practice*. (Krieger ed. 2nd).
73. M. H. Al-Dahhan, Y. Wu, M. P. Dudukovic, *Industrial & Engineering Chemistry Research* **34**, 741 (1995).
74. Hindle.K.T, Jackson.S.D, Webb.G, *Current topics in catalysis* **7**, 115 (2008).
75. S. D. Jackson, S. Rugmini, *Journal of Catalysis* **251**, 59 (2007).
76. H.-S. Kim, S. A. Zygmunt, P. C. Stair, P. Zapol, L. A. Curtiss, *The Journal of Physical Chemistry C* **113**, 8836 (2009).
77. M. Baltes *et al.*, *Physical Chemistry Chemical Physics* **2**, 2673 (2000).
78. K. V. R. Chary, G. Kishan, *The Journal of Physical Chemistry* **99**, 14424 (1995).
79. S. D. Jackson, S. Rugmini, P. C. Stair, Z. Wu, *Chemical Engineering Journal* **120**, 127 (2006).
80. J. McGregor *et al.*, *Catalysis Today* **142**, 143 (2009).
81. Z. Wu, H.-S. Kim, P. C. Stair, S. Rugmini, S. D. Jackson, *The Journal of Physical Chemistry B* **109**, 2793 (2005).
82. A. Khodakov, B. Olthof, A. T. Bell, E. Iglesia, *Journal of Catalysis* **181**, 205 (1999).
83. J. M. Kanervo, M. E. Harlin, A. O. I. Krause, M. A. Bañares, *Catalysis Today* **78**, 171 (2003).
84. D. R. Still, E. F. Westerum Jr, G. C. Sinke, *The chemical thermodynamics of organic compounds*. (John Wiley & sons Inc, 1987).
85. D. Ambrose *et al.*, *The Journal of Chemical Thermodynamics* **7**, 1143 (1975).
86. J. R. Pound, *The Journal of Physical Chemistry* **35**, 1496 (1931).
87. K. Sato, H. Abe, S. Ohara, *Journal of the American Chemical Society* **132**, 2538.
88. V. Santos, M. Zeni, C. P. Bergmann, J. M. Hohemberger, *Rev. Adv.Mater.Sci* **17**, 62 (2008).
89. G. Y. Guo, Y. L. Chen, *Journal of Materials Science* **39**, 4039 (2004).
90. Y. Sakata, C. A. van Tol-Koutstaal, V. Ponec, *Journal of Catalysis* **169**, 13 (1997).
91. R. Pestman, R. M. Koster, J. A. Z. Pieterse, V. Ponec, *Journal of Catalysis* **168**, 255 (1997).
92. E. H. Shreiber, M. D. Rhodes, G. W. Roberts, *Applied Catalysis B: Environmental* **23**, 9 (1999).
93. B. Li, R. D. Gonzalez, *Applied Catalysis A: General* **174**, 109 (1998).

94. B. Li, R. D. Gonzalez, *Applied Catalysis A: General* **165**, 291 (1997).
95. K. W. Bartz, *US Patent 2,947,728*, (1960).
96. G. Fráter, J. A. Bajgrowicz, P. Kraft, *Tetrahedron* **54**, 7633 (1998).
97. K. A. D. Swift, *Flavours and fragrances*. (RSC information services, 1997).
98. R. M. Rioux, M. A. Vannice, *Journal of Catalysis* **216**, 362 (2003/6//).
99. *Handbook of Heterogeneous Catalysis*. H. K. a. J. W. M. Kraus. In: G. Ertl, Ed., (Wiley-VCH, 1997), vol. 4.
100. Y. J. Tu, C. Li, Y. W. Chen, *Journal of Chemical Technology & Biotechnology* **59**, 141 (1994).
101. A. Guerrero-Ruiz, I. Rodriguez-Ramos, J. L. G. Fierro, *Applied Catalysis* **72**, 119 (1991).
102. H. Adkins, R. Connor, *Journal of the American Chemical Society* **53**, 1091 (1931).
103. R. Prasad, *Materials Letters* **59**, 3945 (2005).
104. G. Horn, C. D. Frohning, *US patent 5,320,569*, (1994).
105. R. Prasad, V. Shankar, *Advances in catalyst science & Engineering*. (Wiley Eastern Ltd, ed. T.S.R. Prasad Rao, 1985).
106. Y.-J. Tu, Y.-W. Chen, C. Li, *Journal of Molecular Catalysis* **89**, 179 (1994).
107. Y. S. Prasad, B. D. Padaliax, S. K. Raman, *Journal of Chemical Technology and Biotechnology. Chemical Technology* **35**, 15 (1985).
108. I. I. Simentsova, A. V. Khasin, L. P. Davydova, T. M. Yurieva, *Reaction Kinetics and Catalysis Letters* **82**, 355 (2004).
109. J. Christopher, I. A. P. S. Murthy, C. S. Swamy, *Thermochimica Acta* **164**, 191 (1990).
110. A. Lupu, *Journal of Thermal Analysis and Calorimetry* **2**, 445 (1970).
111. L. M. Plyasova *et al.*, *Kinetics and Catalysis* **42**, 126 (2001).
112. L. M. Plyasova, I. Y. Molina, T. A. Krieger, L. P. Davydova, T. M. Yurieva, *Journal of Molecular Catalysis A: Chemical* **158**, 331 (2000).
113. E. H. Shreiber, G. W. Roberts, *Applied Catalysis B: Environmental* **26**, 119 (2000).
114. Y. K. Lee, S.-E. Park, Y. S. Kwo, *Technol. Ciencia Ed* **4**, 34 (1989).
115. R. Rao, A. Dandekar, R. T. K. Baker, M. A. Vannice, *Journal of Catalysis* **171**, 406 (1997).
116. A. Romero, A. Santos, D. Escrig, E. Simón, *Applied Catalysis A: General* **In Press**, **Accepted Manuscript**.

117. I. I. Simentsova, A. V. Khasin, L. P. Davydova, T. M. Yurieva, *Reaction Kinetics and Catalysis Letters* **82**, 355 (2004).
118. T. M. Yurieva, L. M. Plyasova, O. V. Makarova, T. A. Krieger, *Journal of Molecular Catalysis A: Chemical* **113**, 455 (1996).
119. L. M. Plyasova, L. P. Solovyeva, T. A. Krieger, O. V. Makarova, T. M. Yurieva, *Journal of Molecular Catalysis A: Chemical* **105**, 61 (1996).
120. A. A. Khassin *et al.*, *Physical Chemistry Chemical Physics* **11**, 6090 (2009).
121. A. Khasin, I. Simentsova, T. Yur'eva, *Kinetics and Catalysis* **41**, 282 (2000).
122. S. P. Tonner, M. S. Wainright, D. L. Trimm, N. W. Cant, *Applied Catalysis* **11**, 93 (1984).
123. M. A. Aramendí *et al.*, *Rapid Communications in Mass Spectrometry* **8**, 599 (1994).
124. F. M. Bautista *et al.*, *Journal of Materials Chemistry* **4**, 311 (1994).
125. R. Rajeev *et al.*, *Thermochimica Acta* **254**, 235 (1995).
126. Y.-Y. Zhu *et al.*, *Catalysis Letters* **135**, 275.
127. J. A. Moura *et al.*, *Journal of Thermal Analysis and Calorimetry* **79**, 435 (2005).
128. C.-Y. Shiau, J. C. Tsai, *Journal of Chemical Technology & Biotechnology* **73**, 414 (1998).
129. X. Sun, N. W. Jones, J. C. Gesick, L. Xu, G. W. Roberts, *Applied Catalysis A: General* **231**, 269 (2002).
130. V. Z. Fridman, A. A. Davydov, K. Titievsky, *Journal of Catalysis* **222**, 545 (2004).
131. *Dictionary of Chemistry*. J. Daintith, Ed., (Oxford university press, ed. 5th).
132. <http://www.organic-chemistry.org/namedreactions/tishchenko-reaction.shtm>.
133. N. Ichikawa, S. Sato, R. Takahashi, T. Sodesawa, K. Inui, *Journal of Molecular Catalysis A: Chemical* **212**, 197 (2004).
134. J. Clayden, N. Greeves, N. Warren, P. Wothers, *Organic chemistry*. (Oxford university press).
135. M. V. Twigg, M. S. Spencer, *Applied Catalysis A: General* **212**, 161 (2001).
136. C.-Y. Shiau, S. Chen, J. C. Tsai, S. I. Lin, *Applied Catalysis A: General* **198**, 95 (2000).
137. R. B. C. Pillai, *Catalysis Letters* **26**, 365 (1994).
138. A. Cao, R. Lu, G. Veser, *Physical Chemistry Chemical Physics* **12**, 13499 (2010).
139. P. Forzatti, L. Lietti, *Catalysis Today* **52**, 165 (1999).
140. A. Cao, G. Veser, *Nat Mater* **9**, 75 (2010).
141. J. Cunningham, G. H. Al-Sayyed, J. A. Cronin, C. Healy, W. Hirschwald, *Applied Catalysis* **25**, 129 (1986).

142. V. M. Palekar, J. W. Tierney, I. Wender, *Applied Catalysis A: General* **103**, 105 (1993).
143. R. B. C. Pillai, K. K. Bhattacharyya, C. N. Pillai, *Indian Journal of chemistry* **29 A**, 1115 (1990).
144. M. Besson, P. Gallezot, *Catalysis Today* **81**, 547 (2003).
145. C. Keresszegi, T. Mallat, A. Baiker, *New Journal of Chemistry* **25**, 1163 (2001).
146. T. Okubo *et al.*, *Industrial & Engineering Chemistry Research* **30**, 614 (1991).
147. G. Wang, Y. Zuo, M. Han, J. Wang, *Reaction Kinetics, Mechanisms and Catalysis* **101**, 443 (2010).
148. E. D. Guerreiro, O. F. Gorrioz, J. B. Rivarola, L. A. Arrúa, *Applied Catalysis A: General* **165**, 259 (1997).
149. *Studies in surface science and catalysis: Catalyst deactivation*. (Elsevier Science Publishers B.V), vol. 68.
150. S. Lambert, C. Cellier, F. Ferauche, É. M. Gaigneaux, B. Heinrichs, *Catalysis Communications* **8**, 2032 (2007).
151. V. R. Choudhary, S. O. Pataskar, *Thermochimica Acta* **95**, 87 (1985).
152. R. Connor, K. Folkers, H. Adkins, *Journal of the American Chemical Society* **54**, 1138 (1932).
153. H. Adkins, E. E. Burgoyne, H. J. Schneider, *Journal of the American Chemical Society* **72**, 2626 (1950).
154. F. M. Capece *et al.*, *Journal of Electron Spectroscopy and Related Phenomena* **27**, 119 (1982).
155. S. A. Bocanegra, A. A. Castro, A. Guerrero-Ruíz, O. A. Scelza, S. R. de Miguel, *Chemical Engineering Journal* **118**, 161 (2006).
156. H. Pines, W. O. Haag, *Journal of the American Chemical Society* **82**, 2471 (1960).
157. K. Jirátová, L. Beránek, *Applied Catalysis* **2**, 125 (1982).
158. Sachett.C *et al.*, *Bulletin de la Société Chimique de France* 357 (1989).
159. A. B. M. Saad, V. A. Ivanov, J. C. Lavalley, P. Nortier, F. Luck, *Applied Catalysis A: General* **94**, 71 (1993).
160. M. Arai, S. Nishiyama, S. Tsuruya, M. Masai, *Journal of the Chemical Society, Faraday Transactions* **92**, 2631 (1996).
161. J. Llorca, N. Homs, J. Sales, J.-L. G. Fierro, P. Ramírez de la Piscina, *Journal of Catalysis* **222**, 470 (2004).
162. M. M. Fein, P. A. Colgate, R. A. Kent, *US Patent 3,935,128*, (1976).

163. M. Ishige, K. Sakai, M. Kawai, K. Hata, *Bulletin of the Chemical Society of Japan* **44**, 1095 (1971).
164. M. Twigg, *Catalyst Handbook*. (Wolfe Publishing Ltd, 1989).
165. B. Denise, R. P. A. Sneed, B. Beguin, O. Cherifi, *Applied Catalysis* **30**, 353 (1987).
166. F. Pepe, R. Polini, *Journal of Catalysis* **136**, 86 (1992).
167. S. Göbölös, M. Hegedüs, I. Kolosova, M. Maciejewski, J. L. Margitfalvi, *Applied Catalysis A: General* **169**, 201 (1998).
168. C. Sivaraj, B. M. Reddy, P. K. Rao, *Applied Catalysis* **45**, L11 (1988).
169. Klier, K., *Advanced catalysis* **31**, 242 (1982).
170. A. Onda, Y. Suzuki, S. Takemasa, K. Kajiyoshi, K. Yanagisawa, *Journal of Materials Science* **43**, 4230 (2008).
171. A. Santos, P. Yustos, A. Quintanilla, G. Ruiz, F. Garcia-Ochoa, *Applied Catalysis B: Environmental* **61**, 323 (2005).
172. G. Jeon, G. Seo, J. Chung, *Korean Journal of Chemical Engineering* **13**, 412 (1996).
173. J. N. Keuler, L. Lorenzen, S. Miachon, *Applied Catalysis A: General* **218**, 171 (2001).
174. H.-F. Chang, C.-F. Yang, *Industrial & Engineering Chemistry Research* **36**, 2080 (1997).
175. J. D. Stroupe, *Journal of the American Chemical Society* **71**, 569 (1949).